ONONDAGA LAKE CAPPING, DREDGING, HABITAT AND PROFUNDAL ZONE (SMU 8) FINAL DESIGN

APPENDIX B – CAP MODELING

Prepared for:

Honeywell

301 Plainfield Road, Suite 330
Syracuse, NY 13212

Prepared by:

PARSONS

301 Plainfield Road, Suite 350
Syracuse, NY 13212

ANCHOR QEA

290 Elwood Davis Road, Suite 318
Liverpool, NY 13088
Phone: (315) 451-1905

MARCH 2012

TABLE OF CONTENTS

PAGE

1.0 EXECUTIVE SUMMARY 1

2.0 MODELING OBJECTIVES 3

3.0 DESIGN MODELS 3
- 3.1 Analytical Steady State Model 3
- 3.2 Numerical Model 4
- 3.3 Model Conservatism 5

4.0 MODELING AREAS 7

5.0 MODEL INPUTS 9

6.0 DESIGN OPTIMIZATION CONSIDERING VARIABILITY IN SITE CONDITIONS 9
- 6.1 Extensive Data Collection and Bench Testing 10
- 6.2 Small Model Areas to Minimize Spatial Variability 10
- 6.3 Initial Conservative Modeling Used Maximum Porewater Concentrations 10
- 6.4 Model Conservatisms Offset Potential Impacts of Variability 10
- 6.5 Mean Values Used as Best Estimate 11
- 6.6 Conservative Probabilistic Modeling Used to Evaluate Robustness of Design 11

7.0 MODELING APPROACH AND RESULTS 11
- 7.1 Mercury 14
- 7.2 VOCs and Phenol 15
- 7.3 PAHs/PCBs 16
- 7.4 Cap in 6-9 Meter Zone of Remediation Areas A and E 18
- 7.5 Sub-area Modeling 19
- 7.6 Sources of Uncertainty in Model Results 21

8.0 CONCLUSIONS 22

9.0 REFERENCES 23

TABLE OF CONTENTS (CONTINUED)

LIST OF TABLES

Table 1 Summary of Compounds Meeting Performance Criteria Assuming Initial Conservative Analytical Steady State and Transient Model Evaluations

Table 2 Carbon Application Rate Evaluation

Table 3 Monte Carlo Modeling Results at Final GAC Application Rates

Table 4 Summary of Compounds Meeting Performance Criteria using Initial Conservative Analytical Steady State and Transient Model Evaluations of 6-9 M Zones and Sub-areas Modeling

Table 5 Carbon Application Rate for 6-9 M Zones and Sub-areas Modeling

LIST OF FIGURES

Figure B-1 Remediation and Model Areas Location Map

Figure B-2 Remediation Area A Porewater Sample Locations

Figure B-3 Remediation Area B Porewater Sample Locations

Figure B-4 Remediation Area C Porewater Sample Locations

Figure B-5 Remediation Area D Porewater Sample Locations

Figure B-6 Remediation Area E Porewater Sample Locations

Figure B-7 Remediation Area A Sediment Sample Locations

Figure B-8 Remediation Area B & Wastebeds 1-8 Connected Wetlands Sediment Sample Locations

Figure B-9 Remediation Area C Sediment Sample Locations

Figure B-10 Remediation Area D & Wastebed B/Outboard Area Sediment Sample Locations

Figure B-11 Remediation Area E Sediment Sample Locations

Figure B-12 Remediation Area A Mercury Concentration

Figure B-13 Remediation Area A Benzene Concentration

Figure B-14 Remediation Area A Toluene Concentration

Figure B-15 Remediation Area A Ethylbenzene Concentration

Figure B-16 Remediation Area A Total Xylene Concentration

Figure B-17 Remediation Area A Chlorobenzene Concentration

Figure B-18 Remediation Area A Total DCB Concentration

Figure B-19 Remediation Area A Total TCB Concentration

TABLE OF CONTENTS (CONTINUED)

LIST OF FIGURES

Figure B-20 Remediation Area A Naphthalene Concentration

Figure B-21 Remediation Area A Calculated Phenol Concentration

Figure B-22 Remediation Area A Sediment pH

Figure B-23 Remediation Area B & Wastebeds 1-8 Connected Wetland Mercury Concentration

Figure B-24 Remediation Area B & Wastebeds 1-8 Connected Wetland Benzene Concentration

Figure B-25 Remediation Area B & Wastebeds 1-8 Connected Wetland Toluene Concentration

Figure B-26 Remediation Area B & Wastebeds 1-8 Connected Wetland Ethylbenzene Concentration

Figure B-27 Remediation Area B & Wastebeds 1-8 Connected Wetland Total Xylenes Concentration

Figure B-28 Remediation Area B & Wastebeds 1-8 Connected Wetland Chlorobenzene Concentration

Figure B-29 Remediation Area B & Wastebeds 1-8 Connected Wetland Total DCB Concentration

Figure B-30 Remediation Area B & Wastebeds 1-8 Connected Wetland Total TCB Concentration

Figure B-31 Remediation Area B & Wastebeds 1-8 Connected Wetland Naphthalene Concentration

Figure B-32 Remediation Area B & Wastebeds 1-8 Connected Wetland Calculated Phenol Concentration

Figure B-33 Remediation Area B & Wastebeds 1-8 Connected Wetland Sediment pH

Figure B-34 Remediation Area C Mercury Concentration

Figure B-35 Remediation Area C Benzene Concentration

Figure B-36 Remediation Area C Toluene Concentration

Figure B-37 Remediation Area C Ethylbenzene Concentration

Figure B-38 Remediation Area C Total Xylene Concentration

Figure B-39 Remediation Area C Chlorobenzene Concentration

Figure B-40 Remediation Area C Total DCB Concentration

Figure B-41 Remediation Area C Total TCB Concentrations

Figure B-42 Remediation Area C Naphthalene Concentration

Figure B-43 Remediation Area C Calculated Phenol Concentration

TABLE OF CONTENTS (CONTINUED)

LIST OF FIGURES

Figure B-44 Remediation Area C Sediment pH
Figure B-45 RA-D & WBB/HB Outboard Area Mercury Concentration
Figure B-46 RA-D & WBB/HB Outboard Area Benzene Concentration
Figure B-47 RA-D & WBB/HB Outboard Area Toluene Concentration
Figure B-48 RA-D & WBB/HB Outboard Area Ethylbenzene Concentration
Figure B-49 RA-D & WBB/HB Outboard Area Total Xylenes Concentration
Figure B-50 RA-D & WBB/HB Outboard Area Chlorobenzene Concentration
Figure B-51 RA-D & WBB/HB Outboard Area Total DCB Concentration
Figure B-52 RA-D & WBB/HB Outboard Area Total TCB Concentration
Figure B-53 RA-D & WBB/HB Outboard Area Naphthalene Concentration
Figure B-54 RA-D & WBB/HB Outboard Area Calculated Phenol Concentration
Figure B-55 RA-D & WBB/HB Outboard Area Sediment pH
Figure B-56 Remediation Area E Mercury Concentration
Figure B-57 Remediation Area E Benzene Concentration
Figure B-58 Remediation Area E Toluene Concentration
Figure B-59 Remediation Area E Ethylbenzene Concentration
Figure B-60 Remediation Area E Total Xylenes Concentration
Figure B-61 Remediation Area E Chlorobenzene Concentration
Figure B-62 Remediation Area E Total DCB Concentration
Figure B-63 Remediation Area E Total TCB Concentration
Figure B-64 Remediation Area E Naphthalene Concentration
Figure B-65 Remediation Area E Calculated Phenol Concentration
Figure B-66 Remediation Area E Sediment pH

TABLE OF CONTENTS (CONTINUED)

LIST OF ATTACHMENTS

ATTACHMENT 1 **MODEL INPUT**

ATTACHMENT 2 **PARTITIONING COEFFICIENTS AND SEDIMENT TO POREWATER CALCULATIONS**

ATTACHMENT 3 **MODEL VALIDATION**

ATTACHMENT 4 **MODEL FILES**

ATTACHMENT 5 **NINEMILE CREEK SPITS EVALUATION**

ATTACHMENT 6 **ADDITIONAL SENSITIVITY EVALUATIONS**

1.0 EXECUTIVE SUMMARY

The Onondaga Lake cap will meet performance criteria established to be protective of human health and the environment for 1,000 years or longer. Design of the chemical isolation layer for the Onondaga Lake sediment cap was accomplished through a rigorous modeling effort. This appendix and its attachments summarize the objectives, application, inputs, results and recommendations from this modeling effort.

The models and modeling framework referenced in this appendix were developed by experts and have been published in peer-reviewed journals and publications such as the Journal of Soil and Sediment Contamination (Lampert and Reible, 2009) and "Guidance for In Situ Subaqueous Capping of Contaminated Sediments" (Palermo et al., 1998).

Design of the chemical isolation layer of the cap, which covers more than 450 acres over five remediation areas of the lake and three adjacent areas, was accomplished through an extensive series of model simulations. Two models were used for these evaluations: an analytical steady state model and a time-variable numerical model. Both deterministic and probabilistic model evaluations were used in developing the chemical isolation layer design, to ensure that the cap provides long-term protection of human health and the environment. The modeling approach described in this appendix was used to develop the chemical isolation layer design in each of the model areas by simulating the fate and transport within the cap of each of the 26 contaminants for which cap performance criteria have been established.

The chemical isolation layer will consist primarily of sand. Based on treatability testing, amendments will be incorporated into the chemical isolation layer in certain areas to ensure long-term effectiveness of the cap. These amendments will consist of siderite (a naturally occurring mineral) to neutralize elevated pH and maintain conditions conducive to long-term biological decay of key contaminants within the cap, and granular activated carbon (GAC) to improve sorption of contaminants within the cap and provide an added level of protectiveness. Amendments to the cap will be included in Remediation Areas B, C, D, the Wastebed B/Harbor Brook (WBB/HB) Outboard Area and the Wastebeds 1-8 connected wetlands, and in portions of Remediation Areas A (including the Ninemile Creek spits) and E. Modeling was conducted for both GAC-amended and non-amended caps.

An initial evaluation of the chemical isolation layer was completed based on the maximum concentrations for contaminant porewater measured (or estimated based on sediment concentrations and partitioning theory for those contaminants for which porewater data was not available) within each respective modeling area and best estimates (mean values) for all other model input parameters (model input parameters are described in Attachment 1 to this Appendix). Mercury, polychlorinated biphenyls (PCBs) and most polycyclic aromatic hydrocarbons (PAHs) are predicted to be below cap performance criteria everywhere for over 1,000 years based on the conservative initial model evaluations that were completed. Many VOCs are also predicted to be below their criteria for over 1,000 years in several of the model areas based on these conservative simulations. This initial evaluation was based on analytical steady state and transient numerical modeling of a 1-ft. thick chemical isolation layer.

Based on the results from the initial conservative modeling, an evaluation of GAC amendment performance and more rigorous modeling were required for select VOCs and PAHs in several model areas. The recommended design application rate of GAC to isolate these VOCs and PAHs in each model area was determined using a numerical model that simulated the effects of GAC, based on conservative upper bound (defined as 95th percentile) porewater concentrations and best estimates (mean values) for other model input parameters over a long-term (1,000 year) evaluation period.

As a final evaluation of the robustness of the cap design, probabilistic model simulations were completed to assess GAC performance over the full range of potential input parameter values and conditions specific to each model area. The probabilistic evaluation was performed over a long-term (1,000 years) evaluation period and incorporated the worst-case values for model input parameters as they pertain to predictions of cap performance. GAC application rates from these evaluations based on the 90th percentile of the model outputs were developed. In cases where these GAC application rates exceeded those determined from the prior model runs, the GAC application rate was increased accordingly, providing even greater assurance that the cap would provide complete chemical isolation throughout the 1,000-year model evaluation period and beyond.

This modeling approach is very conservative and as a result, underestimates the long-term effectiveness of the cap. There are natural processes and several engineering/constructability considerations that will significantly enhance the long-term performance of the cap, but are difficult to precisely quantify; however, once the cap is constructed in the field, they will contribute to enhanced performance and protectiveness. Specific natural processes and engineering/constructability considerations that were not incorporated into the model, but will result in an even higher level of long-term chemical isolation and protection of human health and the environment than predicted by the model include:

- Additional cap thickness beyond the design-specified minimum will be placed during construction to ensure that the minimum thickness is achieved everywhere. This material over-placement will result in increased contaminant sorption, biological decay, and amendment application, and will lower concentrations throughout the cap and extend its long-term performance. The amount of over-placement and resulting chemical isolation conservatism will vary over the area of the cap.
- Additional GAC beyond the design-specified minimum will be incorporated into the chemical isolation layer to account for potential unequal mixing of the GAC with the sand. A capping field demonstration was completed in late 2011 using full-scale capping equipment. The capping field demonstration confirmed that the hydraulic placement equipment proposed for the Onondaga Lake cap can consistently place GAC mixed throughout a sand layer at the specific water depths required for the Onondaga Lake project. The capping field demonstration provided information relative to determining the amount of extra GAC addition required. The final amount of additional GAC required will be determined during the capping start-up period, as detailed in the Construction Quality Assurance Plan (CQAP).

- Rapid aerobic biodegradation will occur within the upper portion of the cap's habitat layer. This will result in lower contaminant concentrations at the surface of the cap, where essentially all benthic activity occurs.
- Additional material will be placed to account for mixing of the bottom of the cap with the underlying sediment.

A complete list of model conservatisms is presented in Section 3.3.

2.0 MODELING OBJECTIVES

Contaminant transport modeling was conducted to design a chemical isolation layer for the cap that will meet the ROD requirements and ensure long-term effectiveness. Specifically, the chemical isolation layer performance criterion is to meet the individual probable effects concentrations (PECs) for the 23 contaminants that were linked to toxicity on a lake-wide basis and the New York State Department of Environmental Conservation (NYSDEC) sediment screening criteria (SSC) for benzene, toluene, and phenol[1] throughout the habitat layer.

As stated in the ROD, the compliance point for the cap is the bottom of the habitat restoration layer. To ensure protectiveness, the isolation layer has been designed to prevent concentrations of contaminants from exceeding their performance criteria (PEC or SSC) throughout the habitat restoration layer.

3.0 DESIGN MODELS

Design evaluations were conducted using two models: an analytical steady state model and a more complex numerical model, which allows for time-varying evaluations and simulation of GAC performance. Both models are described below. The method for applying these two models is provided in Section 7.

3.1 Analytical Steady State Model

The analytical steady state model was developed to simulate cap performance and develop an appropriate chemical isolation layer design for containment of contaminated sediments. Simulated transport processes within the typically homogeneous chemical isolation layer include porewater advection, diffusion and dispersion, reaction (where appropriate), and equilibrium partitioning between the dissolved and sorbed phases of the contaminant. Within the overlying habitat layer, the analytical steady state model includes these same processes, as well as sediment mixing and porewater pumping via bioturbation within the upper zone of that layer. The analytical steady state model thus allows the complexities of the biologically-active layer to be considered while maintaining an analytical form for convenient and rapid evaluation. The analytical steady state model evaluates a single material matrix in the chemical isolation layer and is not capable of modeling non-linear sorption processes, which is necessary for evaluating GAC adsorption. The schematic below indicates the general structure and processes included in the analytical steady state cap model.

FILE

1 Benzene, toluene and phenol are not associated with lake-wide toxicity. Model results for benzene, toluene and phenol are compared to NYSDEC acute criteria. Comparison to acute criteria is consistent with comparison to PEC values which are based on acute toxicity.

ILLUSTRATION OF CAP PROCESSES MODELED AND STRUCTURE OF ANALYTICAL STEADY STATE MODEL

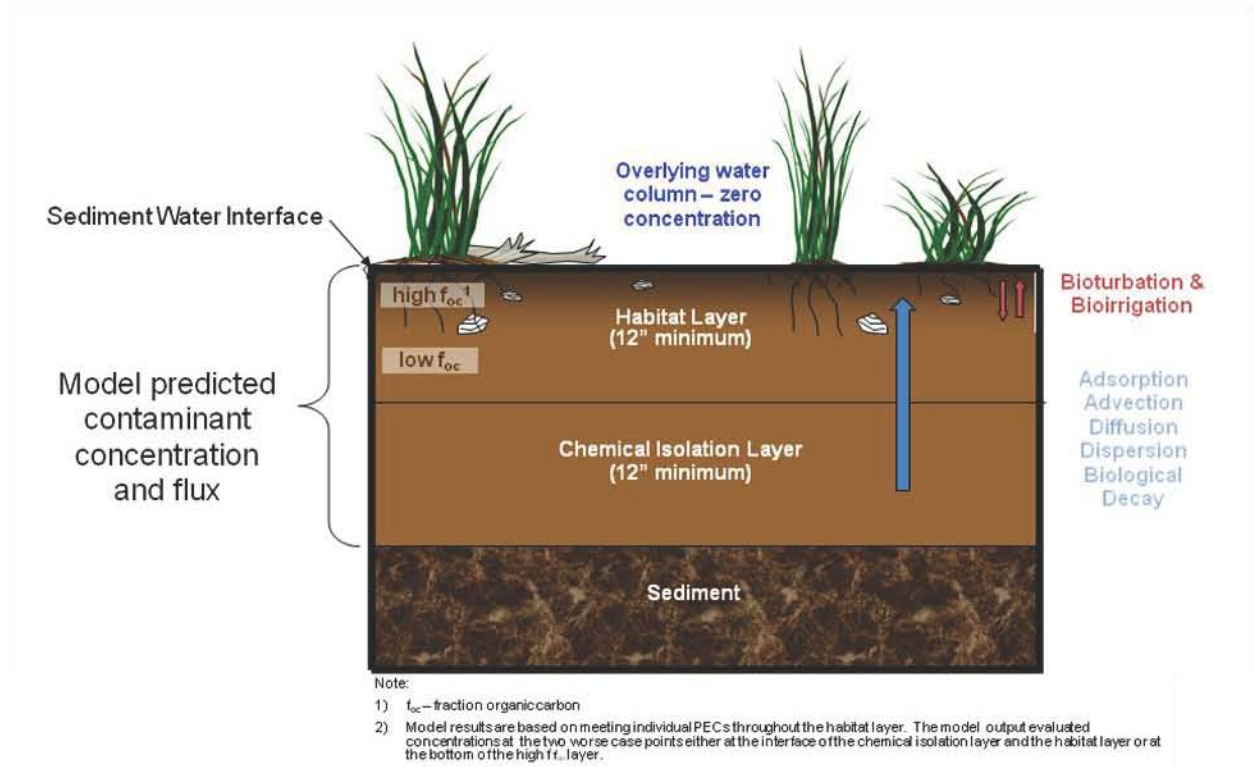

The analytical steady state model was developed by experts in the field of contaminant transport modeling, and has been published in the peer-reviewed Journal of Soil and Sediment Contamination (Lampert and Reible, 2009). Validation of the analytical steady state model code was completed in accordance with Parsons standard procedures for software verification and validation. Model results for various test cases were also compared with calculations from well-documented 1-D solute transport equations by an independent reviewer; the model gave similar results using the same parameters and boundary conditions. A complete model validation report is included in Attachment 3.

3.2 Numerical Model

The general structure and processes included in the Onondaga Lake numerical cap model are consistent with those of the analytical steady state model. In addition, the numerical model simulates diffusional gradients in the underlying sediment, non-linear sorption within the isolation layer, porewater advection due to settlement-inducted consolidation of the underlying sediment, and time-varying biodegradation rates through use of a lag period. The numerical solution scheme of this model also allows for time-variable simulations of the aforementioned processes. The USEPA guidance document entitled "Guidance for In Situ Subaqueous Capping

of Contaminated Sediments: Appendix B: Model for Chemical Containment by a Cap" describes the general modeling processes and basis for the numerical model (Palermo et al., 1998). The model code is the result of an extensive development process (fourth generation model) within the research group at the University of Texas (Go, J. et al, 2009 and Lampert and Reible, 2009). The University of Texas has developed and implemented the code within the MATLAB platform.

Both the analytical steady state and numerical modeling described herein assume an infinite source of contaminants is present in the underlying sediments. Upwelling velocities in the cap areas are relatively low, so transport from the underlying sediments upwards into the cap will be dominated by diffusion. This causes a concentration gradient to develop at the sediment/cap interface, which results in a decrease in chemical concentration in the sediments just below the sediment/cap interface over time. This, in turn, affects the overall rate of upward transport. In order to represent this process, the sediment underlying the cap is explicitly included as a layer in the numerical model. The sediment layer is modeled as 250 cm thick, with an infinite source boundary condition at the bottom of that layer. Model sensitivity analyses evaluating how alternate values for the thickness affect the cap design are documented in Attachment 6. The processes modeled in the underlying sediment layer include advective and diffusive transport and partitioning. Biological decay or other source depletion processes in the underlying sediment are conservatively not included in this modeling evaluation. This explicit representation of the underlying sediment is not included in the analytical steady state model, which is an additional conservatism of that model.

Validation of the numerical model was completed in accordance with Parsons standard procedures for software validation and verification. An independent validation of this model was performed by S.S. Papadopoulos and Associates. Multiple test scenarios were simulated with the numerical model and compared to results from MT3D (Zheng and Wang, 1998), a widely used groundwater transport model that has been extensively verified, as well as an analytical solution to the governing equation of the model (Neville, 2005). Additional validation was provided by Parsons and Anchor QEA, who found that the results of long-term simulations of the numerical model were consistent with the results of the analytical steady state model and with other solutions to the governing one dimensional contaminant transport equation. A complete model validation report is included in Attachment 3. Several updates were made to the model code to enhance its functionality during the course of the cap design; these updates are also documented in Attachment 3.

3.3 Model Conservatism

To ensure that the cap design is conservative and will provide long-term chemical isolation, the modeling used to develop the design of the chemical isolation layer does not incorporate numerous natural processes and engineering/constructability considerations that will significantly contribute to the long-term performance of the cap. Specific concepts and processes that were not incorporated into the model but will result in an even higher level of long-term chemical isolation than predicted by the model are listed below.

- Additional cap thickness beyond the design-specified minimum will be placed during construction to ensure that the minimum thickness is achieved everywhere. This

material over-placement will result in increased contaminant sorption, biological decay, and amendment application, and will lower concentrations throughout the cap and extend its long-term performance. The over-placement thickness is anticipated to average 3 in. or greater for each separate cap layer, which may result in the constructed thickness of the chemical isolation layer to be greater than the design thickness by 25 percent or more. The amount of over-placement and resulting chemical isolation conservatism will vary over the area of the cap.

- Additional GAC (amount to be specified in the Construction Quality Assurance Plan) beyond the design-specified minimum will be incorporated into the chemical isolation layer to account for potential unequal mixing of the GAC with the sand. A capping field demonstration was completed in late 2011 using full-scale capping equipment. The capping field demonstration confirmed that the hydraulic placement equipment proposed for the Onondaga Lake cap can consistently place GAC mixed throughout a sand layer at the specific water depths required for the Onondaga Lake project. The capping field demonstration provided information relative to determining the amount of extra GAC addition required. The final amount of additional GAC required will be determined during the capping start-up period, as detailed in the CQAP. .
- Additional material will be placed to account for mixing of the bottom of the cap with the underlying sediment. The bottom 3 in. of cap material placed is assumed to mix with the underlying sediment, and is not considered when meeting the minimum required isolation layer thickness. This material may mix with the underlying sediment and reduce contaminant concentrations in the zone immediately underlying the cap. It is also possible/likely that a portion of this dedicated mixing layer will not mix with the underlying sediment and therefore would provide even more protection as part of the cap.
- Rapid aerobic biodegradation will occur within the upper portion of the cap's habitat layer. This will result in lower contaminant concentrations at the surface of the cap, where essentially all benthic activity occurs.
- The analytical steady state model assumes a constant porewater concentration at the cap/sediment interface. However, as discussed above, mass conservation principles dictate that in order for diffusion to move contaminant mass out of the underlying sediment, a concentration gradient must be established at the sediment/cap interface. Mass transport out of the sediment, as well as any source depletion due to natural decay processes, are not considered in the analytical steady state model. Although the numerical model includes decreasing concentrations at the cap/sediment interface, the numerical model assumes an infinite source of constant concentration 2.5 meters below the sediment/cap interface.
- The numerical model considers diffusion/dispersion processes in the underlying sediment, which are in part dependant on sediment porosity. Porosity is set at a fixed value which does not change during the model run (the model input value is based on sediment samples collected in a given Remediation Area, as noted in Table A1.1 of Attachment 1). However, subsequent to cap placement, in those areas where significant dredging has not occurred prior to cap placement, consolidation of

underlying sediments will occur as a result of cap placement, which will reduce the porosity and permeability of the underlying sediments. The change will reduce the effective diffusion coefficient in the underlying sediments, which will result in a reduction in contaminant flux.

- In instances where multiple results exist for a given sampling location, maximum sample concentrations were selected from the analytical database. For example, if duplicate samples were collected at a particular location, the maximum value measured was used in the modeled dataset.

4.0 MODELING AREAS

The isolation cap will cover more than 450 acres of the lake bottom in Remediation Areas A, B, C, D, E, and F, as well as in the Wastebed 1-8 connected wetlands, WBB/HB Outboard Area and the Ninemile Creek spits. For cap design purposes, these remediation areas were subdivided into 17 model areas to account for the spatial variability observed in two of the key model input parameters: groundwater upwelling velocity and porewater contaminant concentrations. Each model area was evaluated independently. Cap design, including recommendations for isolation layer thickness and mass application rate of GAC, was based on the modeling results for each model area and is specific to the conditions present in each area. The 17 model areas are shown on Figure B-1. Supporting information such as figures showing contaminant porewater concentration and pH distributions in each area are provided in Figures B-2 through B-66, and the development of groundwater upwelling distributions for each model area is presented in Appendix C of this design report. The model areas are discussed below.

Remediation Area A was divided into two model areas due to the relatively elevated pH and porewater concentrations of VOCs observed at the mouth of Ninemile Creek and the higher measured groundwater upwelling in this area. The area at the mouth of Ninemile Creek has been designated as Model Area A2, and the remaining portion of the remediation area, where pH and VOCs are generally low, is designated as A1. There are isolated locations in Model Area A1 where pH exceeds 8.0, as shown on Figure B-22. However, these locations are not co-located in areas where phenol or other VOCs are present at levels that impact the design; therefore these locations did not factor into model area delineation. There are also some VOCs detected in Model Area A1 northwest of Model Area A-2, however, the concentrations are low and do not impact the design, and therefore Model Area A-2 does not include this area.

Model area delineation in Remediation Areas B and C was based on consideration of VOC and phenol concentrations and groundwater upwelling conditions (including identifying the portions of these areas that will be influenced by hydraulic barriers that have been or will be constructed and operated along the shoreline, as discussed in Appendix C). Based on this information, Remediation Area B was divided into two model areas (B1 and B2) and Remediation Area C was divided into three model areas (C1, C2, and C3). Model Areas B1 and C1 were then combined into a single model area (referred to hereafter as B1/C1) given the similar levels of concentrations of key compounds such as phenol and benzene and similarities in upwelling velocities.

Remediation Area D was divided into four sub-areas based on chemical concentrations and distributions. Appendix G presents the basis for development of these sub-areas, designated as the SMU 2, West, Center, and East sub-areas of Remediation Area D, as shown on Figure B-1. Due to the measured differences in contaminant concentrations and distributions as well as predicted groundwater upwelling velocities, each of these Remediation Area D sub-areas was modeled independently.

Remediation Area E was divided into three model areas due to the higher porewater concentrations of VOCs observed immediately adjacent to Remediation Area D (Model Area E2) and the elevated concentration of naphthalene offshore and at the mouth of Onondaga Creek (Model Area E3). Groundwater upwelling estimates are consistent throughout Remediation Area E and did not factor into model area delineation. There are isolated locations in Model Area E1 where pH exceeds 8.0, as shown on Figures B-66. However, these locations are not co-located with areas where phenol or other VOCs are present at levels that impact the design; therefore these locations did not factor into model area delineation.

Remediation Area F consists of two small areas totaling less than one acre. These areas were delineated based on sediment mercury concentrations that exceed the mercury PEC. Cap modeling was not conducted for these areas. These areas are not close to shore; therefore, groundwater upwelling velocities are expected to be low. Mercury concentrations are much lower in these areas than in other areas where modeling indicates that a 1-ft. chemical isolation layer will be sufficient. Therefore, the chemical isolation layer thickness in this area will be a minimum of 1 ft. consistent with the ROD. The pH in these areas is not elevated, so no amendments are necessary.

The Wastebed 1-8 connected wetland consists of 2.3 acres of connected wetlands that will be constructed adjacent to Remediation Area B. The Wastebeds 1-8 connected wetlands area (referred to hereafter as WB1-8) was evaluated as a single model area, as groundwater upwelling, pH, and contaminant concentrations do not exhibit significant variation across this small area.

The WBB/HB Outboard Area is a 16-acre area that lies between Onondaga Lake and the WBB/HB barrier wall alignment. It includes the mouth of Harbor Brook and areas of wetlands to be restored/constructed along the lake shoreline adjacent to Remediation Area D. The WBB/HB Outboard Area has been divided into three model areas for isolation cap design: east, center, and west (referred to hereafter as WBB-East, WBB-Center, and WBB-West, respectively). In general, elevated levels of VOCs and pH are observed throughout the WBB-West and WBB-Center model areas, and groundwater upwelling velocities are somewhat higher in these areas as well. The contaminant distributions are relatively similar between WBB-West and WBB-Center, while the upwelling increases going from WBB-Center to WBB-West, which formed the basis for modeling these two areas separately. The WBB-East area has lower levels of VOCs, generally low pH (with the exception of a few samples), and groundwater upwelling is lower in this area as well.

The spits of land that extend into Model Area A2 at the mouth of Ninemile Creek were incorporated into the cap design as part of Model Area A2. As documented in the Ninemile Creek OU-2 ROD (NYSDEC and USEPA, October 2009), remediation of the spits includes

sediment removal, placement of a cap/backfill material, and habitat restoration, consistent with the remediation of adjacent lake areas in Remediation Area A. Specific modeling considerations for this area are summarized in Section 7.5. Attachment 5 describes the data collected in the spits and provides additional detail on the inclusion of the spits in the Model Area A2 evaluation.

5.0 MODEL INPUTS

Accurate characterization of site conditions and cap material performance are critical to developing appropriate model input parameters. Model inputs for the cap were derived from extensive site sampling efforts, bench scale testing, and literature in some cases. Site-specific data have been collected in each model area to accurately characterize the underlying sediment and groundwater flow regime, assess cap material performance under model area specific conditions, and to inform input parameter selection on a model area basis.

Key model input parameters, including underlying porewater chemical concentrations and groundwater upwelling velocities, have been evaluated in each individual model area over the course of the seven year pre-design investigation (PDI). These data are supplemented by data from the remedial investigation, resulting in an extensive database that forms the basis for specifying the cap model inputs. Sorption parameters (including partitioning to sand cap materials and to GAC amendments) are also a key model input. Site specific data in model areas, as well as a multi-phase series of bench-scale evaluations were conducted between 2006 and 2011 to increase understanding and provide site-specific information for these key parameters. Model input parameters for which extensive site-specific field investigation and bench-scale laboratory studies have been performed include:

- Porewater chemical concentration
- Fraction of organic carbon (foc) in the isolation layer and at the cap surface (i.e., the bioturbation zone within the upper portion of the habitat layer)
- Groundwater upwelling velocity
- Organic carbon partitioning coefficient (Koc) for cap materials (as well as the underlying sediments)
- Parameters from the Freundlich isotherm equation to describe the non-linear sorption of VOCs and phenol to GAC
- Biological degradation rate
- Chemical isolation layer porosity

Attachment 1 contains details on the model input parameters, including the basis for specification of each input (i.e., applicable references and data sources), and a discussion of the statistical distributions used in probabilistic modeling evaluations.

6.0 DESIGN OPTIMIZATION CONSIDERING VARIABILITY IN SITE CONDITIONS

Understanding and accounting for variability in site conditions that constitute the basis for the model input parameters were critical components of completing the modeling to ensure it is truly predictive of future conditions. Variability in the data used to model cap performance

originated from two sources: 1) spatial variations due to natural and anthropogenic processes such as contaminant loadings to the lake and heterogeneity in permeability, deposition and erosion; and 2) measurement variability associated with sampling, processing and laboratory analysis, and data interpretation. Characterizing and accounting for these sources of variability to ensure that the cap is protective everywhere was a significant focus of the modeling effort described herein. Details are provided below.

6.1 Extensive Data Collection and Bench Testing

As discussed in Section 5, site-specific data were utilized in the model to maximize the accuracy and reliability of the results. An extensive site-specific database for the most important model input parameters was developed based on the RI and seven years of PDI data and laboratory studies. This database includes the analytical results from over 7,000 sediment samples and 5,500 porewater samples. In addition, site-specific measurements of groundwater upwelling velocity were taken at over 350 locations throughout the lake. Finally, extensive bench-scale testing was completed to accurately characterize important processes such as GAC adsorption and biological decay. As a result of this exhaustive data collection effort, uncertainty in input parameters has been minimized and variability can be accurately characterized and taken into consideration during modeling.

6.2 Small Model Areas to Minimize Spatial Variability

Remediation areas were developed to be reflective of localized conditions within the lake, such as contaminant sources and characteristics, water depth, and physical conditions. As discussed in Section 4, the five remediation areas of the lake were further divided into even smaller model areas to ensure that the cap would be designed specific to conditions in an area based on key model input parameters such as groundwater upwelling velocity and contaminant porewater concentrations. This same approach was taken in dividing up the WBB/HB Outboard Area into smaller model areas. By developing these smaller model areas, the spatial variability within each model area is significantly reduced, since zones of high/low concentration and/or upwelling velocity are modeled separately.

6.3 Initial Conservative Modeling Used Maximum Porewater Concentrations

To reduce the number and complexity of subsequent modeling simulations, the first phase of modeling conservatively used maximum porewater contaminant concentrations for analytical steady state simulations and for numerical simulations over a 1,000 year evaluation period. Porewater contaminant concentrations are one of the most significant model input parameters. As detailed in Section 7, the results from this initial conservative modeling indicated that cap performance criteria would be met for over 1,000 years for a majority of the contaminants in each area.

6.4 Model Conservatisms Offset Potential Impacts of Variability

As discussed in Section 3.3, the model underestimates the effectiveness of the cap because it does not incorporate several natural processes and engineering/constructability considerations that will significantly contribute to the long-term performance of the cap, including over-placement of cap materials during construction. For example, in all amended cap areas except Model Areas E2, E3, and WBB-East, the minimum thickness of the GAC-amended isolation

layer is 9 in., which is the basis for the modeling and establishment of GAC application rates in these areas. Average over-placement of GAC-amended sand during construction is expected to be approximately 3 in. As a result, the carbon application rate and resulting cap performance in such areas will be approximately 33 percent greater than the design application rate determined from the modeling. In Model Areas E2, E3, and WBB-East, the GAC-amended isolation layer will be 12 in. (since pH amendments are not being used in these areas), for which a 3 in. over-placement would translate into a 25 percent increase in application rate.

6.5 Mean Values Used as Best Estimate

For modeling that used best estimates of parameters other than porewater concentration (Section 7), the mean rather than median values were used as the best estimate of each input parameter in a given model area. The mean values used were always greater than the median.

6.6 Conservative Probabilistic Modeling Used to Evaluate Robustness of Design

Probabilistic evaluations with the numerical model, which explicitly considered site-specific data on the variability of model inputs, were performed as part of the modeling used to determine GAC application rates. Probabilistic analysis is commonly used to account for input variability in models with multiple parameters (e.g., USEPA, 1997). The first step in performing a probabilistic analysis is to estimate a statistical distribution for each key input parameter, based on the data (for example, a normal distribution). Next, a model simulation is performed, selecting randomly from the distribution for each parameter. This represents one “realization,” and produces one possible outcome, in this case, one estimate of sorbed-phase and porewater concentrations within the cap. The model calculation is then repeated many times (5,000 realizations were used in this modeling evaluation), each time selecting a new value for each input parameter from its distribution. This produces a frequency distribution of computed concentrations. Management decisions can then be made using a chosen percentile of this distribution (e.g., 80th, 90th, or 95th percentile).

Probabilistic modeling based on the 90th percentile was used as a final conservative evaluation of the carbon application rates that were initially established by deterministic modeling with 95th percentile porewater concentrations and best estimate (mean) values for other input parameters (see Section 7 for discussion of the modeling approach). Distributions for the probabilistic analysis were developed for each key input parameter based on an analysis of the site data, in light of the underlying physical, chemical, and biological processes, as detailed in Attachment 1.

To ensure conservatism around two parameters that were not varied in probabilistic modeling (sediment consolidation in Remediation Area D and underlying sediment thickness) sensitivity analyses were conducted. These are included in Attachment 6, and demonstrate a negligible impact on model results.

7.0 MODELING APPROACH AND RESULTS

The modeling approach described below was used to develop the chemical isolation layer design in each of the 17 model areas described in Section 4, taking into consideration each of the 26 contaminants for which cap performance criteria were established, as listed below.

SUMMARY OF MODELED COMPOUNDS

Class	Compounds
Mercury	Mercury
VOCs and Phenol (9)	Benzene, Toluene, Ethylbenzene, Xylenes, Chlorobenzene, Dichlorobenzenes, Trichlorobenzenes, Naphthalene, Phenol
PCBs / PAHs (16)	Total PCBs, Fluorene, Phenanthrene, Acenaphthene, Acenaphthylene, Anthracene, Pyrene, Benzo(a)anthracene, Benzo(b)fluoranthene, Benzo(k)fluoranthene, Chrysene, Fluoranthene, Benzo(a)pyrene, Dibenz(a,h)anthracene, Indeno(1,2,3-cd)pyrene, Benzo(g,h,i)perylene

The cap modeling was generally based on a 12 in. isolation layer and a 12 in. habitat layer. As stated in the ROD, the compliance point for the cap is the bottom of the habitat restoration layer. To ensure protectiveness, the isolation layer has been designed to prevent concentrations of contaminants from exceeding their performance criteria (PEC or SSC) throughout the habitat restoration layer. Ensuring compliance throughout the habitat layer provides protection for benthic organisms in the actively mixed upper portion of the habitat layer as well as in the lower portion of the habitat layer (15-30 cm) where occasional deeper bioturbation may occur.

A general schematic of the amended cap is shown below; a schematic of the processes modeled is included in Section 3.1. In areas where amendments are not required to achieve long-term chemical isolation, the profile will be similar except that the chemical isolation layer will consist of a minimum of 12 in. of sand only.

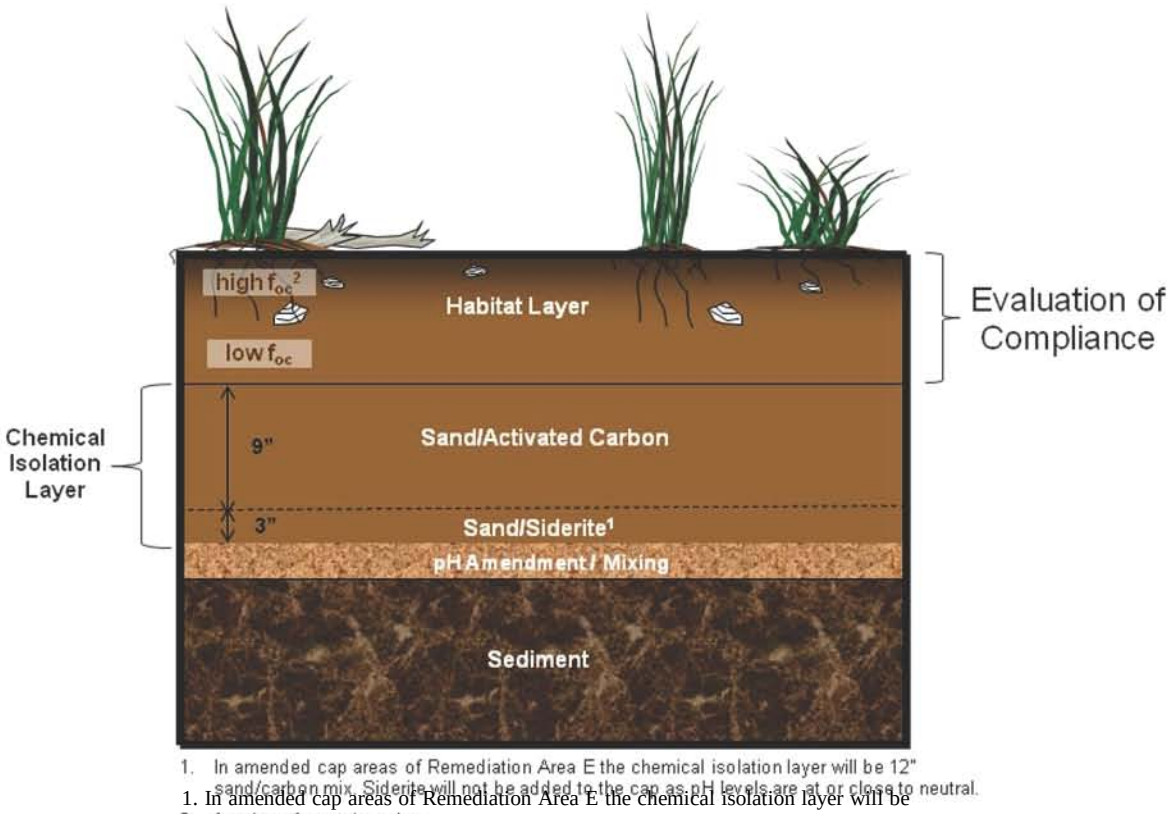

1. In amended cap areas of Remediation Area E the chemical isolation layer will be 12" sand/carbon mix. Siderite will not be added to the cap as pH levels are at or close to neutral.

2. f_{oc} – fraction of organic carbon

Example Schematic of an Amended Cap

For contaminants and/or areas where the attenuation of contaminant flux is provided by the thickness of the sand cap material and not GAC, modeling was based on an 8 in. isolation layer, to allow for an additional level of conservatism in evaluating these cases. This model configuration was used for mercury in all areas and for all contaminants in Model Areas A1 and E1 (since initial modeling indicated that no GAC is needed in these two areas). For the remaining contaminants/areas, which include GAC to ensure long term effectiveness across all contaminants (except mercury as noted above), increasing the cap thickness would not have a significant impact on protectiveness (because the GAC application rate is the main determinant of its long-term performance). For those contaminants that rely on GAC to ensure long-term effectiveness, significant conservatism is already incorporated into the modeling and minimum compliance period of 1,000 years, as summarized in Section 3.3. The modeled thicknesses of each layer are detailed in the table below.

MODELED CAP LAYER THICKNESSES

Cap Model Layers	Sand Cap Areas	Amended Cap Areas	
		GAC and pH Amendment	GAC Only
	A1 and E1	A2, B1/C1, B2, C2, C3, D, WB1-8, WBB-West, and WBB-Center	E2, E3, and WBB-East
Habitat Layer	12 in.		
Chemical Isolation Layer	Start with 8 in. and increase if needed.	12 in. isolation layer including 9 in. sand/GAC and 3 in. sand/siderite layer. For mercury an 8 in. sand isolation layer was modeled.	12 in. sand/GAC amendment isolation layer. For mercury an 8 in. sand isolation layer was modeled.

For areas where the cap will include a pH amendment, the upper 3 in. of that sand/siderite layer was included in the chemical isolation layer, and is therefore represented in the model, including simulation of biological decay in this layer. To facilitate biodecay in this layer, the siderite layer was modeled/designed to ensure that the pH in this layer remains less than 8 for at least 1,000 years, following the initial period of higher porewater flux resulting from consolidation of underlying sediments (see Appendix I).

The modeling approach consisted of an initial highly-conservative evaluation based on analytical steady state modeling of a sand only chemical isolation layer, followed by more refined evaluations using the transient numerical model to simulate GAC performance (including probabilistic modeling in some cases) for chemicals/areas that did not meet the performance criteria based on the conservative set of input assumptions used during the initial steady state evaluation. The modeling approach differed slightly by chemical class and is described below along with a discussion of the results. Detailed model results are provided in Tables 1 through 5 and model input and output files are included in Attachment 4.

7.1 Mercury

Mercury was initially evaluated in each model area using the analytical steady state model. Deterministic simulations were performed using the following inputs:

- Maximum mercury concentration measured in porewater
- Best estimate (mean value) of all other parameters

Based on results from this modeling, if the maximum mercury concentration throughout the habitat layer was less than the PEC, then no further modeling of mercury was required for a given area. As shown on Table 1, mercury concentrations in Model Areas B2, C3, WB1-8, WBB-West, and WBB-Center were predicted to be lower than the PEC throughout the habitat layer based on this analytical steady state modeling evaluation. Therefore, no further modeling was performed for mercury in these areas.

Given the long time periods required to reach steady state for a more highly sorbing compound such as mercury, a secondary set of conservative model runs using the numerical model was employed. In the model areas remaining following the steady state evaluation described above, mercury was evaluated using the numerical model to evaluate long-term effectiveness under transient conditions using the approach listed below:

- Apply the same parameters used in the steady state analysis (maximum values for porewater concentration, best estimate for all others)
- Evaluate mercury concentrations, using a deterministic simulation, throughout the habitat layer over a 1,000-year evaluation period
- Conservatively ignore reductions in porewater concentrations that will result from siderite and GAC (where present)

If the maximum mercury concentration throughout the habitat layer was predicted to be less than the PEC based on this conservative transient modeling, then no further modeling of mercury was required for a given area. This transient modeling evaluation indicated that an 8 in. sand chemical isolation layer would be sufficient to ensure mercury remains below the mercury PEC throughout the habitat layer in all modeling areas for at least 1,000 years (see Table 1).

7.2 VOCs and Phenol

The eight VOCs (see table above) and phenol were initially evaluated within each model area using the analytical steady state model, assuming no GAC was present. Deterministic simulations were performed using the following input configuration:

- Maximum contaminant concentrations measured in porewater (or calculated based on sediment concentrations and partitioning theory for phenol)
- Biological decay was assumed to be zero with the exception of phenol in areas having a native pH of 8 or less (i.e., Areas A1, E1, E2, E3)
- Best estimate (mean value) of all other parameters

Based on the results from these simulations, if the maximum concentration throughout the habitat layer was less than the performance criteria (i.e., PEC or SSC), then no further modeling of that compound was conducted in a given model area.

Results for VOCs and phenol in each model area based on the initial conservative analytical steady state modeling are provided in Table 1. As shown in that table, in Model Areas A1 and E1 all eight VOCs and phenol were predicted to be less than the performance criteria throughout the habitat layer at steady state. This was true in Model Areas B2 and WBB-East as well, with the exception of phenol and naphthalene, respectively. For the remaining areas, concentrations of two or more of the nine compounds (i.e., eight VOCs plus phenol) were predicted to be higher than the performance criteria under this conservative modeling evaluation. Therefore, the remaining contaminants in each model area were further simulated with the numerical model to evaluate long-term effectiveness of a GAC amended cap under transient conditions based on the approach described below.

- Iterative deterministic simulations were performed over a 1,000 year evaluation period using the 95th percentile porewater concentration and best estimate (mean value) for all other inputs to determine the GAC application rate required to meet the performance criteria (i.e., each remaining compound's PEC/SSC). Biological decay rates were based on the slow end of literature rates as defined in the Feasibility Study and supported by the site specific bench and column testing described in Section 4 of the design report. Based on the results of the site specific bench testing, safety factors (as described in Attachment 1) were applied to the Feasibility Study decay rates for benzene, chlorobenzene, and naphthalene.
- To allow adequate time for a biological community to establish in the cap material, a lag period during which no biological decay would occur was specified in the model. The lag period was set at 5 years for those areas where no pH amendment is required (Model Areas A1, E1, E2, and E3). The lag period was set at 100 years in areas requiring pH amendment. This extended lag period in the pH amendment areas conservatively allows time for a robust biological community to establish after pH conditions within the cap reach steady-state (on the order of 1-2 years), thereby buffering pH throughout the full thickness of the cap.
- Following the iterative deterministic simulations described above, iterative probabilistic simulations were performed (see Section 6.6). The probabilistic simulations (based on full distributions for all key inputs, as available) were used to further evaluate the GAC application rate required to meet the performance criteria (i.e., each remaining compound's PEC/SSC) over a 1,000-year evaluation period. Starting with the GAC application rates established by the deterministic modeling (described above), probabilistic simulations were conducted, and the GAC application rate was increased if needed, until 90 percent of the realizations were predicted to meet the performance criteria over the 1,000-year evaluation period.
- Following the deterministic and probabilistic evaluations described above, GAC application rates were selected for each model area based on the more conservative estimate of GAC application rate--i.e., the higher of the two rates determined from the deterministic or probabilistic evaluation.

The GAC application rates and the contaminant that dictated the carbon amendment requirement in each area are presented in Table 2. In addition, the results from the Monte Carlo modeling at the final GAC application rates are provided in Table 3. The table lists the percent realizations meeting the PEC/SSC for all CPOIs included in the numerical probabilistic modeling at various points in time (100, 200, 500, 750, and 1,000 years).

7.3 PAHs/PCBs

Total PCBs and 15 PAHs were initially evaluated in each model area using the analytical steady state model assuming no GAC was present. Deterministic simulations were performed using the following inputs:

- Maximum porewater concentration was calculated from sediment data as described in Attachment 2
- Biological decay was assumed to be zero

- Best estimate (mean value) of all other parameters

Based on these results, if the maximum concentration throughout the habitat layer was predicted to be less than the PEC at steady state, then no further modeling of that compound was required in a given area. In Model Areas A1, A2, B2, ILWD-East, E1, E3, and WB1-8 all fifteen PAHs were predicted to be less than the performance criteria throughout the habitat layer at steady state. This was true in Model Areas B1/C1, E2 and WBB-East as well, with the exception of one PAH in each area (phenanthrene, fluorene, and anthracene, respectively). Total PCBs were predicted to be less than the performance criteria throughout the habitat layer in all model areas. Table 1 provides the results from this steady state evaluation for PCBs/PAHs.

Given the long time periods required to reach steady state for strongly sorbing compounds such as PAHs, a secondary set of conservative model runs using the numerical model was conducted. The remaining PAHs in each remaining model area (i.e., B1/C1, C2, C3, the remaining three subareas of ILWD, E2, and the three subareas of the WBB/HB Outboard Area) were further evaluated using the numerical model to evaluate long-term effectiveness under transient conditions using the approach listed below:

- Apply the same input parameters used in the steady state analysis (i.e., maximum values for porewater concentration, best estimate for all others)
- Use the GAC application rates established from the modeling analysis conducted for VOCs and phenol described above in Section 7.2, conservatively assuming that sorption to GAC for all PAHs is described by the site-specific measurements for naphthalene
- Evaluate concentrations, using a deterministic simulation, throughout the habitat layer over a 1,000-year evaluation period

If the maximum concentration throughout the habitat layer was predicted to be less than the PEC for 1,000 years, then no further modeling was required for a given PAH/area. The results from these conservative transient simulations for PAHs are provided in Table 1. As Table 1 shows, in Model Areas B1/C1, C3, D-West, D-Center, D-SMU2, E2 and WBB-East, all PAHs simulated were predicted to remain below the performance criteria throughout the habitat layer for 1,000 years.

The remaining PAHs in Model Areas C2 (11 compounds) and WBB-West and WBB-Center (two compounds each) were further evaluated using the numerical model to evaluate long-term effectiveness under transient conditions using the approach described below. These runs were conducted to evaluate whether the GAC application rates determined based on the modeling of VOCs and phenol described above needed to be increased further to address any of the individual PAHs.

- Deterministic simulations were performed over the 1,000-year evaluation period used for VOCs and phenol based on the 95th percentile porewater concentration and best estimate (mean value) for all inputs to evaluate if the PAHs met their performance criteria over this period.

- Probabilistic simulations (based on full distributions for all key inputs, as available) were also used to verify that 90 percent or more of realizations meet each individual PAH's PEC over a 1,000-year evaluation period.

If the results from the modeling described above indicated that the performance criteria were not met from the deterministic (1,000-year evaluation period) or probabilistic (1,000 year evaluation period) model simulations, then the GAC application rate was increased to address the PAHs. The results from this additional PAH modeling indicated that the GAC application rates established for VOCs and phenol (i.e., as shown in Table 2) would not need to be increased to address PAHs in Model Areas WBB-Center and WBB-West. However, the results for Model Area C2 indicated that PAHs required additional GAC (beyond that which was required to meet performance criteria for VOCs and phenol). The GAC application rate and the contaminant that dictated the carbon amendment requirement in that area are presented in Table 2 and the results from the Monte Carlo modeling of PAHs (where required) at the final GAC application rates are provided in Table 3.

7.4 Cap in 6-9 Meter Zone of Remediation Areas A and E

As discussed in Section 4.1.7 of the design report, a modified cap containing a 0.5 ft. chemical isolation layer was considered for the portions of Remediation Areas A and E having water depths from 20 ft. to 30 ft. (6 to 9 meters), since the ROD specified that a thin-layer cap may be appropriate for such areas. To evaluate the effectiveness of a 6 in. chemical isolation layer in these areas, a series of steady-state model simulations with a 4 in. chemical isolation layer (to provide for additional conservatism) was conducted for the 6 to 9 m zones of Model Areas A1, E1 and E3. Given the relatively higher VOC concentrations and the proximity to the ILWD, a modified cap was not considered for the 6 to 9 m zone of Model Area E2, which covers a relatively small area. The model inputs for these simulations were the same as those described above (except that the isolation layer thickness was set to 4 in. for steady state modeling and transient mercury modeling and to 6 in. for GAC performance modeling [where needed]).

Simulations were first performed with the steady state analytical model using the same approach as described in Sections 7.1 through 7.3 (i.e., maximum values for porewater concentration, mean values for all other inputs, no simulation of GAC). The results from these simulations, which are presented in Table 4, indicated that:

- All chemicals except mercury were predicted to be below performance criteria at steady state in Model Areas A1 and E1 with the thinner isolation layer.
- Mercury, a few VOCs, and one PAH were predicted to be above performance criteria in Model Area E3, which is generally consistent with the results from the initial conservative steady state modeling of these areas summarized in Table 1.

To further assess mercury in these three areas, deterministic simulations with the transient numerical model were conducted using the same approach described in Section 7.1 (i.e., maximum values for porewater concentration, mean values for all other inputs, 1,000 year evaluation period), for a 4 in. chemical isolation layer thickness. The results from these simulations indicated that the predicted concentrations throughout the habitat layer were below the mercury PEC for over 1,000 years.

To evaluate the remaining VOCs and PAH in the 6-9 m zone of Model Area E3 (i.e., those that were not screened out by the initial steady state modeling), additional transient numerical modeling of a GAC-amended cap was performed based on the following approach:

- Deterministic simulations of the VOCs (i.e., ethylbenzene, xylenes, dichlorobenzene, and naphthalene) with the transient numerical model were conducted using the same approach described in Section 7.2 (i.e., 95th percentile pore water concentrations, and mean values for all other inputs, 1,000 year evaluation period), for a 6-in. isolation layer composed of sand and GAC. The model was run iteratively to determine the GAC application rate needed to meet the PEC of all four compounds for 1,000 years, as summarized in Table 5. Based on that GAC application rate, probabilistic modeling was then conducted using the same approach described above Section 7.2 (model inputs sampled from full distributions, and GAC application rate increased as needed until 90 percent or more of the realizations met the PECs over the 1,000 year simulations). No increase in GAC application rate in the 6-9 m zone of Model Area E3 was required based on the results of this probabilistic modeling.
- For the one PAH (i.e., acenaphthylene) a secondary set of conservative model runs with the transient model was performed, following the approach described in Section 7.3 (i.e., maximum pore water concentrations, mean values for all other inputs, GAC application rate determined based on VOC modeling, 1,000 year evaluation period) to evaluate whether the additional GAC would be needed to address PAHs. The results of these simulations indicated that additional GAC is not necessary.

Based on the results of the simulations of the 6 to 9 m zones of Remediation Areas A and E, the following can be concluded with respect to the effectiveness of a modified cap (see Tables 4 and 5):

- A 6 in. sand chemical isolation layer will meet performance criteria for 1,000 years or longer for all chemicals in Model Areas A1 and E1 and for mercury in all of the model areas evaluated (i.e., A1, E1, E3).
- In the Model Area E3 6 to 9 m zone, a 6 in. chemical isolation layer amended with GAC (at an application rate that is slightly higher than that of the larger model area) will meet performance criteria for 1,000 years or longer for all chemicals.

7.5 Sub-area Modeling

Additional modeling was performed for several sub-areas, where certain measurements were not consistent with the characteristic ranges of values used to represent these model areas in the model input distributions or where there were slight differences in the cap design specifications or design criteria as compared to the modeling approach described above. These sub-areas included the following:

- One sampling location in Model Area A2
- Two sampling locations in Remediation Area D-Center
- One sampling location in Model Area E1
- The Remediation Area D shoreline

- The Ninemile Creek spits

For each such location, the isolation cap design was based on the sub-area modeling described below.

Sampling Location OL-VC-40197 in Model Area A2

In Model Area A2, porewater concentrations of ethylbenzene and xylene at location OL-VC-40197 were elevated in comparison to all other porewater concentrations in Model Area A2 (see Figures B-15 and B-16) and therefore data from this location were not included in the data set for Model Area A2. A GAC application rate was developed using iterative deterministic transient model simulations based on the maximum porewater concentration measured at this location. All other model inputs were set to the best estimate (mean value) established for Model Area A2. Additionally, Monte Carlo simulations based on mean porewater concentration at the OL-VC-40197 location and all other parameters varying according to their respective distributions were performed to evaluate the robustness of the GAC application rate determined through the deterministic modeling (i.e., by confirming that 90% or more of the realizations met the PECs at 1,000 years, consistent with the probabilistic modeling approach described in Section 7.2). Due to the higher porewater concentrations, a higher GAC application rate was required for this localized area relative to that needed for the larger Model Area A2 (Table 5). The areal extent of this sub-area where this higher GAC rate will be applied is shown in Figure 4.1.

Sample Locations OL-VC-10140 and OL-VC-10138 in Model Area D-Center

In Model Area D-Center, benzene porewater concentrations at two locations were elevated in comparison to other porewater data collected in that area, including samples collected from depths deeper than the data selected to define porewater concentrations in the ILWD cap modeling, which were based on samples from 1-meter above to 2-meters below the dredge elevation at a given sample location (see Attachment 1). A GAC application rate specific to concentrations measured in the vicinity of these two sample locations was therefore developed using deterministic simulations based on an alternate porewater data set (data from Model Area D-Center for 1-meter above to 3-meters below the dredge elevation, which includes the high benzene concentrations at depth from locations OL-VC-10140 and OL-VC-10138) and all other inputs the same (i.e., mean values) as those used in the base modeling for Model Area D-Center. Due to the higher porewater concentrations in the alternate data set used to evaluate these two locations, a higher GAC application rate was required for this localized area relative to that needed for the larger Model Area D-Center (Table 5). The areal extent of this sub-area where this higher GAC rate will be applied is shown in Figure 4.4.

Sample Location OL-GP-60155 in Model Area E1

The upwelling velocity at sample location OL-GP-60155 (16.8 cm/yr) in Model Area E1 was an order of magnitude higher than the average upwelling velocity in the overall model area. Sediment porewater concentrations are low throughout Model Area E1, and concentrations in the vicinity of OL-GP-60155 are generally at the low end of the area's overall distribution. To evaluate the elevated groundwater velocity at this location, the Model Area E1 steady state model was used based on the approach discussed in Sections 7.1-7.3, except that 1) the

porewater concentration was set equal to the maximum value measured at sample locations in the vicinity of OL-GP-60155 (approximately a 7 acre area), and 2) the upwelling velocity was set to 16.8 cm/yr. The results of this model analysis, which are shown in Table 4, indicated that concentrations were predicted to be less than the performance criteria throughout the habitat layer at steady state for all CPOIs (i.e., mercury, VOCs, phenol, PCBs, and PAHs). Consistent with the larger Model Area E1, these results indicate that an 8 in. sand isolation layer would be protective in this localized area as well.

Remediation Area D Shoreline

The in-lake planting area within Remediation Area D, which covers a 25-ft strip along the shoreline adjacent to Model Areas D-East, D-Center, and D-West, were also considered for sub-area modeling. This 25-ft strip is being designed to contain higher total organic carbon (TOC) in the cap's habitat layer as compared to the remainder of Remediation Area D. To evaluate the higher habitat layer TOC specific to these areas, sensitivity analyses were conducted to evaluate the impacts on carbon amendments (see Attachment 6). The results of these sensitivity analyses indicated that the differences in GAC application rate were small, and considering the other model conservatisms associated with how these areas are modeled (e.g., see Section 3.3), sub-area-specific GAC application rates are not needed for this relatively limited portion of Remediation Area D.

Ninemile Creek Spits

The Ninemile Creek spits have been incorporated into the cap design for Remediation Area A and were evaluated using the model inputs developed for Model Area A2. However, the cap effectiveness criteria within the spits are established in the Ninemile Creek ROD and differ from those defined in the lake ROD. As discussed in more detail in Attachment 5, the only CPOI that required additional modeling in the spits was mercury. Therefore, using the model inputs for Model Area A2, the approach described in Section 7.1 was followed for the evaluation of the spits, with the exception that model results for mercury were compared to the criterion established in the Ninemile Creek ROD for mercury of 0.15 mg/kg. As discussed in Attachment 5, the model results indicated that the cap design specified for Model Area A2 would also be protective of the Ninemile Creek ROD criteria for 1,000 years in the spits.

7.6 Sources of Uncertainty in Model Results

The input parameters to which the model is most sensitive are porewater concentration, groundwater upwelling velocity, biodegradation rate, and contaminant sorption parameters (including GAC Freundlich coefficients). For each of these parameters, extensive data sets derived from field investigation and bench-scale testing were developed to provide site-specific information. As described in Section 6 specific model areas were developed to address spatial variability and to develop cap designs (i.e., GAC application rates) specific to the conditions in each area. Additional sources of variation and parameter uncertainty were addressed by a combination of conservative initial modeling (e.g., based on maximum measured pore water concentrations) and probabilistic modeling that accounted for the full range of variation in key input parameters (including worst case conditions).

Sources of uncertainty in the modeling have been addressed through the extensive data gathering effort used to support model input specification, the conservatisms described in Section 3.3 and the design optimization process described in Section 6.0.

8.0 CONCLUSIONS

Design of the Onondaga Lake sediment cap chemical isolation layer considers an extensive collection of site-specific data and evaluation of performance based on the rigorous modeling effort described above. Recommended cap profiles and GAC application rates based on a 1,000 year evaluation period are presented in the table below. The cap thicknesses and carbon amendment doses listed below are the minimums required based on design evaluations and do not include over-placement or over-dosing required to meet these minimums during construction.

CHEMICAL ISOLATION LAYER DESIGN SUMMARY

Model Area	Design Thickness and Profile	GAC Application Rate
A1 (0-6m)	12-in. (8-in. required) sand cap	None
A2 (including Ninemile Creek Spits)	12-in. amended cap (9-in. GAC, 3-in. sand/siderite)	0.66 lb/sf
B1/C1	12-in. amended cap (9-in. GAC, 3-in. sand/siderite)	0.60 lb/sf
B2	12-in. amended cap (9-in. GAC, 3-in. sand/siderite)	1.22 lb/sf
C2	12-in. amended cap (9-in. GAC, 3-in. sand/siderite)	0.01 lb/sf
C3	12-in. amended cap (9-in. GAC, 3-in. sand/siderite)	0.24 lb/sf
D-SMU2	12-in. amended cap (9-in. GAC, 3-in. sand/siderite)	0.044 lb/sf
D-West	12-in. amended cap (9-in. GAC, 3-in. sand/siderite)	1.33 lb/sf
D-Center	12-in. amended cap (9-in. GAC, 3-in. sand/siderite)	0.93 lb/sf
D-East	12-in. amended cap (9-in. GAC, 3-in. sand/siderite)	0.44 lb/sf
E1 (0-6m)	12-in. (8-in. required) sand cap	None
E2	12-in. GAC amended cap	0.27 lb/sf
E3 (0-6m)	12-in. GAC amended cap	0.008 lb/sf
WBB-East	12-in. GAC amended cap	0.02 lb/sf
WBB-Center	12-in. amended cap (9-in. GAC, 3-in. sand/siderite)	0.50 lb/sf
WBB-West	12-in. amended cap (9-in. GAC, 3-in. sand/siderite)	0.61 lb/sf
WB1-8	12-in. amended cap (9-in. GAC, 3-in. sand/siderite)	1.20 lb/sf
6-9 Meter Zone		
A1	6-in. (4-in. required) sand cap	None
E1	6-in. (4-in. required) sand cap	None
E3	6-in. GAC amended cap	0.084 lb/sf

Sub-Areas		
A2 (40197)	12-in. amended cap (9-in. GAC, 3-in. sand/siderite)	6.6 lb/sf
D-Center (10138 and 10140)	12-in. amended cap (9-in. GAC, 3-in. sand/siderite)	5.0 lb/sf

9.0 REFERENCES

Go, J., D.J. Lampert, J.A. Stegman, D.D. Reible. 2009. Predicting Contaminant Fate and Transport in Sediment Caps: Mathematical Modeling Approaches, Journal of Applied Geochemistry, 24, 7, 1347-1353.

Lampert, D. J. and Reible, D. 2009. An Analytical Modeling Approach for Evaluation of Capping of Contaminated Sediments, Soil and Sediment Contamination: An International Journal,18:4,470 – 488.

Neville, C. 2005. ADFL Analytical Solution – Version 4, User's Guide. S.S. Papadopulos & Associates, Inc. Bethesda, MD.

New York State Department of Environmental Conservation and United States Environmental Protection Agency Region 2. 2009. Record of Decision. *Operable Unit 2 of the Geddes Brook/Ninemile Creek Site.* Operable Unit of the Onondaga Lake Bottom Subsite of the Onondaga Lake Superfund Site. October 2009.

Palermo, M.R., S. Maynord, J. Miller, and D. Reible. 1998. Guidance for *In Situ* Subaqueous Capping of Contaminated Sediments. Environmental Protection Agency, EPA 905-B96-004, Great Lakes.

Parsons. 2009a. Lake Pre-Design Investigation: Phase VI Work Plan. Prepared for Honeywell, Morristown, New Jersey and Syracuse, New York.

Parsons, 2009b. Draft Onondaga Lake Capping and Dredge Area and Depth Initial Design Report, Appendix B Attachment 3.2. Prepared for Honeywell.

USEPA. 1997. Guiding Principles for Monte Carlo Analysis. Risk Assessment Forum, U.S. Environmental Protection Agency. EPA/630/R-97/001.

Zheng, C., and P. Wang. 1998. MT3DMS: A Modular Three-Dimensional Multispecies Transport Model for Simulation of Advection, Dispersion and Chemical Reactions of Contaminants in Groundwater Systems. Documentation and User's Guide. U.S. Army Corps of Engineers Technical Report, June 1998.

TABLES

TABLE 1

SUMMARY OF COMPOUNDS MEETING PERFORMANCE CRITERIA ASSUMING INITIAL CONSERVATIVE ANALYTICAL STEADY STATE AND TRANSIENT MODEL EVALUATIONS[1]

Group	Chemical	Model Area																
		A1	A2	B1/ C1	B2	C2	C3	S[2]	W[2]	C[2]	E[2]	E1	E2	E3	WB1-8	WBB -West	WBB-Center	WB-East
Mercury	Mercury	✓✓	✓✓	✓✓	✓	✓✓	✓	✓✓	✓✓	✓✓	✓✓	✓✓	✓✓	✓✓	✓	✓	✓	✓✓
VOCs	Benzene	✓	✓		✓	✓	✓					✓	✓	✓		✓	✓	✓
	Toluene	✓	✓		✓	✓	✓	✓				✓	✓	✓				✓
	Ethylbenzene	✓		✓	✓	✓						✓						✓
	Xylenes	✓			✓	✓						✓						✓
	Chlorobenzene	✓		✓	✓	✓	✓	✓				✓		✓	✓			✓
	Dichlorobenzenes	✓		✓	✓	✓		✓				✓		✓				✓
	Trichlorobenzenes	✓	✓	✓	✓	✓	✓	✓				✓		✓	✓			✓
	Naphthalene	✓	✓		✓							✓						
	Phenol	✓					✓					✓	✓	✓				✓
PAHs/ PCB	Total PCBs	✓	✓	✓	✓	✓	✓	✓	✓	✓	✓	✓	✓	✓	✓	✓	✓	✓
	Fluorene	✓	✓	✓	✓		✓✓	✓✓	✓✓	✓✓	✓	✓	✓✓	✓	✓			✓
	Phenanthrene	✓	✓	✓✓	✓		✓✓	✓✓	✓✓	✓✓	✓	✓	✓	✓	✓			✓
	Acenaphthene	✓	✓	✓	✓		✓	✓	✓✓	✓	✓	✓	✓	✓	✓	✓✓	✓✓	✓
	Acenaphthylene	✓	✓	✓	✓	✓	✓	✓	✓✓	✓	✓	✓	✓	✓	✓	✓✓	✓✓	✓
	Anthracene	✓	✓	✓	✓		✓✓	✓✓	✓✓	✓✓	✓	✓	✓	✓	✓	✓✓	✓✓	✓✓
	Pyrene	✓	✓	✓	✓		✓	✓	✓✓	✓	✓	✓	✓	✓	✓	✓✓	✓✓	✓
	Benzo(a)anthracene	✓	✓	✓	✓		✓	✓	✓✓	✓	✓	✓	✓	✓	✓	✓✓	✓✓	✓
	Benzo(b)fluoranthene	✓	✓	✓	✓		✓	✓	✓	✓	✓	✓	✓	✓	✓	✓	✓	✓
	Benzo(k)fluoranthene	✓	✓	✓	✓	✓	✓	✓	✓	✓	✓	✓	✓	✓	✓	✓	✓	✓
	Chrysene	✓	✓	✓	✓		✓	✓	✓✓	✓	✓	✓	✓	✓	✓	✓✓	✓✓	✓
	Fluoranthene	✓	✓	✓	✓		✓	✓	✓	✓	✓	✓	✓	✓	✓	✓✓	✓✓	✓

TABLE 1 (CONTINUED)

SUMMARY OF COMPOUNDS MEETING PERFORMANCE CRITERIA ASSUMING INITIAL CONSERVATIVE ANALYTICAL STEADY STATE AND TRANSIENT MODEL EVALUATIONS[1]

Group	Chemical	Model Area																
		A1	A2	B1/ C1	B2	C2	C3	S[2]	W[2]	C[2]	E[2]	E1	E2	E3	WB1-8	WBB -West	WBB-Center	WB-East
	Benzo(a)pyrene	✓	✓	✓	✓		✓	✓	✓	✓	✓	✓	✓	✓	✓	✓✓	✓✓	✓
	Dibenz(a,h)anthracene	✓	✓	✓	✓	✓	✓	✓	✓	✓	✓	✓	✓	✓	✓	✓	✓	✓
	Indeno(1,2,3-cd)pyrene	✓	✓	✓	✓		✓	✓	✓	✓	✓	✓	✓	✓	✓	✓	✓	✓
	Benzo(g,h,i)perylene	✓	✓	✓	✓	✓✓	✓	✓	✓	✓	✓	✓	✓	✓	✓	✓	✓	✓

Notes:

1) Table summarizes the results from the conservative analytical steady state (✓) and 1,000 year transient evaluations (✓✓) performed using maximum concentrations discussed in Sections 7.1 through 7.3. These compounds were not subject to additional modeling. Check marks (✓) indicate cases where performance criteria were met.
2) ILWD Subareas: SMU2 (S), West (W), Center (C), East (E)

TABLE 2

CARBON APPLICATION RATE EVALUATION

Model Area	Acres	Application rate based on Deterministic Modeling[1]		Application rate based on Probabilistic Modeling[2]		Final Carbon Application Rate (lb/sf)
		Controlling Chemical(s)	Carbon Application Rate (lb/sf)	Controlling Chemical(s)	Carbon Application rate (lb/sf)	
A1 (0-6m)[3]	39.8	Sand Cap Only				
A2[5]	16.1	Xylenes	0.66	NA	No additional carbon	0.66
B1/C1	15.5	Phenol	0.60	NA	No additional carbon	0.60
B2	7.0	Phenol	1.22	NA	No additional carbon	1.22
C2	8.8	Fluorene	0.01	NA	No additional carbon	0.01
C3	12.1	Xylenes	0.24	NA	No additional carbon	0.24
D-SMU2	7.1	Naphthalene	0.044	NA	No additional carbon	0.044
D-West[4]	11.0	Phenol	1.33	NA	No additional carbon	1.33
D-Center[4,5]	33.0	Xylenes	0.93	NA	No additional carbon	0.93
D-East[4]	53.1	Chlorobenzene	0.44	NA	No additional carbon	0.44
E1 (0-6m)[3]	65.6	Sand Cap Only				
E2	21.2	Chlorobenzene	0.27	NA	No additional carbon	0.27
E3 (0-6m)[3]	60.5	Ethylbenzene and Naphthalene	0.008	NA	No additional carbon	0.008
WB1-8	2.4	Xylenes	1.11	NA	1.20	1.20
WBB-West	5.7	Chlorobenzene, Dichlorobenzenes, and Naphthalene	0.61	NA	No additional carbon	0.61
WBB-Center	4.7	Dichlorobenzenes	0.50	NA	No additional carbon	0.50
WBB-East	6.0	Naphthalene	0.02	NA	No additional carbon	0.02

Notes:

1) Application rate needed to achieve criteria over 1,000-year evaluation period in deterministic simulation based on 95th percentile porewater concentrations and best estimates for other model inputs.

2) Application rate needed to achieve criteria over 1,000-year evaluation period in 90% or more of realizations from probabilistic modeling (Monte Carlo Analysis).

3) The 6-9 meter zone in this model area was evaluated separately, results are provided in Table 5. Acreages do not include the 6-9 meter zone.

4) ILWD sub-area acreage values include portions of the addendum cap area adjacent to each sub-area. Carbon application rates for each sub-area will be applied to the portion of the addendum cap area adjacent to each sub-area.

5) A2 and D-Center total acreages include 40197 and 10138/10140 areas, respectively. The acreage for each of these sub-areas is provided in Table 5.

TABLE 3

MONTE CARLO MODELING RESULTS AT FINAL GAC APPLICATION RATES

Model Area	Chemical	Carbon Dose (lb/sf)	Percent Realizations Meeting PEC				
			1,000 years	750 years	500 years	200 years	100 years
A2	Ethylbenzene	0.66	97.2	97.8	98.7	99.8	100.0
	Xylenes		93.5	95.4	97.2	99.6	100.0
	Chlorobenzenes		100.0	100.0	100.0	100.0	100.0
	Dichlorobenzenes		100.0	100.0	100.0	100.0	100.0
	Phenol		98.2	98.2	98.2	98.2	98.3
B1/C1	Benzene	0.6	95.2	95.2	95.2	95.2	95.2
	Toluene		100.0	100.0	100.0	100.0	100.0
	Xylenes		99.9	100.0	100.0	100.0	100.0
	Naphthalene		100.0	100.0	100.0	100.0	100.0
	Phenol		95.4	95.4	95.4	95.4	95.4
B2	Phenol	1.22	92.6	92.6	92.6	92.6	92.6
C2	Naphthalene	0.01	96.7	96.7	96.7	96.7	96.7
	Phenol		95.4	95.4	95.4	95.4	95.4
	Fluorene		94.5	95.5	97.0	98.6	99.3
	Phenanthrene		95.3	96.3	97.8	99.2	99.4
	Acenaphthene		98.7	99.0	99.2	99.8	100.0
	Anthracene		97.5	98.2	98.8	99.5	99.9
	Pyrene		99.3	99.3	99.3	99.7	99.9
	Benzo(a)anthracene		99.3	99.4	99.7	100.0	100.0
	Benzo(b)fluoranthene		99.4	99.6	99.9	100.0	100.0
	Chrysene		99.5	99.7	99.9	100.0	100.0
	Fluoranthene		99.1	99.3	99.3	99.7	100.0
	Benzo(a)pyrene		99.6	99.8	99.9	100.0	100.0

Model Area	Chemical	Carbon Dose (lb/sf)	Percent Realizations Meeting PEC				
			1,000 years	750 years	500 years	200 years	100 years
	Indeno(1,2,3-cd)pyrene		99.8	100.0	100.0	100.0	100.0
C3	Ethylbenzene	0.24	100.0	100.0	100.0	100.0	100.0
	Xylenes		91.0	94.1	97.7	100.0	100.0
	Dichlorobenzenes		99.9	99.9	100.0	100.0	100.0
	Naphthalene		98.2	99.1	99.9	100.0	100.0
ILWD-SMU2	Benzene	0.044	99.6	99.6	99.6	99.6	99.6
	Ethylbenzene		96.2	96.2	96.2	96.2	96.4
	Xylenes		93.6	93.6	93.6	93.9	94.7
	Naphthalene		93.3	93.3	93.4	94.6	97.9
	Phenol		96.0	96.0	96.0	96.0	96.0
ILWD-West	Benzene	1.33	98.4	98.5	98.5	99.0	99.8
	Toluene		99.8	99.8	99.9	99.9	100.0
	Ethylbenzene		100.0	100.0	100.0	100.0	100.0
	Xylenes		99.6	99.9	100.0	100.0	100.0
	Chlorobenzenes		100.0	100.0	100.0	100.0	100.0
	Dichlorobenzenes		100.0	100.0	100.0	100.0	100.0
	Trichlorobenzenes		100.0	100.0	100.0	100.0	100.0
	Naphthalene		99.90	99.98	100.0	100.0	100.0
	Phenol		93.06	93.06	93.06	93.06	93.1
ILWD-Center	Benzene	0.93	93.8	93.8	93.8	93.9	94.2
	Toluene		99.8	99.8	99.8	99.9	100.0
	Ethylbenzene		99.8	99.9	99.9	100.0	100.0
	Xylenes		92.2	95.7	97.7	100.0	100.0
	Chlorobenzenes		96.1	97.4	99.5	100.0	100.0
	Dichlorobenzenes		100.0	100.0	100.0	100.0	100.0
	Trichlorobenzenes		99.9	99.9	99.9	99.9	99.9

Model Area	Chemical	Carbon Dose (lb/sf)	Percent Realizations Meeting PEC				
			1,000 years	750 years	500 years	200 years	100 years
	Naphthalene		97.4	97.6	98.1	100.0	100.0
	Phenol		99.6	99.6	99.6	99.6	99.6
ILWD-East	Benzene	0.44	100.0	100.0	100.0	100.0	100.0
	Toluene		100.0	100.0	100.0	100.0	100.0
	Ethylbenzene		100.0	100.0	100.0	100.0	100.0
	Xylenes		96.3	97.0	97.9	99.9	100.0
	Chlorobenzenes		94.1	94.9	95.7	97.1	99.8
	Dichlorobenzenes		97.9	98.8	99.9	100.0	100.0
	Trichlorobenzenes		100.0	100.0	100.0	100.0	100.0
	Naphthalene		98.0	98.3	99.1	100.0	100.0
	Phenol		97.3	97.3	97.3	97.3	97.3
E2	Ethylbenzene	0.27	99.9	99.9	99.9	100.0	100.0
	Xylenes		98.7	99.2	99.4	99.9	100.0
	Chlorobenzenes		94.6	96.3	98.4	99.9	100.0
	Dichlorobenzenes		96.8	98.3	99.2	99.9	100.0
	Trichlorobenzenes		100.0	100.0	100.0	100.0	100.0
	Naphthalene		97.9	98.6	99.2	100.0	100.0
E3	Ethylbenzene	0.0008	94.6	94.6	94.6	94.6	94.6
	Xylenes		99.4	99.4	99.4	99.4	99.4
	Naphthalene		94.2	94.2	94.2	94.2	94.2
WBB-East	Naphthalene	0.02	93.0	93.9	95.7	100.0	100.0
WBB-West	Toluene	0.61	100.0	100.0	100.0	100.0	100.0
	Ethylbenzene		100.0	100.0	100.0	100.0	100.0
	Xylenes		98.3	99.4	99.8	100.0	100.0
	Chlorobenzenes		91.8	93.7	96.8	99.8	100.0
	Dichlorobenzenes		93.3	96.7	98.9	100.0	100.0

Model Area	Chemical	Carbon Dose (lb/sf)	Percent Realizations Meeting PEC				
			1,000 years	750 years	500 years	200 years	100 years
	Trichlorobenzenes		99.6	99.7	99.7	99.8	99.8
	Naphthalene		93.7	96.1	98.7	99.9	100.0
	Phenol		98.7	98.7	98.7	98.7	98.7
	Fluorene		99.3	99.3	99.4	99.9	100.0
	Phenanthrene		99.6	99.9	100.0	100.0	100.0
WBB-Center	Toluene	0.5	99.9	99.9	99.9	99.9	99.9
	Ethylbenzene		100.0	100.0	100.0	100.0	100.0
	Xylenes		98.0	99.0	99.8	100.0	100.0
	Chlorobenzenes		92.9	94.2	96.8	99.8	99.9
	Dichlorobenzenes		93.5	97.2	99.0	100.0	100.0
	Trichlorobenzenes		99.5	99.6	99.7	99.8	99.8
	Naphthalene		94.0	96.6	98.6	99.9	100.0
	Phenol		98.4	98.4	98.4	98.4	98.4
	Fluorene		99.3	99.3	99.4	100.0	100.0
	Phenanthrene		99.7	99.9	99.9	100.0	100.0
WB 1-8	Benzene	1.2	99.3	99.3	99.3	99.7	99.9
	Toluene		100.0	100.0	100.0	100.0	100.0
	Ethylbenzene		99.9	100.0	100.0	100.0	100.0
	Xylenes		90.3	96.5	99.5	100.0	100.0
	Dichlorobenzenes		100.0	100.0	100.0	100.0	100.0
	Naphthalene		95.9	98.9	99.8	100.0	100.0
	Phenol		93.7	93.7	93.7	93.7	93.7
E3 (6-9m Zone)	Ethylbenzene	0.084	99.3	99.3	99.3	99.3	99.3
	Xylenes		99.4	99.5	99.7	100.0	100.0
	Dichlorobenzene		99.9	99.9	99.9	100.0	100.0
	Naphthalene		94.6	95.1	96.3	98.9	99.8

Model Area	Chemical	Carbon Dose (lb/sf)	Percent Realizations Meeting PEC				
			1,000 years	750 years	500 years	200 years	100 years
OL-VC-40197	Benzene	6.56	100.0	100.0	100.0	100.0	100.0
	Toluene		100.0	100.0	100.0	100.0	100.0
	Ethylbenzene		99.2	100.0	100.0	100.0	100.0
	Xylenes		97.0	100.0	100.0	100.0	100.0
	Chlorobenzenes		100.0	100.0	100.0	100.0	100.0
	Dichlorobenzenes		100.0	100.0	100.0	100.0	100.0
	Trichlorobenzenes		99.9	100.0	100.0	100.0	100.0
	Naphthalene		100.0	100.0	100.0	100.0	100.0

Note:

1) Monte Carlo modeling was performed on areas and chemicals that did not meet the PEC during the conservative screening using maximum porewater concentrations.

TABLE 4

SUMMARY OF COMPOUNDS MEETING PERFORMANCE CRITERIA USING INITIAL CONSERVATIVE ANALYTICAL STEADY STATE AND TRANSIENT MODEL EVALUATIONS OF 6-9 M ZONES AND SUB-AREA MODELING [1]

Group	Chemical	Model Area			
		A1 (6-9 M ZONE)	E1 (6-9 M ZONE)	E3 (6-9 M ZONE)	E1 Location OL-GP-60155
Mercury	Mercury	✓✓	✓✓	✓✓	✓
VOCs	Benzene	✓	✓	✓	✓
	Toluene	✓	✓	✓	✓
	Ethylbenzene	✓	✓		✓
	Xylenes	✓	✓		✓
	Chlorobenzene	✓	✓	✓	✓
	Dichlorobenzenes	✓	✓		✓
	Trichlorobenzenes	✓	✓	✓	✓
	Naphthalene	✓	✓		✓
	Phenol	✓	✓	✓	✓
PAHs/ PCB	Total PCBs	✓	✓	✓	✓
	Fluorene	✓	✓	✓	✓
	Phenanthrene	✓	✓	✓	✓
	Acenaphthene	✓	✓	✓	✓
	Acenaphthylene	✓	✓	✓✓	✓
	Anthracene	✓	✓	✓	✓
	Pyrene	✓	✓	✓	✓
	Benzo(a)anthracene	✓	✓	✓	✓
	Benzo(b)fluoranthene	✓	✓	✓	✓
	Benzo(k)fluoranthene	✓	✓	✓	✓
	Chrysene	✓	✓	✓	✓
	Fluoranthene	✓	✓	✓	✓

TABLE 4 (CONTINUED)

SUMMARY OF COMPOUNDS MEETING PERFORMANCE CRITERIA USING INITIAL CONSERVATIVE ANALYTICAL STEADY STATE AND TRANSIENT MODEL EVALUATIONS OF 6-9 M ZONES AND SUB-AREA MODELING [1]

Group	Chemical	Model Area			
		A1 (6-9 M ZONE)	E1 (6-9 M ZONE)	E3 (6-9 M ZONE)	E1 Location OL-GP-60155
	Benzo(a)pyrene	✓	✓	✓	✓
	Dibenz(a,h)anthracene	✓	✓	✓	✓
	Indeno(1,2,3-cd)pyrene	✓	✓	✓	✓
	Benzo(g,h,i)perylene	✓	✓	✓	✓

Notes:

1) Table summarizes the results from the conservative analytical steady state (✓) and 1000 year transient evaluations (✓✓) performed using maximum concentrations discussed in Sections 7.1 through 7.3. These compounds were not subject to additional modeling. Check marks (✓) indicate cases where performance criteria were met.

TABLE 5

CARBON APPLICATION RATE FOR 6-9 M ZONES AND SUB AREA MODELING

Model Area / Location	Acres	Application rate based on Deterministic Modeling[1]		Application rate based on Probabilistic Modeling[2]		Final Carbon Application Rate (lb/sf)
		Controlling Chemical(s)	Carbon Application Rate (lb/sf)	Controlling Chemical(s)	Carbon Application rate (lb/sf)	
A1 (6-9 M)	29.9	Sand Cap Only				
E1 (6-9 M)	12.6	Sand Cap Only				
E3 (6-9 M)	15.6	Naphthalene	0.084	NA	No additional carbon	0.084
A2 OL-VC-40197	0.2	Xylenes	6.6	NA	No additional carbon	6.6
D-Center OL-VC-10138 & OL-VC-10140	1.6	Benzene	5.0	Not modeled		5.0
E1 OL-GP-60155	NA	Sand Cap Only				
Ninemile Creek Spits[3]	1.9	NA	0.66	Not modeled		0.66

Notes:

1) Application rate needed to achieve criteria over 1,000-year evaluation period in deterministic simulation based on 95th percentile porewater concentrations and best estimates for other model inputs.

2) Application rate needed to achieve criteria over 1,000-year evaluation period in 90% or more of realizations from probabilistic modeling (Monte Carlo Analysis).

3) Cap design for Ninemile Creek spits same as Model Areas A2 (see Attachment 5)

FIGURES

ATTACHMENT 1

MODEL INPUTS

1.0 MODEL INPUT PARAMETERS

Model inputs were derived from extensive site sampling efforts and bench-scale testing, as well as literature in some cases. Based on the initial modeling conducted during the FS, as well as analyses conducted since that time, model predictions have been found to be most sensitive to underlying porewater concentration, groundwater upwelling velocity, biological decay rate and sorption parameters (including partitioning to sand cap materials and to GAC amendments). Therefore, an extensive data collection effort and a series of bench-scale evaluations were conducted between 2005 and 2011 to increase understanding and provide site-specific information for these key parameters. The following subsections describe the data collection efforts and basis for developing the input values used for these key model input parameters.

Both deterministic and probabilistic model evaluations were used in developing the chemical isolation layer design. Input parameters for the deterministic simulations were fixed values specified based on the references and rationale provided in detail in Table A1.1. Probabilistic model simulations were completed to assess cap performance against the full range of potential input parameter values (including the "worst-case" values as they pertained to predications of cap performance). Statistical distributions were developed for key input parameters and used in these probabilistic modeling evaluations. The distributions used for such model input parameters, and the basis for their selection (including applicable references and data sources) are also provided in Table A1.1.

1.1 Porewater Concentrations

Multiple sampling methods were used to measure porewater concentrations within the remediation areas of the lake. These methods are described further in the Onondaga Lake Phase I Pre-Design Investigation Porewater Methods Evaluation Report (Parsons, 2006). Sampling methods included *in situ* diffusion samplers (peepers), groundwater upwelling pumps and porewater generated via centrifugation of sediment. Peepers and centrifuged samples, in general, produced consistent results and provided readily implementable approaches for collecting a large number of porewater samples. Therefore, data from all three methods (i.e., centrifugation, peepers, and upwelling pumps) were generally used to develop model inputs for porewater concentration.

In consultation with the NYSDEC, correction factors were developed and applied to the porewater data to account for any potential losses during sample collection, handling or analysis. Correction factors varied by compound and sampling methodology. Correction factors for peeper data were based on the results of the Phase II Pre-Design Investigation: Data Summary Report, Appendix J - Diffusion Sampler Equilibrium Study (Parsons, 2009a). For porewater samples generated via centrifugation, correction factors were based on average Matrix Spike/Matrix Spike Duplicate (MS/MSD) recoveries. Groundwater data collected from upwelling pumps in 2002/2003 were discarded, with the exception of mercury and phenol results, due to the potential for losses along the pump tubing. Groundwater data collected from the upwelling pumps, following modification of the tubing during the Phase I Pre-Design Investigation (PDI), were incorporated into the model data set without correction factors. Table A1.2 provides a summary of the correction factors employed.

For certain contaminants, the ability to collect porewater samples was limited by the volume required for analysis. Therefore, in the case of PAHs, phenol and PCBs, sediment data from the lake PDI as well as the Remedial Investigation (RI) were used (in conjunction with measurements of TOC, bulk density, and porosity) to calculate porewater concentrations based on equilibrium partitioning equations for use in the modeling effort. Attachment 2 to Appendix B of this design report describes the calculation of porewater concentrations for these compounds.

Initial concentrations used in the model inputs were based on the data selection and calculation methods described above and are further detailed in Table A1.1. Based on the porewater concentration data set for each compound in each model area, empirical distributions were developed. Addendum 1 describes the approach for generating these cumulative distribution functions (CDFs) for each compound in each model area. For deterministic simulations, either the maximum value (for initial conservative screening level modeling) or the 95th percentile of the distribution was used (as described in Appendix B). Probabilistic modeling was based on sampling from the full distributions. Plots of the full distributions for each compound are provided with the electronic model input files in Appendix B Attachment 4.

1.2 Groundwater Upwelling Velocities

Appendix C to this design report details the field effort and results of the extensive groundwater upwelling investigation conducted on the lake, and describes the development of the groundwater upwelling inputs that were used in cap modeling. This work was completed to characterize the groundwater upwelling velocities that the sediment cap will be subjected to following construction.

Direct measurements of groundwater upwelling velocity were collected in most of the remediation areas, as detailed in Appendix C. Thus, the measurements of groundwater upwelling velocity collected in the capping areas of Remediation Areas A, E, and in Model Area C2 were used to generate the groundwater upwelling data sets (i.e., empirical CDFs) used in the cap modeling for those areas.

The upwelling rates used in the cap modeling for the four subareas in Remediation Area D, Model Areas B1/C1, B2, C3, WBB-West, WBB-Center, WBB-East and the WB1-8 connected wetlands were based on predictions of conditions that would exist once the upland hydraulic containment systems are in place. Estimates of these future upwelling distributions were developed based on calculations of vertical flow through the underlying silt and clay unit based on measurements of thickness, vertical hydraulic conductivity, and hydraulic gradient of that unit in each of these areas. Additional discussion is provided in Appendix C.

For all modeling areas, the specific upwelling velocities used in the model runs were based on the upwelling velocity distributions developed as described above (i.e., based on empirical data or estimated based on calculations of flow through the slit and clay unit). For deterministic simulations, the best estimate (i.e., mean value) of the distribution was used, and probabilistic modeling was based on sampling from the full distributions, as provided in Appendix C.

1.3 Consolidation Induced Porewater Expression

Settlement calculations indicate that there will be some upward expression of porewater associated with sediment consolidation due to cap placement. This porewater expression would be equivalent to an additional advective flux into the cap during the time that such consolidation occurs. That flux will occur over a relatively short timeframe, after which the long-term conditions represented by the steady-state model would prevail. For steady state model behavior, such an initial expression of porewater does not change the ultimate steady state concentration profile calculated by the model. Therefore, consolidation effects were not included in the steady state analytical modeling. Porewater expression may have a more significant impact on shorter-term performance evaluations of amended cap effectiveness, as simulated with the numerical transient modeling. Therefore, porewater expression was represented in the transient modeling of amended cap areas by adding the calculated porewater flux during the consolidation period to the base upwelling velocity (described above). Appendix E of this design report presents the basis for how predictions of settlement induced porewater expression as a function of time were developed for the purposes of the cap modeling, and Table A1.1 provides more detail on how this process was simulated in the model.

1.4 Sorption Parameters for Sediment and Sand Cap Material

As noted above, porewater concentrations within the sediment beneath the cap used for modeling were based on direct measurements of porewater concentrations, as well as calculations of porewater concentrations from sediment data and partitioning theory, as described in Section 1.1. Partitioning theory was also used to predict partitioning between porewater and sediments beneath the cap and between porewater and the cap materials. The basis for specification of the sorption parameters used in the model is summarized in Table A1.1; details are provided in Attachment 2 to Appendix B of this design report.

1.5 GAC Adsorption Parameters

Site-specific isotherms for various solid media with potential for use as an amendment material were generated for VOCs, mercury and naphthalene during the Phase IV PDI (Parsons, 2009b). Additional isotherm testing for the same list of parameters, with the addition of phenol, was conducted during the Phase VI PDI to validate the Phase IV PDI results and evaluate each isotherm point in triplicate to reduce variability (as compared to the initial testing). Screening studies conducted during the Phase VI isotherm experiments indicated a potential influence of pH on GAC sorption for some compounds. As a result, a second round of isotherms was conducted at neutral pH. Results from the Phase VI adjusted pH isotherms were generally consistent with or more conservative than the Phase IV results. Because of this and the higher levels of QA/QC employed in the Phase VI studies, the Phase VI amended pH GAC isotherms were used in the cap modeling evaluation for all cap areas within the lake and the WB1-8 connected wetlands to simulate GAC amendments, where used. Isotherm data were also generated within the Outboard Area following a similar methodology. Adjusted pH isotherms were developed based on porewater from the WBB-West area, and unadjusted isotherms were developed based on porewater from the WBB-East area. These data were used for modeling GAC amendments in these areas.

GAC isotherm data for PAHs and PCBs were not included in the scope of the site-specific evaluations. In order to model these compounds, the site-specific results for naphthalene were conservatively used to represent PAHs and PCBs. PAHs are composed of multiple benzene rings bonded in a planar configuration. With only two bonded benzene rings, naphthalene is the simplest and smallest of the PAH compounds. All other PAHs consist of greater numbers of bonded benzene rings and are therefore of higher molecular weight, larger molecular size, and greater hydrophobicity; the same is true of PCBs, as these compounds consist of two benzene rings to which between one and ten chlorine atom(s) are bonded. These characteristics all lend themselves to higher relative GAC sorbability than naphthalene. For example, in one study the equilibrium sorbed concentration values for naphthalene and phenanthrene at a water concentration of 0.1 mg/L were determined to be 50 mg/g and 80 mg/g, respectively (USEPA, 1980). Since the addition of each benzene ring (or chlorine atoms in the case of PCBs) will increase the sorptivity relative to naphthalene, applying the site-specific derived Freundlich parameters for naphthalene to the other PAHs and PCBs will yield a highly conservative modeling estimate for the GAC cap amendment.

Model inputs from the Phase VI and Outboard Area studies included site-specific Freundlich isotherm parameters (Kf and 1/n) for each compound, as described in Table A1.1. Kf and 1/n values used for the deterministic simulations of each chemical were based on the best estimate for these two parameters as determined through nonlinear regression analysis of the isotherm data. A 95 percent confidence interval was also generated directly from the experimental data using joint uncertainty bounds for the two parameters in the fitted Freundlich equations (Kf, 1/n). In order to quantify uncertainty around the best estimate of Kf and 1/n for the probabilistic simulations, coefficient pairs were generated by randomly sampling from within these 95 percent confidence regions.

1.6 Biological Decay

Biological degradation of organic contaminants within the chemical isolation layer is an important contaminant fate process considered in the design of the chemical isolation layer. Over time, natural biological processes will degrade organic contaminants as they slowly migrate upwards into the cap and reduce contaminant concentrations throughout the isolation layer and the overlying habitat layer. Several stages of bench-scale experiments were conducted to evaluate the rate of biological decay anticipated to occur within the cap for key compounds present in lake sediments and porewater (Parsons 2008, 2009a, 2009c, 2009d).

Rapid decay under aerobic conditions (which will occur within the upper portion of the cap's habitat layer) was consistently observed for all VOCs evaluated in the bench studies. Based on test results, anaerobic biodegradation is expected to occur within the chemical isolation layer for benzene, toluene, ethylbenzene, xylene, chlorobenzene, dichlorobenzenes, naphthalene, and phenol, provided porewater pH is 8 or less. Thus, there is evidence from the laboratory testing and in the literature that over time biological decay will occur in the isolation cap for all of the volatile organic compounds (VOCs), including naphthalene evaluated with the cap model. Given the inherent complexities in replicating long-term environmental processes in the relatively short-term investigation period, it was difficult to generate a robust data set to adequately quantify site-specific biological degradation rates for all organic contaminants of concern evaluated with the

cap model. Therefore, when simulating decay for VOCs, including naphthalene, and phenol, the rates were based on the slow end of the literature range developed during the FS (as discussed in Table A1.1). Based on the degree of variability in the results from the site specific bench testing, safety factors were applied to the FS decay rates for three CPOIs: benzene, chlorobenzene, and naphthalene (see Table A1.1). Although development of site-specific degradation rates was difficult based on the batch studies, the range of literature-based rates from the FS used in the cap model are well within the range of rates supported by the batch study results.

To account for a period of time over which a sufficient microbial community is established and acclimated such that it can achieve these decay rates within the chemical isolation layer in areas where pH is elevated above 8, a lag period before biodegradation is assumed to become effective was incorporated into the modeling. This lag period was set to 5 years in model areas with pH <=8 (Model Areas A1, E1, E2 and E3) and to 100 years in areas where pH is elevated above 8 (Model Area A2, all model areas in Remediation Areas B, C, and D, WB1-8 and the WBB-West and WBB-Center areas). Degradation was conservatively excluded from the model in the WBB-East Model Area since there are a few samples in that area with elevated pH, but a pH amendment is not being included in the cap for that area.

2.0 REFERENCES

Parsons. 2006. *Onondaga Lake Phase I Pre-Design Investigation: Porewater Methods Evaluation Report*. Prepared for Honeywell, Morristown, New Jersey and Syracuse, New York.

Parsons. 2008. *Onondaga Lake Pre-Design Investigation: Phase IV Work Plan*. Prepared for Honeywell, Morristown, New Jersey and Syracuse, New York.

Parsons. 2009a. *Onondaga Lake Pre-Design Investigation: Phase II Data Summary Report, Appendix J – Diffusion Sampler Equilibrium Study*. Prepared for Honeywell, Morristown, New Jersey and Syracuse, New York.

Parsons. 2009b. *Onondaga Lake Pre-Design Investigation: Phase IV Data Summary Report*. Prepared for Honeywell, Morristown, New Jersey and Syracuse, New York

Parsons. 2009c. *Onondaga Lake Pre-Design Investigation: Phase III Data Summary Report*. Prepared for Honeywell, Morristown, New Jersey and Syracuse, New York

Parsons. 2009d. *Onondaga Lake Pre-Design Investigation: Phase V Work Plan*. Prepared for Honeywell, Morristown, New Jersey and Syracuse, New York.

USEPA. 1980. *Carbon Adsorption Isotherms for Toxic Organics*. U.S. Environmental Protection Agency. EPA/600/8-80-023. April 1980.

TABLE A1.1
MODEL INPUT PARAMETERS AND BASIS

Model Input	Site-specific or Literature Based	Reference	Rationale
Initial porewater concentration in underlying sediment: Fixed value (maximum concentration or 95th percentile) used for deterministic simulations. Distribution (CDF) used for probabilistic simulations.	Site-specific	Based on concentrations measured in porewater for the following contaminants: benzene, toluene, ethylbenzene, xylene, chlorobenzene, dichlorobenzenes, trichlorobenzenes, naphthalene, phenol, and mercury (where available). Porewater concentrations for the following contaminants were calculated based on sediment concentrations and equilibrium partitioning formulae: phenol, PAHs, and total PCBs (see Attachment 2). Phenol and mercury data from groundwater upwelling pumps were used, where available, to supplement these values. Data were selected from the following depth intervals: 1 meter above to 2 meters below the dredge cut in Remediation Area D, 0-3 m in Remediation Areas A, B, C and E, 0-5 meters in WBB-East and WBB-West/Center and 0-6 meters in WB 1-8. Correction factors were applied as appropriate (see Table A1.2). Depth intervals were selected considering the proposed dredge plan and generally include the data from above to at least two meters below the maximum dredge cut in an area which provides a robust data set and reflects the concentrations that will directly influence the cap. Modeling in sub areas was conducted around sample locations OL-VC-10138 and OL-VC-10140 in the ILWD Center; for this evaluation, data were selected from the IWD Center from 1 meter above to 3 meters below the dredge cut. *Honeywell Onondaga Lake Locus Database, 2010.*	Spatial variability exists across the lake capping areas. The ILWD has been broken into four subareas to account for larger-scale differences in contaminant concentration distributions. Likewise, Remediation Areas A, B, C and E have each been separated into smaller Modeling Areas: A1, A2, B1/C1, B2, C2, C3 and E1, E2, E3 based on differences in porewater concentration. WB1-8 was modeled as a single area due to its small size and limited variation in porewater concentrations. The Outboard Area was broken into 3 areas (WBB-West, WBB-Center, and WBB-East) based on differences in porewater concentration and upwelling. Because no spatial differences in porewater concentration were observable between WBB-West and WBB-Center, the data from those two areas were combined to develop CDFs that were used in both areas. Probabilistic simulations were based on empirical CDFs developed from the concentration datasets for each CPOI within a given modeling area (except in the case of the sub-area probabilistic modeling conducted for location OL-VC-40197, which was based on the mean concentration at that sample location). CDFs are provided in Attachment 5. Further explanation of the

Model Input	Site-specific or Literature Based	Reference	Rationale
			development of the CDFs is provided in Addendum 1.
Molecular diffusion coefficient: Fixed value	Literature	Fixed value by compound. *Lyman, W.J, Reehl, W.F. and Rosenblatt D.H. 1990. Handbook of Chemical Property Estimation Methods. American Chemical Society, Washington, D.C.*	Little to no spatial variability or uncertainty anticipated.
Hydrodynamic dispersivity: Fixed value	Literature	Conservative value fixed at 10 percent of the total cap thickness. Homogenous cap layer expected to exhibit significantly smaller dispersivity. *Domenico and Schwartz (1990), Physical and Chemical Hydrogeology, John Wiley*.	Upper bound employed, model is not sensitive to this parameter.
Partition coefficient (Koc / Kd) for isolation sand and underlying sediment: Fixed value used for VOCs in deterministic simulations (best estimate – mean value). Distribution used for VOCs in probabilistic simulations. For mercury, phenol,	Site-specific for VOCs and mercury Literature for PCBs, PAHs, and phenol	Log Koc values for VOCs (mean and standard error[1]) calculated using regression of paired sediment/porewater measurements from Phase I-VI data. Normal distribution of log Koc specified based on these values for probabilistic simulations. Paired data were also used for estimating mercury Kd's in the native sediments (for use in numerical modeling); *see Attachment 2.* No paired sediment/porewater data existed for the WB1-8 and the WBB Outboard areas, so Koc/Kd values were set equal to those estimated for lake areas based on similarities in properties (e.g., due to elevated pH conditions and presence of	The variability observed is likely due to sampling methodology and analytical limitations. To evaluate the impact of this variability, the distribution for log Koc is modeled by a normal distribution defined by the mean and standard error, with the standard error representing uncertainty about the mean value. For the literature-based values used for PAH, PCB, and phenol modeling, uncertainty was not represented, since there is no information available to estimate site-specific variation in the values derived from NYSDEC Guidance.

1 The uncertainty in the mean is characterized by the standard error, as opposed to the standard deviation, which characterizes the variability of individual values. Therefore, distributions used in the probabilistic analysis were mostly normal or lognormal distributions developed using the mean and the standard error (= standard deviation / sqrt (number of observations)) of the data (or the log transformed data in the case of a lognormal distribution).

Model Input	Site-specific or Literature Based	Reference	Rationale
PCBs, and PAHs: a fixed value was used for all simulations.		waste material in the WBB-West area, the Koc/Kd values were based on those from ILWD). Literature value used for phenol based on *NYSDEC Technical Guidance for Screening Contaminated Sediment (NYSDEC, 1999))*. Values used to represent partitioning to cap material for PAHs and PCBs based on NYSDEC screening guidance values; corrected literature values to represent partitioning in underlying sediment, as described in *Attachment 2*. Mercury partitioning coefficients for sand based on data from: *Reible, D, 2009. Phase IV Addendum 2 Report –Isotherm Experiments with Organic Contaminants of Concern with Sand, Organoclay and Peat and for Mercury with Sand, Organoclay, Peat and Activated Carbon.*	
Porosity (isolation and habitat layers): Fixed value	Literature	Fixed value of 0.4, based on porosity testing of the capping material conducted in January 2012.	Little to no spatial variability or uncertainty anticipated. Given the relatively small percent by weight or volume of GAC that will be present in the isolation layer the value of 0.4 is also appropriate for the bulk mixed media. In places where the habitat layer will consist of gravel material, use of this value is also appropriate because: 1) the porosity of typical gravel material would likely only be slightly lower than this value; 2) the model is not sensitive to such small differences in

Model Input	Site-specific or Literature Based	Reference	Rationale
			porosity. For example, Domenico and Schwarz (1990) list the following ranges of porosity values for sands and gravels: • Gravel, coarse: 0.24 to 0.36 • Gravel, fine: 0.25 to 0.38 • Sand, coarse: 0.31 to 0.46 • Sand, fine: 0.26 to 0.53
Porosity (underlying sediment): Fixed value	Site-specific	Average porosity in each area modeled (A1, E1, E2, etc.) was calculated from sediment/soil samples collected in that area. *Honeywell Onondaga Lake Locus Database, 2010.*	The critical model input parameter is the initial porewater concentration (C_0), which was either measured or calculated from sediment data. Since the calculated value is a function of sediment characteristics such as fraction organic carbon, porosity and particle density (along with sediment contaminant level), it is difficult to coherently apply distributions to all these parameters simultaneously. The decision was made to prioritize C_0, and use fixed values for the underlying sediment characteristics. Model is not sensitive to this parameter.
Particle density of sand cap material (un-amended isolation layer and habitat layer) and underlying sediment: Fixed value	Literature	Fixed value of 2.6 g/cm^3 *Freeze, R.A., Cherry, J.A. 1979. Groundwater. Prentice-Hall, Inc., Englewood Cliffs, New Jersey.*	Little to no spatial variability or uncertainty anticipated. Model is not sensitive to this parameter. This value is appropriate for either a sand or gravel habitat layer.
GAC concentration in GAC amended	Design parameter	The transient numerical model was developed to primarily simulate a sorptive amendment as a thin layer that consists	Value for each amended cap area determined as part of design to establish

Model Input	Site-specific or Literature Based	Reference	Rationale
layer: Fixed value		entirely of amendment material (i.e., placement as a mat). In order to simulate a bulk mixture of sand and GAC in a single layer, the input parameters for the "active layer" in the model are specified such that the thickness of the layer equals the thickness of the bulk media, and that the specified thickness, along with the input values for "particle density", which in this case refers to the GAC concentration (mass of GAC per unit volume of mixed media), and porosity of that layer result in the desired GAC application rate. For example, to achieve a GAC application rate of 0.3 lb/ ft^2 over a 12" layer of bulk sand and GAC, the following are specified for model inputs in that layer: • thickness: 30.48 cm • porosity: 0.4 • GAC concentration: 0.008 g/cm^3 and the resulting GAC application rate is: *(0.008 g/cm^3) * (1-0.4) * (30.48 cm) * (1 lb / 453.6 g) * (30.48 cm / $ft)^2$ = 0.3 lb/ft^2* Essentially, the input value for GAC concentration accounts only for the mass of GAC amendment in the layer. Setting the parameters in this way implicitly (and conservatively) assumes that the sand material in the amended isolation layer has no sorptive capacity.	recommended GAC application rate.
foc (sand material used for isolation layer and lower portion of habitat layer): Fixed value	Site-specific	Model input value based on the average foc of 0.022 percent (222 mg/kg) measured in samples of the sand cap material during the Phase VI PDI. *Honeywell Onondaga Lake Locus Database, 2010.*	Little to no spatial variability or uncertainty anticipated. This value for foc is also applicable in the lower portion of the habitat layer (e.g., below the upper mixing zone). In areas where the habitat layer will consist of gravel materials, the foc is

Model Input	Site-specific or Literature Based	Reference	Rationale
			anticipated to be minimal, so this value is applicable for gravel habitat layer material as well.
foc (underlying sediment): Fixed value	Site-specific	Average values calculated from individual sediment/soil sample results collected in each modeling area. *Honeywell Onondaga Lake Locus Database, 2010.*	The critical model input parameter is the initial C_0, which was either measured or calculated from sediment data. Since the calculated value is a function of sediment characteristics such as fraction organic carbon, porosity and particle density (along with sediment contaminant level), this makes it difficult to coherently apply distributions to all these parameters simultaneously. The decision was made to prioritize C_0, and use fixed values for the underlying sediment characteristics. Model is not sensitive to this parameter.
foc (upper 6 inches of the habitat layer in lake areas or upper 8 inches of the habitat layer in wetland areas): Fixed value (best estimate) for deterministic simulations. Distribution for probabilistic simulations.	Site-specific and literature	For lake model areas except Remediation Area A: Normal distribution based on mean and standard error of site-specific (ln-transformed) TOC data in the top 6 inches of lesser-impacted non-ILWD SMUs (SMU 4 and 5); length weighted averages were developed for cores where multiple sample intervals were collected in the top 0-6". *Honeywell Onondaga Lake Locus Database, 2010.* For wetland model areas (WB1-8, WBB-West, WBB-Center, WBB-East): average value of 10 percent was used for deterministic simulations and uniform distribution ranging from 5 to 15 percent was used for probabilistic simulations. These same values were used for modeling Remediation Area A (due to the presence of an in-lake planting habitat module over a large portion of that area) and for location-specific modeling conducted to evaluate the 25-ft wide planting areas	Inherent uncertainty exists in trying to estimate the ultimate post-remedy TOC that will be established in the upper layer of the sediment cap within the lake. Site-specific data may provide a suitable estimate of this input parameter in areas of the lake not impacted (or impacted to a lesser degree) by Metro processes and Solvay Waste materials, both of which tend to produce higher TOC values. To address the uncertainty around future TOC levels in the upper layer of the cap data in the 0-6 inches interval from SMUs 4 and 5 were used to develop a range of surficial TOC. The SMU 4/5 data do not exhibit any spatial structure and are expected to be an overestimate of post-remedy TOC given recent decreases in

Model Input	Site-specific or Literature Based	Reference	Rationale
		along the Remediation Area D shoreline. Expected range of foc in wetland soils of 5 to 15 percent is generally consistent with site-specific data (SYW-10 and Geddes Brook floodplain) as well as literature (e.g., Bruland et al. 2006). *Bruland, G. L., and C. J. Richardson. 2006. Comparison of soil organic matter in created, restored and paired natural wetlands in North Carolina. Wetlands Ecology and Management 14:245–251.*	organic loading and lake productivity associated with Metro upgrades. This data set was described by a log normal distribution represented by the mean and standard error. This value for foc is based on the assumption that clean sediment will be deposited in the habitat layer over time. This assumption is not impacted by the application of a sand or gravel habitat layer material. Higher foc values for wetland areas based on literature and measurements in other constructed wetlands.
Freundlich coefficients for GAC: Fixed value (best estimate based on nonlinear regression of isotherm data) for deterministic simulations. Distribution for probabilistic simulations based on sampling from 95 percent joint confidence region.	Site-specific	Isotherm experiments were conducted by Carnegie-Mellon to establish sorption characteristics of the proposed activated carbon to be used. Parsons conducted a series of isotherm experiments during the Phase VI PDI to verify the Carnegie Mellon results, reduce variability through analysis of triplicate samples, and account for impacts of neutralized pH. Model inputs were based on the Phase VI isotherm data and data collected following the same methodology for the Wastebed B Outboard Area. *Draft Report submitted in February 2011, updated draft report provided in October 2011 which included results from WBB isotherm studies.* Naphthalene isotherm parameters were conservatively used to represent isotherm parameters for PAHs and PCBs.	The best estimates of Kf and 1/n (as determined by nonlinear regression of the isotherm data) were used for deterministic model runs. In order to quantify uncertainty around the mean values used for Kf and 1/n, a 95 percent confidence region was generated around the means, and estimates of the coefficient pairs randomly taken from within that range were used for the probabilistic simulations. The 95 percent confidence interval was generated directly from experimental data (a two parameter (Kf, 1/n) nonlinear sorption isotherm).

Model Input	Site-specific or Literature Based	Reference	Rationale
Boundary layer mass transfer coefficient: Fixed value	Site-specific	Fixed value of 0.363 cm/hr. Eqn 11 of *Thibodeaux and Becker, 1982 (4 m/s windspeed, 5m water depth, benzene, 500m fetch). Thibodeaux, L. J., and Becker, B., (1982). "Chemical transport rates near the sediment of a wastewater impoundments", Environmental Progress, Vol 1; no. 4, p 296-300.*	Little to no spatial variability or uncertainty anticipated.
Particle biodiffusion coefficient (upper mixing zone [top 6"] of habitat layer): Fixed value (best estimate) for deterministic simulations. Distribution for probabilistic simulations.	Literature	Normal distribution of log transformed values. *Thoms, S.R., Matisoff, G., McCall, P.L., and Wang, X. 1995. Models for Alteration of Sediments by Benthic Organisms, Project 92-NPS-2, Water Environment Research Foundation, Alexandria Virginia*	Uncertainty associated with size, depth and distribution of benthic organisms. Data from freshwater sites employed to generate a lognormal distribution.
Porewater biodiffusion coefficient (upper mixing zone [top 6"] of habitat layer): Fixed value (best estimate) for deterministic simulations. Distribution for probabilistic simulations.	Literature	Normal distribution based on mean and standard error of log transformed values derived from literature. *Wood, L.W. (1975) Role of oligochaetes in the circulation of water and solutes across the mud-water interface. Verhandlungen der Internationalen Vereinigung fur Theoretische und Angewandte Limnologie. 19: 1530-1533. Svensson, J.M., and L. Leonardson. (1996) Effects of bioturbation by tube-dwelling chironomid larvae on oxygen uptake and denitrification in eutrophic lake sediments. Freshwater Biology. 35: 289-300. Cunningham (2003) Unpublished PhD dissertation, Louisiana State University, D. Reible, Advisor.*	Uncertainty associated with size, depth and distribution of benthic organisms. Data from freshwater sites employed to generate a lognormal distribution.

Model Input	Site-specific or Literature Based	Reference	Rationale
Darcy velocity: Fixed value (best estimate – mean value) for deterministic simulations. Distribution for probabilistic simulations.	Site-specific	Site-specific groundwater upwelling data used to generate an empirical cumulative distribution function for the data sets in Model Areas A1, A2, C2 and Remediation Area E (Model Areas E1, E2, and E3 combined). Upwelling velocities used in Remediation Areas B, C (excluding Model Area C2) D, WBB-East, WBB-Center, WBB-West, and WB 1-8 were based on the best estimate of conditions that would exist once the upland hydraulic containment systems are in place. To represent these anticipated conditions in the cap modeling, a probabilistic simulation approach was used to calculate a distribution of upwelling velocities within each modeling area. These simulated distributions were generated based on the variations in hydraulic conductivity, hydraulic gradient, and thickness of the underlying clay layer, and were found to closely follow lognormal distributions, which formed the basis of the model inputs. Further detail is provided in Appendix C. In all cases, the best estimate (i.e., mean value) of the distribution was used for deterministic simulations, and probabilistic modeling was based on sampling from the full distributions (empirical CDF or lognormal), as provided in Appendix C.	Simulation of separate sub-areas and model areas (with the exception of Remediation Area E as described below) captures major spatial variation in upwelling rate (resulting from differences in underlying clay thickness and underlying sediment/soil structure). The impacts of smaller-scale variations in upwelling within these subareas/model areas are quantified by the probabilistic results (i.e., the distribution in outputs captures measurement uncertainty as well as spatial variability). No significant spatial variability was observed within Remediation Area E; thus, data from the three model areas were pooled and used to specify the same CDF for each individual area. Additional discussion on groundwater data sets used in the modeling is provided in Appendix C.
Biological decay rate (isolation and habitat layers): Fixed value	Site-specific	Anaerobic biological degradation rates for VOCs including benzene, toluene, xylene, ethylbenzene, chlorobenzene, dichlorobenzene, trichlorobenzene, phenol and naphthalene based on slow end of literature range used in the FS. Based on the results of the site specific bench testing, safety factors were applied to the FS decay half lives for benzene, chlorobenzene and naphthalene (1.5, 3.0, and 2.0, respectively). Resulting decay half lives used in the modeling were as follows: benzene	The modeling evaluation employed literature-based degradation rates that are consistent with or more conservative than anaerobic decay rates measured in the site specific testing. Safety factors were applied to benzene, chlorobenzene and naphthalene half lives to account for variable results in the site-specific testing. Degradation was

Model Input	Site-specific or Literature Based	Reference	Rationale
		1,080 days, chlorobenzene 1,800 days, dichlorobenzene 720 days, ethylbenzene 228 days, toluene 365 days, trichlorobenzene 720 days, xylene 767 days, naphthalene 450 days, phenol 28 days. *Howard, P.H., R.S. Boethling., W.F. Jarvis., W.M. Meylan, and E.M. Michalenko. 1991. Handbook of Environmental Degradation Rates. Lewis Publishers, Inc., Chelsea, Michigan.* *Interim Report on Phase V PDI Biotreatability Study Interim Report submitted in July 2010, results of additional testing and supplemental analysis provided to DEC via e-mail in May and June 2011.*	also conservatively omitted in the WBB-East Model Area since a few porewater samples in that area indicate elevated pH, and no pH amendment is included in the cap for that area.
Lag time for biological decay: Fixed value	Literature	Lag time is used in the model to represent a period over which microbial populations capable of degrading the compounds of interest (i.e., VOCs) build up and acclimate. Lag time of 5 years was specified for areas with native pH <=8; lag time of 100 years was specified for pH-amended areas.	Longer lag times used in pH amendment areas given expected time for pH equilibration in cap following initial consolidation period (see Appendix I).
Consolidation induced porewater expression: Fixed value that varies over time	Site-specific	For each remediation area, a power function was used to represent the cumulative consolidation-induced porewater flux over time. These functions were developed based on conservative estimates of the consolidation flux (primary and secondary) for each remediation area: • Within non-ILWD areas, the maximum settlement magnitude and corresponding time rate of settlement within each remediation area, which takes into account the full range of sediment characteristics and consolidation parameters, was used to develop power function parameters. • For the ILWD, the consolidation flux parameters of	Values selected to represent conservative estimates of the total porewater flux associated with consolidation and timeframe over which such consolidation would occur in each remediation area based on settlement estimates, as described in Appendix E.

Model Input	Site-specific or Literature Based	Reference	Rationale
		the subarea within ILWD having the highest settlement estimate (using average/representative consolidation parameters within that subarea) was used for modeling of all four ILWD model areas. Model sensitivity analyses were conducted to evaluate alternate upper bound values as well (see Attachment 6 to Appendix B of this design report). The total consolidation used in the model ranges from 0.67 ft (Remediation Area D) to 3.1 ft (Remediation Area E). The time to reach 90 percent of those values varies from approximately 3 years (Remediation Areas A, B, and E) to around 20 years (Remediation Area D). The time-derivative of the resulting consolidation vs. time curve is used by the model to calculate a time-varying upwelling velocity that is added to the base-upwelling rate input to the model. This process was modeled over a 30-year timeframe (because at longer times, the incremental upwelling velocity becomes negligible). Details are provided in Appendix E.1 for non-ILWD areas and in Appendix E.2 for the ILWD and the Outboard Area. Consolidation in WB 1-8 was assumed to be the same as that estimated for the adjacent Remediation Area B.	

TABLE A1.2
CORRECTION FACTORS FOR POREWATER CONCENTRATIONS

Porewater Sample Collection Method	Correction Factor
Peepers (Phases I, II & III)	
Xylenes (total)	1.1
Chlorobenzene	1.1
Toluene	1.1
Ethylbenzene	1.1
Benzene	1.1
1,3-Dichlorobenzene (phases I & II)	1.2
1,3-Dichlorobenzene (phase III)	1.1
1,4-Dichlorobenzene (phases I & II)	1.2
1,4-Dichlorobenzene (phase III)	1.1
1,2-Dichlorobenzene (phases I & II)	1.2
1,2-Dichlorobenzene (phase III)	1.1
Naphthalene (phases I & II)	1.2
Naphthalene (phase III)	1.1
Mercury (Tuffryn)	1.1
1,2,4-Trichlorobenzene (phases I & II)	1.2
1,2,4-Trichlorobenzene (phase III)	1.1
1,2,3-Trichlorobenzene (phases I & II)	1.2
1,2,3-Trichlorobenzene (phase III)	1.1
1,3,5-Trichlorobenzene (phases I & II)	1.2
1,3,5-Trichlorobenzene (phase III)	1.1
Centrifuge (Phases I, II, III & IV)	
Xylenes (total)	1.11
Chlorobenzene	1.11
Toluene	1.08
Ethylbenzene	1.07
Benzene	1.09
1,3-Dichlorobenzene	1.10
1,4-Dichlorobenzene	1.14
1,2-Dichlorobenzene	1.15
Naphthalene	1.54
Mercury	1.06
1,2,4-Trichlorobenzene	1.45
1,2,3-Trichlorobenzene	1.53
1,3,5-Trichlorobenzene	1.07

ADDENDUM 1

CUMULATIVE DISTRIBUTION FUNCTIONS FOR POREWATER CONCENTRATION

The contaminant concentrations in the porewater of the sediments underlying the cap were characterized by data collected in Onondaga Lake. There were certain cases where the presence of a relatively high proportion of non-detect results introduced uncertainty at the lower end of the concentration distribution. For example, Figure A.1 shows the distribution of ethylbenzene concentrations in SMU 2, with non-detect sample concentrations plotted at the detection limit (5 ug/L) as green open symbols. Clearly, assuming all non-detect results are equal is inappropriate, whether at the detection limit which would be overly conservative or at zero which is equally inappropriate.

The approach used to estimate the full distribution of contaminant concentrations was based on the observation that the detected concentrations generally follow a log-normal distribution (that is, the detected data are roughly linear in Figure A.1); thus a reasonable and logical assumption is that the non-detect concentrations follow this same distribution. A cumulative distribution function was derived based on the detected concentrations, and this function was then used to estimate values for the non-detect results. Specifically, a truncated log-normal distribution was fit to only the detected concentrations by fitting a linear regression to predict log-concentration from the normal z-score values (i.e., a regression through the green filled symbols was used to generate the resulting black line in Figure A.1). Z-score values were assigned assuming all of the detected concentrations were higher than the non-detect sample results. The fitted regression line was then used to predict log-concentrations for the normal z-score values attributed to the non-detect samples (see open symbols in Figure A.1). Finally, the empirical cumulative distribution function was used to characterize the distribution of porewater concentrations for the probabilistic simulations, restricted to the range of detected and estimated concentrations. This approach is recommended by Ginevan and Splitstone 2004.

Figure A.1

Ethylbenzene concentrations in the porewater of sediment from SMU2

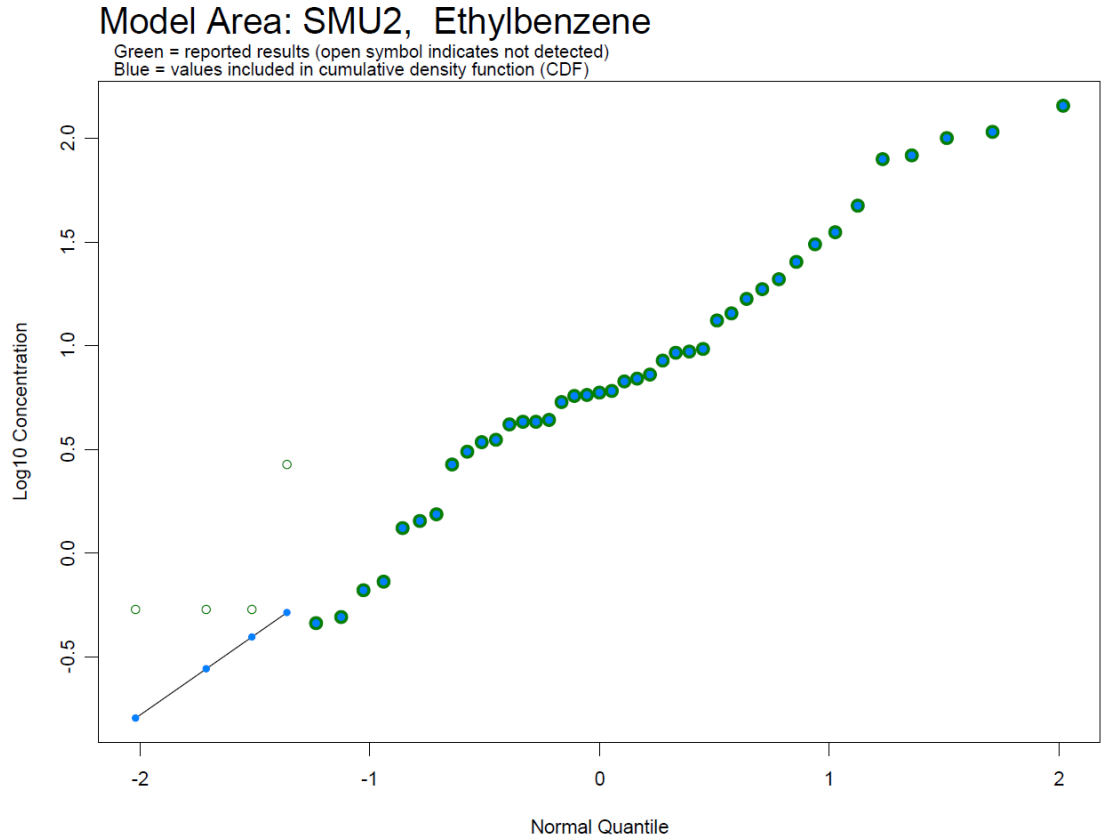

Reference:

Ginevan, Michael E., and Douglas E. Splitstone, 2004. Statistical tools for environmental quality measurement. CRC Press LLC. p. 229.

ATTACHMENT 2

PARTITIONING COEFFICIENTS AND SEDIMENT TO POREWATER CALCULATIONS

ATTACHMENT 2

PARTITIONING COEFFICIENT EVALUATION AND SEDIMENT TO POREWATER CALCULATION BASIS

Partitioning coefficients were employed in various aspects of the cap modeling evaluation to describe the equilibrium relationship between contaminant concentrations in the dissolved and sorbed-to-sediment phases within the cap materials as well as in the underlying sediments. This attachment discusses the basis for the selected partitioning coefficients as well as the calculations used to derive porewater concentrations from sediment data or vice versa.

The following sections describe the methods used to estimate partition coefficients for use in the model based on site-specific data or literature studies. Due to differences in data availability, varying methods were used to develop partition coefficients for the different classes of modeled CPOIs (i.e., VOCs, mercury, phenol, PAHs and PCBs). As such, the classes of CPOIs are discussed separately in the sections below.

1.0 PARTITIONING COEFFICIENT EQUATIONS

Partitioning coefficients, by definition, relate equilibrium porewater concentrations to sorbed-to-sediment concentrations. Since the laboratory-reported sediment concentrations for this project account for contaminants in all phases (i.e., sorbed, dissolved, vapor, and NAPL) per dry weight of sediment, the calculation of a partitioning coefficient must relate to this total sediment concentration. The partitioning equation derived from the EPA's Soil Screening Guidance (EPA, 1996) equation 22 of Part 2 (reorganized) for non-NAPL-impacted material is:

$$K_d = \frac{C_{sed}}{C_{pw}} - \frac{\theta}{\rho_b}$$

where

C_{sed} equals the total sediment concentration (dry weight) of the CPOI (µg/kg),
C_{pw} equals the core dissolved porewater concentration (µg/l),
θ is porosity, and
ρ_b is dry bulk density (kg/L).

For hydrophobic organics, the equation is:

$$K_{oc} = \frac{\left[\frac{C_{sed}}{C_{pw}} - \frac{\theta}{\rho_b} \right]}{f_{oc}}$$

where

f_{oc} is the mass fraction of organic carbon of the raw sediment.

The equation, as laid out, assumes there is no NAPL in the sample. The principal reason for doing this is that it is not possible to test for the presence of NAPL using a sample's CPOI

concentrations without first knowing the Koc values. Therefore, the use of this equation would provide an overestimate of mean Koc values since a NAPL-impacted sample would exhibit a higher total sediment concentration than what would be indicated by equilibrium with its porewater phase. This issue affects the assessment of sediments in SMU 1, where NAPL has been observed. However, it is not expected that the presence of NAPL in some of the samples would materially affect the overall estimates, given the large number of usable data pairs in SMU 1 and the lognormal distribution of the data.

As noted above, partition coefficients relate equilibrium porewater concentrations to sorbed-to-sediment concentrations, not to the total sediment concentration as measured in the PDI sampling program. While this distinction, which suggests it is important to account for contaminant mass in the dissolved-phase of a sample, is meaningful for low sorptivity compounds, it is not actually important for highly sorptive compounds. This is due to the fact that for highly sorptive compounds, such as PAHs and PCBs, very little contaminant mass is held in the dissolved-phase of a sediment sample. Therefore in calculating PAH and PCB porewater concentrations from measured sediment concentrations, it is only necessary to also know the f_{oc} of the sediment sample. This procedure actually adds a very small element of conservatism to the estimation of porewater concentration, since complete accounting for the dissolved-phase mass in the sample would lower the estimate of porewater concentration.

For PAHs and PCBs, the equation for calculating the local porewater concentration is:

$$C_{pw} = \frac{C_{sed}}{K_{oc} \bullet f_{oc}}$$

2.0 DEVELOPMENT OF SITE SPECIFIC PARTITIONING COEFFICIENTS FOR VOCs

The analysis of paired sediment and porewater samples, generated via centrifugation procedures in Phases I through VI of the PDI, provided an opportunity to estimate site-specific partitioning coefficients for Onondaga Lake sediments, in the form of an organic carbon-water partitioning coefficient (K_{oc}) for Benzene, Toluene, Ethylbenzene, Xylene, Tri-cholorobenzene, Di-chlorobenzene, chlorobenzene and naphthalene. This section describes the sample processing procedures, and the calculations and analysis methods used to estimate the partitioning coefficients from the sample data (including filtering of the dataset to eliminate unusable results). Results are presented in graphical and tabular formats. The site specific partitioning coefficients generated as described in the following subsections were used in cap modeling to predict partitioning within the sand cap materials used in the chemical isolation and habitat layers, as well as within the underlying sediments for the numerical modeling.

2.1 SAMPLE COLLECTION AND PROCESSING

In Phase I of the PDI, samples of sediment and porewater were collected at 33 locations in SMU 1 and SMU 6. No paired sampling was conducted in Phase II for the purpose of estimating partitioning coefficients. The total number of sample pairs was greatly increased by work

conducted in Phases III through IV. In total over 1,000 samples pairs were collected across the remediation areas over the course of the PDI.

In Phase I, three cores were collected at each location and depth interval to provide material for sediment and porewater analyses. Upon receipt in the lab, the cores were opened and freestanding water decanted and discarded. No homogenization of sediments occurred. One core was used for raw sediment analysis, and the other two were used to fill between four and six centrifuge bottles, which were then centrifuged to generate porewater. All generated porewater was then composited prior to sub-sampling for the various analyses. One of the centrifuged bottles provided material for the dewatered sediment analysis. A sample pair from Phase I, for the purposes of calculating partition coefficients, was comprised of a dewatered sediment sample and an associated porewater sample.

In Phases III through VI, long cores were cut into 2-ft. sections. Upon receipt in the lab the 2-ft. cores were opened, and freestanding water carefully decanted for compositing with porewater subsequently generated by centrifugation of the sediment sample. A portion of the sediment sample from the top of the core was sub-sampled for raw sediment analyses. The balance of the sediment from the 2-ft. core was weighed and placed in centrifugation bottles. The sample bottle was centrifuged and supernatant water was separated and collected. The aqueous sample for volatile organic compounds (VOCs) was then centrifuged again, decanted and placed in volatile organic analyte (VOA) vials for analysis. A sample pair from Phases III through VI, for the purposes of calculating partition coefficients, was comprised of a raw sediment sample and an associated porewater sample.

2.2 AREA-WIDE PARTITION COEFFICIENT ANALYSIS

The partition coefficients estimated from the site data used in the cap modeling effort were developed based on the hypothesis that a single mean partition coefficient could be used to describe the site data within a given area, and that sample-to-sample differences within these areas stem primarily from measurement variability. This is consistent with the fact that partition coefficients are often taken to be chemical-specific properties (after properly normalizing for organic carbon content as appropriate). To estimate the effective partition coefficient for an area containing numerous sediment-porewater sample pairs, the sorbed-to-sediment phase concentration was first calculated for each sample pair. This concentration was calculated by taking the reported total dry weight concentration (Csed in the equations above) and subtracting off the porewater mass (using the measured corrected porewater concentration (see Table A1.2), bulk density, and porosity):

$$C_s = C_{sed} - \left(C_{pw} \frac{\theta}{\rho_b} \right)$$

where Cs is the sorbed-to-sediment phase concentration of a CPOI (µg/kg).

After calculating Cs for all samples within an area, the concentrations were normalized by foc and plotted against their paired porewater concentrations. Plotting these values against porewater concentration in linear space produces a relationship with a slope that is equivalent to Koc. Thus, a least squares regression analysis can be used to calculate the Koc for a given area (and the confidence interval of the regression line can describe its variability). Preliminary analyses indicated that such regressions could be strongly influenced by the highest concentration data pairs. Given that porewater concentrations within the cap would be expected to be within a lower range, the underlying regression equation (Cs/foc = Koc*Cpw) was log-transformed to remove the effect of a few high concentration samples driving the regression and therefore all measurements were treated as having the same standard error. By doing this, it was equivalent to the model: log (Cs/foc) = log (Koc) + log (Cpw). Least squares regression formulae were derived for this case, which produced a best estimate of log Koc and an associated standard error. The log-transform was judged appropriate since Koc values are typically found to be lognormally distributed (and are hence typically reported as log Koc).

For the cap modeling effort, the analysis method described above was used to estimate a Koc value for each modeled VOC. The data from Remediation Areas A and E were pooled together, and data from Remediation Area D were analyzed separately since previous analyses had suggested partitioning within ILWD materials differs from that in sediments from other areas of the lake. Data from Remediation Areas B and C were compared with these two groupings and found to exhibit a relationship between particulate and dissolved phase that more closely resembled that of the ILWD. As such, the data from Remediation Areas B, C, and D were combined for the purposes of calculating Koc values for the VOCs. Koc values were also required for modeling of the Wastebed 1-8 connected wetlands (referred to hereafter as WB1-8) and in the three model areas of the Wastebed B Outboard area (referred to hereafter as WBB-West, WBB-Center, and WBB-East). No paired sediment/soil and porewater samples were collected during the investigations conducted in these areas. Therefore, Koc values for these areas were assigned based on those developed from areas of the lake having similar sediment characteristics.

2.3 FILTERING OF DATA PAIRS

After compiling the data from PDI Phases I through VI, any data pair (sediment and porewater) which involved a non-detect result was excluded from the analysis, given the uncertainty of the resulting calculation. Additionally, any result which produced a negative value for the sorbed-to-sediment concentration from the above equation was deleted. This would occur when the CPOI mass measured in the porewater phase exceeded the total CPOI mass measured in the bulk sediment (i.e., solids plus porewater). Since such a scenario—where the total contaminant mass (bulk sediment concentration) is insufficient to produce the measured mass in the dissolved-phase (porewater concentration)—is not possible, even though the analytical results support it, the assumption is that there is some error in one or more of the analyses, and therefore the data pair does not allow for calculation of a partitioning coefficient. Such occurrences were rare (≈ 8% of sample pairs), with nearly half involving benzene, the least sorptive of the compounds considered in this analysis.

In an effort to assess the potential effects of surface water on porewater concentrations in the surficial samples, the data set was also sorted and samples collected in the 0-1 ft interval were eliminated.

2.4 RESULTS

Following the filtering step described in Section 2.3, the log-transformed regression analyses described in Section 2.2 were conducted. Figures 1 through 12 present these regressions, the resulting Koc values, and standard errors (derived from the confidence limit on the regression line). The data and regression lines on Figures 1-12 indicate that while there is scatter in the data (the degree to which varies by CPOI), when taken together, data from Areas A/E and from Areas B/C/D exhibit a relatively consistent relationship between sorbed-to-sediment and porewater concentrations, with standard errors of regression equal to or less than 0.1 log units (for CPOIs with at least 50 sample pairs or more). The presence of such a relationship is consistent with the concept of the area-based approach used in this analysis. The resulting Koc values tend to differ between Areas B/C/D and Areas A/E, with the former group's values being somewhat higher (on average approximately one-third of a log value across CPOIs) – this difference is consistent with results from previous analyses and likely attributable to the effects of elevated pH within the ILWD materials and/or differences related to the solid matrix of waste material versus natural sediment.

For each CPOI, Table 1 presents the number of data pairs, the resulting Koc values and associated standard errors, and includes a comparison to a range of literature values. The differences in resulting Koc values among these CPOIs follow expected trends (e.g., Koc of chlorbenzenes increases with chlorination level from monochlorobenzene to dichlorobenzenes to trichlorobenzenes), and the calculated values are within the range of the literature values.

As such, the values listed in Table 1 for Areas A/E were used to describe the partitioning of VOCs to sand capping materials in all model areas. These same values were used to simulate partitioning of VOCs within the underlying sediment in the application of the numerical model to Remediation Areas A and E, as well as the WBB-East area, which is similar to these two lake

areas in that there is limited to no impact from ILWD-like materials. Likewise, the Koc values estimated from the Remediation Area B/C/D data set were used to describe partitioning within the underlying sediment/waste materials within those areas, for use in the transient numerical modeling. These values were also used in transient modeling of the underlying sediment in WB1-8, WBB-Center, and WBB-West, because the soil/sediments in these areas are similar in nature to those in the ILWD. The differences in Koc between ILWD and non-ILWD materials are believed to be due to elevated pH and/or solid matrix differences between ILWD materials and natural sediment as discussed above; however, the Koc values derived from non-ILWD data were used to simulate sorption to sand capping materials within the ILWD, Remediation Areas B and C, and Model Areas WB1-8, WBB-West, and WBB- Center because the pH amendment to the cap is designed to lower pH in the isolation layer. Thus, the amended cap approach within these high pH areas is designed to eliminate these effects and result in partitioning behavior within the isolation layer that is consistent with that in other capped areas of the lake.

2.5 MERCURY PARTITIONING COEFFICIENTS

Unlike VOCs, the partition coefficients used for simulating mercury were expressed as a Kd value, since organic carbon is not the only significant sorbing phase for mercury. The values used in the cap modeling conducted for mercury were developed as follows:

- Kd values for the underlying sediment (used in the transient numerical modeling) were calculated from the values for paired sediment / porewater data (i.e., using the data sets/filtering methods described above for VOCs), and the average log Kd for each area was used in the model. This simpler method for calculating the sediment Kd (as compared to the regression-based approach used for VOCs) was used since this parameter only describes the partitioning within the underlying sediment in the numerical model, which has much less influence on predicted concentrations in the cap than the Kd values used to describe partitioning onto capping materials (which are described below). Separate values for the underlying sediment log Kd were calculated for Remediation Areas A, B/C, D, and E, and are presented in Table 2. For the model areas lacking paired sediment-porewater data, underlying sediment mercury Kd values were assigned based on those calculated from data in areas having similar characteristics. Specifically, the Kd for WB1-8 was set equal to that calculated from Remediation Area B and C sediment data, the Kd for WBB-West and WBB-Center was set equal to that calculated from Remediation Area D sediment data, and the Kd for WBB-East was set equal to the average of those calculated from Remediation Area A and E sediment data (due to the generally lower pH and limited to no impact from ILWD-like materials in these areas). The variation in estimated Kd values among these Remediation Areas is believed to reflect differences in the nature of the materials, including elevated pH.

- Kd values for sorption of mercury onto sand capping material in Remediation Areas A and E and in the WBB-East Model Area were estimated based on the data from isotherm studies conducted using porewater from SMU 6/7 sediments (Parsons, 2008). These data were found to best be described by a Freundlich isotherm equation

(Parsons, 2008). As such, the best fit SMU 6/7 isotherm equation was used to calculate a Kd based on the maximum measured porewater concentration in each applicable modeling area. This approach is conservative because at the lower concentrations that would be present in the cap (as compared to the maximum underlying porewater concentration), the SMU 6/7 isotherm relationship produces Kd values that are higher than those calculated for that maximum porewater concentration (thus resulting in even slower transport). The resulting log Kd values for each applicable modeling area (i.e., Model Areas A1, A2, E1, E2, E3, and WBB-East) are presented in Table 2.

- Kd values for sorption onto sand capping material in areas impacted by ILWD-like materials and elevated pH conditions (i.e., Remediation Areas B, C, and D and the WB1-8, WBB-West, and WBB-Center Model Areas) were derived from data generated from isotherm studies performed with SMU 1 porewater (Parsons, 2008). These data were found to follow a linear relationship, so a regression-based approach was used, in which the slope of a linear regression line fit through a plot of sorbed-to-sediment phase mercury concentrations versus porewater concentrations was used to estimate the Kd. The resulting log Kd value is presented in Table 2.

In areas where the isolation cap material will consist of sand mixed with activated carbon as a sorptive amendment, the Kd values described above do not account for any increased sorption of mercury that may occur as a result of the amendment.

3.0 PHENOL PARTITIONING COEFFICIENT

Site-specific porewater data for phenol were limited given the large volumes required or analysis. Additionally, sediment-porewater pairs were not available for the direct estimate of a phenol partitioning coefficient. In lieu of a site specific Koc value the NYSDEC Technical Guidance (NYSDEC, 1999) value for phenol was used to describe partitioning of phenol to both the underlying sediment, to supplement existing porewater data, and to simulate partitioning to the cap material. Similar to VOC compounds, phenol partitioning in the cap model is simulated through use of a Koc value. The Technical Guidance document directly provides an octanol/water partition coefficient or Kow. The Technical Guidance suggests that when applying the equilibrium partitioning methodology Koc and Kow values are very similar, for un-chlorinated phenol the Log Kow value is 2.0 (NYSDEC, 1999). This value was used for phenol in all model simulations.

4.0 PCB AND PAH PARTITIONING COEFFICIENTS

Site specific porewater data were not available for PAH and PCB model simulations. Porewater collected during the 2002/2003 groundwater upwelling investigation were mostly non-detect for PAHs and PCBs (Parsons, 2003 and Parsons, 2007). In the absence of site-specific data for PAHs and PCBs a literature review of partitioning of these compounds was conducted. This information was used to calculate initial porewater concentrations in model simulations as well as to describe partitioning to cap materials.

Modeling conducted during the Feasibility Study had used Kow values reported in New York State Department of Environmental Conservation Guidance (NYSDEC, 1999) as estimates of Koc and measured foc values to estimate the concentrations of PAHs and PCBs in sediment porewater beneath the cap. This same approach was taken in the here when modeling fate and transport of PAHs and PCBs within the sand capping material; however, a growing body of literature indicates that the conventional approach of calculating PAH and PCB porewater concentrations in underlying sediments will overestimate actual PAH or PCB porewater concentrations (for discussions see Arp et al., 2009; Hawthorne et al., 2006; and McGroddy et al., 1996). The primary cause of this discrepancy is that natural sediments are composed of different types of organic carbon, with some phases of organic carbon ("hard" carbon, generally derived from anthropogenic sources) sorbing hydrophobic contaminants stronger but more slowly than other phases ("soft" carbon, generally natural organic matter). For purposes of calculating initial porewater concentrations in the underlying sediment, measured foc values and field-derived effective Koc values measured in natural sediment at other sites that account for strongly-sorbing carbon fractions of sediment, were used. Addendum 1 provides a detailed description of the literature review and partitioning coefficient recommendations.

Recommendations from the evaluation presented in Addendum 1 support the use of corrected PAH and PCB Koc values to most accurately model and predict porewater PAH and PCB concentrations within the underlying Lake sediment in the absence of direct measurements. Based on the data presented in Addendum 1 an increase in effective Koc values of 10X from PAH Kow values is recommended for derivation of PAH porewater concentrations in the non-ILWD impacted sediments (which was taken to consist of Remediation Areas A and E, as well as the WBB-East Model Area). Likewise, based on the data presented in Addendum 1, an increase in effective Koc values of 5X from PCB Kow values is recommended for derivation of PCB porewater concentrations in the non-ILWD impacted sediments. Effective Koc values are based on the values presented in the NYSDEC Technical Guidance. Partitioning in the underlying sediments of the ILWD and within Remediation Areas B and C and the WB1-8, WBB-West, and WBB-Center Model Areas is based directly on the Technical Guidance values, as the presence of ILWD-like material and the unusual pH and DOC conditions in those areas create conditions at variance with natural sediments and so are not addressed by the literature cited above. Partitioning to the cap material is simulated in the model using uncorrected values from the Technical Guidance. Fixed values were used for PAHs and PCBs in all model simulations.

5.0 REFERENCES

NYSDEC, 1999. Technical Guidance for Screening Contaminated Sediments. January 1999.

Parsons, 2003. Groundwater Upwelling Investigation for Onondaga Lake, Syracuse New York. Prepared for Honeywell, Morristown, New Jersey. Syracuse, New York.

Parsons, 2007. Onondaga Lake Pre-Design Investigation, Phase I Data Summary Report. Prepared for Honeywell, Morristown, New Jersey. Syracuse, New York.

Parsons, 2008. Onondaga Lake Pre-Design Investigation: Phase IV Work Plan - Addendum 2 Cap Amendment Isotherm Development. Prepared for Honeywell, Morristown, New Jersey. Syracuse, New York.

USEPA, 1996. Soil Screening Guidance: Technical Background Document, Part 2, page 36, EPA/540/R-95/128, May 1996.

TABLES

Table 1. Summary of log K_{OC} values determined by regression analysis, compared to literature-based values.

	Model Areas B,C, and D			Model Areas A & E			Range of log K_{OC} from regression-based formulas in literature[1]		Range of log K_{OC} from published studies (Mackay, et al.)[2]	
	No. of data pairs	log K_{OC}	std error of regression	No. of data pairs	log K_{OC}	std error of regression	Min	Max	Min	Max
Benzene	192	1.78	0.040	131	1.69	0.051	1.63	1.97	1.26	2.01
Toluene	278	2.34	0.030	140	2.18	0.059	2.31	2.64	2.25	2.39
Ethylbenzene	187	2.77	0.041	127	2.59	0.045	2.77	3.10	2.21	
Xylene	306	2.76	0.029	188	2.53	0.046	2.77	3.10	2.22	2.52
Chlorobenzene	197	2.51	0.037	143	2.29	0.056	2.46	2.79	1.92	2.73
1,2-Dichlorobenzene	191	3.00	0.036	77	2.64	0.073	3.00	3.32	2.26	3.51
1,3-Dichlorobenzene	14	2.77	0.20	126	2.72	0.066	3.00	3.32	2.14	4.60
1,4-Dichlorobenzene	200	3.08	0.038	99	2.60	0.068	3.00	3.32	2.78	3.26
1,2,3-Trichlorobenzene	7	3.67	0.15	1	3.21	--	3.87	4.19	2.30	4.70
1,2,4-Trichlorobenzene	39	3.54	0.057	32	2.82	0.141	3.87	4.19	3.09	4.70
1,3,5-Trichlorobenzene	--	--	--	52	3.05	0.100	3.87	4.19	2.85	5.10
Naphthalene	331	2.86	0.032	114	2.47	0.077	2.99	3.31	2.66	5.00

Notes:

1. Range from several representative regression formulas that correlate K_{OW} to K_{OC} (log K_{OW} values presented in Table 1 of NYDEC's *Technical Guidance for Screening Contaminated Sediments* (http://www.dec.ny.gov/docs/wildlife_pdf/seddoc.pdf) were used).

   These formulas were pooled from the following studies:
   - DiToro, D.M., 1985. A Particle Interaction Model of Reversible Organic Chemical Sorption. *Chemosphere 14* :1503-1538.
   - Karickhoff, S.W., 1981. Semi-empirical estimation of sorption of hydrophobic pollutants on natural sediments and soil. *Chemosphere 10:* 833-846.
   - Means, J.C., S.G. Wood, J.J. Hassett and W.L. Banwart, 1980. Sorption of polynuclear aromatic hydrocarbons by sediments and soils. *Environmental Science & Technology 14:* 1524-1528.
   - Shimizu, Y., S.Yamazaki and Y. Terashima, 1992. Sorption of anionic pentachlorophenol (PCP) in aquatic environments: The effect of pH. *Water Science & Technology 25:* 41-48.
2. Range of values taken from *Illustrated Handbook of Physical-Chemical Properties and Environmental Fate for Organic Chemicals,* Donald Mackay, Wan Ying Shiu, and Kuo Ching Ma, 1992. Only values from studies utilizing field measurements were included.

Table 2. Summary of log K_d values for Mercury.

	Mercury log Kd	
	Underlying Sediment	Sand Cap
Model Area A-1	4.7 [1]	3.3 [3]
Model Area A-2		2.8 [3]
Remediation Areas B & C	2.5 [1]	3.1 [4]
Wastebed 1-8 Wetland	2.5 [2]	
Remediation Area D	3.1 [1]	
WBB Outboard Area West and Center	3.1 [2]	
WBB Outboard Area East	4.4 [2]	4.0 [3]
Model Area E-1	4.2 [1]	3.3 [3]
Model Area E-2		3.8 [3]
Model Area E-3		3.2 [3]

Notes:

1. Values caluclated from paired sediment and porewater data.
2. Values assigned based on data from other lake areas having similar characteristics.
3. Values calculated based on isotherm developed from testing of SMU 6/7 porewater and max. measured porewater concentration in given area.
4. Value based on isotherm developed from testing of SMU 1 porewater.

FIGURES

Relationship between porewater concentration and carbon-normalized sediment concentration (with log-transformed regression)

BENZENE – Model Areas B, C, and D

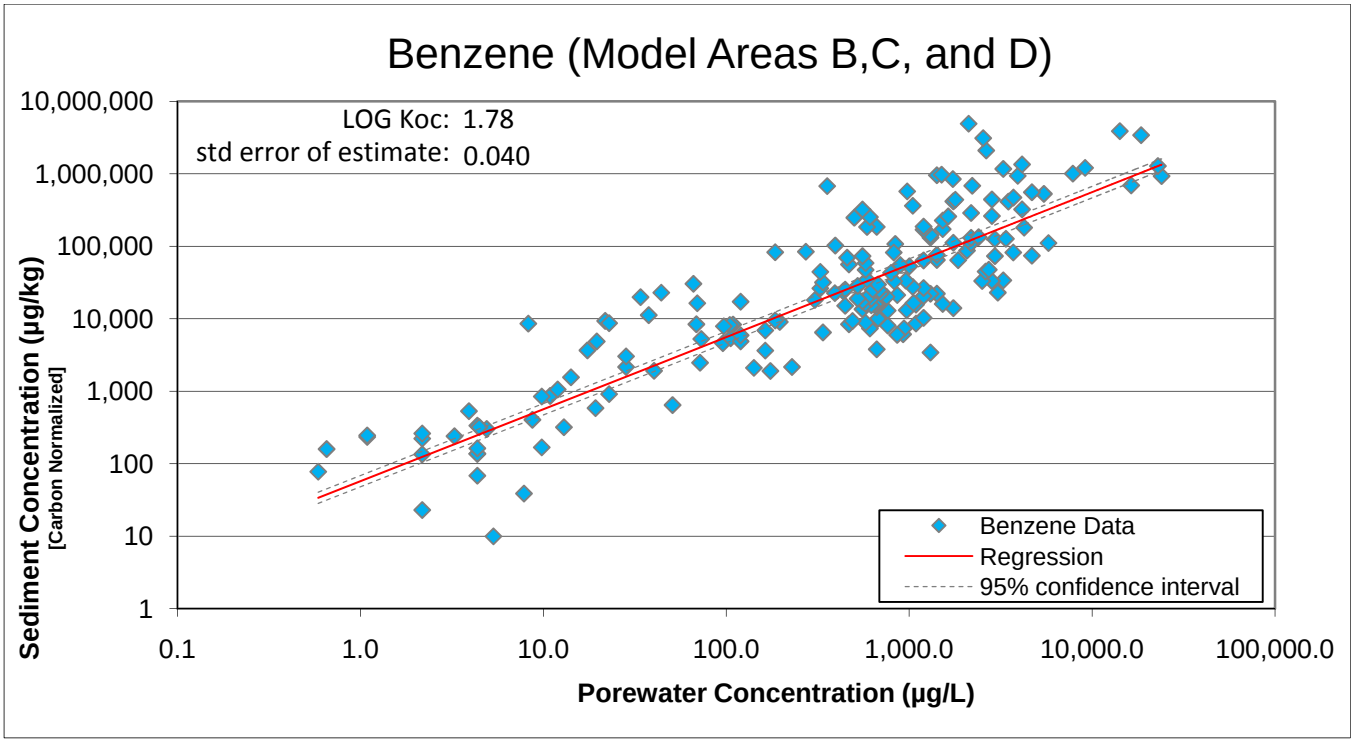

BENZENE – Model Areas A & E

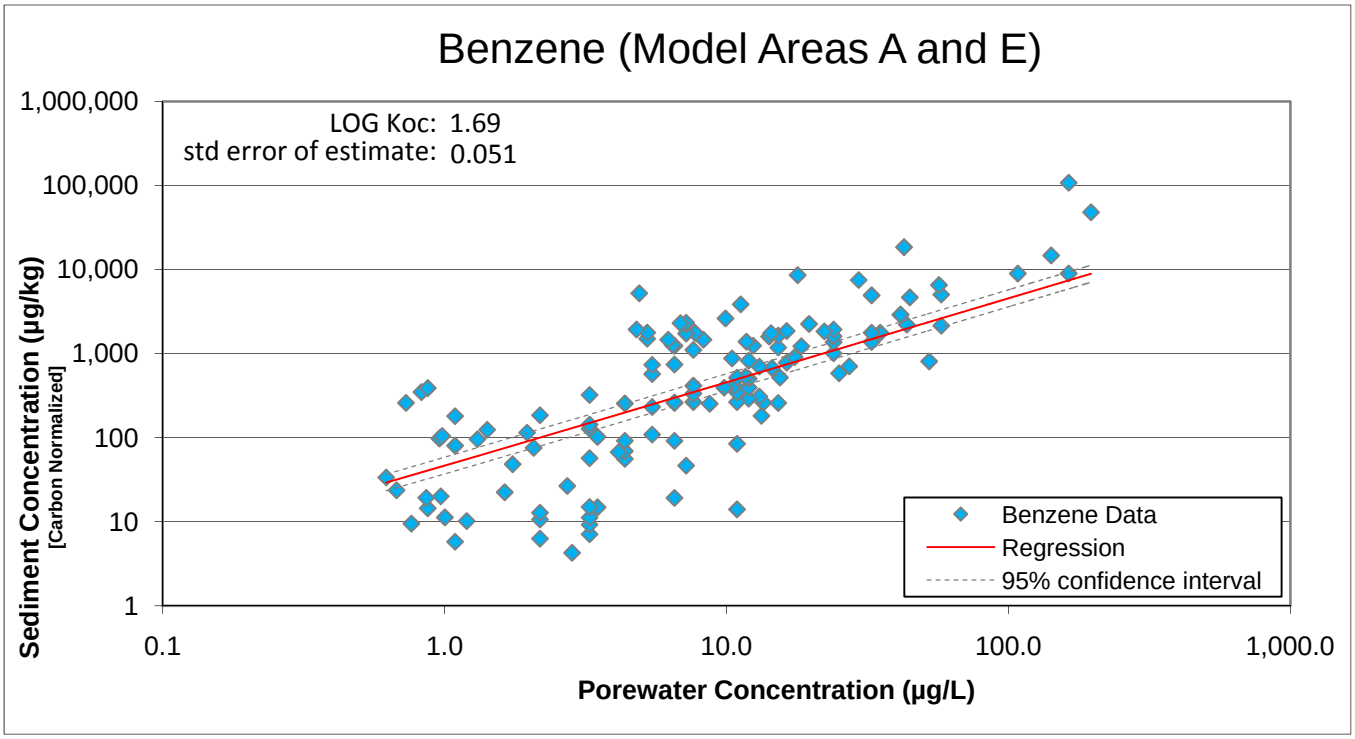

Figure 1. Relationship between *benzene* porewater concentration and carbon-normalized sediment concentration (with log-transformed regression).

TOLUENE – Model Areas B, C, and D

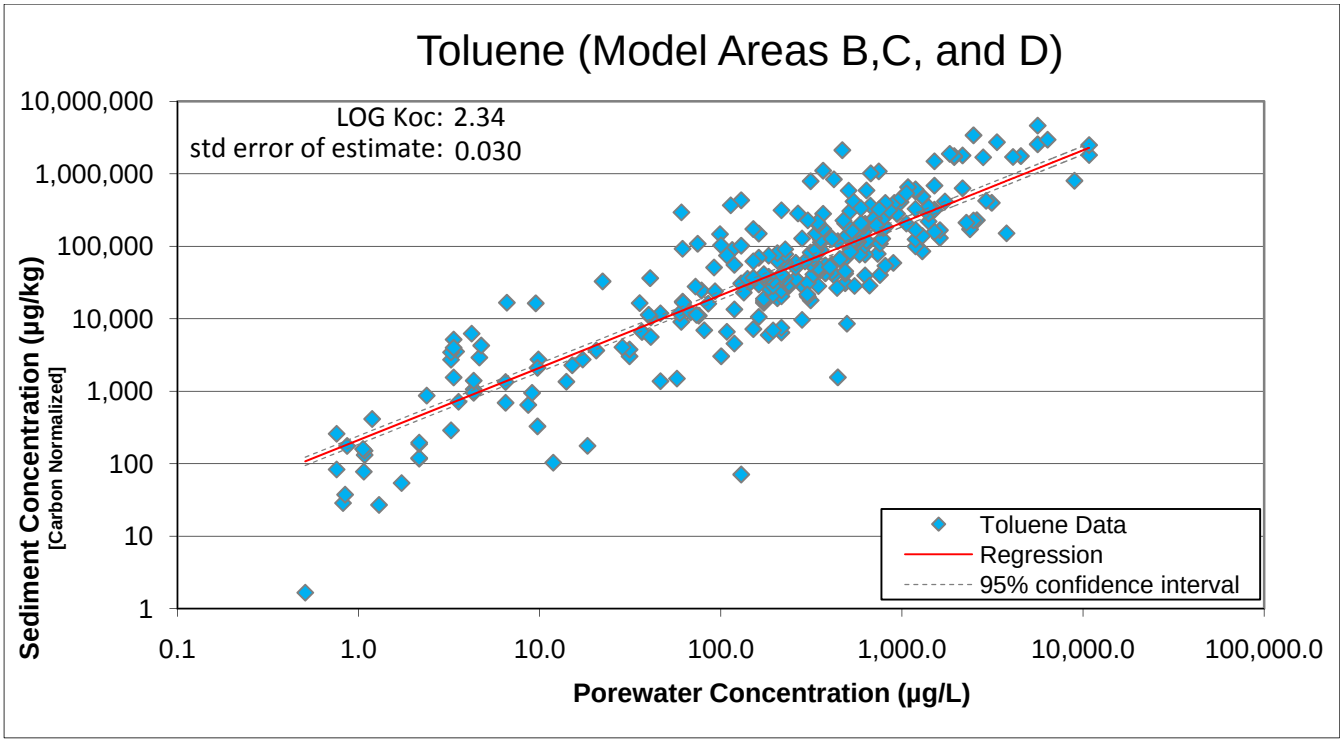

TOLUENE – Model Areas A & E

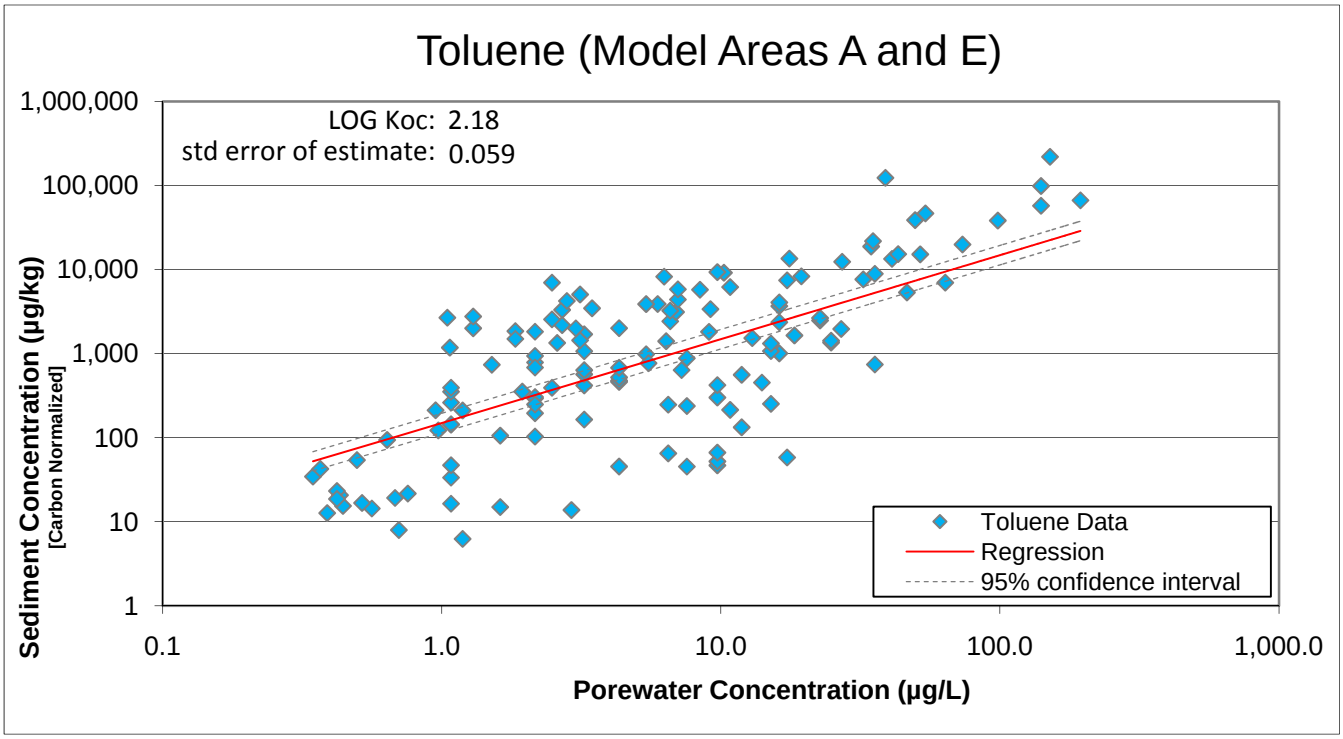

Figure 2. Relationship between *toluene* porewater concentration and carbon-normalized sediment concentration (with log-transformed regression).

ETHYLBENZENE – Model Areas B, C, and D

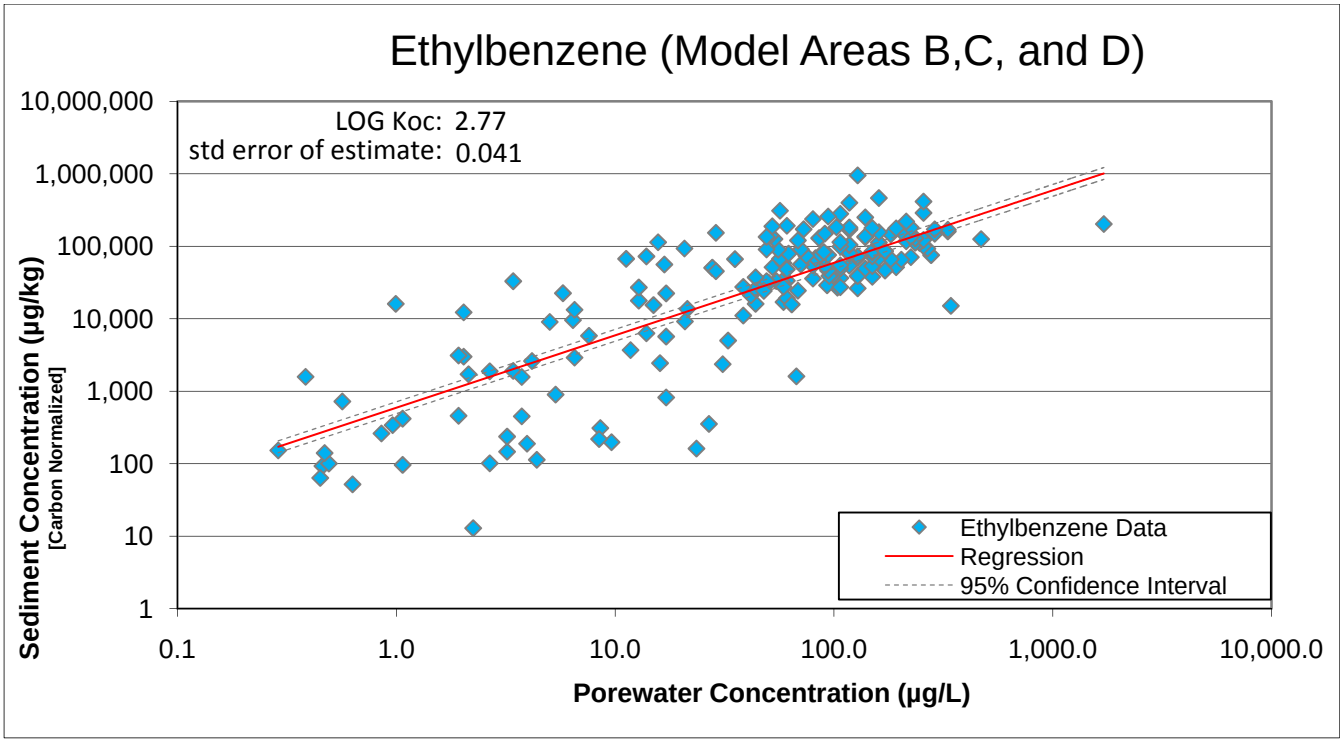

ETHYLBENZENE – Model Areas A & E

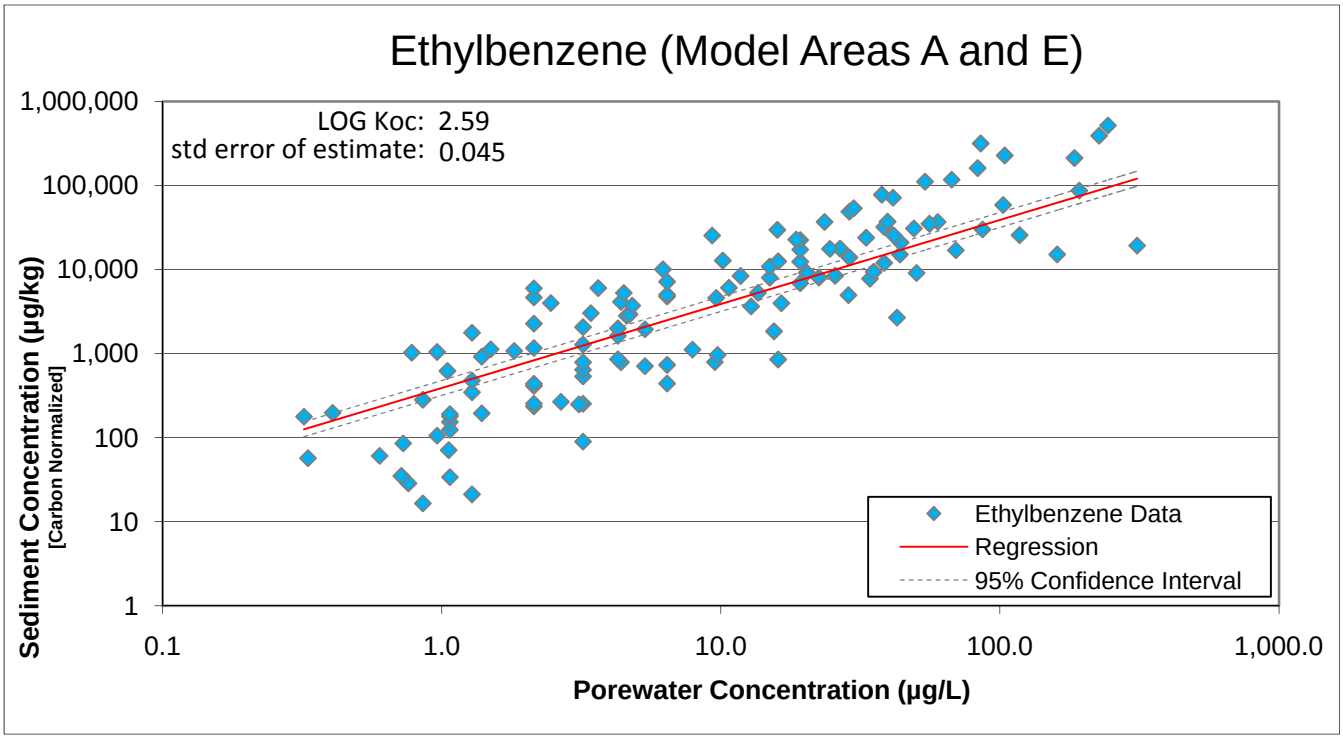

Figure 3. Relationship between *ethylbenzene* porewater concentration and carbon-normalized sediment concentration (with log-transformed regression).

XYLENE – Model Areas B, C, and D

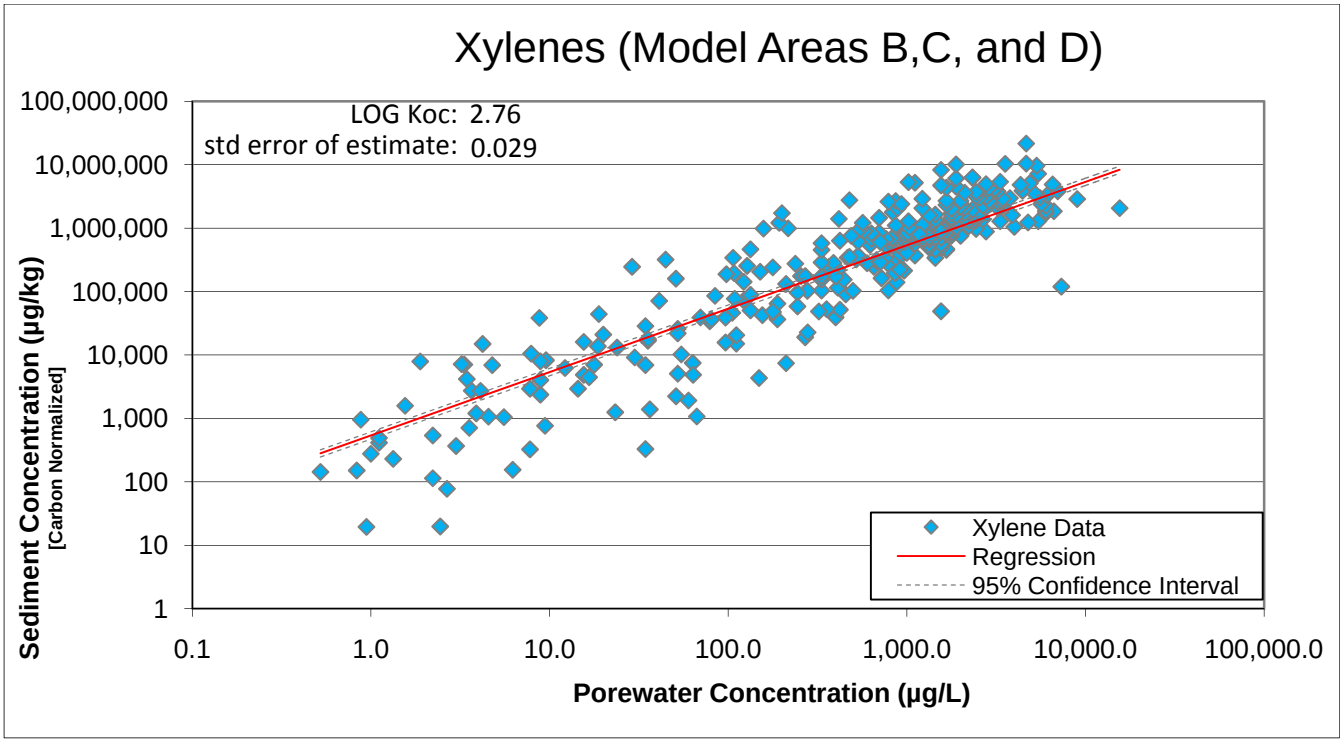

XYLENE – Model Areas A & E

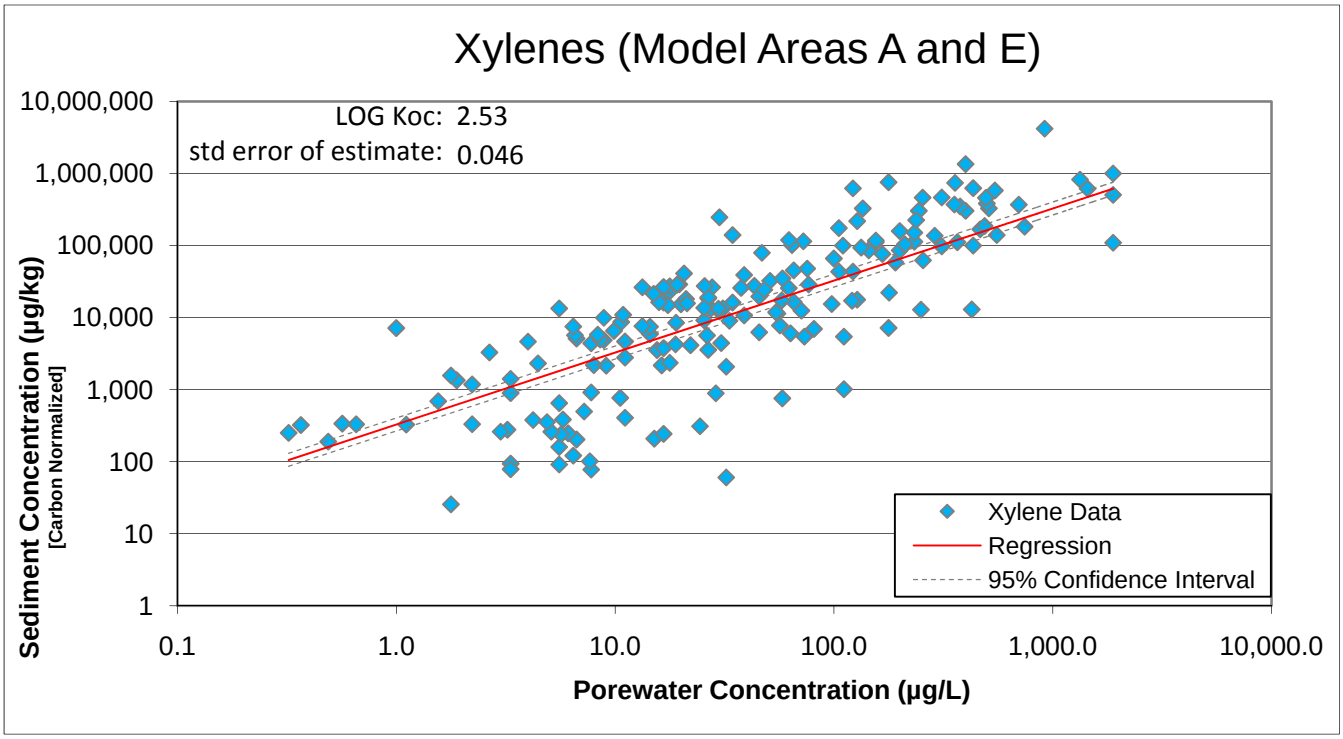

Figure 4. Relationship between *xylene* porewater concentration and carbon-normalized sediment concentration (with log-transformed regression).

CHLOROBENZENE – Model Areas B, C, and D

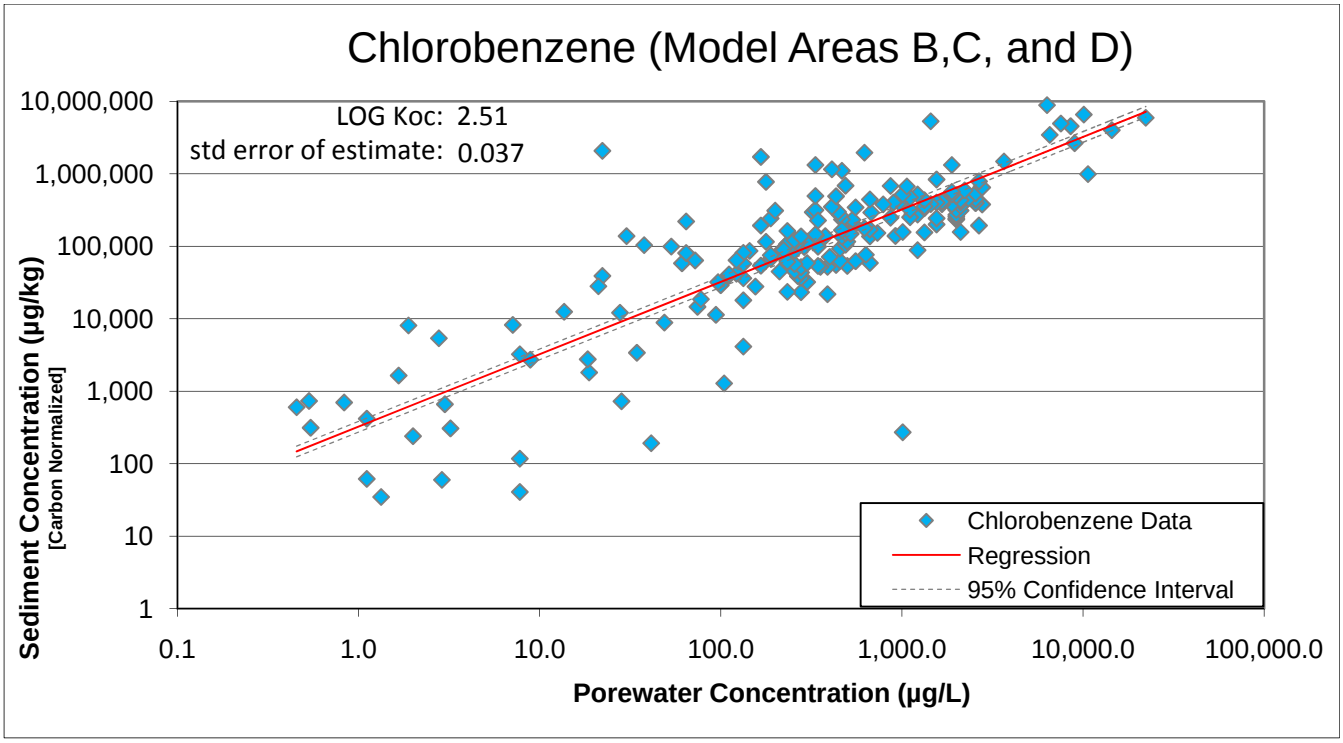

CHLOROBENZENE – Model Areas A & E

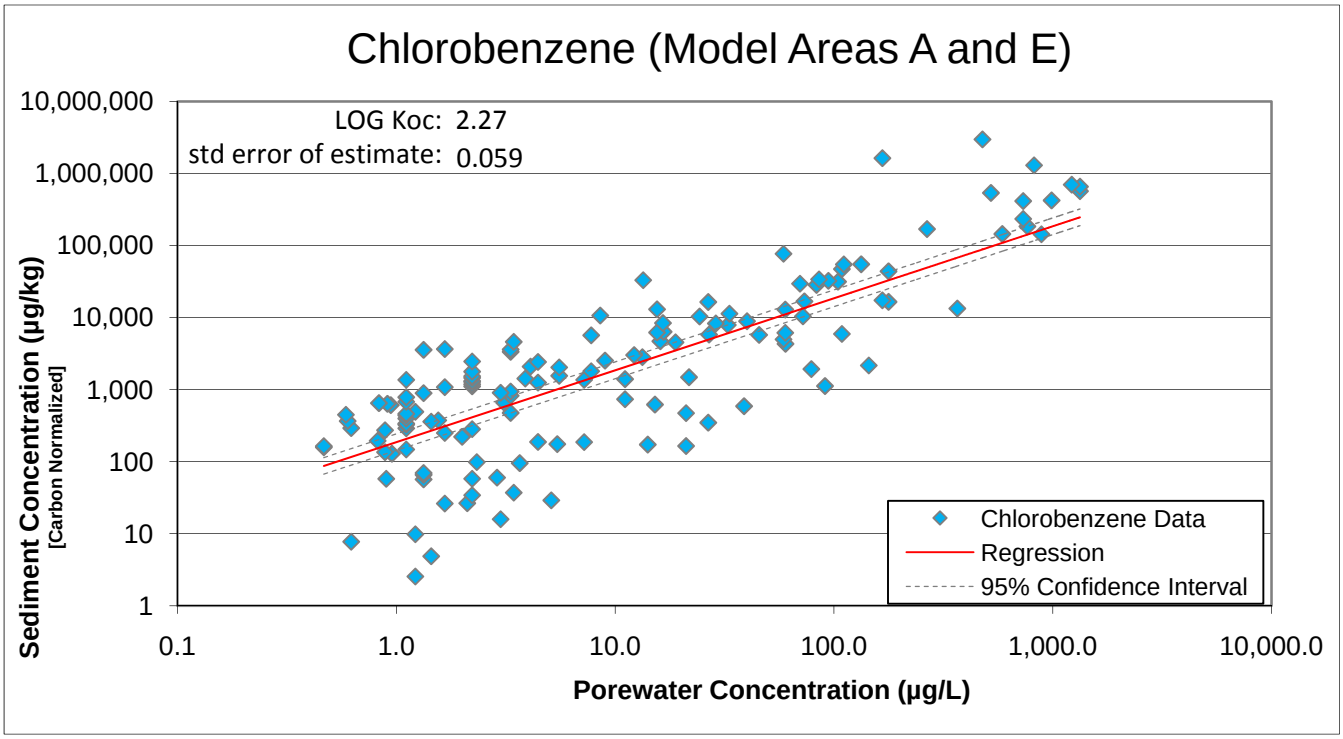

Figure 5. Relationship between *chlorobenzene* porewater concentration and carbon-normalized sediment concentration (with log-transformed regression).

1,2-DICHLOROBENZENE – Model Areas B, C, and D

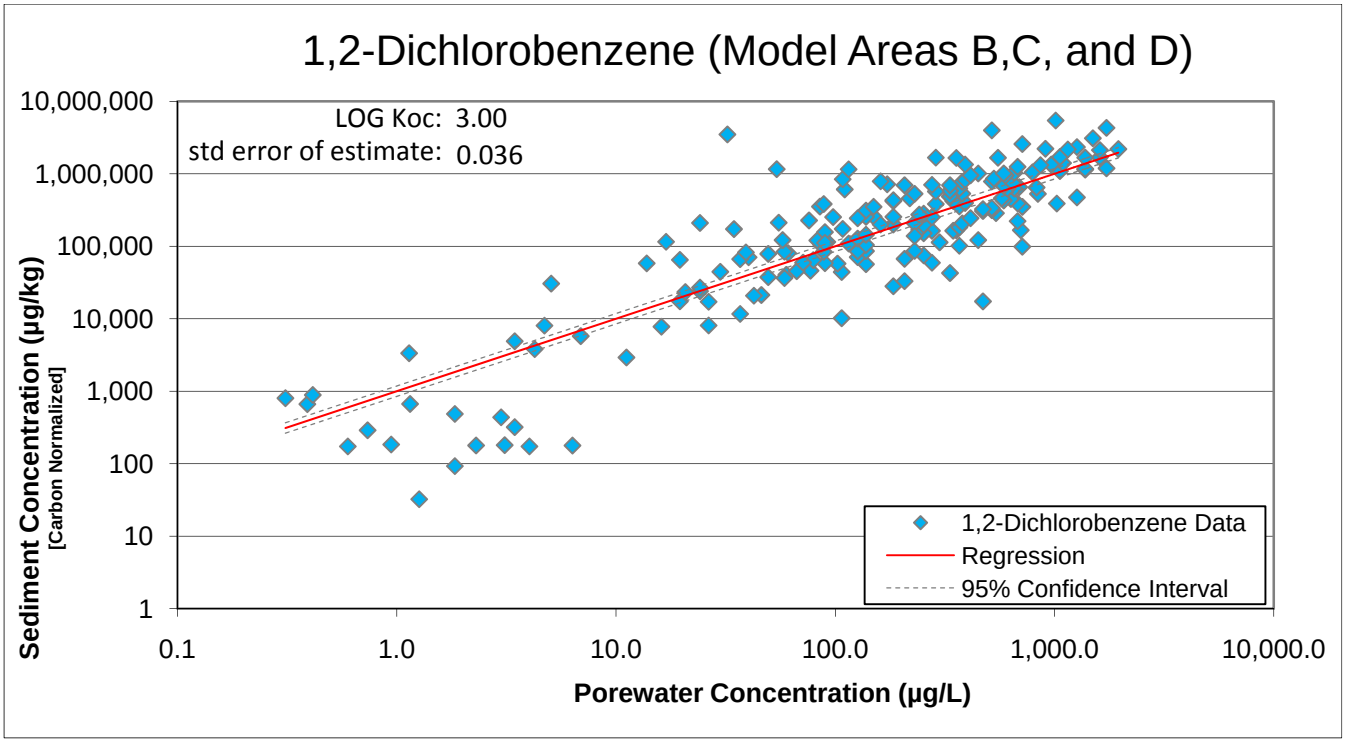

1,2-DICHLOROBENZENE – Model Areas A & E

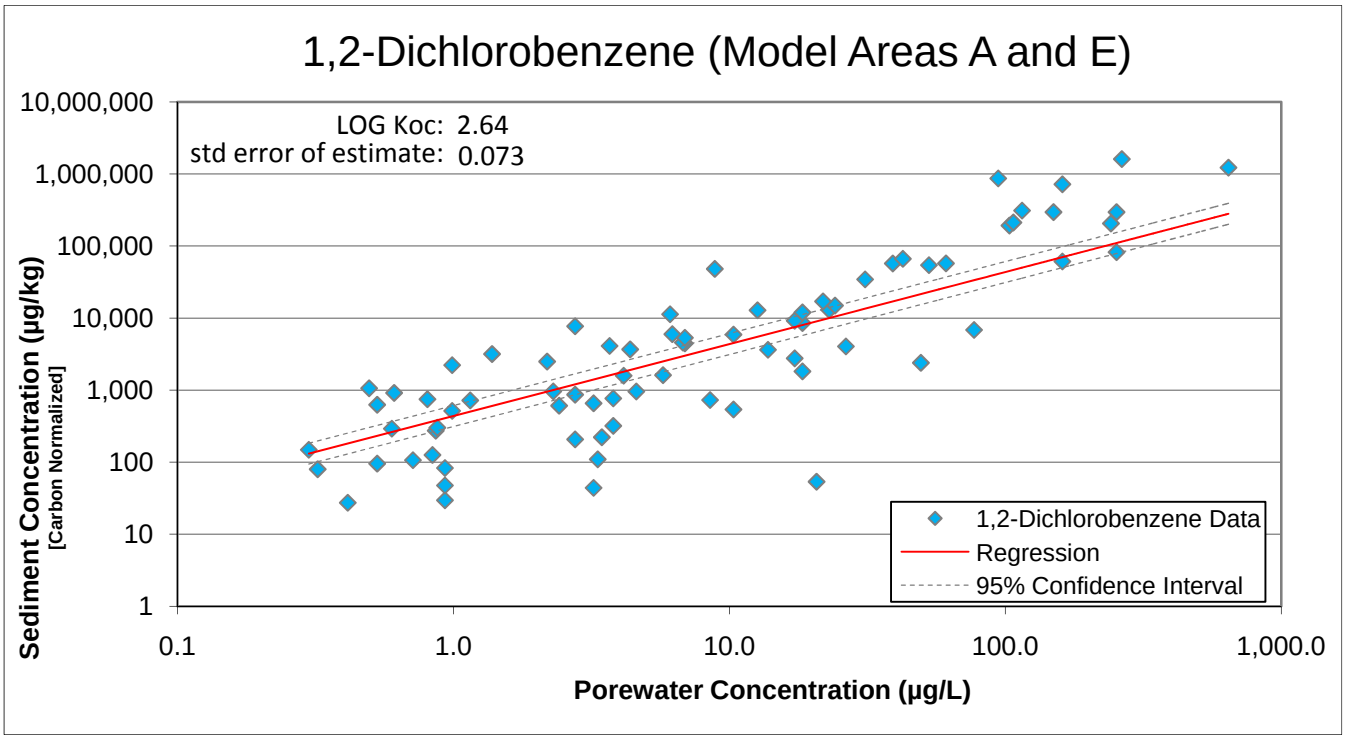

Figure 6. Relationship between *1,2-dichlorobenzene* porewater concentration and carbon-normalized sediment concentration (with log-transformed regression).

1,3-DICHLOROBENZENE – Model Areas B, C, and D

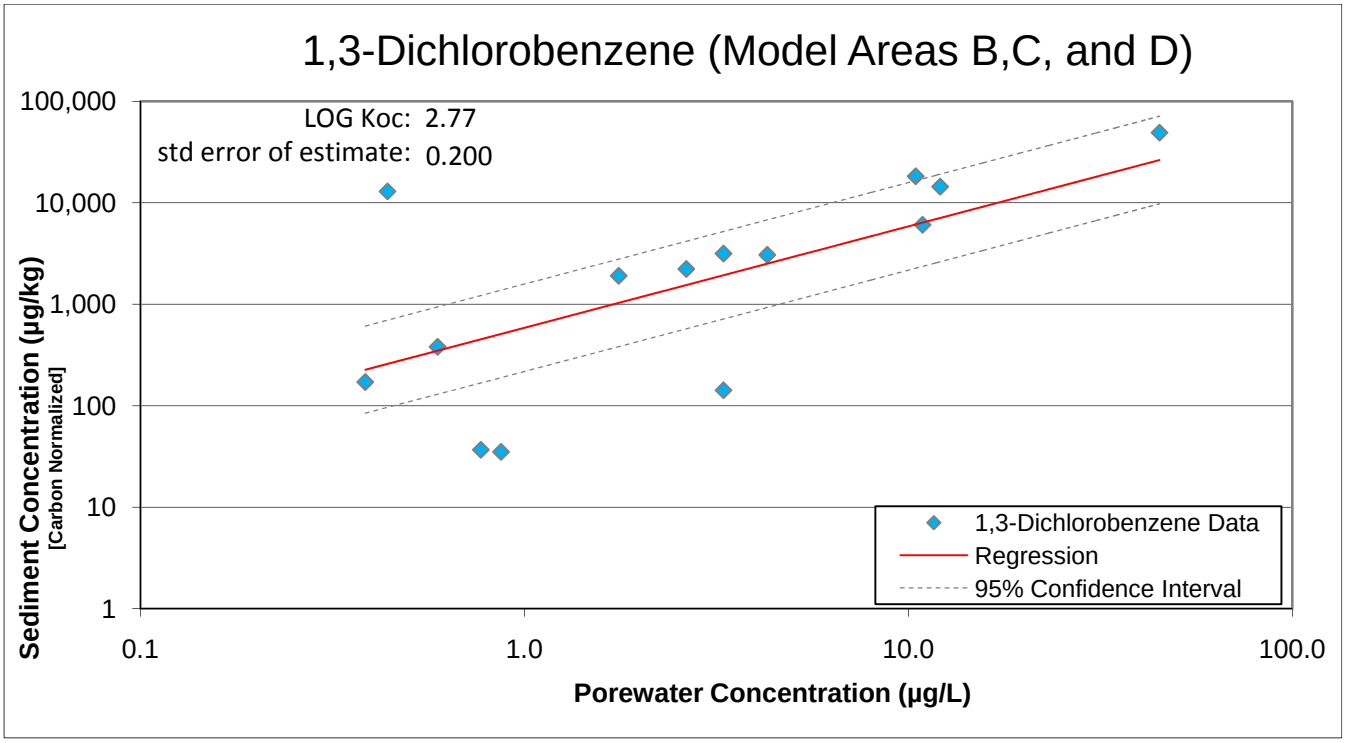

1,3-DICHLOROBENZENE – Model Areas A & E

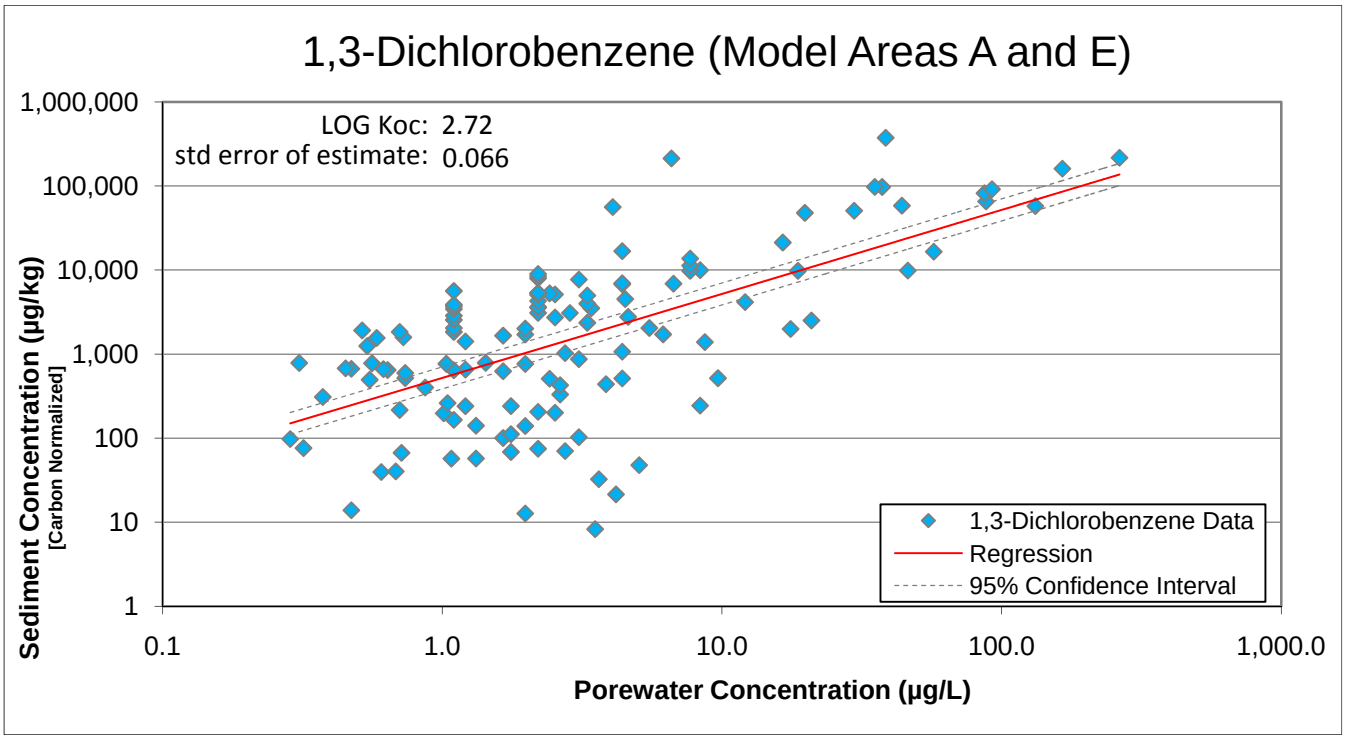

Figure 7. Relationship between *1,3-dichlorobenzene* porewater concentration and carbon-normalized sediment concentration (with log-transformed regression).

1,4-DICHLOROBENZENE – Model Areas B, C, and D

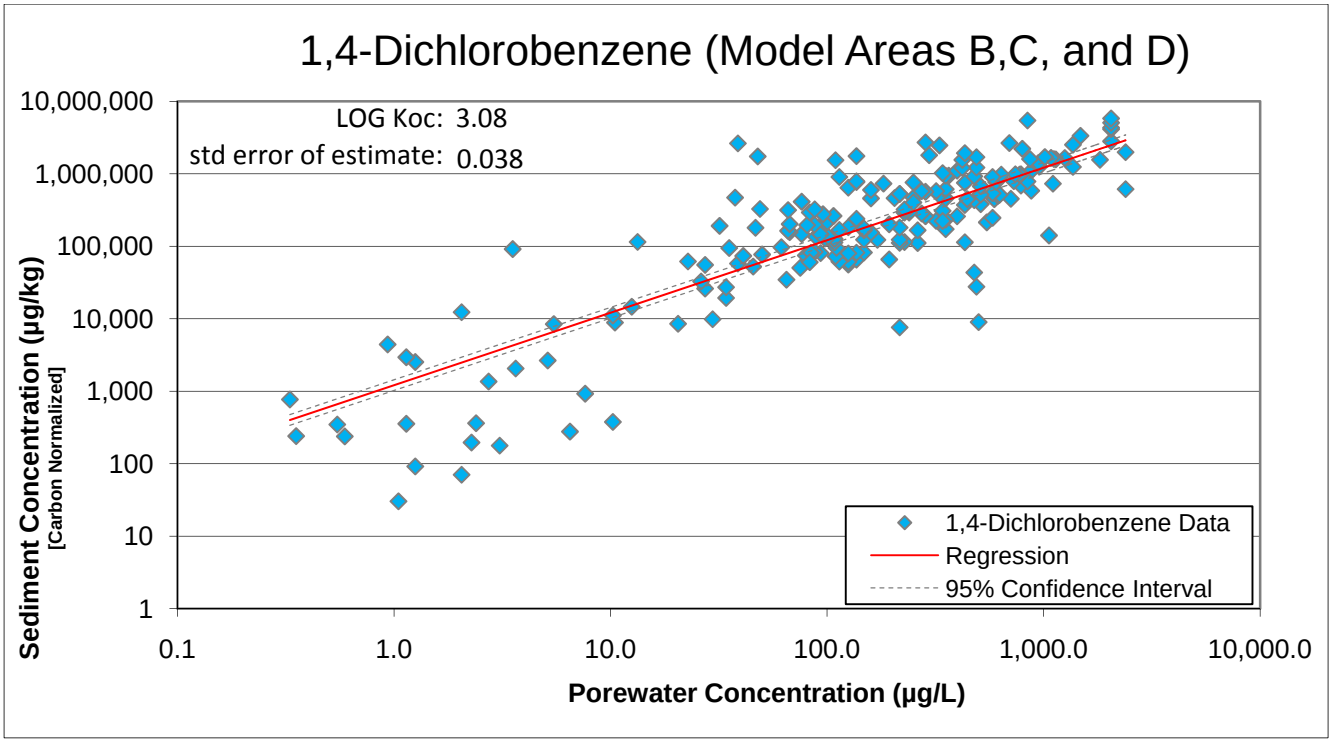

1,4-DICHLOROBENZENE – Model Areas A & E

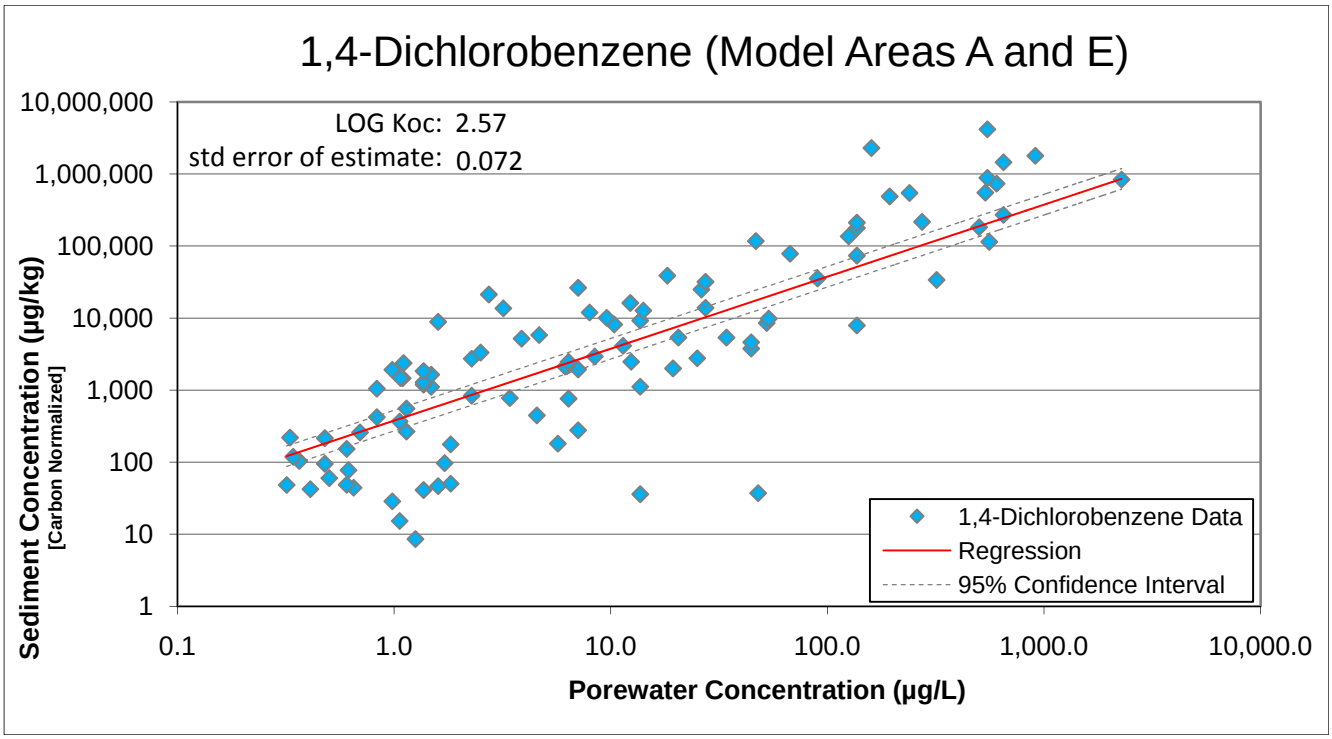

Figure 8. Relationship between *1,4-dichlorobenzene* porewater concentration and carbon-normalized sediment concentration (with log-transformed regression).

1,2,3-TRICHLOROBENZENE – Model Areas B, C, and D

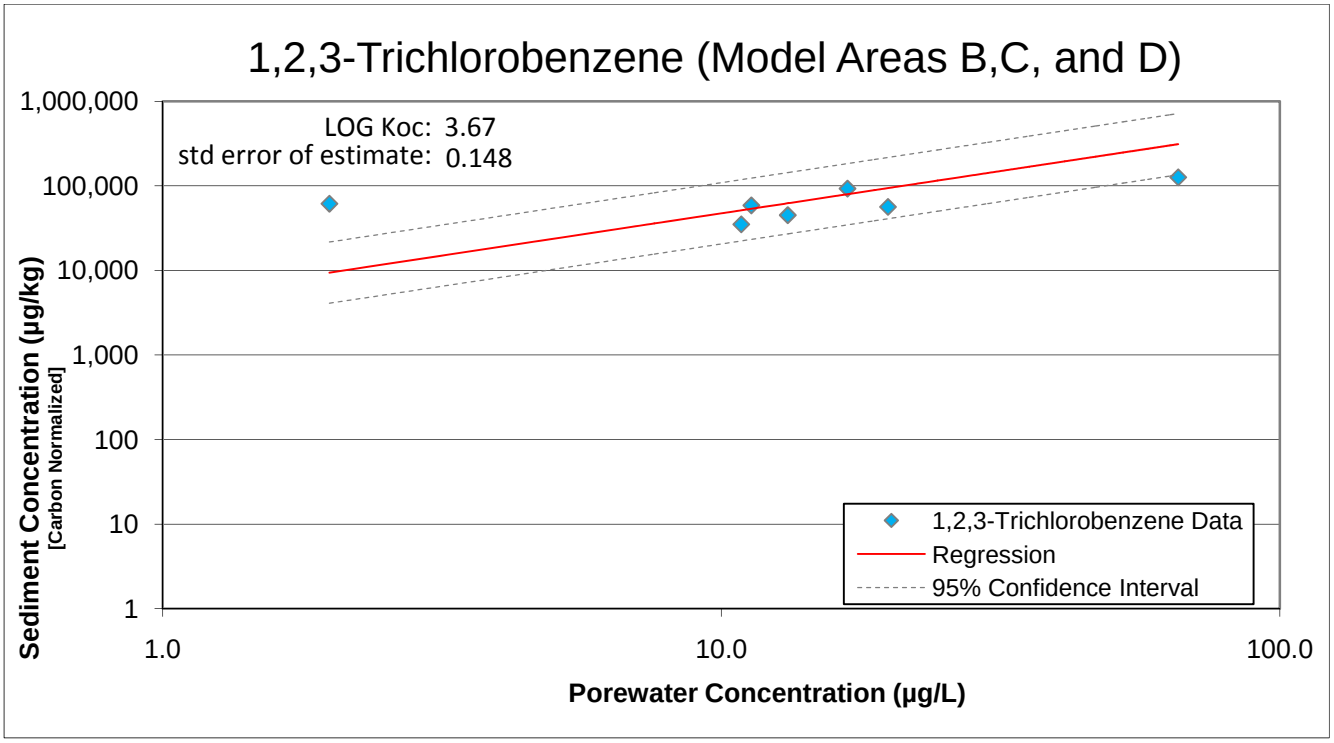

1,2,3-TRICHLOROBENZENE – Model Areas A & E

THERE WAS ONLY A SINGLE USABLE DATA PAIR FOR 1,2,3-TRICHLOROBENZENE IN MODEL AREAS A and E (plot not shown)

Figure 9. Relationship between *1,2,3-trichlorobenzene* porewater concentration and carbon-normalized sediment concentration (with log-transformed regression).

1,2,4-TRICHLOROBENZENE – Model Areas B, C, and D

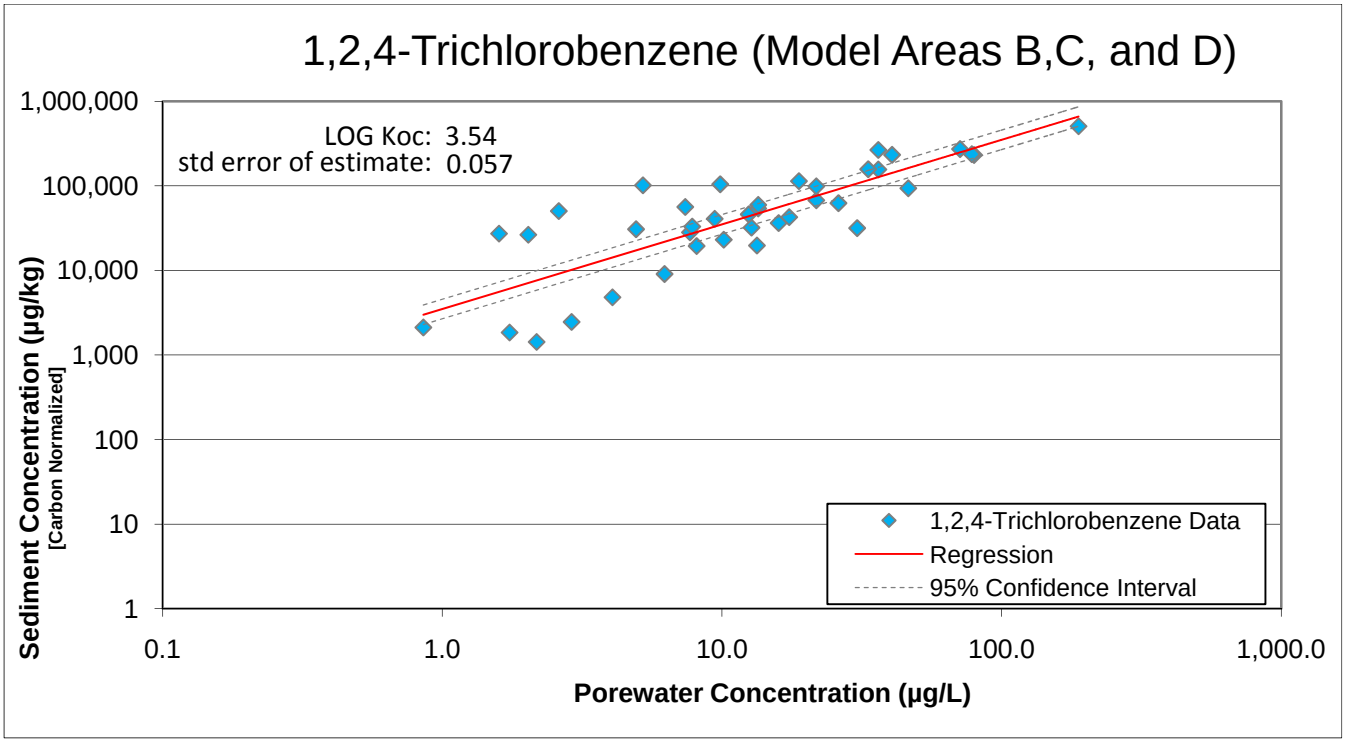

1,2,4-TRICHLOROBENZENE – Model Areas A & E

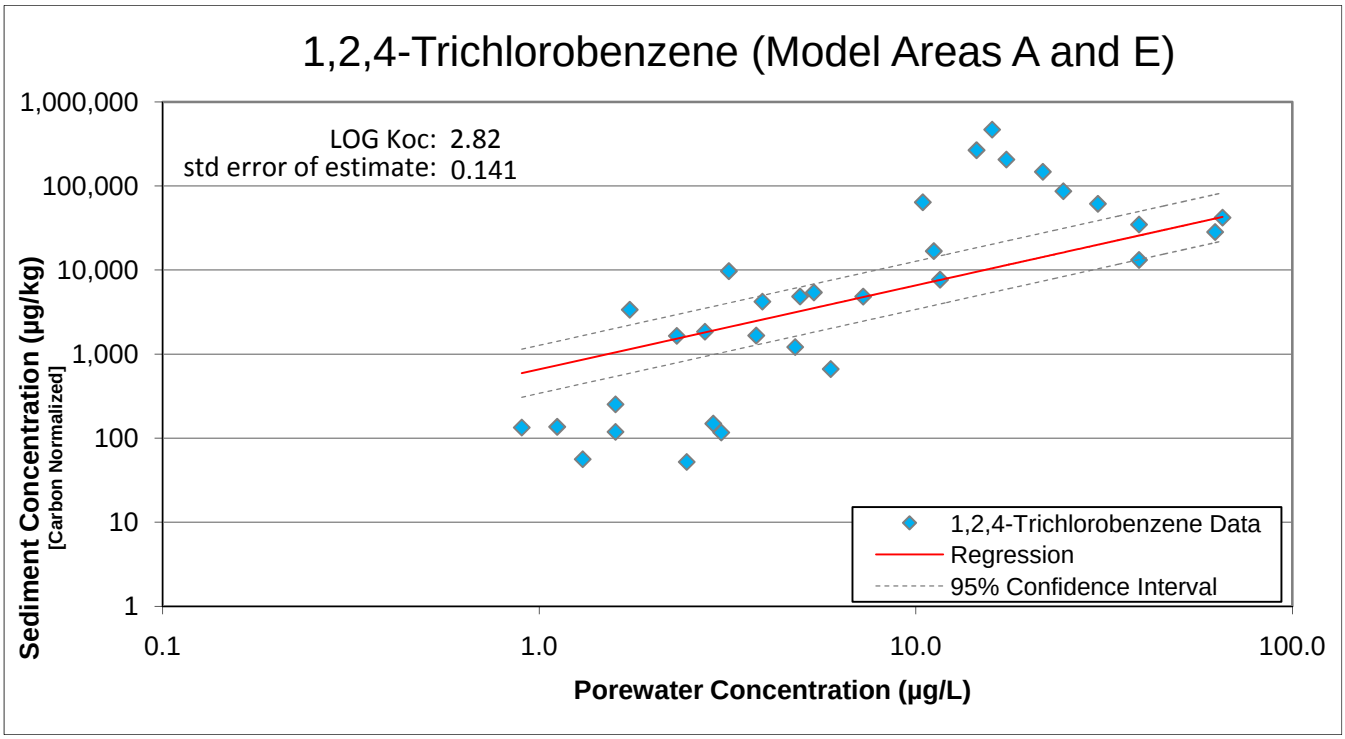

Figure 10. Relationship between *1,2,4-trichlorobenzene* porewater concentration and carbon-normalized sediment concentration (with log-transformed regression).

1,3,5-TRICHLOROBENZENE – Model Areas B, C, and D

THERE WERE NO USABLE DATA PAIRS FOR 1,3,5-TRICHLOROBENZENE IN MODEL AREAS B, C, and D (plot not shown)

1,3,5-TRICHLOROBENZENE – Model Areas A & E

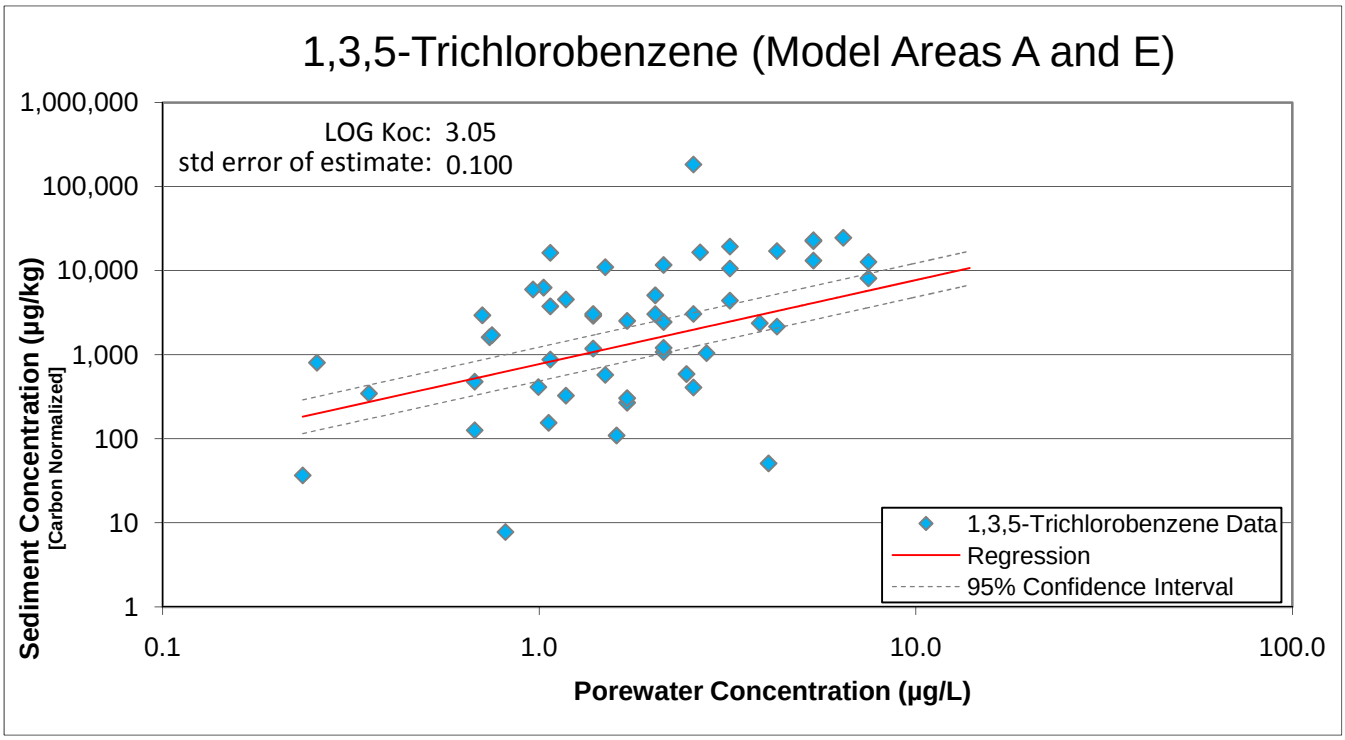

Figure 11. Relationship between *1,3,5-trichlorobenzene* porewater concentration and carbon-normalized sediment concentration (with log-transformed regression).

NAPHTHALENE – Model Areas B, C, and D

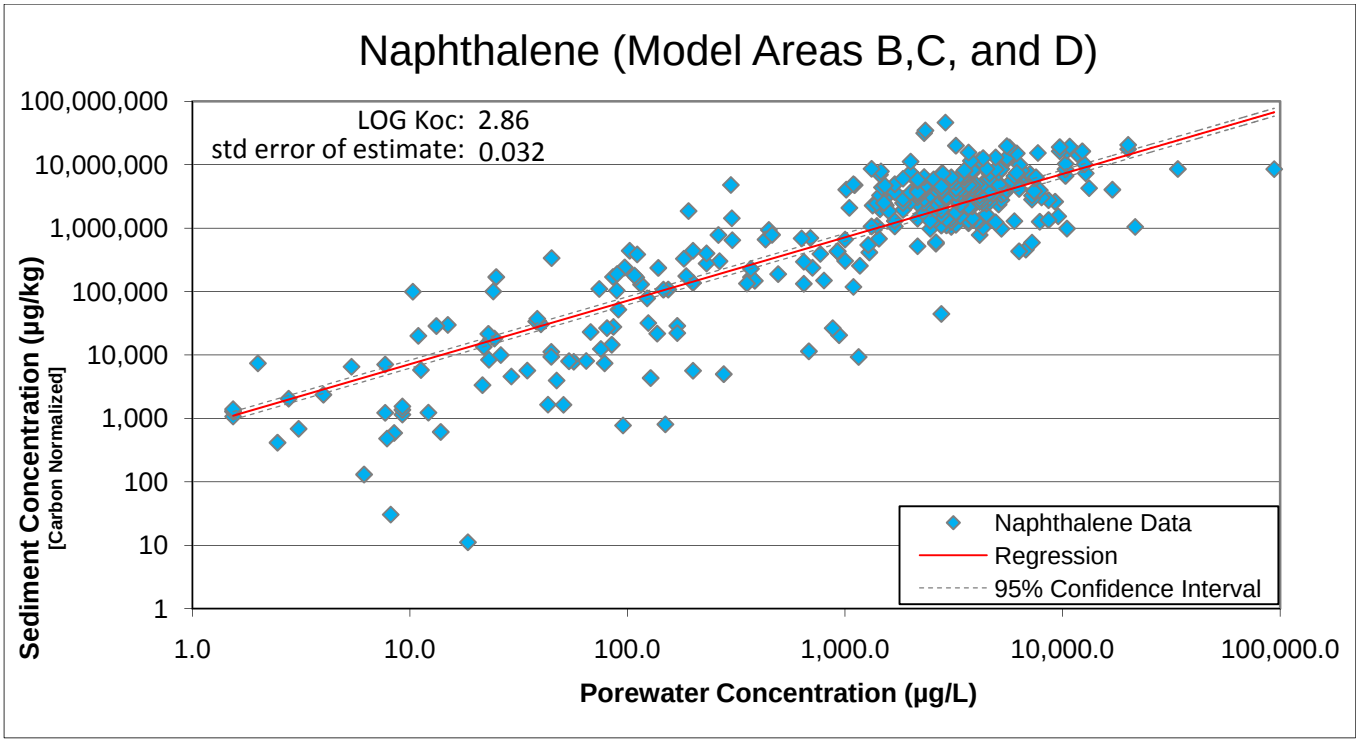

NAPHTHALENE – Model Areas A & E

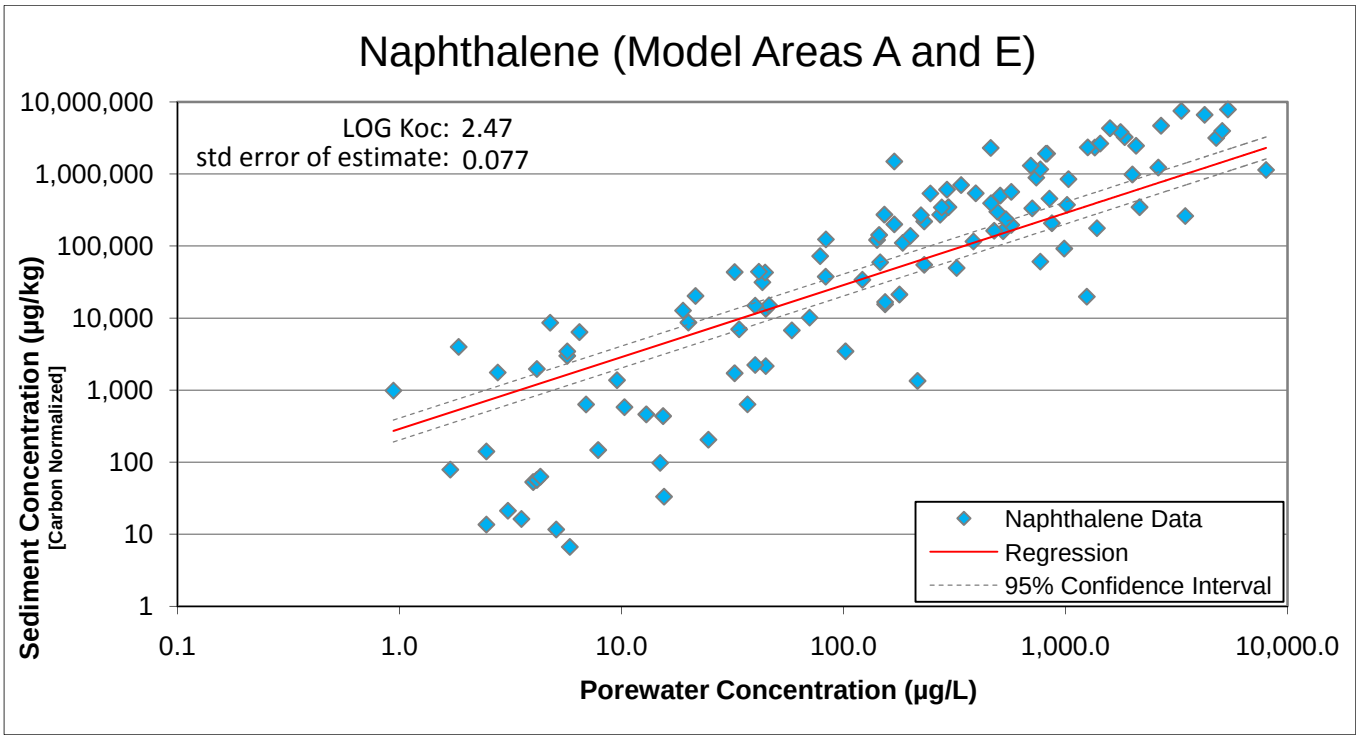

Figure 12. Relationship between *naphthalene* porewater concentration and carbon-normalized sediment concentration (with log-transformed regression).

ADDENDUM 1

Geosyntec consultants

130 Research Lane, Suite 2
Guelph, Ontario, Canada N1G 5G3
PH 519.822.2230
FAX 519.822.3151

TECHNICAL MEMORANDUM

Date: 09 December 2009

To: Edward Glaza – Parsons

Copies to: Caryn E. Kiehl-Simpson and John Nolan – Parsons

From: Tom Krug and David Himmelheber - Geosyntec Consultants
Danny Reible – University of Texas at Austin

Subject: Establishing Representative PAH Sediment-Porewater Partitioning Coefficients Within Sediments for Input into Transport Modeling, Onondaga Lake, Syracuse, New York

---

1. BACKGROUND AND SCOPE

This memorandum has been prepared by Geosyntec Consultants, Inc. (Geosyntec) to provide recommended values for effective sediment-porewater partitioning coefficients (K_{oc}) in lake sediments to be used to calculate sediment porewater concentrations. The values are intended to be incorporated into transport modeling at areas of Onondaga Lake, Syracuse, New York (the "Site") not impacted by in-lake waste deposits (ILWD) that are to be managed with an *in situ* sediment cap. A focused literature review of select datasets was performed to examine the phenomenon of porewater polycyclic aromatic hydrocarbon (PAH) and polychlorinated biphenyl (PCB) concentrations measured in actual sediment samples being lower than expected based upon conventional estimates derived from octanol-water distribution coefficients (K_{ow}) and bulk sediment concentration. Direct measurement of porewater concentrations of these compounds are unavailable, hence the need to make the best prediction of porewater concentration for the purposes of modeling.

One approach of estimating porewater concentrations of hydrophobic contaminants, such as PAHs and PCBs, in sediments has been to measure bulk sediment concentration (C_s), then assume linear partitioning into the aqueous phase (C_w) based on solid-liquid distribution coefficients (K_d). The distribution coefficient has been generalized as the product of the fraction organic carbon (f_{oc}) in the sediment and K_{oc}:

$$C_w = \frac{C_s}{K_d} = \frac{C_s}{K_{oc} \times f_{oc}} \qquad (1)$$

While this approach does not account for mass held in the dissolved-phase associated with the sediment solids, the correction is extremely small for highly sorptive compounds such as PAH

and PCB. Therefore, pore water concentrations can be related to bulk sediment concentrations (which is based on mass in all phases) with negligible adjustment. Measured f_{oc} values are site-specific while K_{oc} values are chemical-specific and can either be determined experimentally or calculated based on chemical structure and/or properties (e.g., octanol-water partitioning coefficient [K_{ow}]). Note that K_{ow} values are physical constants of a particular compound but that values of K_{oc} are partially dependent upon the particular compound and are also influenced by environmental conditions (including factors such as the nature of the f_{oc}) and whether compounds are sorbing or desorbing. Modeling conducted to date has used K_{ow} values reported in New York State Department of Environmental Conservation Guidance (NYSDEC, 1999) as estimates of K_{oc} and measured f_{oc} values to estimate the concentrations of PAHs and PCBs in sediment porewater beneath the cap. A growing body of literature indicates that this conventional approach of calculating PAH and PCB porewater concentrations in sediments will overestimate actual PAH or PCB porewater concentrations (for discussions see Arp et al., 2009; Hawthorne et al., 2006; and McGroddy et al., 1996). The primary cause of this discrepancy is that natural sediments are composed of different types of organic carbon, with some phases of organic carbon ("hard" carbon) sorbing hydrophobic contaminants stronger but more slowly than other phases ("soft" carbon). An illustration of how different forms of carbon present in sediments results in different effective K_{oc} values for phenanthrene was compiled by Ghosh et al. (2003) and reproduced in this document as Figure 1. As a result, when PAHs or PCBs are introduced into sediments, a portion of the contaminant is sorbed strongly to the "hard" carbon component of organic matter and effectively resistant to desorption. This desorption-resistance is not inherently incorporated into the conventional K_{oc} x f_{oc} approach of estimating porewater concentrations since compilations of K_{oc} are often based upon short-term sorption experiments in the laboratory or equivalent correlations with K_{ow}. This discrepancy ultimately leads to lower field measurement of porewater PAH concentrations than are predicted by literature K_{oc} values.

A more realistic approach to modeling PAH and PCB transport within sediments is to use measured f_{oc} values and field-derived effective K_{oc} values measured in natural sediment that account for strongly-sorbing fractions of sediment. A compilation of field-derived effective K_{oc} values from several literature sources has been performed.

2. COMPILATION OF DATASETS COMPARING MEASURED PAH POREWATER CONCENTRATIONS WITH ESTIMATED POREWATER CONCENTRATIONS

Figures 2 and 3 present graphs plotting K_{ow} values for PAHs versus field-derived effective K_{oc} values. PAHs included in the analysis are listed in Table 1. Plotted K_{ow} values were obtained from the NYSDEC Guidance Document (1999) for all but three PAH compounds (acenaphthylene, benzo[ghi]perylene, and dibenz[a,h]anthracene) whose K_{ow} values were obtained from Syracuse Research Corporation's (SRC) KowWIN database. The K_{ow} values utilized in this assessment are the same values being employed for modeling efforts to date. The data utilized for the field-derived observed K_{oc} values were actual porewater sampling and

analysis, providing an accurate measurement of aqueous phase PAH concentrations (Arp et al., 2009). Figure 2 contains the compilation of all sediment site data compiled and Figure 3 contains data from sites with freshwater and brackish conditions (i.e., excluding marine sediments).

The K_{ow} values consistently underestimate observed effective K_{oc} values and thus overestimate PAH porewater concentrations associated with sediment containing a known concentration of PAH compared with the field-derived values. On average, the field-derived PAH K_{oc} values are greater than the K_{ow} values currently utilized in modeling efforts by 1.07 ± 0.14 log units (average ± 95% confidence interval) when examining all the data, and 1.05 ± 0.15 when considering just freshwater and brackish sediment sites. Figures 2 and 3 indicate that adjusting the log K_{ow} values currently employed in modeling efforts by one log unit, or a factor of 10, closely approximates the statistical best-fit lines in both Figures 2 and 3 and falls within the 95% confidence bands of each respective regression line.

3. COMPILATION OF DATASETS COMPARING MEASURED PCB POREWATER CONCENTRATIONS WITH ESTIMATED POREWATER CONCENTRATIONS

Figures 4 and 5 presents graphs of K_{ow} values for PCBs versus field-derived effective K_{oc} values from Arp et al 2009. PCBs included in the analysis are presented in Table 2. Plotted K_{ow} values in Figures 4 and 5 were obtained from the Hawker et al 1988 and Lu et al 2007 respectively.

The K_{ow} values consistently underestimate observed effective K_{oc} values and thus overestimate PCB porewater concentrations associated with sediment containing a known concentration of PCB compared with the field-derived values. On average, the field-derived PCB K_{oc} values are greater than the literature K_{ow} values by a factor of five. Figures 4 and 5 indicate that adjusting the K_{ow} values currently employed in modeling efforts by a factor of five, closely approximates the statistical best-fit lines in both Figures 4 and 5 and falls within the 95% confidence bands of each respective regression line.

4. RECOMMENDATIONS

The literature review described above and relevant experience at other sediment sites supports the use of corrected PAH and PCB K_{oc} values to most accurately model and predict porewater PAH and PCB concentrations within the Onondaga Lake sediment in the absence of direct measurements. Based on the data presented in Figures 2 and 3 an increase in effective K_{oc} values of 10 from PAH K_{ow} values is recommended for derivation of PAH porewater concentrations in the non-ILWD impacted sediments at this time. Based on the data presented in Figures 4 and 5 an increase in effective K_{oc} values of 5 from PCB K_{ow} values is recommended for derivation of PCB porewater concentrations in the non-ILWD impacted sediments.

5. REFERENCES

Arp, H.P.H., Breedveld, G.D., and Cornelissen, G., 2009. Estimating the in situ sediment-porewater distribution of PAHs and chlorinated aromatic hydrocarbons in anthropogenic impacted sediments. *Environ. Sci. Technol.. 43*, 5576–5585.

Cornelissen, G., Gustafsson, O., Bucheli, T. D., Jonker, M. T. O., Koelmans, A. A., and VanNoort, P. C.M., 2005. Extensive sorption of organic compounds to black carbon, coal, and kerogen in sediments and soils: Mechanisms and consequences for distribution, bioaccumulation, and biodegradation. *Environ. Sci. Technol., 39* (18), 6881–6895.

Ghosh, U., Zimmerman, J.R., and Luthy, R.G., 2003. PCB and PAH speciation among particle types in contaminated harbor sediments and effects on PAH bioavailability. *Environ. Sci. Technol.*, *37*, 2209–2217.

Hawker, D.W., and Connell, D.W., 1988. Octanol-water partition coefficients of polychlorinated biphenyls congeners. *Environ. Sci. Technol*., 22:382-385.

Hawthorne, S.B., Grabanski, C.B., and Miller, D.J., 2006. Measured partitioning coefficients for parent and alkyl polycyclic aromatic hydrocarbons in 114 historically contaminated sediments: Part 1. K_{oc} values. *Environ. Toxicol. Chem.*, *25* (11), 2901-2911.

Lohmann, R., MacFarlane, J. K., and Gschwend, P. M., 2005. Importance of black carbon to sorption of native PAHs, PCBs, and PCDDs in Boston and New York Harbor sediments. *Environ. Sci. Technol., 39* (1), 141–148.

Lu, X., Reible, D.D., and Fleeger, J.W., 2006. Bioavailability of polycyclic aromatic hydrocarbons in field-contaminated Anacostia River (Washington, DC) sediment. *Environ. Toxicol. Chem., 25,* (11), 2869-2874.

Lu, W., Chen, Y., Liu, M., Chen, X. and Hu, Z., 2007. QSPR prediction of n-octonal/water partitioning coefficient for polychlorinated biphenyls. *Chemosphere,* 69 (2007), 469-478.

McGroddy, S. E., Farrington, J. W., and Gschwend, P. M., 1996. Comparison of the in situ and desorption sediment-water partitioning of polycyclic aromatic hydrocarbons and polychlorinated biphenyls. *Environ. Sci. Technol., 30* (1), 172–177.

New York State Department of Environmental Conservation (NYSDEC), 1999. Technical Guidance for Screening Contaminated Sediments. Division of Fish, Wildlife and Marine Resources.

Table 1 - Literature Values for Kow and Koc for Polycyclic Aromatic Hydrocarbons

Data Source in Arp et al, 2009	CAS #	Compound	Average Log Koc Arp et al, 2009	Log Kow NYSDEC, 1999	Log Kow SRC
7	208-96-8	Acenaphthylene	5.11	ns	3.94
9	208-96-8	Acenaphthylene	4.48	ns	3.94
10	208-96-8	Acenaphthylene	4.47	ns	3.94
4	120-12-7	Anthracene	6.24	4.45	
6	120-12-7	Anthracene	6.08	4.45	
7	120-12-7	Anthracene	5.75	4.45	
9	120-12-7	Anthracene	5.41	4.45	
14	120-12-7	Anthracene	6.61	4.45	
15	120-12-7	Anthracene	5.26	4.45	
1	56-55-3	Benz[a]anthracene	7.14	5.61	
4	56-55-3	Benz[a]anthracene	7.38	5.61	
6	56-55-3	Benz[a]anthracene	6.77	5.61	
7	56-55-3	Benz[a]anthracene	6.55	5.61	
8	56-55-3	Benz[a]anthracene	6.95	5.61	
9	56-55-3	Benz[a]anthracene	6.45	5.61	
14	56-55-3	Benz[a]anthracene	7.81	5.61	
6	50-32-8	Benzo(a)pyrene	7.03	6.04	
1	50-32-8	Benzo[a]pyrene	7.77	6.04	
4	50-32-8	Benzo[a]pyrene	8.37	6.04	
7	50-32-8	Benzo[a]pyrene	6.68	6.04	
8	50-32-8	Benzo[a]pyrene	7.96	6.04	
9	50-32-8	Benzo[a]pyrene	6.85	6.04	
11	50-32-8	Benzo[a]pyrene	7.25	6.04	
12	50-32-8	Benzo[a]pyrene	6.79	6.04	
13	50-32-8	Benzo[a]pyrene	6.15	6.04	
14	50-32-8	Benzo[a]pyrene	7.81	6.04	
4	205-99-2	Benzo[b]fluoranthene	7.99	6.04	
6	205-99-2	Benzo[b]fluoranthene	7.06	6.04	
8	205-99-2	Benzo[b]fluoranthene	7.42	6.04	
9	205-99-2	Benzo[b]fluoranthene	6.91	6.04	
15	205-99-2	Benzo[b]fluoranthene	6.59	6.04	
1	191-24-2	Benzo[ghi]perylene	8.25	ns	6.70
4	191-24-2	Benzo[ghi]perylene	9.01	ns	6.70
6	191-24-2	Benzo[ghi]perylene	7.58	ns	6.70
7	191-24-2	Benzo[ghi]perylene	7.13	ns	6.70
8	191-24-2	Benzo[ghi]perylene	7.84	ns	6.70
9	191-24-2	Benzo[ghi]perylene	6.94	ns	6.70
14	191-24-2	Benzo[ghi]perylene	8.91	ns	6.70
15	191-24-2	Benzo[ghi]perylene	6.67	ns	6.70
4	207-08-9	Benzo[k]fluoranthene	8.16	6.04	
6	207-08-9	Benzo[k]fluoranthene	7.25	6.04	
8	207-08-9	Benzo[k]fluoranthene	7.41	6.04	
9	207-08-9	Benzo[k]fluoranthene	6.90	6.04	
12	207-08-9	Benzo[k]fluoranthene	6.74	6.04	
15	207-08-9	Benzo[k]fluoranthene	6.41	6.04	

notes:

ns - not specified

Table 1 - Literature Values for Kow and Koc for Polycyclic Aromatic Hydrocarbons

Data Source in Arp et al, 2009	**CAS #**	**Compound**	**Average Log Koc** Arp et al, 2009	**Log Kow** NYSDEC, 1999	**Log Kow** SRC
4	53-70-3	Dibenz[a,h]anthracene	8.06	ns	6.70
6	53-70-3	Dibenz[a,h]anthracene	7.62	ns	6.70
7	53-70-3	Dibenz[a,h]anthracene	6.82	ns	6.70
9	53-70-3	Dibenz[a,h]anthracene	6.88	ns	6.70
6	206-44-0	Fluorantene	6.25	5.19	
1	206-44-0	Fluoranthene	6.26	5.19	
4	206-44-0	Fluoranthene	6.37	5.19	
7	206-44-0	Fluoranthene	5.79	5.19	
8	206-44-0	Fluoranthene	6.04	5.19	
9	206-44-0	Fluoranthene	5.89	5.19	
13	206-44-0	Fluoranthene	6.43	5.19	
14	206-44-0	Fluoranthene	7.41	5.19	
15	206-44-0	Fluoranthene	6.15	5.19	
16	206-44-0	Fluoranthene	6.34	5.19	
7	86-73-7	Fluorene	4.71	4.18	
9	86-73-7	Fluorene	4.65	4.18	
10	86-73-7	Fluorene	4.17	4.18	
15	86-73-7	Fluorene	4.69	4.18	
16	86-73-7	Fluorene	6.49	4.18	
7	91-57-6	2-Methylnaphthalene	4.56	3.86	
16	91-57-6	2-Methylnaphthalene	7.03	3.86	
7	91-20-3	Naphthalene	4.26	3.37	
9	91-20-3	Naphthalene	3.39	3.37	
10	91-20-3	Naphthalene	3.14	3.37	
1	85-01-8	Phenanthrene	5.87	4.45	
4	85-01-8	Phenanthrene	6.15	4.45	
6	85-01-8	Phenanthrene	5.83	4.45	
7	85-01-8	Phenanthrene	5.20	4.45	
8	85-01-8	Phenanthrene	5.70	4.45	
8	85-01-8	Phenanthrene	5.70	4.45	
9	85-01-8	Phenanthrene	5.30	4.45	
10	85-01-8	Phenanthrene	5.03	4.45	
11	85-01-8	Phenanthrene	5.25	4.45	
12	85-01-8	Phenanthrene	4.76	4.45	
13	85-01-8	Phenanthrene	6.50	4.45	
14	85-01-8	Phenanthrene	6.91	4.45	
15	85-01-8	Phenanthrene	4.99	4.45	
16	85-01-8	Phenanthrene	6.59	4.45	
4	129-00-0	Pyrene	6.38	5.32	
6	129-00-0	Pyrene	5.86	5.32	
7	129-00-0	Pyrene	5.82	5.32	
8	129-00-0	Pyrene	6.05	5.32	
9	129-00-0	Pyrene	5.97	5.32	
10	129-00-0	Pyrene	5.08	5.32	
11	129-00-0	Pyrene	5.90	5.32	
12	129-00-0	Pyrene	5.43	5.32	
13	129-00-0	Pyrene	6.06	5.32	
14	129-00-0	Pyrene	6.71	5.32	
15	129-00-0	Pyrene	5.75	5.32	
16	129-00-0	Pyrene	6.80	5.32	

notes:

ns - not specified

Table 2 - Literature Values for Kow and Koc of PCB Congeners

PCB Congener	Log Kow Hawker et al 1988	Log Kow Lu et al 2007	Ave Log Koc Arp et al 2009
PCB-18	5.24	5.33	5.94
PCB-18	5.24	5.33	5.54
PCB-28	5.67	5.71	6.25
PCB-28	5.67	5.71	6.44
PCB-28	5.67	5.71	7.18
PCB-28	5.67	5.71	6.28
PCB-31	5.67	5.68	6.99
PCB-44	5.75	5.73	6.48
PCB-44	5.75	5.73	5.9
PCB-52	5.84	5.79	6.46
PCB-52	5.84	5.79	6.7
PCB-52	5.84	5.79	7.01
PCB-52	5.84	5.79	6.51
PCB-52	5.84	5.79	6.03
PCB-66	6.2	5.98	6.8
PCB-72	6.26	na	6.01
PCB-77	6.36	na	7.32
PCB-77	6.36	na	6.86
PCB-81	6.36	na	7.38
PCB-95	6.13	5.92	6.35
PCB-101	6.38	na	6.56
PCB-101	6.38	na	7.54
PCB-101	6.38	na	7.71
PCB-101	6.38	na	6.95
PCB-101	6.38	na	6.55
PCB-105	6.65	6.79	8.06
PCB-105	6.65	6.79	7.51

PCB Congener	Log Kow Hawker et al 1988	Log Kow Lu et al 2007	Ave Log Koc Arp et al 2009
PCB-118	6.74	6.57	6.83
PCB-118	6.74	6.57	8.02
PCB-118	6.74	6.57	7.58
PCB-118	6.74	6.57	6.85
PCB-118	6.74	6.57	6.86
PCB-126	6.89	na	7.7
PCB-138	6.83	6.73	8.19
PCB-138	6.83	6.73	8.25
PCB-138	6.83	6.73	7.55
PCB-138	6.83	6.73	7.15
PCB-153	6.92	6.8	8.33
PCB-153	6.92	6.8	8.32
PCB-153	6.92	6.8	7.46
PCB-153	6.92	6.8	7.01
PCB-156	7.18	7.44	8.13
PCB-156	7.18	7.44	7.82
PCB-156	7.18	7.44	7.38
PCB-167	7.27	7.29	7.94
PCB-169	7.42	7.55	7.96
PCB-170	7.27	7.08	8
PCB-180	7.36	7.21	7.35
PCB-180	7.36	7.21	8.31
PCB-180	7.36	7.21	8.3
PCB-180	7.36	7.21	7.86
PCB-187	7.17	6.99	7.79
PCB-195	7.56	7.35	7.85
PCB-204	7.3	7.48	8.24

Figure 1 - Phenanthrene K_{oc} values for different types of organic carbon.
Reproduced from Ghosh et al., 2003.

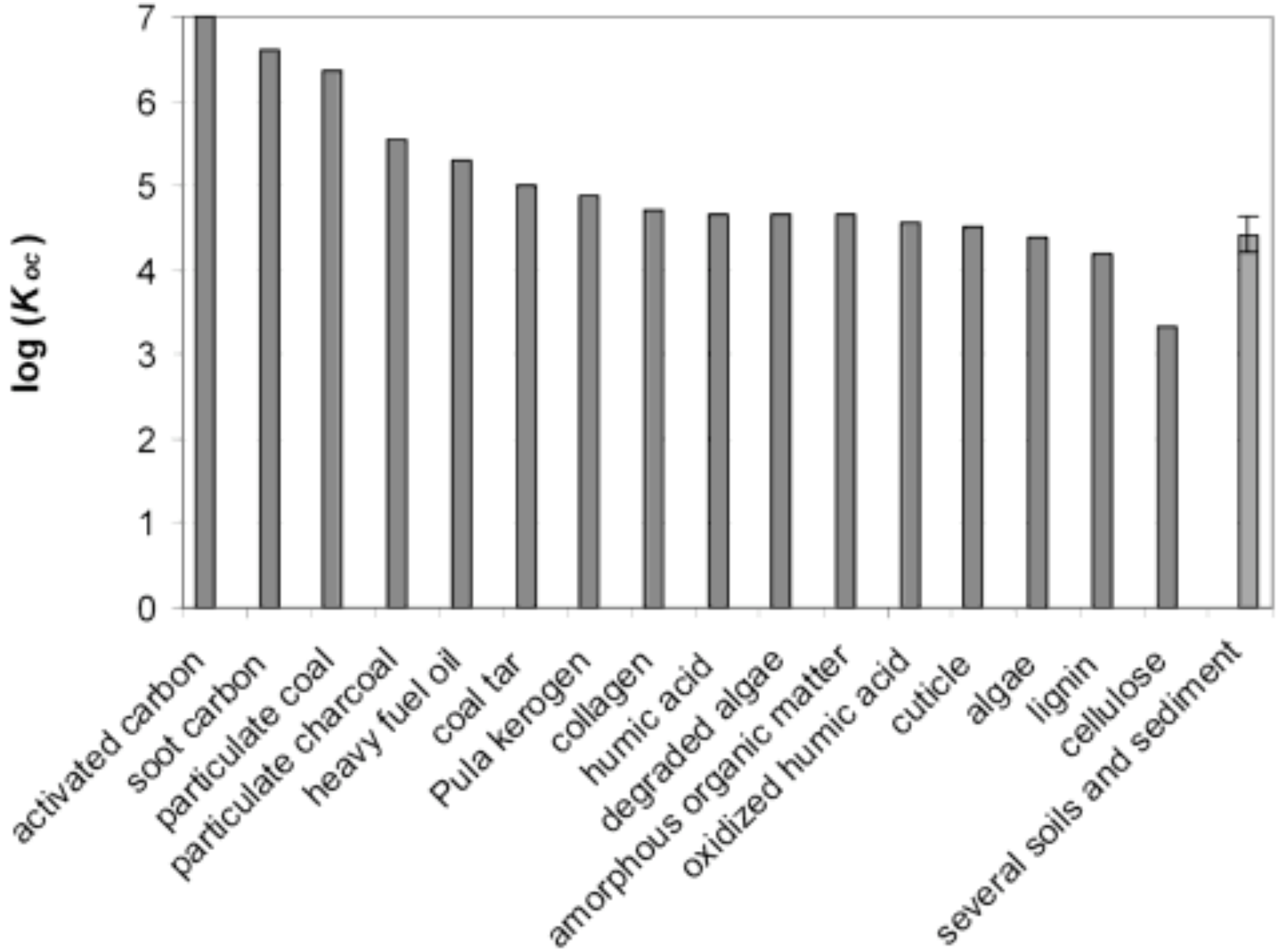

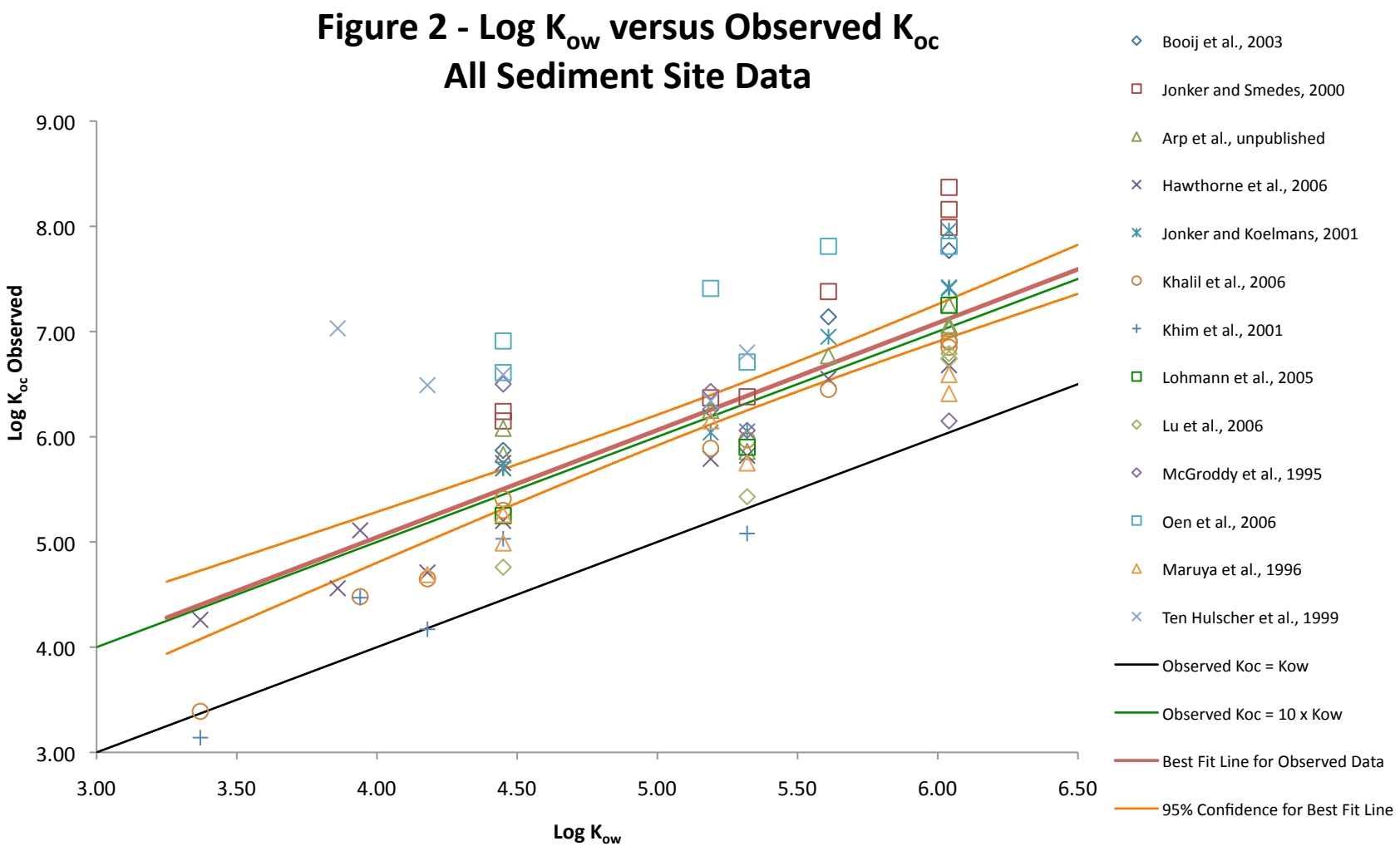
Figure 2 - Log K_{ow} versus Observed K_{oc}
All Sediment Site Data
Log K_{oc} Observed
Log K_{ow}
9.00
8.00
7.00
6.00
5.00
4.00
3.00
3.00
3.50
4.00
4.50
5.00
5.50
6.00
6.50
Booij et al., 2003
Jonker and Smedes, 2000
Arp et al., unpublished
Hawthorne et al., 2006
Jonker and Koelmans, 2001
Khalil et al., 2006
Khim et al., 2001
Lohmann et al., 2005
Lu et al., 2006
McGroddy et al., 1995
Oen et al., 2006
Maruya et al., 1996
Ten Hulscher et al., 1999
Observed Koc = Kow
Observed Koc = 10 x Kow
Best Fit Line for Observed Data
95% Confidence for Best Fit Line

Figure 3 - Log K_{ow} versus Observed K_{oc}
Freshwater to Brackish Sediment Sites

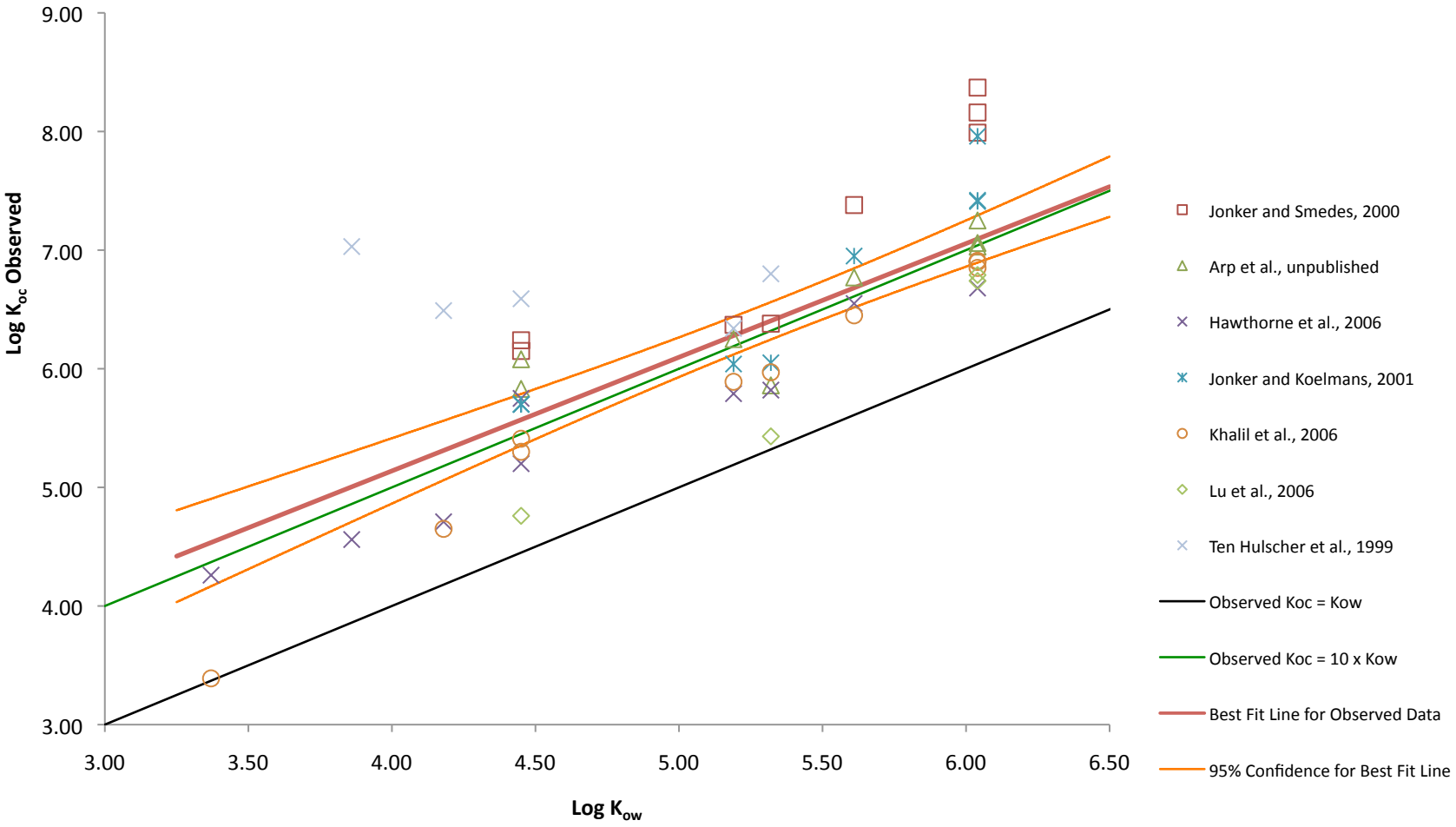

Figure 4 - Log K_{ow} vs Observed Log K_{oc}

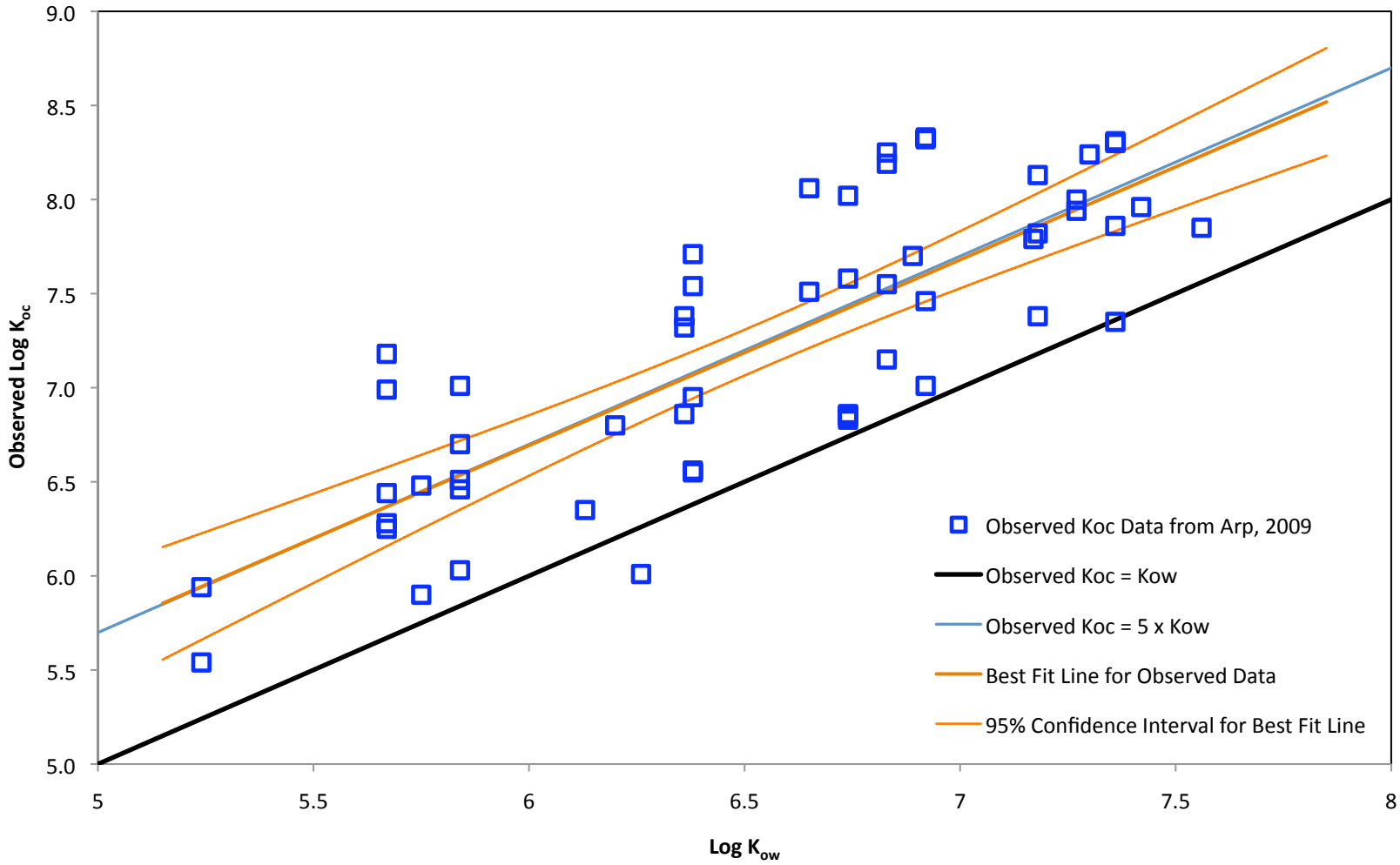

Log K_{ow} values from Hawker, 1988

Figure 5 - Log K_{ow} vs Observed Log K_{oc}

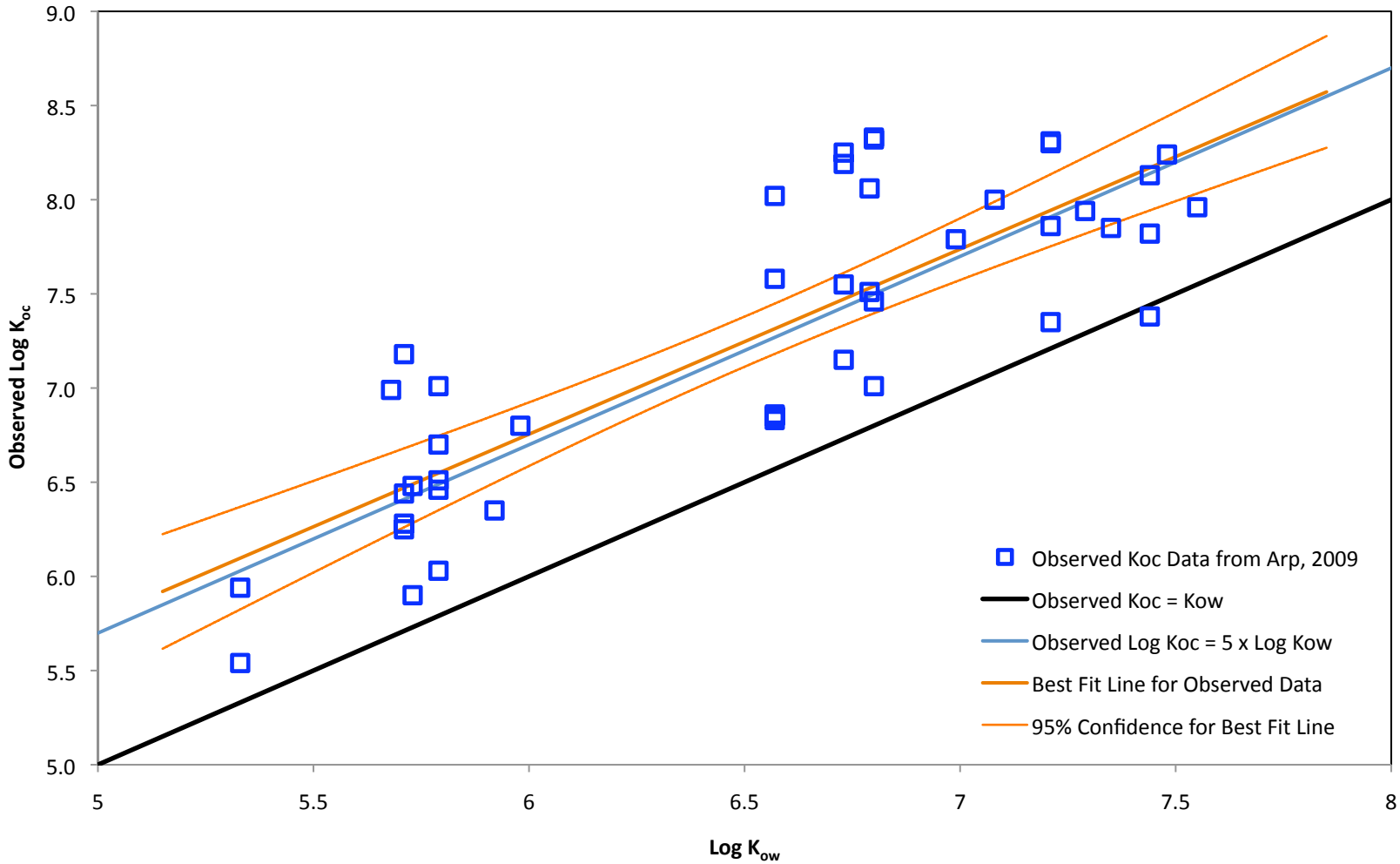

Log K_{ow} values from Lu et al. 2007

ATTACHMENT 3

MODEL VALIDATION

Parsons Engineering Department

Certificate of Software Validation

User Discipline HYDROGEOLOGY **Certification No.** HY-009

Software Title. Active Capping Transport Model **Date of Validation** 01/06/09

Software Supplier REIBLE[1] **Validated Version** Version 2.0

Software Description and Use 1-Dimensional, solute transport model through a sediment cap, also see attached documentation.

System Requirements:

Operating System	Windows XP/Vistas
RAM	512K
Hard Disk	yes
Math Coprocessor	yes
Windows	yes
Other	Matlab version 7.7 or later

Restrictions/Limitations see attached documentation

The above-named software is certified as a validated software. The scope of this validation is as follows:

a. The software has demonstrated satisfactory function for its intended tasks, through the following verification methods (check all pertinent items):

- **(2) By independent verification testing.**
- ___ **By extensive use on active projects.**
- ___ **Industry tested and proven.**
- ___ **NRC/other agency approved (list agency and number if possible).**
- **(1) Supplier-performed verification.**
- ___ **Other (describe)**

b. All users have received/will receive suitable instructions/sufficient documentation to use the software.

Submitted: **Software Custodian** _____ **Date** _____

Approved: **Section Manager** _____ **Date** _____

(1) Danny Reible, Ph.D., Bettie Margaret Smith Professor of Environmental Health Engineering, Department of Civil, Architectural, Environmental Engineering, The University of Texas at Austin, 1 University Station C1786, Austin, TX 78712-0273.

(2) Model results were compared with well-documented 1-D solute transport equations by Charles Andrews. See attached memorandum.

Printed copies of this document are uncontrolled copies.

This article was downloaded by: *[reible@mail.utexas.edu]*
On: *24 June 2009*
Access details: *Access Details: [subscription number 912623667]*
Publisher *Taylor & Francis*
Informa Ltd Registered in England and Wales Registered Number: 1072954 Registered office: Mortimer House, 37-41 Mortimer Street, London W1T 3JH, UK

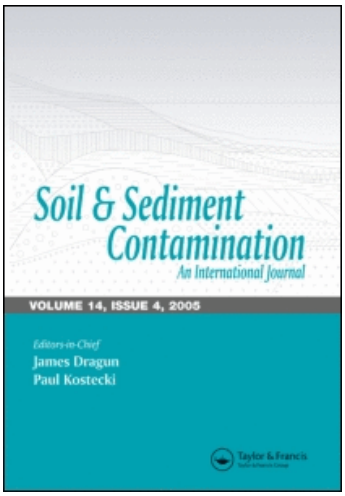

Soil and Sediment Contamination: An International Journal
Publication details, including instructions for authors and subscription information:
http://www.informaworld.com/smpp/title~content=t713401148

An Analytical Modeling Approach for Evaluation of Capping of Contaminated Sediments

David J. Lampert [a]; Danny Reible [a]
[a] Department of Civil, Architectural, Environmental Engineering, The University of Texas at Austin, Austin, TX, USA

Online Publication Date: 01 July 2009

To cite this Article Lampert, David J. and Reible, Danny(2009)'An Analytical Modeling Approach for Evaluation of Capping of Contaminated Sediments',Soil and Sediment Contamination: An International Journal,18:4,470 — 488

To link to this Article: DOI: 10.1080/15320380902962387

URL: http://dx.doi.org/10.1080/15320380902962387

PLEASE SCROLL DOWN FOR ARTICLE

Full terms and conditions of use: http://www.informaworld.com/terms-and-conditions-of-access.pdf

This article may be used for research, teaching and private study purposes. Any substantial or systematic reproduction, re-distribution, re-selling, loan or sub-licensing, systematic supply or distribution in any form to anyone is expressly forbidden.

The publisher does not give any warranty express or implied or make any representation that the contents will be complete or accurate or up to date. The accuracy of any instructions, formulae and drug doses should be independently verified with primary sources. The publisher shall not be liable for any loss, actions, claims, proceedings, demand or costs or damages whatsoever or howsoever caused arising directly or indirectly in connection with or arising out of the use of this material.

Soil and Sediment Contamination, 18:470–488, 2009
Copyright © Taylor & Francis Group, LLC
ISSN: 1532-0383 print / 1549-7887 online
DOI: 10.1080/15320380902962387

Taylor & Francis
Taylor & Francis Group

An Analytical Modeling Approach for Evaluation of Capping of Contaminated Sediments

DAVID J. LAMPERT AND DANNY REIBLE

Department of Civil, Architectural, Environmental Engineering,
The University of Texas at Austin, Austin, TX, USA

Downloaded By: [reible@mail.utexas.edu] At: 00:03 24 June 2009

An analytical design tool is developed to predict performance of a cap for containment of contaminated sediments. Transient conditions within a cap can be modeled by advection, diffusion, and reaction within the typically homogeneous chemical isolation layer for which analytical models exist. After contaminant penetration of the chemical isolation layer, a steady state model is proposed that incorporates pore water advection and diffusion, sediment erosion and deposition, sediment re-working and pore water pumping via bioturbation, and reaction. The steady state model allows the complexities of the biologically active layer to be considered while maintaining an analytical form for convenient and rapid evaluation. In this paper, the model framework, behavior, and limitations are presented.

Keywords Capping, contaminated sediments, modeling

Introduction

Remediation of contaminated sediments is one of the most challenging problems in environmental engineering today. One of the primary risks associated with contaminated sediments is bioaccumulation in benthic organisms, which is a route of entry into the food chain. Thus an important goal of sediment remediation is reducing concentrations to these organisms.

Few alternatives exist for management of contaminated sediments. One promising technology for reducing exposure and risk to contaminated sediments *in situ* is through the use of capping with clean media. Capping with clean media has been shown to reduce surficial sediment concentrations in the lab and to agree well with traditional mass transport models (Thoma et al., 1991). In a field study, Azcue et al. (1998) found that the flux of metals was reduced significantly one year after capping. Zeman and Patterson (1997) discuss the successful implementation of a sand cap in Hamilton Harbor, Ontario, Canada. A capping project in the St. Paul Waterway near Tacoma, Washington, successfully demonstrated habitat restoration (Parametrix, 1998). Ten years of monitoring showed minimal cap disturbance and the ability of capping to contain contaminants. As an added benefit, sand capping restored shallow-water habitat that had been reduced by 90% over the past

Address correspondence to Danny Reible, Bettie Margaret Smith Professor of Environmental Health Engineering, Department of Civil, Architectural, Environmental Engineering, The University of Texas at Austin, 1 University Station C1786, Austin, TX 78712-0273, USA. E-mail: reible@mail.utexas.edu

100 years. Simpson et al. (2002) found that capping was successful at reducing metal fluxes, particularly due to organism-induced mixing (bioturbation) in the clean cap material rather than in the sediments.

The primary purposes of a cap over contaminated sediments are:

1. Armoring contaminated sediments to ensure they are not re-suspended in high flow conditions.
2. Physically isolating contaminated sediments from benthic organisms that typically populate only the upper few cm of sediment.
3. Providing resistance to transport processes that result in chemical release from the sediments.

Because many sediment contaminants are highly sorptive, their migration through a cap can be retarded due to accumulation on the clean cap material. A portion of the cap is typically compromised by the following processes: intermixing between sediment and the lower layer of the cap, expression of contaminated pore water by consolidation of underlying sediment, and bioturbation (organism-related mixing) of the near surface layer. The remaining layer is termed the chemical isolation layer. It has been estimated that the time for typical sediment contaminants to migrate through strongly sorbing chemical isolation layers may be hundreds or thousands of years (Murphy et al., 2006). For other less sorbing caps where the breakthrough time is shorter, capping can serve as a mass transport resistance to reduce the steady state flux and surficial concentrations near the sediment-water interface.

Evaluation and design of sediment caps require a model to predict the relationship of design parameters to chemical fate and transport processes that take place within the contaminated sediment cap containment system. Chemical migration in porous containment layers can be estimated using a transient advection-diffusion model as described by Bear (1972). For example, numerous approaches to the transport of contaminants through soil containment layers have been presented (e.g. Rowe and Booker, 1985; Rubin and Rabideau, 2000; Malusis and Shackelford, 2002). The majority of this work has been applied to soil slurry liners, which differ from sediment caps in several important ways.

The top of the sediment cap (hereafter referred to as the bioturbation layer) is subject to significantly different transport processes and rates than in the underlying cap layer and may exhibit significantly different physical and chemical characteristics, such as increased organic carbon content and sharp gradients in redox conditions. The organisms that reside in this zone also re-work sediment particles; this process significantly affects chemical transport. It is also within this zone that chemical reactivity is highest due to the exchange of nutrients, labile organic matter, and electron acceptors with the overlying water. The thickness of the cap may increase due to deposition or decrease due to erosion. Finally, mass transport at the sediment-water interface requires different boundary conditions than those used in soil slurries due to the presence of turbulent motion in the overlying surface water.

The EPA has provided guidance for *in situ* cap design (Palermo et al., 1998). The important considerations for cap design are minimizing erosion, reducing contaminant flux to biological receptors, and providing appropriate thickness to account for consolidation of the surficial sediments. The EPA guidance document presents a simplistic approach for evaluating contaminant fluxes and concentrations in a sediment cap. In this approach, the transient migration and flux through the cap system is assumed to be controlled by the chemical isolation layer and estimated by advection or diffusion. This approach does not include

Downloaded By: [reible@mail.utexas.edu] At: 00:03 24 June 2009

important processes such as degradation and cannot predict contaminant concentrations or fluxes in the biologically active zone that is often of primary importance.

In this paper, an approach is presented to address these limitations. The result is a set of analytical models that can be used for initial screening and evaluation of sediment capping. Because the models are analytical, they can be used for rapid evaluation across a range of parameter values and can be used as a check for more complex numerical models, which may be applied to situations where no exact solution to the governing equations exists.

The models developed here enable an assessment of the concentration within the chemical isolation layer of a cap at any time, the time over which a cap is effective, and the potential exposure in the biologically active zone after contaminant penetration of the chemical isolation layer. The recommended approach is to employ a one-layer analytical transient model under the assumption of a semi-infinite domain until penetration of the chemical isolation layer occurs (i.e. while the assumption is valid). Upon penetration of the chemical isolation layer, the relatively rapid transport processes in the surface layer will subsequently quickly lead to steady state conditions. Under steady state conditions it is possible to consider the complexities of the upper boundary and still employ relatively simple analytical solutions to the chemical transport equations. Through use of a steady state model, it is possible to estimate the maximum contaminant concentration and flux that may ever be achieved within the biologically active zone. Thus the model can be used to determine a conservative cap design through estimation of the maximum concentrations and fluxes in the biologically active zone. The transient model presented here is equivalent to the one presented in the EPA guidance document (Palermo et al., 1998) but is included for completeness and discussion of how to adapt the model to evaluate other processes such as burial by sediment deposition. The combination of the transient model for the chemical isolation layer and the steady state model for the chemical isolation and bioturbation layers presented here provide:

1. the concentration profiles during contaminant migration through the chemical isolation layer;
2. the time of complete separation of the benthos from the contaminants;
3. the maximum concentration and flux that will be achieved after penetration of the cap assuming constant concentration in the underlying sediment.

Downloaded By: [reible@mail.utexas.edu] At: 00:03 24 June 2009

Conceptual Model

The conceptual model divides the system into five different parts: the underlying sediment, the chemical isolation layer, the biologically active or bioturbation layer, the sediment-water interface (benthic boundary) layer, and the overlying water column. The placed cap layer, with thickness h_{cap}, consists of both the chemical isolation layer, with thickness h_{eff}, and the bioturbation layer, with thickness h_{bio}. The underlying sediment layer also includes the zone in which cap and sediment have intermixed during placement as the pore water concentrations in this region are essentially indistinguishable from those in the underlying sediment. In transient calculations any portion of the cap compromised by chemical migration due to consolidation should also be considered part of the underlying sediment (Palermo et al., 1998). Under steady state conditions, however, pore water expression and consolidation do not influence contaminant behavior.

The underlying sediment concentration is assumed constant. In a real sediment capping system, as contaminants are transported from the former sediment-water interface to the clean cap material the concentrations in the underlying sediment would change. The

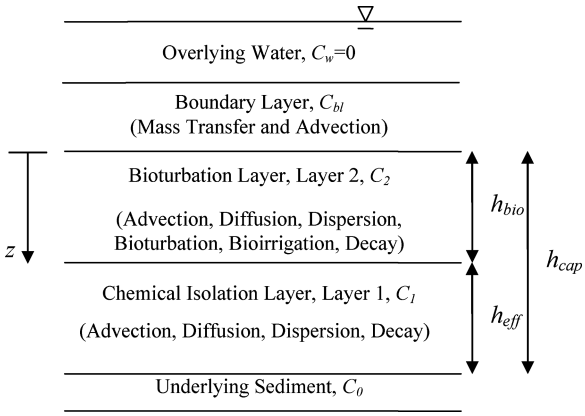

Figure 1. Sediment cap system and parameter definition.

Downloaded By: [reible@mail.utexas.edu] At: 00:03 24 June 2009

concentration at the bottom of the cap would likely decrease with depletion of mass to the capping materials. However, as shown by Rabideau and Kandelwahl (1998), the most conservative boundary condition for the underlying contaminated material in a containment system is constant concentration. Any change in the actual concentration would likely be a decrease as mass is lost to the cap material, which provides further conservatism to this assumption. An alternative to constant concentration in the sediment would be to model the entire sediment layer; this approach is more robust but would require numerical simulation to describe behavior in the sediment column and capping layer.

The transport processes in the chemical isolation layer are advection, diffusion/dispersion, and decay. For the bioturbation layer, bioturbation-induced movement of particles and bioirrigation of pore water are also considered. Bioturbation-related processes are considered quasi-diffusive and hence are assumed to increase the effective diffusion/dispersion coefficient. Transport through the aqueous boundary layer is dictated by the benthic boundary layer mass transfer coefficient (Boudreau and Jorgensen, 2001). Benthic boundary layer mass transfer is controlled by the turbulence in the overlying water. For river systems, this process is controlled by parameters such as current and water depth. In lake systems, this coefficient is typically controlled by lake mixing processes. Imberger and Hamblin (1982) provide an excellent overview of mechanisms of mixing processes in lakes; mechanisms of lake mixing including wind, wave and buoyancy-driven circulation. Figure 1 shows the conceptual model of the sediment cap system along with the model coordinate system.

Due to the low solubility of most sediment contaminants, the bulk sediment loading, W (mass of contaminant on solid phase per mass of solid phase), is the parameter that is typically used for quantifying contaminant levels in sediments instead of the pore water (mobile phase) concentration. W depends upon the sorption properties of the sediment or cap layer, however, and is potentially discontinuous while the pore water concentration is both continuous across interfaces and directly represents the mobile phase contaminants. Under the assumption of linear partitioning, the bulk sediment loading can be related to the pore water concentration, C, through the following relationship, assuming local equilibrium:

$$W = K_d C \tag{1}$$

Where K_d represents the effective sediment-water partition coefficient in the cap material. It is generally reasonable to assume local equilibrium with the pore water at some effective (measured) partition coefficient due to the relatively slow contaminant migration rates within the sediment bed. Of critical importance to the rate of migration of contaminants in the cap material is the ratio of the total concentration (mass per unit volume) in the porous cap matrix to that of the mobile phase concentration, or the retardation factor, R_1 (defined in terms of model parameters subsequently).

For organic contaminants, the contaminant partition coefficient is often estimated as the product of the fraction organic carbon f_{oc} and the organic carbon partition coefficient, K_{oc}. This is likely a crude assumption in the underlying sediment that has been shown to exhibit a different relationship due to desorption resistance (McGroddy and Farrington, 1995) but may be a good assumption for the cap material and the new (clean) sediment. For typical sand, the organic carbon fraction tends to be less than 0.1%. At these low organic carbon contents, mineral sorption tends to become important even for organic compounds; so the assumption of 0.01–0.1% organic carbon is likely a lower bound to the effective sorption of organic contaminants on sandy cap materials (Schwarzenbach et al., 2003).

Due to the limited sorptive capacity of sand caps, permeable adsorptive caps, sometimes referred to as active caps, have been proposed (Reible et al., 2007; McDonough et al., 2007). These caps may contain organic sorbents such as activated carbon, organo-modified clays, coke, or metal sorbents such as apatite. These could be incorporated in the modeling approach herein by using the appropriate effective partition coefficient, although for sorbents exhibiting nonlinear sorption behavior, such as activated carbon, the model results are only approximate. Permeable reactive caps with enhanced degradation characteristics have also been proposed, although their long-term efficacy has not been demonstrated.

The approach presented here is developed using pore water concentrations, which represent the mobile contaminant phase in a stable cap and may be more closely related to the contaminants available for bioaccumulation (e.g. Lu et al., 2006; Beckles et al., 2007). Based on the assumptions listed above, the domain of the model for the cap system consists of two layers: the chemical isolation layer and the bioturbation layer. The underlying sediment, benthic layer, and overlying water are utilized to develop boundary conditions.

Downloaded By: [reible@mail.utexas.edu] At: 00:03 24 June 2009

Transient Model and Containment Breakthrough Time

The governing transport equation for the chemical isolation layer (Layer 1) is:

$$R_1 \frac{\partial C_1}{\partial t} - U \frac{\partial C_1}{\partial z} = D_1 \frac{\partial^2 C_1}{\partial z^2} - \varepsilon_1 \lambda_1 C_1 \tag{2}$$

Where C_1 is the pore water concentration in the isolation layer, z is the depth downward from the cap-water interface, t is the time, λ_1 is the decay rate constant, R_1 is the retardation factor in the layer (defined here as the ratio of the total concentration to that in the mobile phase), U is the effective advective velocity (assumed to be directed upward although a negative value is still appropriate), and ε_1 is the porosity in the layer. The decay of the contaminant is assumed to be first-order and to occur only in the pore water. Thus seemingly large decay rate constants may have only a minimal impact on mass degradation rate since only a small fraction of the contaminants resides in the pore water. The strong sorptive nature of most sediment contaminants limits the rate of degradation due to limited bioavailability (Hyun et al., 2006; Beckles et al., 2007).

For an active capping system, the chemical isolation layer must be further subdivided into sand and active layer(s), which would require introduction of additional governing and appropriate boundary conditions (continuity of concentration and flux) for each layer. The transport equation for each layer would be essentially the same, with the primary difference arising from the retardation term. For sorbing cap materials such as organoclays and peats that obey linear partitioning relationships, the governing equations would differ only in the value of the retardation factor. For a nonlinear sorption model (such as activated carbon) the governing equations would be almost the same, although the retardation factor would no longer be constant but a function of concentration. Note that in either case at steady state the sorption term disappears and the steady state model developed herein still applies.

For the chemical isolation layer, the bottom boundary condition is assumed to be a first-type or Dirichlet boundary with a concentration of C_0:

$$C_1(z = h_{cap}) = C_0 \tag{4}$$

For modeling during the transient period, i.e. before significant penetration of the overlying biologically active layer, the chemical isolation layer may be approximated as semi-infinite, which produces the second boundary condition:

$$\lim_{z \to -\infty} \frac{\partial C_1}{\partial z} = 0 \tag{5}$$

For an initially clean cap, the initial condition is:

$$C_1(t = 0) = 0 \tag{6}$$

The transient behavior can be estimated using an analytical solution to Equation (2) subject to the conditions in (4), (5), and (6). The solution to this problem was presented by van Genuchten (1981):

$$C(z,t) = \frac{C_0}{2} \left\{ \begin{array}{l} \exp\left[\dfrac{(U-u)(h_{cap}-z)}{2D_1}\right] \operatorname{erfc}\left[\dfrac{R_1(h_{cap}-z)-ut}{\sqrt{4D_1R_1t}}\right] + \\ \exp\left[\dfrac{(U+u)(h_{cap}-z)}{2D_1}\right] \operatorname{erfc}\left[\dfrac{R_1(h_{cap}-z)+ut}{\sqrt{4D_1R_1t}}\right] \end{array} \right\} \tag{7}$$

$$u = \sqrt{U^2 + 4\varepsilon\lambda_1 D_1}$$

The transient model (7) is appropriate until the time when the isolation layer is completely compromised by migration from below by the processes of advection, diffusion, and dispersion. For a diffusion-dominated problem with no decay, Equation (7) reduces to the well-known complementary error function solution:

$$C = C_0 erfc\left(\frac{R_1^{0.5}(h_{cap}-z)}{\sqrt{4D_1t}}\right) \tag{8}$$

This equation can be assumed valid while the concentration at the boundary of the containment and bioturbation layers is small; the complementary error function is equal to about 0.01 when the argument is about two (i.e. when the concentration predicted at the top of the cap layer is 1% of the underlying sediment concentration). Therefore, a conservative

Downloaded By: [reible@mail.utexas.edu] At: 00:03 24 June 2009

estimate of penetration time for a diffusion-dominated system is:

$$t_{diff} = \frac{R_1 h_{eff}^2}{16 D_1} \tag{9}$$

For an advection-dominated system with no decay, Equation (7) reduces to a front or step function with velocity U/R_1 ; hence an appropriate time for penetration is:

$$t_{adv} = \frac{R_1 h_{eff}}{U} \tag{10}$$

Because advection and diffusion/dispersion act together to compromise the chemical isolation layer, the time for penetration of the layer can be estimated by assuming the processes act in parallel. Thus, a time scale characteristic of the advective-diffusive migration through the isolation layer can be written:

$$t_{adv/diff} \approx \frac{1}{1/t_{diff} + 1/t_{adv}} \approx \frac{1}{16 D_1/(R_1 h_{eff}^2) + U/(R_1 h_{eff})} \approx \frac{R_1 h_{eff}^2}{16 D_1 + U h_{eff}} \tag{11}$$

For times long compared to $t_{adv/diff}$ a steady state model will describe concentrations and fluxes in the cap. The transient time through the biologically active layer is typically negligible compared to that in the chemical isolation layer due both to its small thickness (5–15 cm) and the rapid sediment reworking and contaminant migration rates in this layer. Thus for times long compared to $t_{adv/diff}$, a steady state model is applicable to both the chemical isolation layer and the overlying bioturbation layer.

To verify the applicability of the relatively simple approach in Equation (11), the time required to achieve a concentration at the top of the chemical isolation layer equal to 1% of the concentration at the sediment-cap interface ($C/C_0 = 0.01$) and the time required to achieve a flux at the top of the chemical isolation layer 1% of the flux at the sediment-cap interface, $F/F_0 = 0.01$, were calculated from a full advection-diffusion model and compared to the prediction of Equation (11). The ratio of the flux at the top of the chemical isolation layer to the flux at the sediment-cap interface was calculated by,

$$F/F_0 = \frac{F(z = h_{bio}, t)}{F(z = h_{cap}, t)} = \frac{UC(z = h_{bio}, t) + D_1 \frac{\partial C(z=h_{bio},t)}{\partial z}}{UC(z = h_{cap}, t) + D_1 \frac{\partial C(z=h_{cap},t)}{\partial z}} \tag{12}$$

The results were computed for dimensionless time, τ, in terms of the dimensionless Peclet number, Pe, which is defined as:

$$\tau = \frac{t D_1}{R_1 h_{eff}^2} \tag{13}$$

$$Pe = \frac{U h_{eff}}{D_1} \tag{14}$$

The times to concentration or flux equal to 1% of that at the bottom of the sediment were calculated for two solutions to Equation (2), a semi-infinite cap layer and a finite cap layer with a zero concentration at the cap-water interface ($z = 0$). The calculated times were identical for both boundary conditions, since the top boundary does not affect the solution until significant penetration of the complete chemical isolation layer has occurred. The results in Figure 2 show that the prediction of breakthrough based on Equation (11)

Downloaded By: [reible@mail.utexas.edu] At: 00:03 24 June 2009

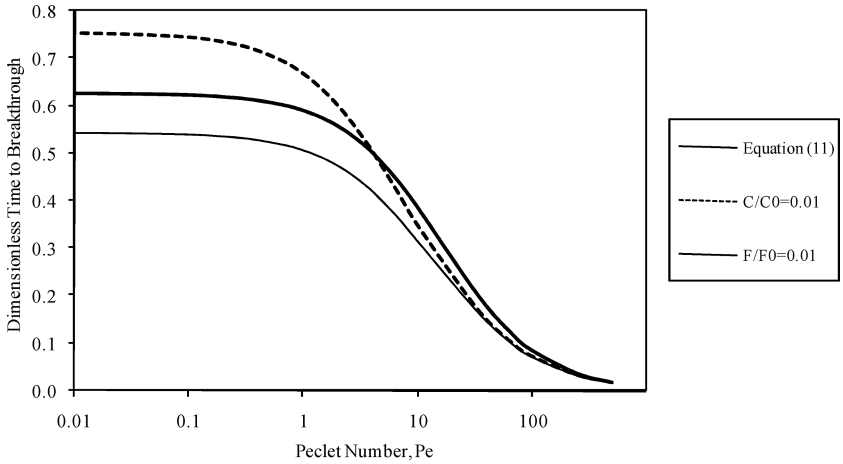

Figure 2. Comparison of breakthrough time approaches. Time required to achieve concentration (C) or flux (F) at top of the chemical isolation layer equal to 1% of the concentration (C_0) or flux (F_0) at the bottom of the layer from full solutions of Equation (2).

Downloaded By: [reible@mail.utexas.edu] At: 00:03 24 June 2009

fall between those based on flux and concentration at low *Pe*, while at high *Pe* Equation (11) slightly over-predicts breakthrough for both cases. The maximum over prediction compared with an F/F_0 value of 0.01 basis was 23%. It appears that Equation (11) provides a reasonable estimate for penetration time for a non-reactive solute over the entire range of *Pe* and, in particular, provides a good estimate of the time before conditions in the biologically active layer will begin to influence concentration profiles within the cap. Any decay would retard the breakthrough time and as a result the predictions from Equation (11) would be conservative.

The Bioturbation Layer and the Sediment-Water Interface

The transport equation for the bioturbation layer has the same general form as the chemical isolation layer; however, the processes of bioturbation are assumed to increase the effective diffusion/dispersion coefficient. The decay rate and retardation factor in the bioturbation layer may also be different than those observed in the chemical isolation layer. The Darcy velocity U must be the same for water (assumed incompressible). The transport equation for the bioturbation layer (Layer 2) is:

$$R_2 \frac{\partial C_2}{\partial t} - U \frac{\partial C_2}{\partial z} = D_2 \frac{\partial^2 C_2}{\partial z^2} - \varepsilon_2 \lambda_2 C_2 \tag{15}$$

Where C_2 is the concentration in the bioturbation layer, R_2 is the retardation factor in the bioturbation layer, D_2 is the effective diffusion/dispersion coefficient for the bioturbation layer, λ_2 is the decay rate for the bioturbation layer, and ε_2 is the porosity in the layer.

At the interface between the chemical isolation layer and the bioturbation layer, the concentrations and fluxes in the two layers must be equal. Recognizing that the advective flux is the same in each layer, the following represent appropriate boundary conditions at the interface between the bioturbation and underlying containment layers (here C_{bio} is

defined as the concentration at the interface):

$$C_1(z = h_{bio}) = C_2(z = h_{bio}) = C_{bio} \tag{16}$$

$$-D_1 \frac{\partial C_1(z = h_{bio})}{\partial z} = -D_2 \frac{\partial C_2(z = h_{bio})}{\partial z} \tag{17}$$

The boundary condition at the cap-water interface is the most complex, as it essentially requires the effluent boundary condition from a porous medium, which has a long history and is the subject of many papers (Hulbert, 1944; Danckwerts, 1953; Wehner and Wilhelm, 1956). The concept of a benthic boundary layer mass transfer resistance composed of a laminar (diffusive) sublayer above the sediment-water interface has long been used for modeling mass transport from surficial sediments and is widely accepted in soil and marine science (see Boudreau, 1997). A complete mass balance on the interface results in the following expression (Boudreau and Jorgensen, 2001):

$$UC_2(z = 0^+) - D_2 \frac{\partial C_2(z = 0^+)}{\partial z} + R' = U_{bl} C_{bl}(z = 0^-) + k_{bl}(C_{bl} - C_w) \tag{18}$$

Where *R'* represents transport of contaminants from the exposed surficial sediment to the overlying water, and U_{bl}, $k_{bl,}$, and $C_{bl}(z)$ represent the effective advective velocity, effective mass transfer coefficient, and concentration in the benthic boundary layer, respectively. The value of R' has been shown to be small relative to the other processes (Boudreau and Jorgensen, 2001). The effective mass transfer coefficient in the benthic boundary layer can also be thought of as a diffusion in a laminar sublayer of thickness, δ, separating the cap-water interface from the bulk overlying water of concentration, C_w:

$$k_{bl}(C_{bl} - C_w) = D_{bl} \frac{C_{bl} - C_w}{\delta} \tag{19}$$

The value in the overlying surface water is taken to be zero without loss of generality (all other concentrations are taken relative to this surface water concentration). Combining these assumptions results in the following boundary condition of the third kind (Boudreau and Jorgensen, 2001):

$$D_2 \frac{\partial C_2(z = 0^+)}{\partial z} = k_{bl} C_{bl}(z = 0^-) = k_{bl} C_2(z = 0^+) \tag{20}$$

Steady State Model

To evaluate the concentrations in the combined containment and bioturbation layers, the relative importance of the different transport mechanisms can be evaluated with the following dimensionless numbers, which are defined as:

$$Pe_1 = \text{Peclet number in chemical isolation layer} = \frac{U h_{eff}}{D_1} = \frac{\text{Rate of advection}}{\text{Rate of diffusion}} \tag{21}$$

$$Da_1 = \text{Damkohler number in chemical isolation layer} = \frac{\varepsilon_1 \lambda_1 h_{eff}^2}{D_1} = \frac{\text{Rate of decay}}{\text{Rate of diffusion}} \tag{22}$$

Downloaded By: [reible@mail.utexas.edu] At: 00:03 24 June 2009

$$Pe_2 = \text{Peclet number in bioturbation layer} = \frac{Uh_{bio}}{D_2} \tag{23}$$

$$Da_2 = \text{Damkohler number in bioturbation layer} = \frac{\varepsilon_2 \lambda_2 h_{bio}^2}{D_2} \tag{24}$$

$$Sh = \text{Sherwood number at cap-water interface} = \frac{k_{bl} h_{bio}}{D_2} = \frac{\text{Rate of mass transfer}}{\text{Rate of diffusion}} \tag{25}$$

Under steady state conditions the time derivatives in Equations (2) and (15) disappear. Equations (2) and (15) can be re-written in terms of the dimensionless parameters introduced above:

$$h_{eff}^2 \frac{\partial^2 C_1}{\partial z^2} + Pe_1 h_{eff} \frac{\partial C_1}{\partial z} - Da_1 C_1 = 0 \tag{26}$$

$$h_{bio}^2 \frac{\partial^2 C_2}{\partial z^2} + Pe_2 h_{bio} \frac{\partial C_2}{\partial z} - Da_2 C_2 = 0 \tag{27}$$

By assuming a solution of an exponential form, the general solution of (26) and (27) can be obtained. At steady state the concentrations at the boundaries of the domain are constant and assumed to have values of C_0 at the cap-sediment interface, C_{bio} at the boundary of the chemical isolation and bioturbation layers, and C_{bl} at the cap-water interface. The solutions to the governing ordinary differential equations are thus:

$$C_1 = \frac{C_{bio} e^{-\frac{Pe_1}{2}} - C_0 e^{-\beta}}{2 \sinh \beta} \exp\left[\left(\frac{Pe_1}{2} + \beta\right) \frac{h_{cap} - z}{h_{eff}}\right] + \frac{C_0 e^{\beta} - C_{bio} e^{-\frac{Pe_1}{2}}}{2 \sinh \beta} \times \exp\left[\left(\frac{Pe_1}{2} - \beta\right) \frac{h_{cap} - z}{h_{eff}}\right] \tag{28}$$

$$\beta = \sqrt{\frac{Pe_1^2}{4} + Da_1}$$

$$C_2 = \frac{C_{bl} e^{-\frac{Pe_2}{2}} - C_{bio} e^{-\gamma}}{2 \sinh \gamma} \exp\left[\left(\frac{Pe_2}{2} + \gamma\right) \frac{h_{bio} - z}{h_{bio}}\right] + \frac{C_{bio} e^{\gamma} - C_{bl} e^{-\frac{Pe_2}{2}}}{2 \sinh \gamma} \times \exp\left[\left(\frac{Pe_2}{2} - \gamma\right) \frac{h_{bio} - z}{h_{bio}}\right] \tag{29}$$

$$\gamma = \sqrt{\frac{Pe_2^2}{4} + Da_2}$$

The values of C_{bio} and C_{bl} can be determined by applying the boundary conditions (17) and (20) to Equations (28) and (29):

$$C_{bio} = \frac{C_o \frac{Pe_2}{Pe_1} e^{\frac{Pe_1}{2}} \beta \sinh \gamma}{\frac{Pe_2}{Pe_1} \beta \cosh \beta \sinh \gamma + \gamma \sinh \beta \cosh \gamma - \frac{\gamma^2 \sinh \beta}{\left(Sh + \frac{Pe_2}{2}\right) \sinh \gamma + \gamma \cosh \gamma}} \tag{30}$$

Downloaded By: [reible@mail.utexas.edu] At: 00:03 24 June 2009

$$C_{bl} = \frac{C_0 e^{\frac{Pe_1+Pe_2}{2}}}{\left(\frac{Pe_1}{2} + \frac{Pe_1 Sh}{Pe_2}\right)\frac{\sinh\beta\cosh\gamma}{\beta} + \left(\frac{Pe_2}{2} + Sh\right)\frac{\cosh\beta\sinh\gamma}{\gamma} + \frac{Pe_1\gamma\sinh\gamma\sinh\beta}{Pe_2\beta} + \cosh\beta\cosh\gamma} \tag{31}$$

The concentration of contaminants in the bioturbation layer is of particular interest, as benthic organisms in the layer often provide the primary route of entry of contaminants into the food chain. Hence, another important parameter is the average concentration in the bioturbation layer. This concentration can be used to evaluate the potential long-term effectiveness of a sediment cap. Integrating Equation (29) over the bioturbation layer and dividing by the depth of the bioturbation layer provides the average value:

$$(C_{bio})_{avg} = \frac{C_{bl}e^{-\frac{Pe_2}{2}} - C_{bio}e^{-\gamma}}{2\sinh\gamma}\frac{e^{\frac{Pe_2}{2}+\gamma} - 1}{\frac{Pe_2}{2}+\gamma} + \frac{C_{bl}e^{\gamma} - C_{bio}e^{-\frac{Pe_2}{2}}}{2\sinh\gamma}\frac{e^{\frac{Pe_2}{2}-\gamma} - 1}{\frac{Pe_2}{2}-\gamma} \tag{32}$$

The average solids loading in the bioturbation layer, $(W_{bio})_{avg}$, can be determined from the partitioning relationship between the pore water and the sediment, where $(f_{oc})_{bio}$ is the expected fraction of organic carbon in the newly deposited sediment:

$$(W_{bio})_{avg} = (f_{oc})_{bio} K_{oc} (C_{bio})_{avg} \tag{33}$$

Additionally, the flux to the overlying water column, J, may be of interest. This can be evaluated by:

$$J = (k_{bl} + U)C_{bl} \tag{34}$$

Numerical Model Comparison

To check the validity of the analytical solutions for both the transient and steady state models, Equations (2) and (15) subject to boundary conditions (4), (16), (17), and (20) and initial condition (6) were solved independently by numerical analysis. A finite differencing scheme using the Crank-Nicolson method (Crank and Nicolson, 1947) with a forward difference for the advection term and central difference for the diffusion term was employed for the analysis. Reasonable estimates for the parameters were assumed for two cases using the methods described above. Simulations were performed for low and high values of Pe_1. Figure 3 shows that results of the simulations and the analytical solutions (7) and (28–31) are equivalent. Thus the analytical solutions can be used to predict concentrations within the chemical isolation layer during the transient period and to predict the steady state behavior. For estimation of cap behavior in the transition time between $\tau_{\text{adv/diff}}$ and steady state, a numerical model must be employed to approximate the solution to the governing equations.

Characterization of Transport Parameters

The factors R_1 and R_2 as defined here are the ratios of the total concentration in an elementary sediment volume (stationary phase) to that in the pore water (mobile phase) for the containment and bioturbation layers, respectively. A significant proportion of the total concentration in the pore water may be present in colloidal organic matter (Baker et al., 1985; Chin and Gschwend, 1992; Schlautman and Morgan, 1993). Chin and

Downloaded By: [reible@mail.utexas.edu] At: 00:03 24 June 2009

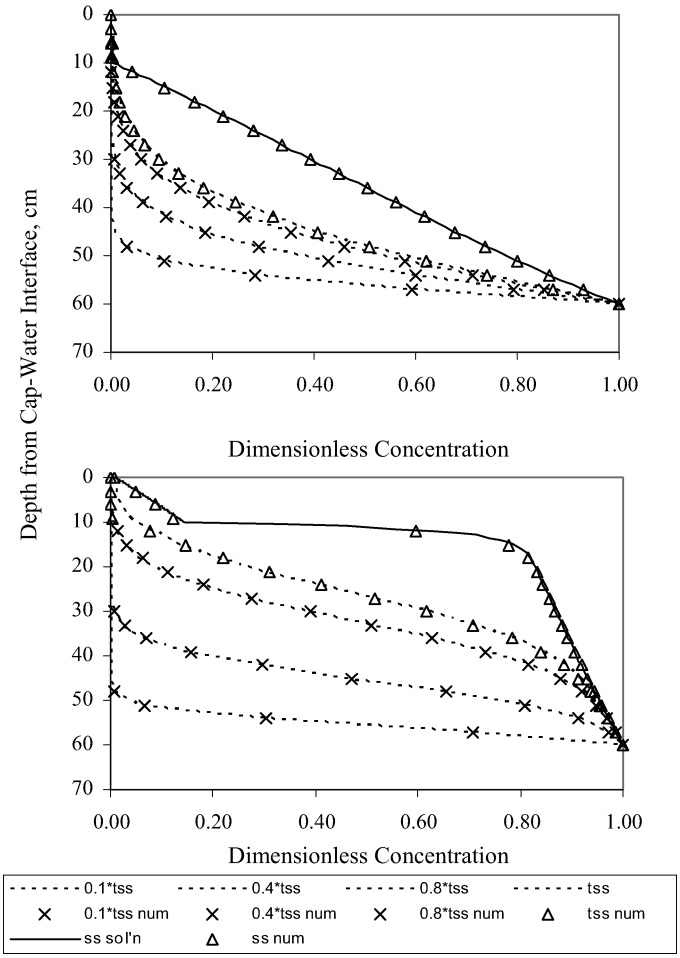

Figure 3. Transient and steady state concentration profiles throughout cap: comparison of analytical with numerical solution. Top: low flow ($Pe_1 = 0.66$); Bottom: high flow ($Pe_1 = 32.8$).

Downloaded By: [reible@mail.utexas.edu] At: 00:03 24 June 2009

Gschwend (1992) found this relationship to be linear. Thus partitioning onto the total organic carbon in the pore water, ρ_{DOC}, with a colloidal organic carbon partition coefficient, K_{DOC}, serves to increase the effective solubility of the compounds. Coupling this assumption with the linear partitioning onto the cap material, and recognizing that the fractional organic carbon in the bioturbation layer, $(f_{oc})_{bio}$ will over time be different from that in the containment layer, $(f_{oc})_{eff}$, produces the following relationships for R_1 and R_2 in terms of ρ_{oc}, K_{DOC}, ε, the particle density ρ_P, and K_{oc}:

$$R_1 = \frac{\varepsilon_1 + \varepsilon_1 \rho_{DOC} K_{DOC} + (1 - \varepsilon_1)\rho_P (f_{oc})_{eff} K_{oc}}{1 + \rho_{DOC} K_{DOC}} \tag{35}$$

$$R_2 = \frac{\varepsilon_2 + \varepsilon_2 \rho_{DOC} K_{DOC} + (1 - \varepsilon_2)\rho_P (f_{oc})_{bio} K_{oc}}{1 + \rho_{DOC} K_{DOC}} \tag{36}$$

The Darcy velocity, U, here accounts for both groundwater upwelling and the effect of erosion/deposition. In a coordinate system fixed relative to the cap-water interface,

deposition or erosion changes the net advective flux. Because particle deposition effectively buries both pore water and solid associated contaminants, the effective advective flux also encompasses both. The effective advective velocity associated with both the Darcy pore water upwelling, V, the velocity of sediment deposition, V_{dep}, and the retardation factor applicable to the cap-sediment layer, R, is:

$$U = V - RV_{dep} \tag{37}$$

Note that although new sediment is typically deposited at the cap–water interface, the mixing in this region is rapid and governed by bioturbation, or particle mixing processes that are not subject to retardation by pore water transport. Transient migration in the underlying cap containment layer is delayed by burial with new sediment and the apparent shifting of the sediment interface. For estimation of the time delay associated with burial, R in Equation (37) can be conservatively estimated by R_1 (the retardation in the underlying sand), despite the fact that typically more sorbing sediment is deposited at the cap-water interface (characterized by R_2). In the event of net erosion rather than deposition the value of V_{dep} is negative. For the purposes of conservative estimates and due to uncertainties over future deposition rates, it is often assumed that the deposition of new sediment is negligible despite the fact that contaminated sediments have typically accumulated in net depositional areas.

The advective flow is perhaps the most important parameter in this analysis, as it will dominate in many natural systems. The flow may be upward or downward, in which case the value is negative. In the absence of direct measurements, the flow may be modeled using Darcy's Law. This approach requires an understanding of the hydrogeology of the area, including the effective hydraulic conductivity of the sediment/groundwater system and the local groundwater elevation levels driving the flow rate. For direct measurement of groundwater flux, seepage meters such as the one described by Lee (1977) may be used to measure the groundwater seepage rate. Alternatively, Cook et al. (2003) describe methods for estimating flux using different kinds of tracers. The local effective hydraulic conductivity for the sediment-cap system is dictated by the layer with the lowest hydraulic conductivity. The hydraulic conductivity of the system is generally unaffected by the presence of a cap (since it is often composed of relatively coarse granular media) although the cap could be constructed to control permeability or may cause consolidation in the underlying sediment, reducing its permeability.

The value of D_1 is the sum of the diffusion and dispersion coefficients. Diffusion through granular porous media is often characterized by an effective diffusion coefficient D_{diff} given by the molecular diffusivity D_w times the porosity (the available diffusion area) and divided by a hindrance parameter (the lengthening of the diffusion path by the media). The model of Millington and Quirk (1961), where the hindrance parameter is taken to be the porosity to the negative one-third power, is widely used for diffusion in granular porous media such as a typical sand cap:

$$D_{diff} = \varepsilon_1^{\frac{4}{3}} D_w \tag{38}$$

Boudreau (1997) suggests an alternative that may be more applicable for fine-grained sediments:

$$D_{diff} = \frac{\varepsilon_1 D_w}{1 - \ln \varepsilon_1^2} \tag{39}$$

Downloaded By: [reible@mail.utexas.edu] At: 00:03 24 June 2009

The molecular diffusivity is a function of temperature and molecular weight and can be estimated from the literature (e.g. Lyman et al., 1990). Mechanical dispersion characterized by D_{disp} of the contaminant through the cap can be modeled as the product of the velocity through the cap and some length scale defined as the dispersivity, α:

$$D_{disp} = \alpha U \tag{40}$$

Thus, the effective diffusion/dispersion coefficient in the containment layer can be determined by:

$$D_1 = \varepsilon_1^{\frac{4}{3}} D_w + \alpha U \tag{41}$$

After placement of a sediment cap, new sediment is deposited at the cap surface. As this deposition occurs, the top of the sediment cap is re-colonized by benthic organisms (worms and other macro invertebrates). These organisms blend the sediments at the top of cap, resulting in relatively rapid transport of contaminants from the bottom of the layer to the overlying water. Provided that the movement of particles and pore water by these organisms is essentially random, the length scale of the movement of the particles is smaller than that being studied (i.e. the cap thickness), and time scale between mixing events is smaller relative to other processes, the transport processes can be taken as quasi-diffusive (Boudreau, 1986). The diffusion-like mixing of particles is known as bioturbation, while the diffusion-like mixing of pore water is bioirrigation. These processes increase diffusion/dispersion coefficient from the containment layer, D_1, to that in the bioturbation layer, D_2. The flux of a chemical species, J^p_{bio}, associated with the diffusion of these particles associated with a bioturbation coefficient of D^p_{bio} and a solid-phase concentration (mass of chemical species per unit volume sediment particle) of M is:

$$J^p_{bio} = -D^p_{bio} \frac{\partial M}{\partial z} \tag{42}$$

If the time for movement of the sediment particles plus the time between particle movement events is large compared with that of desorption of contaminants, local equilibrium can be assumed, and the value of M can be re-written in terms of pore water concentration (noting that ε, ρ_{p}, $(f_{oc})_{bio}$, and K_{oc} are independent of depth):

$$J^p_{bio} = -D^p_{bio}(1-\varepsilon)\rho_P (f_{oc})_{bio} K_{oc} \frac{\partial C_2}{\partial z} \tag{43}$$

In addition to particle mixing, organisms also irrigate the surficial sediments through direct pore water exchange from the underlying sediments to the overlying water. The transport of contaminants associated with this process can be modeled by:

$$J^{pw}_{bio} = -D^{pw}_{bio} \frac{\partial C}{\partial z} \tag{44}$$

Thus the processes of bioturbation and bioirrigation serve to increase the effective diffusion/dispersion coefficient. The values of D^p_{bio} and D^{pw}_{bio} can be measured using radioactive tracers, such as described by McCafree et al. (1980). Thoms et al. (1995) provide an extensive review of measured biodiffusion coefficients at different locations in the United States. The effective diffusion coefficient for the bioturbation layer, D_2, can be determined

Downloaded By: [reible@mail.utexas.edu] At: 00:03 24 June 2009

from the following:

$$D_2 = D_1 + D_{bio}^{pw} + D_{bio}^{p}(1-\varepsilon)\rho_P(f_{oc})_{bio}K_{oc} \tag{45}$$

The decay rates λ_1 and λ_2 are highly compound and site specific. The model taken here is based on first-order kinetics, which may not be appropriate as the degradation may depend on many factors other than the contaminant concentration but provides a relatively simple way of incorporating this important mechanism into a mathematical model. In the absence of a site-specific study, the literature may be used to estimate a degradation rates.

Transport at the cap-water interface is dictated by the benthic boundary layer mass transfer coefficient, which is a function of the turbulence and shear of the overlying water column. Boudreau and Jorgensen (2001) and Thibodeaux (1996) present empirical correlations for k_{bl} based on mixing conditions in the overlying water. The value of k_{bl} should be conservatively estimated, as its value directly affects the surficial sediment concentrations.

Downloaded By: [reible@mail.utexas.edu] At: 00:03 24 June 2009

Steady State Model Behavior

The steady state model presented in (28–31) is a function of only the five parameters (21–25) and the depth of the two layers. To illustrate the behavior of the solution, consider a one-foot (30 cm) thick sand cap with an expected bioturbation depth of 10 cm. For Case I, consider a conservative ($Da_1 = Da_2 = 0$) contaminant, with $Sh = 10$ (minimal mass transfer limitations) and $D_2 = 10D_1$ ($Pe_2 = 0.05Pe_1$). Figure 4 shows the dimensionless concentration profiles for $0.1 < Pe_1 < 200$. For low Pe_1, the solution approaches a straight line in each layer, which is the expected result of a diffusion-dominated steady state profile. The increased diffusivity in the bioturbation layer results in lower concentrations in that layer. This behavior makes sense physically because the increased mixing rate in the layer reduces the concentrations there (contaminants are transported more rapidly in the bioturbation layer). If advection dominates (high Pe_1), the concentration profile approaches unity; again this is the expected result for an advection problem at steady state. The deviation near the boundary layer is a result of the simplifying assumptions made in the formulation of the top boundary condition. For high advection a more appropriate boundary condition would be a zero gradient. However, the profiles still approach the expected result and provide a reasonable estimation of cap performance even under these conditions. Clearly, at steady state in a high upwelling velocity system a cap will have limited effectiveness.

Now consider a system with degradation (Case II). For simplicity, the Damkohler number in the chemical isolation layer is assumed to be four. The value of D_2 was again taken as $10D_1$, and again it is assumed that $Sh = 10$. The decay rate in the bioturbation layer is taken as ten times that in the chemical isolation layer, a reasonable assumption due to higher levels of nutrients, organic matter, and electron acceptors. These assumptions result in $Pe_2 = 0.05Pe_1$ and $Da_2 = 0.25Da_1 = 1$. Figure 4 shows the dimensionless concentration profiles for $0.1 < Pe_1 < 200$. When compared with the no decay situation, the concentration profiles are lower, as expected. In general, the graphs perform as anticipated mathematically. The concentrations in the bioturbation layer are significantly decreased versus the underlying sediment concentrations. Hence, if it can be proven that a contaminant will decay in a cap, capping is an extremely attractive alternative for remediation.

To evaluate the effects of mass transfer resistance on model output, consider the systems presented in Cases I and II with $Sh = 0.1$ rather than 10 (Cases III and IV). Figure 4 also shows the results for these parameters. For Case III, the concentrations in the cap are minimally reduced even when diffusion-dominated (low Pe_1). The performance

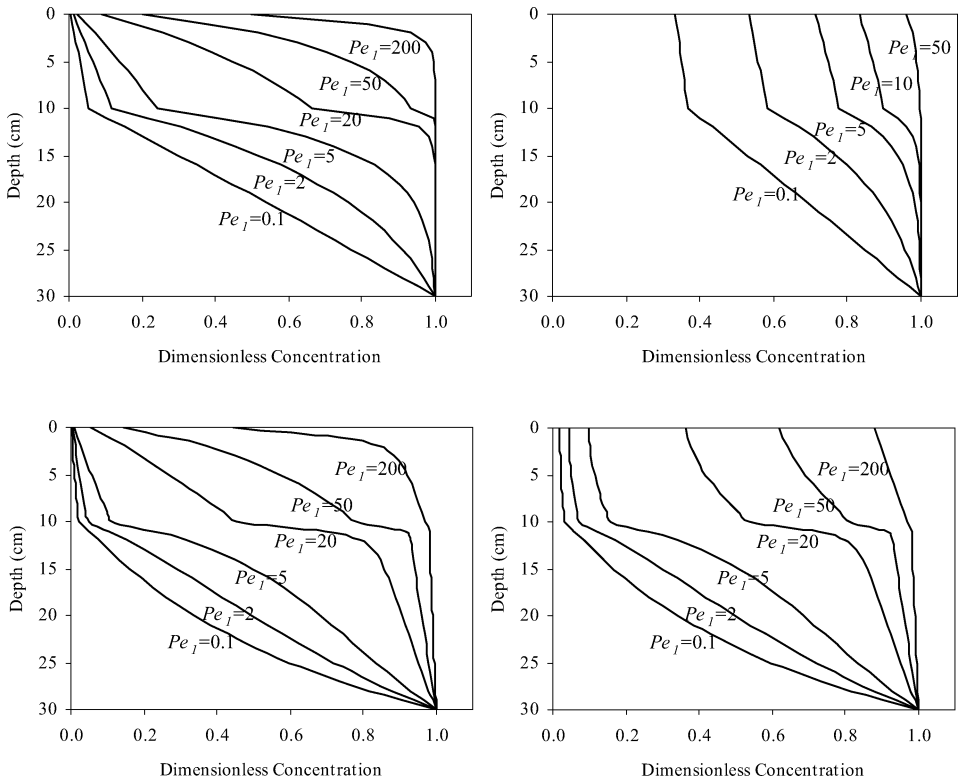

Figure 4. Steady state model behavior. Top left, Case I ($Da_1 = Da_2 = 0$, $Sh = 10$). Bottom left, Case II ($Da_1 = 4$, $Da_2 = 1$, $Sh = 10$). Top right, Case III ($Da_1 = Da_2 = 0$, $Sh = 0.1$). Bottom right, Case IV ($Da_1 = 4$, $Da_2 = 1$, $Sh = 0.1$). The dashed lines represent the interface between the chemical isolation and the bioturbation layers.

is as expected theoretically, with a linear profile in the containment layers at low Pe_1, which approaches a uniform profile for high values of Pe_1. In Case IV, the importance of decay on long term capping success is demonstrated. For a diffusion-dominated system, the bioturbation layer concentrations are drastically reduced over pre-cap levels, even with mass transfer resistance at moderately high advection ($Pe_1 = 5$). Again, as the upwelling velocity is increased, the cap performance is limited.

It is important to note that the model presents steady state concentrations, which may not be realized for many years. Capping may still be a viable option in a case where the transient migration through the containment layer is sufficiently long that natural attenuation processes not included in the models are expected to render the contaminants inconsequential. Steady state predictions beyond this time frame may not be considered important.

These results show the importance of the ground water upwelling velocity in the effectiveness of a cap. The upwelling velocity is a critical parameter in a transient analysis as well as it often controls the steady state flux. Upwelling velocities of the order of cm/day or more may be high enough to effectively negate the effectiveness of a cap even for moderately sorbing contaminants. In addition, the local equilibrium assumption may fail under the influence of extremely high upwelling. So, if capping is under consideration

Downloaded By: [reible@mail.utexas.edu] At: 00:03 24 June 2009

for management of contaminated sediments, it is important for the designer to measure or make a good estimate of the upwelling velocity before making a final decision. Due to the inherent heterogeneity in this parameter, it is also important to evaluate a range of values of upwelling velocity for predicting concentrations that will be used in design and decision making.

The traditional material used for capping sediment is clean sand. However, as demonstrated by these modeling results, a passive sand cap may not be an effective long-term approach for contaminated sediment management for high seepage/low degradation systems. For this reason, one current research focus (Reible et al., 2007; McDonough et al., 2007) is on active capping; that is, capping with materials that may enhance sequestration/degradation in situ or decrease the seepage flow rates through a sediment cap.

Conclusions

In this article, the key processes controlling chemical migration in a cap isolation layer and in the overlying biologically active layer have been highlighted. A simple means for incorporating these processes into an analytical modeling approach has been developed. The approach is subject to a number of limitations. First, several of the models for individual processes are simplistic (e.g. deposition, linear pore water partitioning, first-order decay). The underlying sediment is assumed to maintain a constant concentration. A more robust approach to assessing the concentration in the sediment would be to model fate and transport within the layer based on an initial concentration profile. However, this approach would normally require a numerical simulation in the full-advection diffusion case. Finally, the model is based on two homogeneous layers. Predicting transient concentration profiles in more complex sediment caps with more than two homogeneous layers or with nonlinear sorption would require a more robust approach. The steady state model presented here, however, would still be valid provided the values of diffusion/dispersion coefficients and decay rates were the same. For predicting transient performance of a cap under these scenarios, a numerical solution to the governing equations would be required. The exact solutions presented here represent an important check for future models of this kind.

The model presented here allows calculation of the steady state concentration profile and flux in a sediment cap. When coupled with a transient model of advection, diffusion, and reaction in the chemical isolation layer, this approach forms a relatively simple means of evaluating sediment caps. If the steady state condition is sufficient for achieving remediation objectives, there is no need for a more complicated transient approach. A spreadsheet that computes the analytical model output is available at http://www.caee.utexas.edu/reiblegroup/downloads.html for interested parties.

References

Azcue, J.M., Zeman, A.J., Mudroch, A., Rosa, F., and Patterson, T. 1998. Assessment of sediment and porewater after one year of subaqueous capping of contaminated sediments. *Water Sci. Technol.* **37**, 323–329.

Baker, J.E., Capel, P.D., Eisenreich, S.J. 1985. Influence of colloids on sediment-water partition coefficients of polychlorobiphenyl congeners in natural waters. *Environ. Sci. Technol.* **20**, 1136–1143.

Bear, J. 1972. *Dynamics of Fluids in Porous Media*. Elsevier, New York.

Beckles, D., Chen, W., Hughes, J. 2007. Bioavailability of polycyclic aromatic hydrocarbons sequestered in sediment: microbial study and model prediction. *Environ. Toxicol. Chem.* **26**, 878–883.

Downloaded By: [reible@mail.utexas.edu] At: 00:03 24 June 2009

Boudreau, B. 1986. Mathematics of tracer mixing in sediments, I. Spatially-dependent, diffusive mixing. *Am. J. Sci.* **286**, 161–198.

Boudreau, B. 1997. *Diagenetic Models and Their Implementation: Modeling Transport Reactions in Aquatic Sediments*. Springer-Verlag, New York.

Boudreau, B., and Jorgensen, B. 2001. *The Benthic Boundary Layer*. Oxford University Press, New York.

Chin, Y.P., Gschwend, P.M. 1992. Partitioning of polycyclic aromatic hydrocarbons to marine pore water organic colloids. *Environ. Sci. Technol.* **26**, 1621–1626.

Cook, P.G., Favreau, G., Dighton, J.C., Tickell, S. 2003. Determining natural groundwater influx to a tropical river using radon, chlorofluorocarbons, and ionic environmental tracers. *J. Hydrol.* **277**, 74–88.

Crank, J., and Nicolson, P. 1947. A practical method for numerical evaluation of solutions of partial differential equations of the heat conduction type. *Proc. Camb. Phil. Soc.* **43**, 50–64.

Danckwerts, P.V. 1953. Continuous flow systems. *Chem. Eng. Sci.* **2**, 1–13.

Hulburt, H.M. 1944. Chemical processes in continuous-flow systems: reaction kinetics. *Ind. Eng. Chem.* **36**, 1012–1017.

Hyun, S., Jafvert, C., Lee, L., and Rao, P. 2006. Laboratory studies to characterize the efficacy of sand capping a coal tar-contaminated sediment. *Chemosphere* **63**, 1621–1631.

Imberger, J., and Hamblin, P. 1982. Dynamics of lakes, reservoirs, and cooling ponds. *Annu. Rev. Fluid Mech.* **14**, 153–187.

Lee, D.R. 1977. A device for measuring seepage fluxes in lakes and estuaries. *Limnol. Oceanogr.* **22**, 140–147.

Lu, X., Reible, D.D., and Fleeger, J.W. 2006. Bioavailability of polycyclic aromatic hydrocarbons in field-contaminated Anacostia River (Washington, DC) sediment. *Environ. Toxicol. Chem.* **25**, 2869–2874.

Lyman, W.J, Reehl, W.F. and Rosenblatt, D.H. 1990. *Handbook of Chemical Property Estimation Methods: Environmental Behavior of Organic Compounds*. American Chemical Society, Washington, DC.

Malusis, M., and Shackelford, C. 2002. Theory for reactive solute transport through clay membrane barriers. *J. Contam. Hydrol.* **59**, 291–316.

McCafree, R.J., Myers, A.C., Davey, E., Morrison, G., Bender, M., Luedtke, N., Cullen, D., Froelich, P., and Klinkhammer, G. 1980. The relation between pore water chemistry and benthic fluxes of nutrients and manganese in Narragansett Bay, Rhode Island. *Limnol. Oceanogr.* **25**, 31–44.

McDonough, K., Murphy, P., Olsta, J., Zhu, Y., Reible, D., and Lowry, G. 2007. Development of a sorbent-amended thin layer sediment cap in the Anacostia River. *Soil Sed. Contam.* **16**, 313–322.

McGroddy, S.E., and Farrington, J.W. 1995. Sediment porewater partitioning of polycyclic aromatic hydrocarbons in three cores from Boston Harbor, Massachusetts. *Environ. Sci. Technol.* **29**, 1542–1550.

Millington, R.J., and Quirk, J.M. 1961. Permeability of porous solids. *Trans. Far. Soc.* **57**, 1200–1207.

Murphy, P., Marquette, A., Reible, D. and Lowry, G.V. 2006. Predicting the performance of activated carbon-, coke-, and soil-amended thin layer sediment caps. *J. Environ. Eng.* **132**, 787–794.

Palermo, M., Maynord, S., Miller, J. and Reible, D. 1998. *Guidance Document for In Situ Subaqueous Capping of Contaminated Sediments*, EPA 905-B96–004.

Parametrix. 1998. St. Paul Waterway Area Remedial Action and Habitat Restoration Project. Final 1998 Monitoring Report.

Rabideau, A., and Khandelwal, A. 1998. Boundary conditions for modeling transport in vertical barriers. *J. Environ. Eng.* **124**, 1135–1139.

Reible, D.D, Lampert, D.J., Constant, D., Mutch, R., and Zhu, Y. 2007. Active capping demonstration in the Anacostia River in Washington, DC. *Remed. J.* **17**, 39–53.

Rowe, P.K., and Booker, J.R. 1985. 1-D pollutant migration in soils of finite depth. *J. Geotech. Eng.* **111**, 479–499.

Rubin, H., and Rabideau, A. 2000. Approximate evaluation of contaminant transport through vertical barriers. *J. Contam. Hydrol.* **40**, 311–333.

Downloaded By: [reible@mail.utexas.edu] At: 00:03 24 June 2009

Schlautman, M.A., and Morgan, J.J. 1993. Effects of aqueous chemistry on the binding of polycyclic aromatic hydrocarbons by dissolved humic materials. *Environ. Sci. Technol.* **27**, 961–969.

Schwarzenbach, R., Gshwend, P., and Imboden, D. 2003. Chapter 9, Sorption I: Introduction and sorption processes involving organic matter and Chapter 11: Sorption III: Sorption processes involving inorganic surfaces. *Environmental Organic Chemistry*, 2nd ed., pp. 275–330 and 387–458. Wiley & Sons, Hoboken, New Jersey.

Simpson, S., Pryor, I., Mewburn, B., Batley, G., and Jolley, D. 2002. Considerations for capping metal-contaminated sediments in dynamic estuarine environments. *Environ. Sci. Technol.* **36**, 3772–3778.

Thibodeaux, L.J. 1996. Chapter 5: Chemical exchange between water and adjoining earthen material. *Environmental Chemodynamics*, pp. 255–368. John Wiley, New York.

Thoma, G., Reible, D., Valsaraj, K., and Thibodeaux, L. 1991. Efficiency of capping contaminated bed sediments in situ. 1. Laboratory-scale experiments on diffusion-adsorption in the capping layer. *Environ. Sci. Technol.* **25**, 1578–1584.

Thoms, S.R., Matisoff, G., McCall, P.L., and Wang, X. 1995. *Models for Alteration of Sediments by Benthic Organisms*, Project 92-NPS-2, Water Environment Research Foundation, Alexandria Virginia.

Van Genuchten, M. 1981. Analytical solutions for chemical transport with simultaneous adsorption, zero order production and first order decay. *J. Hydrol.* **49**, 213–233.

Wehner, J., and Wilhelm, R. 1956. Boundary conditions of flow reactor. *Chem. Eng. Sci.* **6** 89–93.

Zeman, A., and Patterson, T. 1997. Preliminary results of demonstration capping project in Hamilton Harbour. *Water Qual. Res. J. Can.* **32**, 439–452.

Downloaded By: [reible@mail.utexas.edu] At: 00:03 24 June 2009

S.S. PAPADOPULOS & ASSOCIATES, INC.
Environmental & Water-Resource Consultants

Memorandum

Date: November 23, 2010

From: Charles Andrews

To: Caryn Kiehl-Simpson

Subject: **Active Capping Transport Model – Version 2.0**

The Active Capping Transport Model is a computer program developed by David Lampert and Danny Reible at the University of Texas. The model calculates one-dimensional vertical transport of a contaminant through a sediment cap considering the processes of advection, diffusion, dispersion, reaction, bioturbation, deposition, consolidation, and retardation with local equilibrium between sediment, pore water, and dissolved organic matter. Excellent background documents that describe the processes simulated with the model are "*Guidance for In-Situ Subaqueous Capping of Contaminated Sediments: Appendix B: Model for Chemical Containment by a Cap*" (Palermo and others 1996) and a paper published in Soil and Sediment Contamination by Lampert and Reible (2009). I highly recommend that all users of Active Capping Transport Model read and familiarize themselves with these background documents.

The Active Capping Transport Model was developed as a MATLAB program and is run within the MATLAB environment. I have reviewed several versions of the Active Capping Transport Model and described the results of my reviews in memoranda dated January 6, 2009 and November 5, 2010. In my reviews, I noted several coding issues in the Active Capping Transport Model. These coding issues have all been addressed.

The Active Capping Transport Model Version 2.0 was developed to simulate contaminant transport in a six layer system; model parameters can vary from layer to layer. The governing equation in the Active Capping Transport Model is:

$$R\frac{\partial C}{\partial t} = -U\frac{\partial C}{\partial x} + D\frac{\partial^2 C}{\partial x^2} - n\lambda C \qquad (1)$$

where: C = concentration;
U = Darcy velocity;
D = effective diffusion/dispersion coefficient (sum of diffusion and dispersive coefficients);
R = retardation factor for compound of interest; and
λ = first-order degradation rate.

The governing equation is solved using a two-point upstream centered finite-difference scheme in space with the Crank-Nicolson method. The model automatically creates a finite-difference grid with sufficiently fine-vertical spacing to minimize numerical dispersion; for typical problems a vertical spacing

7944 WISCONSIN AVENUE, BETHESDA, MARYLAND 20814-3620 • TEL: (301) 718-8900 • FAX: (301) 718-8909
www.sspa.com • e-mail: CAndrews@sspa.com

of 0.5 centimeters is specified. The time step size is increased with time from start of simulation for computational efficiency.

A schematic of the 6-layer system simulated with the Active Capping Transport Model is shown to the right. The bottom two layers represent the underlying sediment. These layers can be specified at a constant concentration, can be specified with a finite thickness with depth varying concentrations to simulate a depleting source with time, and can be specified with a constant concentration at base of sediment layer.

Overlying the sediment layer is the chemical isolation layer, which in turn is overlain by an active layer – a layer containing activated carbon.

Overlying the active layer is the buffer and habitat layer, which in turn is overlain by a bioturbation layer. In the real world, the bioturbation zone develops in the upper part of the buffer and habitat layer. In the model the bioturbation zone is treated as a separate layer with properties that differ from those in the underlying layer. At the top of the bioturbation layer, a mass transfer coefficient (M_{bl}) specifies the rate of contaminant transfer to the overlying lake water.

Lake

Layer #	Layer Description	Parameters
6	Bioturbation Layer	b, f_{oc}, n, ρ_s, λ, M_{bl} D_{bp}, D_{bw}, K_{oc}
5	Buffer and Habitat Layer	b, f_{oc}, n, ρ_s, λ, K_{oc}
4	Active Layer	b, f_{oc}, n, ρ_s, λ,Kf, N
3	Chemical Isolation Layer	b, f_{oc}, n, ρ_s, λ,Koc
2 1	Sediment Layer	b, f_{oc}, n, ρ_s, λ,K_{oc}

↑ groundwater flow

The model parameters that are specified for the layers are shown on the schematic above and are defined as follows (note that parameters must be specified in units listed below):

b = layer thickness (cm)
n = porosity
λ = first order decay rate (1/yr)
N = Freundlich coefficient
ρ_s = particle density (g/cm^3)
M_{bl} = mass transfer coef. (cm/hr)

f_{OC} = fraction organic carbon content
Kf = Freundlich coefficient (ug/kg)(L/ug)^N
D_{bw} = water biodiffusion coefficient (cm^2/yr)
D_{bp} = particle biodiffusion coefficient (cm^2/yr)
K_{OC} = organic carbon partition coefficient for specific contaminant (specified for sediment, sand and bioturbation layers separately, L/kg).

Note that the Freundlich coefficients (Kf and N), which are contaminant specific, are specified only in the active layer, and the particle biodiffusion coefficient and the water biodiffusion coefficient are only specified in the bioturbation layer.

In addition to the model parameters that are layer specific are the following parameters:

Kdoc = colloidal partition coefficient for a specific contaminant (L/kg);
Dw = diffusion coefficient for specific contaminant in water (cm^2/sec);
U = Darcy velocity (cm/yr);
Uss = steady-state Darcy velocity (cm/year),
Uc = Darcy velocity due to consolidation (cm/year),
α = dispersion length (cm); and
C_{oc} = colloidal matter concentration (mg/L).

It is important to note that the governing equation (1) has only four parameters – U, R, D and λ. One of these parameters, the first-order decay rate (λ) is specified directly. The other three parameters are derived from the parameters described above. The derivation of the parameters R, D, and U in the governing equation are described below.

The retardation factor is defined for all layers, except for the active layer, as:

$$R = \frac{n + (1-n)\rho_S K_{OC} f_{OC} + nC_{OC}K_{doc}}{1 + C_{OC}K_{doc}} \tag{2}$$

For the active layer, the retardation factor is defined as follows with sorption described by the Fruendlich isotherm:

$$R = \frac{n + (1-n)\rho_S K_f N C^{(N-1)} + nC_{OC}K_{doc}}{1 + C_{OC}K_{doc}} \tag{3}$$

The effective diffusion/dispersion coefficient (D) is defined for all layers except the sediment layer and the bioturbation layer as follows:

$$D = n^{(4/3)} D_w + \alpha \left|U\right| \tag{4}$$

For the sediment layer the effective diffusion/dispersion coefficient (D) is defined as:

$$D = \frac{nD_w}{1 - \ln(n^2)} + \alpha \ |U| \tag{5}$$

This definition uses a relationship developed by Boudreau (1996) to adjust the water diffusion coefficient for the tortuosity of a porous sediment. This relationship better defines the tortuosity relationship in natural sediments than the term used in equation 4 that is based on a relationship developed by Millington (1959). The Millington relationship works best for relatively uniform sands.

For the bioturbation layer the effective diffusion/dispersion coefficient is defined as:

$$D = n^{(4/3)} D_w + \alpha \ |U| + D_{bp} \rho_S (1-n) K_{OC} f_{OC} + D_{bw} \tag{6}$$

The Darcy velocity in the Active Transport Model consists of two components: a steady-state groundwater velocity and a velocity component due to consolidation as

$$U = Uss + Uc \tag{7}$$

.The velocity component due to consolidation is defined on the basis of two parameters (*a* and *b*) as follows:

$$Uc = 30.48 * a * b * t^{(b-1)} \tag{8}$$

where *a* and *b* are coefficients, and *t* is time in years since placement of the cap.

It is important for the user of Active Capping Transport Model to note that the retardation parameter and the effective diffusion/dispersion parameter as defined by equation 1 are not equivalent to those commonly used in the groundwater literature. The retardation parameter commonly used in the groundwater literature (R') in equal to the retardation parameter defined above divided by the porosity (R = R'/n); and equivalently D = D'/n where D' is the effective diffusion/dispersion coefficient commonly used in the groundwater literature.

.

Review and Verification

I checked the accuracy of the calculated concentrations from the Active Capping Transport Model by simulating eight test cases with this computer code and with other computer codes. The other computer codes I used were MT3D (Zheng, 2006), the most-widely used groundwater transport model that has been extensively verified, and an analytical solution to equation 1 (Neville, 2005). The analytical solution was only used for test case 1 as it requires uniform properties. In using MT3D, the test cases were set up in a similar fashion to that used in the Active Capping Transport Model; a finite-difference grid with a vertical spacing of 0.5 centimeters. The TVD solution method was used in MT3D. Consolidation in MT3D was simulated by adjusting the velocity at each time step.

The input parameter values for the eight verification test cases are listed on Table 1. The various test cases were designed to test the model with various combinations of model parameters and boundary conditions. In five of the test cases, a Darcy velocity of 2 cm/year was used. When this velocity is specified, the contaminant transport is dominated by diffusive processes. The other three test cases used velocities of 10 and 20 cm/year. Only one of the test cases, test case 8, considers consolidation. The results from the test cases are presented on Figure 1 which is a series of plots of concentrations with depth as calculated with the models at various times after placement of the cap.

In test case 1, the calculated concentrations from all three models were nearly identical at all times (Figure 1). This indicates that for a media with uniform properties, that both MT3D and the Active Capping Transport Model correctly solve equation 1. This provides a level of confidence that MT3D is an appropriate code to use for verification of the Active Capping Transport Model.

The calculated concentrations from MT3D and the Active Capping Transport Model for tests cases 2 through 8 at various times since placement of the cap are also shown on Figure 1. For each of the test cases, nearly identical concentrations were calculated by MT3D and the Active Capping Transport Model. This provides confidence that the Active Capping Transport Model correctly solves the governing equation.

Conclusions

The Active Capping Transport Model is an appropriate model to use for the evaluation and design of sediment caps for Onondaga Lake. Based on the evaluations described in this memorandum, the computer model accurately solves the governing equation. The computer code for the model is concisely written and is relatively easy to understand. The model is very efficient which makes it feasible to easily conduct Monte Carlo type simulations.

References

Boudreau, B. 1996. The Diffusive Tortuosity of Fine-Grained Unlithified Sediments: *Geochimica et Cosmochimica Acta* 60, no. 16: 3139-3142.

Lambert, D. and D. Reible, 2009. An Analytical Approach for Evaluation of Capping of Contaminated Sediments. Soil and Sediment Contamination. 18:470-488.

Millington, R.J., 1959. Gas diffusion in porous media. Science, Vol. 130:100-102.

Neville, C., 2005. ADFL Analytical Solution – Version 4, User's Guide. S.S. Papadopulos & Associates, Inc. Bethesda, MD.

Palermo, M.R., S. Maynord, J. Miller, and D. Reible, 1996. Guidance for in-situ subaqueous capping of contaminated sediments. Environmental Protection Agency, EPA 905-B96-004, Great Lakes National Program Office, Chicago, Il. Available at http://www.epa.gov/grtlakes/sediment/iscmain/appndb.pdf.

Zheng, C. 2006. MT3DMS v5.2, A modular three-dimensional multispecies transport model for simulation of advection, dispersion and chemical reactions of contaminants in groundwater systems. Supplemental User's Guide. U.S. Army Corps of Engineers Technical Report, October 2006.

Table 1
Input Parameter Values for Test Cases

Parameter	Case 1	Case 2	Case 3	Case 4	Case 5	Case 6	Case 7	Case 8
Contaminant Properties (Contaminant Specific)								
Contaminant	Toluene	Mercury	Mercury	Mercury	Mercury	Mercury	Mercury	Mercury
log Koc	2.35	2.35	2.35	2.35	2.35	2.35	2.35	2.35
log literature Koc - for sand layers	0	2.35	1.00	2.35	2.35	1.00	2.35	2.35
log Kdoc		0	0	0	0	0	0	0
Dw	5.2E-06	4.7E-06	4.7E-06	4.7E-06	4.7E-06	4.7E-06	4.7E-06	4.7E-06
Flow and System Properties (Site Specific)								
Darcy Velocity	2	2	2	2	10	10	20	2
depositional velocity	0	0	0	0	0	0	0	0
hydrodynamic dispersivity	0.42	6.13	6.13	6.13	6.13	6.13	6.13	6.13
boundary layer mass transfer coeff.	0.33	0.36	0.36	0.36	0.36	0.36	0.36	0.36
colloidal matter concentration	0	0	0	0	0	0	0	0
Sediment Properties (Site Specific)								
sediment porosity	0.4	0.79	0.79	0.79	0.79	0.79	0.79	0.79
sediment particle density	2.6	2.62	2.62	2.62	2.62	2.62	2.62	2.62
sediment foc	0.001	0.1	0.1	0.01	0.1	0.1	0.1	0.1
sediment initial decay rate	0	0	0	0	0	0	0	0
duration for initial decay rate	0	1000	1000	1000	1000	1000	1000	1000
sediment final decay rate	0	0	0	0	0	0	0	0
Chemical Isolation Layer Properties (Design Parameters)								
layer thickness	30	30.48	30.48	30.48	30.48	30.48	30.48	30.48
layer porosity	0.4	0.4	0.4	0.4	0.4	0.4	0.4	0.4
layer particle density	2.6	2.6	2.6	2.6	2.6	2.6	2.6	2.6
layer foc	0.001	1E-07	1E-07	1E-07	1E-07	1E-07	1E-07	1E-07
layer initial decay rate	0	2.1E-09	2.1E-09	2.1E-09	2.1E-09	2.1E-09	2.1E-09	2.1E-09
layer final decay rate	0	2.1E-09	2.1E-09	2.1E-09	2.1E-09	2.1E-09	2.1E-09	2.1E-09
Active Layer Properties (Design Parameters)								
active layer thickness (sand plus AC)	17.0	0.3846	0.3846	0.3846	0.3846	0.3846	0.3846	0.3846
active layer porosity	0.4	0.35	0.35	0.35	0.35	0.35	0.35	0.35
active layer particle density (calculated)	2.6	0.80	0.80	0.80	0.80	0.80	0.80	0.80
active layer Freudlich Kf	0.22	22.36	22.36	22.36	22.36	22.36	22.36	22.36
active layer Freundlich 1/n	1	1	1	1	1	1	1	1
active layer initial decay rate	0	2.1E-09	2.1E-09	2.1E-09	2.1E-09	2.1E-09	2.1E-09	2.1E-09
active layer final decay rate	0	2.1E-09	2.1E-09	2.1E-09	2.1E-09	2.1E-09	2.1E-09	2.1E-09
Buffer and Habitat Restoration Layer Properties (Design Parameters)								
Habitat Restoration Layer thickness	55.7	30.48	30.48	30.48	30.48	30.48	30.48	30.48
Buffer Layer thickness	0	0	0	0	0	0	0	0
layers porosity	0.4	0.4	0.4	0.4	0.4	0.4	0.4	0.4
layers particle density	2.6	2.6	2.6	2.6	2.6	2.6	2.6	2.6
layers foc (CI and non-bio HR)	0.001	0.1	0.1	0.1	0.1	0.1	0.1	0.1
layers initial decay rate	0	2.1E-09	2.1E-09	2.1E-09	2.1E-09	2.1E-09	2.1E-09	2.1E-09
layers final decay rate	0	2.1E-09	2.1E-09	2.1E-09	2.1E-09	2.1E-09	2.1E-09	2.1E-09
Bioturbation Layer Properties (Site Specific)								
bioturbation depth	5.5	15.24	15.24	15.24	15.24	15.24	15.24	15.24
bioturbation layer porosity	0.4	0.4	0.4	0.4	0.4	0.4	0.4	0.4
bioturbation layer particle density	2.6	2.6	2.6	2.6	2.6	2.6	2.6	2.6
bioturbation layer foc	0.001	0.1	0.1	0.1	0.1	0.1	0.1	0.1
bioturbation layer initial decay rate	0	2.1E-09	2.1E-09	2.1E-09	2.1E-09	2.1E-09	2.1E-09	2.1E-09
bioturbation layer final decay rate	0	2.1E-09	2.1E-09	2.1E-09	2.1E-09	2.1E-09	2.1E-09	2.1E-09
Pore Water Biodiffusion Coefficient	0	4.7E-06	4.7E-06	4.7E-06	4.7E-06	4.7E-06	4.7E-06	4.7E-06
Particle Biodiffusion Coefficient	0	0	0	0	0	0	0	0
Bioturbation Layer logKoc	0	2.35	2.35	2.35	2.35	2.35	2.35	2.35
Consolidation Data								
parameter a	0	0	0	0	0	0	0	0.211
parameter b	0	0.235	0.235	0.235	0.235	0.235	0.235	0.235
total time for consolidation (years)	0	30	30	30	30	30	30	30
Simulation Parameters								
Simulation length (years)	100	1,000	1,000	1,000	1,000	1,000	1,000	1,000
Minimum number of grid points	150	150	150	150	150	150	150	150
Minimum number of time steps	400	400	400	400	400	400	400	400
Answer 1 for yes and 0 for no								
Infinite source?	1	1	1	0	1	1	1	1
Infinite source at sediment bottom?	1	1	1	1	1	1	1	1

Note: Shaded cells indicate parameters changed relative to Test Case 2.

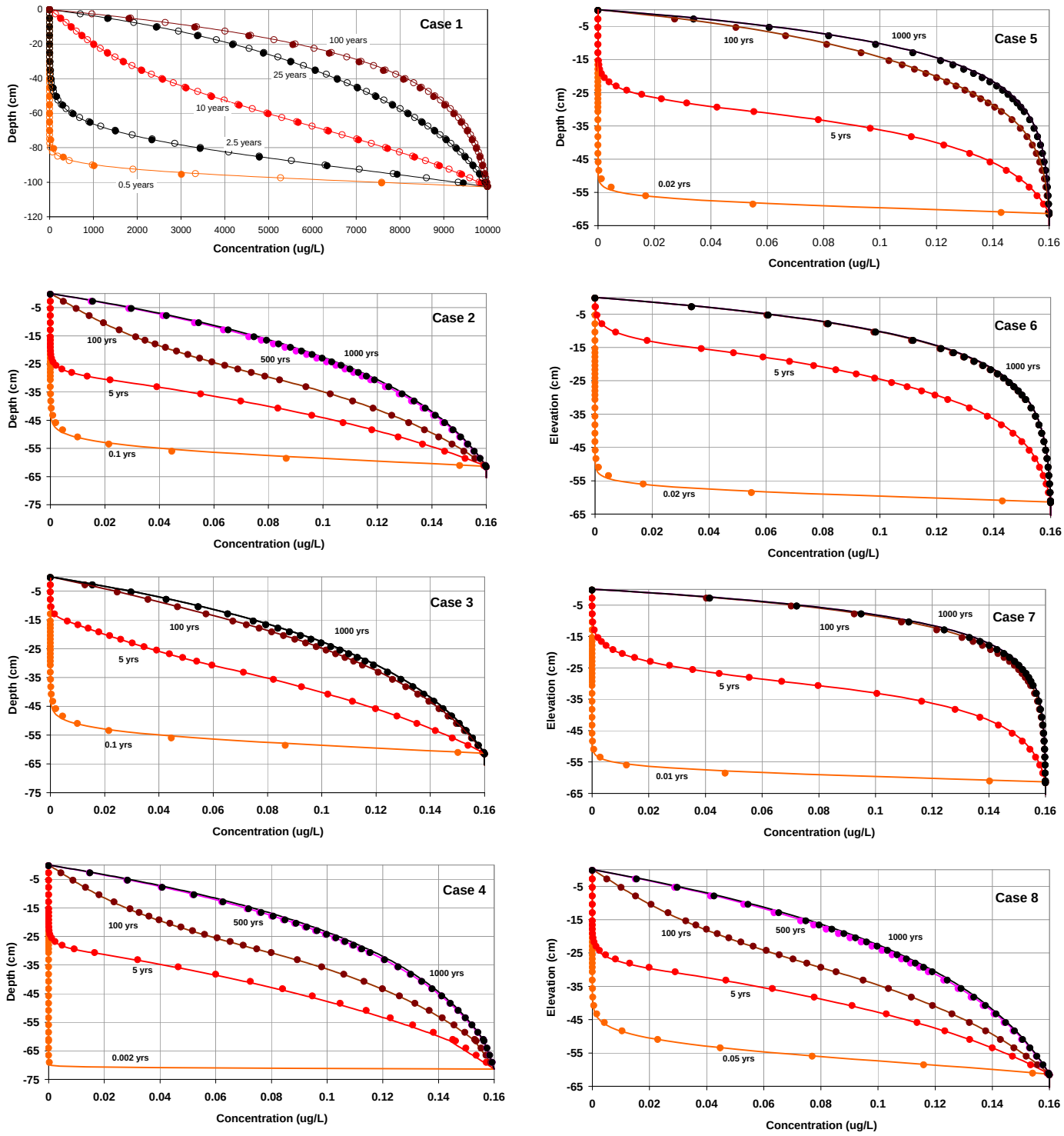

MT3D results plotted as solid dots, Active Capping Transport Model results plotted as solid lines and in Case 1 AFLD results plotted as open circles.

Figure 1 Comparison of Calculated Concentrations for Test Cases 1 through 8

S.S. PAPADOPULOS & ASSOCIATES, INC.
Environmental & Water-Resource Consultants

Memorandum

Date: January 6, 2009

From: Charles Andrews

To: Files

Subject: **Active Capping Transport Model – Version 2.0**

Introduction

Active Capping Transport Model is a computer program developed by David Lampert and Danny Reible at the University of Texas. The model calculates one-dimensional vertical transport of a contaminant through a sediment cap considering the processes of advection, diffusion, dispersion, reaction, bioturbation, deposition and retardation with local equilibrium between sediment, pore water, and dissolved organic matter. An excellent background document that describes the processes simulated with the model is "Guidance for In-Situ Subaqueous Capping of Contaminated Sediments: Appendix B: Model for Chemical Containment by a Cap" (Palermo and others 1996). I highly recommend that all users of Active Capping Transport Model read and familiarize themselves with this background document.

I reviewed Version 2.0 of the Active Capping Transport Model dated December 10, 2008. The model was developed as a MATLAB program and is run within the MATLAB environment. I used MATHLAB Version 7.7 to run the program. The model reads input data from an Excel spreadsheet and writes model outputs to an Excel spreadsheet. The model will not run on earlier versions of MATLAB that do not support reading and writing from Excel files.

Active Capping Transport Model Version 2.0 was developed to simulate contaminant transport in a five layer system; model parameters can vary from layer to layer. The governing equation in the Active Capping Transport Model is:

$$R\frac{\partial C}{\partial t} = -U\frac{\partial C}{\partial x} + D\frac{\partial^2 C}{\partial x^2} - n\lambda C \qquad (1)$$

where: C = concentration;
U = Darcy velocity;
D = effective diffusion coefficient (sum of diffusion and dispersive coefficients);
R = retardation factor for compound of interest; and
λ = first-order degradation rate.

7944 WISCONSIN AVENUE, BETHESDA, MARYLAND 20814-3620 • TEL: (301) 718-8900 • FAX: (301) 718-8909
www.sspa.com • e-mail: CAndrews@sspa.com

To: File
Date: January 6, 2009
Page: 2

The governing equation is solved using a two-point upwind centered finite-difference scheme in space with the Crank-Nicolson method. The model automatically creates a finite-difference grid with sufficiently fine-vertical spacing to minimize numerical dispersion; for typical problems a vertical spacing of 0.5 centimeters is specified. The time step size is increased with time from start of simulation for computational efficiency.

A schematic of the 5-layer system simulated with the Active Capping Transport Model is shown to the right.

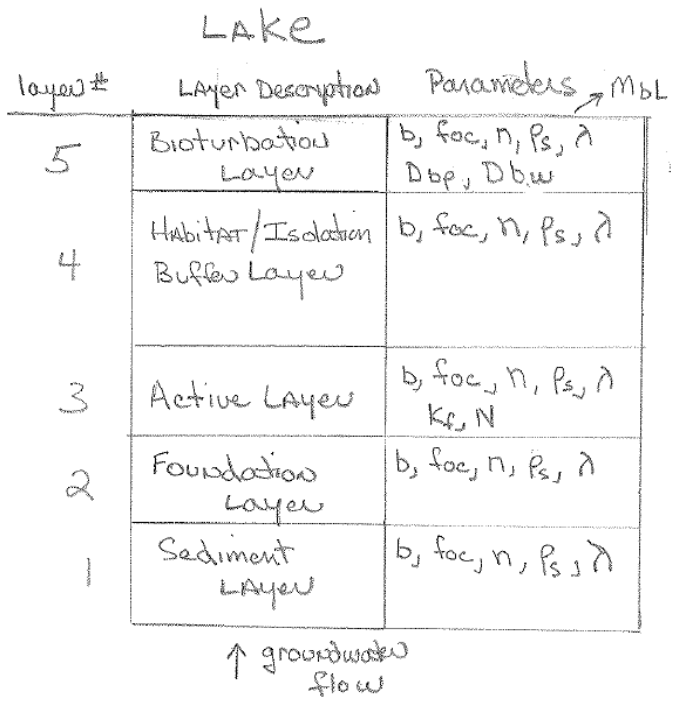

The bottom layer is the sediment layer. This layer can be specified at a constant concentration or it can be specified with a finite thickness with depth varying concentrations to simulate a depleting source with time.

Overlying the sediment layer is the cap foundation layer, which in turn is overlain by an active layer – a layer containing activated carbon.

Overlying the active layer is the habitat/isolation/buffer layer, which in turn is overlain by a bioturbation layer. In the real world, the bioturbation zone develops in the upper part of the habitat/isolation/buffer layer. In the model the bioturbation zone is treated as a separate layer with properties that differ from those in the underlying layer. At the top of the bioturbation layer, a mass transfer coefficient (M_{bl}) specifies the rate of contaminant transfer to the overlying lake water.

The model parameters that are specified for each layer are shown on the schematic above and are defined as follows (note that parameters must be specified in units listed below):

b = layer thickness (cm)
n = porosity
λ = first order decay rate (1/yr)
N = Freundlich coefficient

foc = fraction organic carbon content
ρ_s = particle density (g/cm^3)
Kf = Freundlich coefficient (ug/kg)(L/ug)^N
D_{bp} = particle biodiffusion coefficient (cm^2/yr)
D_{bw} = water biodiffusion coefficient (cm^2/yr)

Note that the Freundlich coefficients (Kf and N), which are contaminant specific, are specified only in the active layer, and the particle biodiffusion coefficient and the water biodiffusion coefficient are only specified in the bioturbation layer.

In addition to the model parameters that are layer specific are the following parameters:

Koc = organic carbon partition coefficient for a specific contaminant (L/kg);
Kdoc = colloidal partition coefficient for a specific contaminant (L/kg);
Dw = diffusion coefficient for specific contaminant in water (cm^2/sec);
U = Darcy velocity (cm/yr);
α = dispersion length (cm);
C_{oc} = colloidal matter concentration (mg/L); and
M_{bl} = upper layer mass transfer coefficient (cm/hr).

It is important to note that the governing equation (1) has only four parameters – U, R, D and λ. Two of these parameters, the Darcy velocity (U) and the first-order decay rate (λ) are specified directly. The other two parameters are derived from the parameters described above. The derivation of the parameters R and D in the governing equation are described below.

The retardation factor is defined for all layers, except for the active layer, as:

$$R = \frac{n + (1-n)\rho_S K_{OC} f_{OC} + nC_{OC}K_{doc}}{1 + C_{OC}K_{doc}} \tag{2}$$

For the active layer, the retardation factor is defined as follows with sorption described by the Fruendlich isotherm:

$$R = \frac{n + (1-n)\rho_S K_f N C^{(N-1)} + nC_{OC}K_{doc}}{1 + C_{OC}K_{doc}} \tag{3}$$

The effective diffusion coefficient (D) is defined for all layers except the sediment layer and the bioturbation layer as follows:

$$D = n^{(4/3)} D_w + \alpha \left|U\right| \tag{4}$$

For the sediment layer the effective diffusion coefficient (D) is defined as:

$$D = \frac{nD_w}{1 - \ln(n^2)} + \alpha \left|U\right| \tag{5}$$

This definition uses a relationship developed by Boudreau (1996) to adjust the water diffusion coefficient for the tortuosity of a porous sediment. This relationship better defines the tortuosity relationship in natural sediments than the term used in equation 4 that is based on a relationship developed by Millington (1959). The Millington relationship works best for relatively uniform sands.

For the bioturbation layer the effective diffusion coefficient is defined as:

$$D = n^{(4/3)} D_w + \alpha \left|U\right| + D_{bp} \rho_S (1-n) K_{OC} f_{OC} + D_{bw} \tag{6}$$

It is important for the user of Active Capping Transport Model to note that the retardation parameter and the effective diffusion parameter as defined by equation 1 are not equivalent to those commonly used in the groundwater literature. The retardation parameter commonly used in the groundwater literature (R') in equal to the retardation parameter defined above divided by the porosity (R = R'/n); and equivalently D = D'/n where D' is the effective diffusion coefficient commonly used in the groundwater literature.

Review and Verification

I checked the computer code for Active Capping Transport Model (parsons.m) to verify that the model input parameters specified for model layers were correctly converted into the parameters used in the governing equation. These conversions are made on lines 99-199 and 329 to 330 of the model code. In the latest version of the code that I reviewed, these conversions were correct except for the calculation of the retardation coefficient with a Freundlich isotherm (equation 3). I modified the code to correctly calculate the retardation coefficient using equation 3 (in the version of the code I reviewed, the term "n+" in the numerator on the right hand side was missing).

I checked the accuracy of the calculated concentrations from the Active Capping Transport Model by simulating four test problems with this computer code and with other computer codes. The other computer codes I used were MT3D (Zheng and Wang, 1998), the most-widely used groundwater transport model that has been extensively verified, and an analytical solution to equation 1 (Neville, 2005). In the first three test cases, a Darcy velocity of 2 cm/year was used. When this velocity is specified, the contaminant transport is dominated by diffusive processes. The fourth test case used a Darcy velocity of 10 cm/year.

To: File
Date: January 6, 2009
Page: 5

The four test problems consisted of the following: 1) problem with uniform properties in the five model layers, 2) problem with uniform properties except for porosity which was varied from layer to layer, 3) problem with sorption in active layer simulated with Freundlich isotherm (in other test problems the Freundlich coefficient N was specified as 1 to simulate linear sorption), and 4) identical to test problem 3 except that Darcy velocity increased from 2 cm/year to 10 cm/year. The model parameters specified for the Active Capping Transport Model for the four test problems are listed below in the format that they appear in the Excel spreadsheet used for model input.

Input Parameter Values for Test Problems

	Test Problem 1	Test Problem 2	Test Problem 3	Test Problem 4	
Contaminant Properties (Contaminant Specific)					
log Koc	2.34947	2.34947	2.34947	2.34947	log L/kg
log Kdoc	0	0	0	0	log L/kg
Dw	5.2187E-06	5.2187E-06	5.2187E-06	4.8541E-06	cm2/s
Flow and System Properties (Site Specific)					
Darcy Velocity	2	2	2	10	cm/yr
depositional velocity	0	0	0	0	cm/yr
hydrodynamic dispersivity	0.42361	0.42361	0.42361	0.42361	cm
boundary layer mass transfer coeff.	0.328	0.328	0.328	0.328	cm/hr
colloidal matter concentration	0	0	0	0	mg/L
Sediment Properties (Site Specific)					
sediment porosity	0.4	0.4	0.4	0.4	
sediment particle density	2.6	2.6	2.6	2.6	g/cm3
sediment foc	0.001	0.001	0.001	0.001	
sediment decay rate	0	0	0	0	yr-1
Foundation Layer Properties (Design Parameters)					
foundation layer thickness	30	30	30	30	cm
foundation layer porosity	0.4	0.5	0.4	0.4	
foundation layer particle density	2.6	2	2.6	2.6	g/cm3
foundation layer foc	0.001	0.001	0.001	0.001	
foundation layer decay rate	0	0	0	0	yr-1
Active Layer Properties (Design Parameters)					
active layer thickness	**17.0**	**17.0**	**17.0**	**17.0**	cm
active layer porosity	0.4	0.8	0.35	0.35	
active layer particle density	2.6	0.8	0.8	0.8	g/cm3
active layer Freudlich Kf	0.22	0.22	5,000.00	5,000.00	$ug/kg*(ug/L)^{-n}$
active layer Freundlich n	1	1	0.44	0.44	
active layer decay rate	0	0	0	0	yr-1
Isolation, Buffer, and Habitat Restoration Layer Properties (Design Parameters)					
Habitat Restoration Layer thickness	40.48	40.48	40.48	40.48	cm
Chemical Isolation Layer thickness	15.24	15.24	15.24	15.24	cm
Buffer Layer thickness	0	0	0	0	cm
isolation layers porosity	0.4	0.3	0.4	0.4	
isolation layers particle density	2.6	2.2286	2.6	2.6	g/cm3
isolation layer foc	0.001	0.001	0.001	0.001	
isolation layer decay rate	0	0	0	0	yr-1
Bioturbation Layer Properties (Site Specific)					
bioturbation depth	5.5	5.5	5.5	5.5	cm
bioturbation layer porosity	0.4	0.4	0.4	0.4	
bioturbation layer particle density	2.6	2.6	2.6	2.6	g/cm3
bioturbation layer foc	0.001	0.001	0.001	0.001	
bioturbation layer decay rate	0	0	0	0	yr-1
Pore Water Biodiffusion Coefficient	0	0	0	0	cm2/yr
Particle Biodiffusion Coefficient	0.00	0.00	0.00	0.00	cm2/yr

The results from the test simulations are shown on the following pages. The analytical solution was only used for test problem 1 as it requires uniform properties. In using MT3D, the problem were set up in a similar fashion to that used in the Active Capping Transport Model; a finite-difference grid with a vertical spacing of 0.5 centimeters was used and the TVD solution method.

In test problem 1 the calculated concentrations from all three models were nearly identical (Figure 1). For the second test problem, the solutions from MT3D and the Active Capping Transport Model compared well (Figure 2). For the third test problem, the solutions from MT3D and the Active Capping Transport Model did not compare well (Figure 3). In the MT3D simulation, based on results for 100 years, it appears that the effective retardation coefficient in the active layer is higher than in the Active Capping Transport Model. Another simulation was made in which the Freundlich coefficient (Kf) in MT3D was reduced by 15.5% to check if the differences between the models were related to specification of retardation coefficient. The results from this MT3D simulation compared very well with the results from the Active Capping Model for test problem 3.

It was determined that the discrepancy between the MT3D solution and the Active Capping Transport Model solution was the result of differences in time-step sizes. The Active Capping Transport Model was rerun for test problem 3 with each time step reduced by a factor of 32 and the solution compared well with the MT3D solution (Figure 4). Test problem 4 was also run with a reduced time step size and the comparison between the MT3D solution and the Active Capping Transport Model solution is good.

The reduction factor of 32 was chosen arbitrarily. Initially chose a factor of 8 and this did not produce acceptable results, the factor was then increased to 32 and the results were acceptable.

Conclusions

The Active Capping Transport Model is an appropriate model to use for the evaluation and design of a sediment cap for Onondaga Lake. Based on our evaluations that computer model accurately solves the governing equation. In addition, note that the computer code for the model is concisely written and is relatively easy to understand. The model is very efficient which makes it feasible to easily conduct Monte Carlo type simulations.

To: File
Date: January 6, 2009
Page: 7

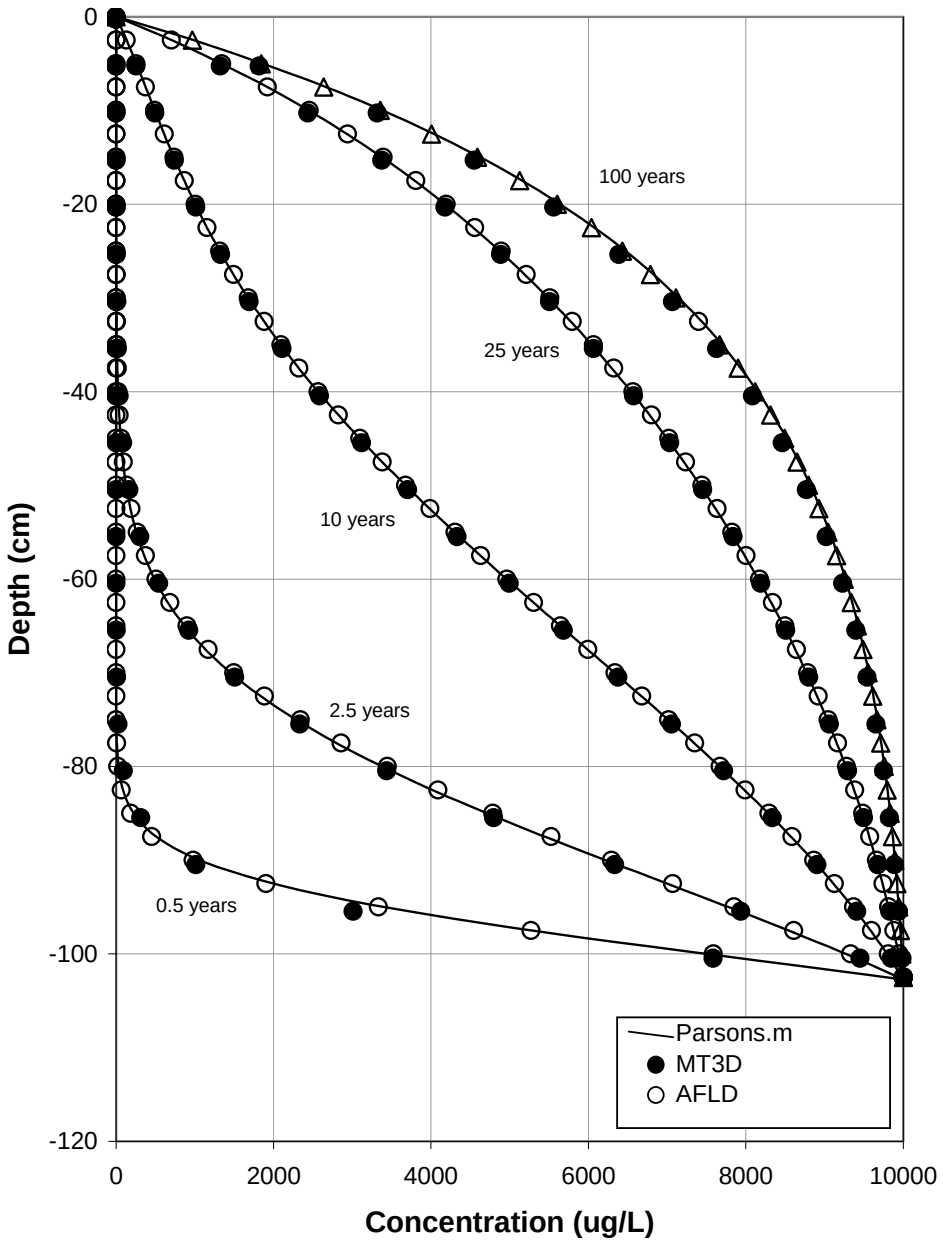

Figure 1 Test Problem 1 Uniform Properties

To: File
Date: January 6, 2009
Page: 8

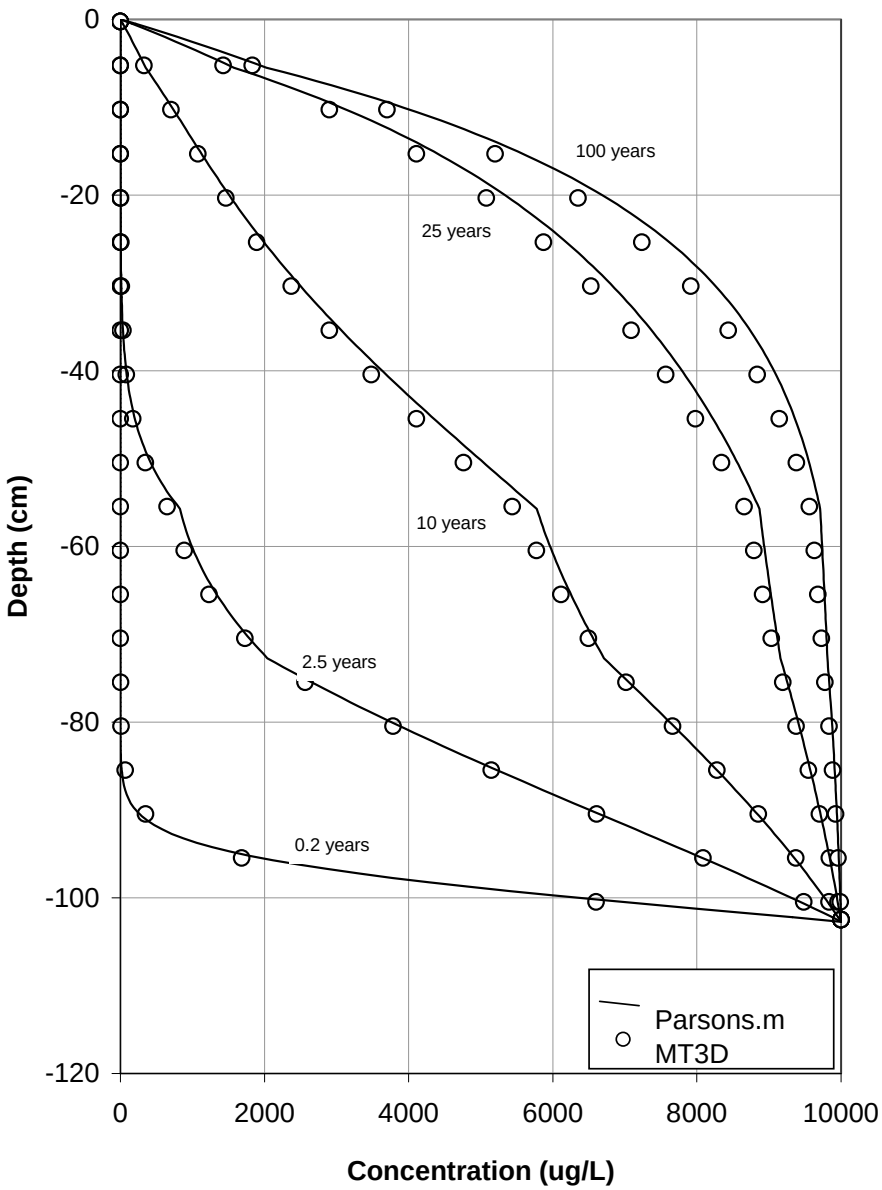

Figure 2 Test Problem 2 -- Non-Uniform Properties (porosity varies among five layers)

To: File
Date: January 6, 2009
Page: 9

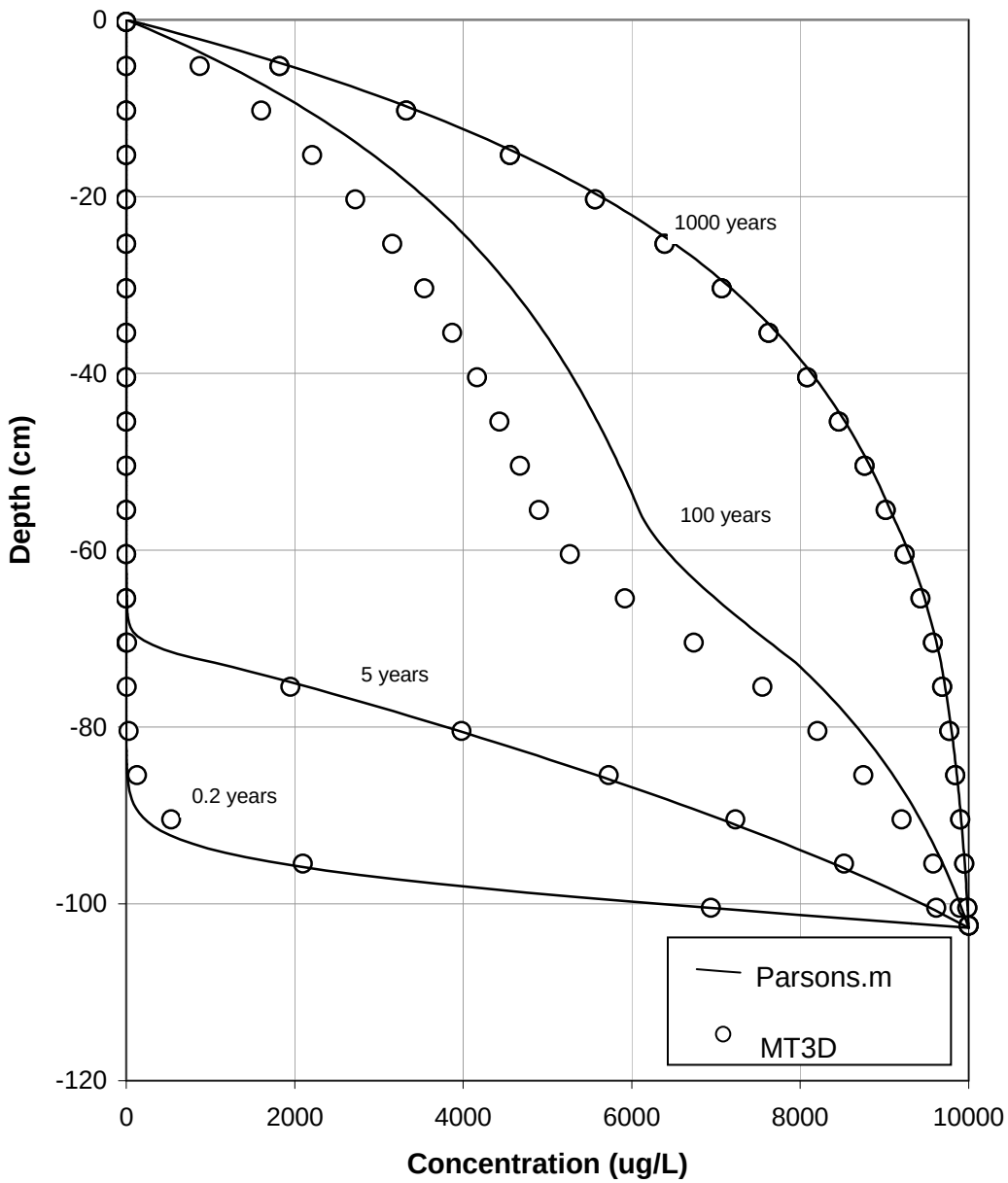

Figure 3 Test Problem 3

To: File
Date: January 6, 2009
Page: 10

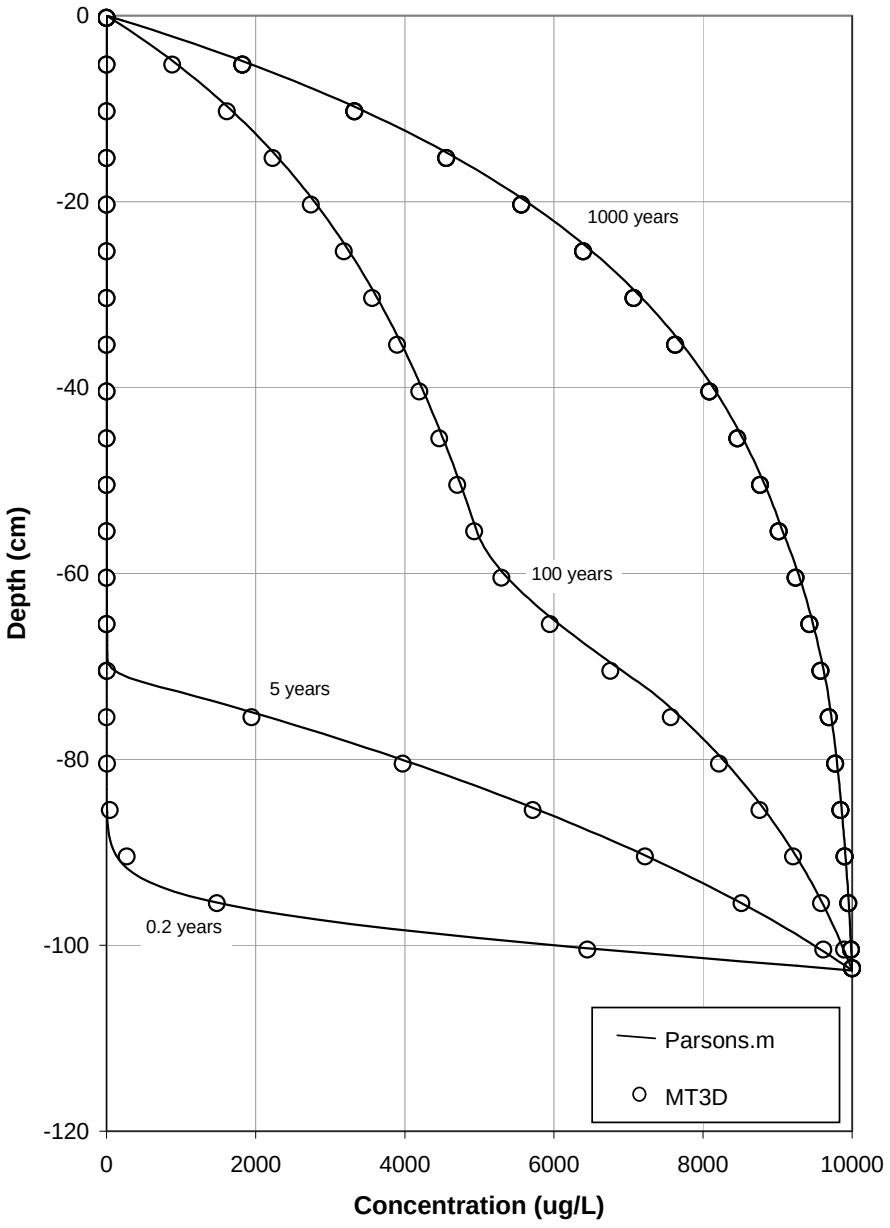

Figure 4 Test Problem 3 (decreased time step size in Parsons.m)

To: File
Date: January 6, 2009
Page: 11

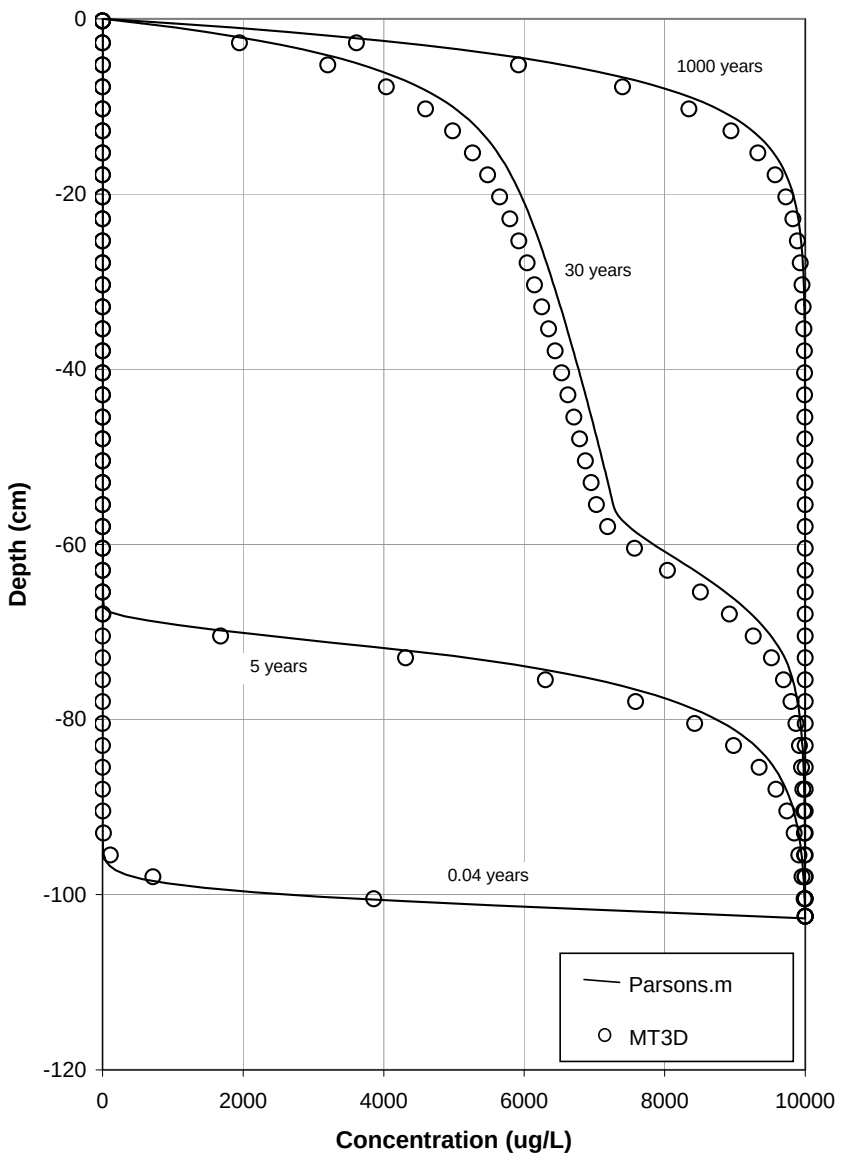

Figure 5 Test Problem 4 (decreased time step size in Parsons.m)

References

Boudreau, B. 1996. The Diffusive Tortuosity of Fine-Grained Unlithified Sediments: *Geochimica et Cosmochimica Acta* 60, no. 16: 3139-3142.

Millington, R.J., 1959. Gas diffusion in porous media. Science, Vol. 130:100-102.

Neville, C., 2005. ADFL Analytical Solution – Version 4, User's Guide. S.S. Papadopulos & Associates, Inc. Bethesda, MD.

Palermo, M.R., S. Maynord, J. Miller, and D. Reible, 1996. Guidance for in-situ subaqueous capping of contaminated sediments. Environmental Protection Agency, EPA 905-B96-004, Great Lakes National Program Office, Chicago, Il. Available at http://www.epa.gov/grtlakes/sediment/iscmain/appndb.pdf.

Zheng, C. and P. Wang, 1998. MT3DMS, A modular three-dimensional multispecies transport model for simulation of advection, dispersion and chemical reactions of contaminants in groundwater systems. Documentation and User's Guide. U.S. Army Corps of Engineers Technical Report, June 1998.

ANCHOR QEA

290 Elwood Davis Road, Suite 340
Liverpool, New York 13088
Phone 315.453.9009
Fax 315.453.9010
www.anchorqea.com

MEMORANDUM

To:	Caryn Kiehl-Simpson, Parsons Ed Glaza, Parsons	**Date:**	March 1, 2012
From:	Deirdre Reidy, Kevin Russell, and Peter Song, Anchor QEA	**Project:**	090139-01.20
Re:	Summary of changes to the numerical cap model code		

This memorandum summarizes changes and updates to the Onondaga Lake numerical cap model (Matlab) code made by Anchor QEA, LLC (Anchor QEA) between May 2011 and February 2012 (i.e., subsequent to the versions of the model code that were included with the Intermediate Design). All changes to the code made by Anchor QEA were reviewed by the original authors (i.e., Danny Reible and Dave Lampert at the University of Texas) and the code has been thoroughly tested to make sure all modifications performed as intended. The code changes described in this memorandum are grouped into three categories: 1) added functionality for site-specific modeling; 2) improvements to numerical methods/computational efficiency; and 3) corrections of minor errors.

CODE MODIFICATIONS TO INCREASE FUNCTIONALITY

- <u>Specification of biodegradation rates for each cap layer in the probabilistic (Monte Carlo) version of the code (May 2011)</u>: The early versions of the probabilistic model input file and model code (e.g., prior to and including the Intermediate Design) allowed the user to specify "initial" and "final" biodegradation rates for the model using two sets of input parameters: one set to specify the "initial" and "final" biodegradation rates for the bioturbation zone and one set of inputs for the remaining layers, the latter of which was specified by the parameter "below bioturbation layer." The input file was updated along with the model code to allow separate "initial" and "final" degradation rates to be specified for each unique layer simulated by the model (i.e., foundation layer, [active] isolation layer, habitat restoration layer, and bioturbation zone). These changes were made to allow biodegradation and lag times to be properly represented in the model.

- Specification of a uniform distribution for bioturbation zone TOC in the Monte Carlo version of the code (August 2011): The probabilistic code was modified to allow for sampling from a uniform distribution for bioturbation zone TOC. Allowing the user to specify the type of distribution was necessary because a uniform TOC distribution was used in the modeling of the wetlands (WB1-8, WBB-West, WBB-Center, and WBB-East) and Remediation Area A, whereas a lognormal distribution was used for all other model areas. This modification also required a slight change to the model input file, which now contains a flag to indicate the distribution used: lognormal or uniform (Cells I24-I39 of the chemical-specific tabs).
- Development of a version of the code that includes an additional model layer for simulating wetland areas (September 2011 to February 2012): In the approach used for the Final Design of modeling wetland areas, the Onondaga Lake cap model code was modified to include an additional model layer that lies between the habitat restoration layer and the chemical isolation layer. This new version of the model was developed by making the following changes:
  - Three unique layers above the chemical isolation layer are needed for the wetland areas: 1) the "Bioturbation Zone," which is upper portion of the high TOC habitat layer, within which mixing occurs (i.e., 6 inches); 2) a layer of high TOC material that has no bioturbation, which is referred to in the model as the "Upper Habitat Restoration Layer"; and 3) a layer of low TOC material, which is referred to in the model as the "Lower Habitat Restoration Layer." Most of the changes made to the code were based on the indexing of the boundary points for the "active" layer and in a couple of places, the code was changed to properly reference the new layer number for the Upper Habitat Restoration Layer. This new seventh layer also required a change to the location of various inputs within the Excel input file (A45 to C52) as well as an increase in the number of elements in the variable arrays within the deterministic and Monte Carlo versions of the code. Indexing of the variables affected indices 5, 6, and 7, which refer to the Lower Habitat Restoration, Upper Habitat Restoration, and Bioturbation Zone layers, respectively. Indexing of the inputs from the Excel input file (variable name "Inputs") affected indices 46 through 71 of the deterministic code.

- When modeling the wetlands in the Final Design, a higher TOC value was simulated in the upper 8 inches of the cap—that is, the Bioturbation Zone (6 inches) and the Upper Habitat Restoration Layer (the next 2 inches), as described above. During the probabilistic modeling of the wetlands, the TOC value for the bioturbation zone was selected from a uniform distribution. The TOC value in the upper habitat layer should vary the same way; however, a separate distribution could not be specified for each because the values would then vary independently for each probabilistic realization. The model input files were, therefore, updated to include a flag indicating whether to use the same TOC values as in the Bioturbation Zone, or to use the static value specified for the Upper Habitat Restoration Layer. The code was then updated to check this flag and use the appropriate values (i.e., either the realization values generated for the bioturbation zone [sampled from a uniform distribution ranging over 5 to 15%] or the static value set in the input file for the Upper Habitat Restoration Layer).

CODE CHANGES TO IMPROVE NUMERICAL METHODS/COMPUTATIONAL EFFICIENCY

- Model timeframe to be as long as the user-specified "Simulation length" (July 2011): In the Intermediate Design versions of the model code, the timeframe for certain model simulations was found to be less than the "Simulation length" specified in the model input file. In order to assess compliance with the design criteria over a set timeframe (1,000 years was used for the Final Design), the model code was updated to ensure that the model runs for at least the length specified in the input file.
- Time domain division to ensure complete simulation length (August 2011): Changes were made to also ensure that the conversions to and from the dimensionless time used in the solution of the governing equation are based on a constant value for the characteristic diffusion time, which was used to specify dimensionless time steps and simulation length.

CODE CORRECTIONS

- User-specified lag time for biodegradation (May 2011): A lag period during which no biological decay would occur was specified in the model to allow adequate time for a biological community to establish in the cap material. This lag period is simulated by specifying two decay rates: an "initial" rate (which was set to zero to simulate no biodegradation) and a "final" rate, the latter of which is used after a user-specified duration (i.e., the lag time). While reviewing results from model tests conducted during development of the Draft Final Design (which was the first time this feature was used for the Onondaga Lake cap design), it was discovered that the final rate was not being applied at the user-specified time, but several years later. Time stepping in the code is performed on two levels—a large-scale time step and finer-scale time step. The code that initiates the "final" decay rate was located within the larger time step and, therefore, the first time step after the lag period specified by the user was several years later. To correct this inconsistency, the code that handles the start of the "final" decay rate was moved inside the second level time loop, which is on a finer scale, so that the "final" decay rate begins at the user-specified time.
- Discrepancy between model output to the screen versus the model output to the *.CSV file (June 2011): As noted in NYSDEC's comments to the Intermediate Design Report, the concentrations at the bottom of the Bioturbation Zone (Wbio) and the bottom of the Habitat Restoration Layer (Whr) printed to the screen did not match those reported in the output file (*.CSV). Throughout the code, the "active" layer (i.e., that which contains a sorptive amendment that is characterize by non-linear [Freundlich] partitioning) is handled separately from the remaining layers. After the model finishes simulating porewater concentrations within a given time step, it calculates the sorbed-phase concentrations using partitioning relationships. At this point in the code, modifications were made to correctly handle the indexing of the "active" layer so that there is no inconsistency in the reported outputs.
- Calculation of retardation factor in probabilistic code (February 2012): The calculation of the retardation factor in the "active" layer at early times was referencing the incorrect porewater concentration from the model input file, using the static value reserved for deterministic runs rather than the probabilistic

value from a given realization. The model code was updated in two places to correct this issue.

ATTACHMENT 4

MODEL FILES

ATTACHMENT 5

NINE MILE CREEK SPITS EVALUATION

ATTACHMENT 5

NINE MILE CREEK SPITS EVALUATION

The Nine Mile Creek spits have been incorporated into the cap design in Remediation Area A. The cap effectiveness criteria within the spits are established in the Ninemile Creek ROD, and differ slightly from those defined in the lake ROD. The Ninemile Creek ROD established criteria for the COCs in Ninemile Creek, which included hexachlorobenzene, benzo(a)pyrene, phenol, total PAHs, lead, arsenic and mercury. Soil concentrations for the locations on the spits were compared to the Ninemile Creek ROD criteria. Results and conclusions from this evaluation are as follows:

- There are no exceedences of the Ninemile Creek criteria in the spits soil data for hexachlorobenzene, benzo(a)pyrene, total PAHs, or lead. Therefore the cap will be protective for these contaminants and modeling of these contaminants was not required.
- There was one exceedence of the Ninemile Creek ROD criterion for phenol; a concentration of 79.32 g/g OC was measured compared with the criterion of 25 ug/g OC. As shown in Table A5-1 below, the phenol concentrations in the spits are lower than those measured in Model Area A2. The performance criterion for phenol is the same for Ninemile Creek and the lake, in that both are based on the NYSDEC SSC. Therefore the cap design in Model Area A2 (including the specified GAC application rate) is conservative for the spits with regard to phenol and no additional modeling is required.
- There were two minor exceedences for both arsenic and PCBs. For PCBs, concentrations of 22.045 and 22.189 ug/g OC were measured compared with the criterion of 19.3 ug/g OC, and two samples of arsenic where concentrations of 34.4 and 34.8 mg/kg were measured compared with the criterion of 33 mg/kg. These exceedences are sporadic and only marginally above the Ninemile Creek criteria; therefore the cap will be protective with regard to these contaminants and modeling of these contaminants was not required.
- Exceedences for the Ninemile Creek mercury criterion of 0.15 mg/kg were present in the spits. Therefore, cap performance with respect to mercury was modeled for the spits (using Model Area A2 inputs), recognizing that the mercury criterion in the spits is 0.15 mg/kg compared with the lake criterion of 2.2 mg/kg. The approach taken and the results are as follows:
    - As shown in Table A5-1 below, mercury concentrations in the spits are similar to those in Model Area A2. Therefore, the mercury concentrations used in Model Areas A2 are applicable to the spits.
    - In addition, groundwater upwelling in the spits is predicted to be consistent with the upwelling in Model Area A2. As stated in Appendix C: No pore-water or sediment-conductivity data were collected along the spits at the mouth of Ninemile Creek. Under existing conditions, the upwelling velocities on the spits are likely downward because of recharge that occurs on the spits. Following

construction of the wetlands, upwelling velocities will be consistent with those observed in adjacent areas in Model Area A2. Therefore, for cap design purposes, the upwelling velocities in the proposed wetland area were assumed to be the same as those in Model Area A2.

- The Model Area A2 model was therefore used to simulate mercury in the spits, comparing the results against the Ninemile Creek performance criteria of 0.15 mg/kg. Results from this modeling are included in Attachment 4. The results show that at the 95th percentile porewater concentration, an isolation layer thickness between 9 and 10 inches would meet the mercury criterion of 0.15 mg/kg for over 1,000 years. Given that the actual thickness of the isolation layer would be 12" and that the modeling does not represent the effects of siderite or GAC on limiting mercury transport, and taking into consideration the other model conservatisms described in Section 3.3 of Appendix B, these model results indicate that the cap specified for Model Area A2 would be also protective for the spits, in that it would meet the Ninemile Creek mercury criterion for 1,000 years.

Table A5-1
Nine Mile Creek Spits Soil and Model Area A-2 Sediment Concentrations

Ninemile Creek Spits Area Soil Locations Concentration* Statistics			
	Maximum	Average	95th Percentile
Mercury (mg/kg)	169	23	112
Phenol (ug/kg)	656	58	104

Model Area A2 Sediment Concentration* Statistics			
	Maximum	Average	95th Percentile
Mercury (mg/kg)	189	30	110
Phenol (ug/kg)	5,900	215	1,435

Notes

* - Non-detects are at half value.

ATTACHMENT 6

ADDITIONAL SENSITIVITY EVALUATIONS

ATTACHMENT 6

ADDITIONAL SENSITIVITY EVALUATIONS

Underlying Sediment Thickness

Model sensitivity evaluations were conducted to evaluate the effect of the specified thickness of the underlying sediment layer on GAC performance. As discussed in Section 3.2 of Appendix B, the model assumes an underlying thickness of 250 cm. To evaluate the sensitivity of the model results to this parameter, thicknesses of 200 and 100 cm were evaluated. This evaluation consisted of repeating the deterministic numerical simulations in which the model was iteratively used to determine the GAC application rate required to meet design criteria (i.e., the approach described in Section 7.2 of Appendix B) for each of these two alternate sediment thicknesses. These simulations were conducted for Model Areas D-West and E3, and the results are listed in the table below:

Sediment Thickness (cm)	Model Area D-West Carbon Application Rate (lb/sf)	Model Area E3 Carbon Application Rate (lb/sf)
250	1.33	0.008
200	1.33	0.008
100	1.33	0.008

The results shown above, which are consistent with those from sensitivity tests conducted in other model areas during previous stages of the design, indicate that the GAC application rates determined with the model are not sensitive to the thickness of underlying sediment included in the model.

Remediation Area D Consolidation Parameters

Model sensitivity analyses were conducted to evaluate the effect of parameters associated with consolidation of the underlying sediment resulting from cap placement Remediation Area D on GAC performance. As described in Attachment 1, conservative values were specified in the base modeling of consolidation in all model areas; in Remediation AreaD, the base consolidation curve results in 0.67 ft of porewater flux over 30 years. To evaluate the sensitivity of this parameter, an alternate set of upper bound parameters for Remediation Area D, in which the total porewater flux was 0.81 ft, was evaluated. The basis for this upper bound estimate of porewater flux is provided in Appendix E of the Final Design. This evaluation consisted of repeating the deterministic numerical simulations in which the model was iteratively used to determine the GAC application rate required to meet design criteria (i.e., the approach described in Section 7.2 of Appendix B) for all four subareas of Remediation Area D for the alternate consolidation parameters. The results of these sensitivity analyses are provided in the table below.

Model Area	Base RA-D Consolidation (0.67 ft)		Alternate Upper Bound RA-D Consolidation (0.81 ft)	
	Controlling Chemical	Carbon Application Rate (lb/sf)	Controlling Chemical	Carbon Application Rate (lb/sf)
D-SMU2	Naphthalene	0.044	Naphthalene	0.045
D-West	Phenol	1.33	Phenol	1.34
D-Center	Xylenes	0.93	Xylenes	0.93
D-East	Naphthalene	0.44	Chlorobenzenes	0.44

The results shown above indicate that the GAC application rates determined with the model are not sensitive to the alternate upper bound consolidation parameters for Remediation Area D.

Remediation Area D Shoreline Planting Area

The in-lake planting area within Remediation Area D, which covers a 25-ft strip along the shoreline adjacent to Model Areas D-East, D-Center, and D-West are being designed to contain higher total organic carbon (TOC) in the cap's habitat layer as compared to the remainder of Remediation Area D. To evaluate the higher habitat layer TOC specific to these areas, sensitivity analyses were conducted to evaluate the impacts on carbon amendments. The sensitivity analyses conducted for these three ILWD model areas consisted of deterministic numerical modeling using the same methods as described in Section 7.2, except that a higher TOC value (10% vs. 4.56%; see Attachment 1) was specified within the upper portion of the habitat layer. The results from these sensitivity analyses are shown in the table below.

Area	Controlling Chemical(s)	Carbon Application Rate (lb/sf)	
		TOC = 4.56%	TOC = 10%
D-West Shoreline	Phenol	1.33	1.33
D-Center Shoreline	Xylenes	0.93	1.02
D-East Shoreline	Chlorobenzene	0.44	0.53

These results indicate that the higher TOC in the planting areas would require GAC application rates that are equal to or only slightly higher than those required in the larger model areas.

Groundwater Upwelling Velocities in Remediation Areas, Onondaga Lake Bottom Subsite

S.S. PAPADOPULOS & ASSOCIATES, INC.
Environmental & Water-Resource Consultants

March 2012

7944 Wisconsin Avenue, Bethesda, Maryland20814-3620• (301) 718-8900

Table of Contents

Page

List of Figures iii

List of Tables iv

List of Attachments iv

Executive Summary v

Section 1 Introduction 1

Section 2 Groundwater Conditions in Remediation Areas 4

Geologic Setting 4
Onondaga Lake and Groundwater Flow 4
Hydraulic Containment Systems 6
Groundwater Flow Model 7
Groundwater Conditions and Model Area Development 7

Section 3 Measurements of Upwelling Velocities 9

Temperature and Conductivity Survey 10
Groundwater Upwelling Investigation – 2003 10
Seepage Meter Investigations 11
Seepage Meters – Phase I Investigation 11
Seepage Meters – Phase III Investigation 12
Chloride-Depth Profiles 14
Description of Method 14
Model Parameters 15
Measurement of Sediment Chloride Concentrations 16
Field Investigations 18
Initial Data Evaluations 18

Section 4 Upwelling Velocities Calculated from Chloride-Depth Profiles 21

Section 5 Upwelling Velocities for Cap Design in Areas without Hydraulic Containment 26

Results 27

Section 6 Evaluation of Uncertainty in Calculated Upwelling Velocities 29

Sensitivity to Model Parameters 29
Reproducibility of Results 29
Model Fit 30
Summary 31

Section 7 Analysis of Upward Groundwater Flow through Silt and Clay Unit 32

Section 8 Upwelling Velocities for Cap Design in Areas with Hydraulic Containment 39

Vertical Hydraulic Conductivity 39

Thickness of Silt and Clay Unit 40
Water Level Differences 40
Monte Carlo Simulation 41
Results 42
Remediation Area A – Model Area A1 44
Section 9 Conclusions 45
Section 10 References 46

List of Figures

Figure 1	Remediation Areas and Cross Section Location Map
Figure 2	Hydrogeologic Setting of Onondaga Lake
Figure 3	Thickness of Silt and Clay Unit
Figure 4	Remediation Area A - Hydrogeologic Cross Section B-B’
Figure 5	Remediation Area D - Hydrogeologic Cross Section H-H’
Figure 6	Remediation Area E - Hydrogeologic Cross Section I-I’
Figure 7	Schematic of Hydraulic Containment System and Groundwater Flow through Silt and Clay Unit
Figure 8	Upwelling Transect and Piezometer Locations
Figure 9	Upwelling Measurement and Seepage Meter Locations – Remediation Area A
Figure 10	Upwelling Measurement Locations – Remediation Area B
Figure 11	Upwelling Measurement Locations – Remediation Area C
Figure 12	Upwelling Measurement and Seepage Meter Locations – Remediation Area E
Figure 13	Average Porosity at Vibracore Locations
Figure 14	Upwelling Velocities in Model Areas A1 and A2
Figure 15	Upwelling Velocities in Remediation Area C
Figure 16	Upwelling Velocities in Model Areas E1, E2, and E3
Figure 17	Locations of Vertical Hydraulic Conductivity Measurements
Figure 18	Average Upwelling Velocities in Remediation Area B
Figure 19	Average Upwelling Velocities in Remediation Area C
Figure 20	Average Upwelling Velocities in Remediation Area D

List of Tables

Table 1	Summary of Upwelling Velocities Used to Develop Cumulative Frequency Distributions for Model Areas A1, A2, and C2, and Remediation Area E
Table 2	Comparison of Upwelling Velocities at Locations with Pore Water and Sediment Conductivity Data
Table 3	Comparison of Upwelling Velocities at Locations with Multiple Sets of Sediment Conductivity Data
Table 4	Measured Values of Vertical Hydraulic Conductivity of Silt and Clay Unit
Table 5	Calculated Vertical Groundwater Velocities across the Silt and Clay Unit at Selected Monitoring Well Locations

List of Attachments

Attachment I	Geologic Sections
Attachment II	Conductivity-Temperature Investigation Results
Attachment III	Upwelling Investigation Results – Transect TR01
Attachment IV	Seepage Meter Investigation Results
Attachment V	Vibracore Water Quality and Porosity Data
Attachment VI	Sediment Conductivity and Pore Water Correlations
Attachment VII	Chloride-Depth Profile Analyses
Attachment VIII	Transient Evaluation of Chloride-Depth Profiles
Attachment IX	Comparison of Upwelling Estimates from Pore Water and Sediment Conductivity Data from Same Location
Attachment X	Evaluation of Velocity in Silt and Clay Unit
Attachment XI	Sensitivity Evaluations
Attachment XII	Results from Diffusion Samplers – Phase III
Attachment XIII	Estimation of Hydraulic Conductivity from Consolidation Test Data

Executive Summary

This report describes the results of extensive field and analytical studies that have quantified the discharge of groundwater to the areas in Onondaga Lake where a sediment cap will be placed as part of the remedial activities undertaken to meet the requirements of the Record of Decision (ROD) for the Onondaga Lake Bottom Subsite. The data and evaluations described in this report provide an excellent foundation for the design of the remedy for Onondaga Lake. The upwelling velocities that are described in this report will be used in the chemical isolation model for purposes of cap design.

The current rates of groundwater discharge in much of Remediation Areas A and E and in the center section of Remediation Area C, which are similar to discharge rates expected after placement of the isolation cap, have been delineated based on the analysis of chloride depth profiles at over 200 locations within and in the vicinity of these remediation areas. In Remediation Area B, Remediation Area D, and the northern and southern sections of Remediation Area C, the rates of groundwater discharge after placement of the isolation cap will be significantly lower than current rates as the result of the construction and operation of hydraulic containment systems along the shoreline. Groundwater discharge rates after placement of the isolation cap in these remediation areas were calculated based on groundwater flow rates upward through the underlying regional confining unit (the silt and clay unit), as the containment systems will capture all groundwater flow to the lake above this unit.

This report describes methods that were implemented in the field to measure groundwater discharge rates, which are commonly referred to as upwelling velocities, within the remediation areas. The evaluation of upward groundwater velocity through the sediment, based on the change in chloride concentrations with depth in sediment pore water, was determined to be the best method for quantifying current upwelling velocities in the remediation areas. This report describes the theoretical basis for the use of this method to measure upwelling velocities and describes the extensive data collected on chloride concentrations in sediment pore water to accurately delineate the current distribution of upwelling velocities within the remediation areas. The mean upwelling velocities determined from this method in Model Areas A1, A2, and C2 and Remediation Area E are 1.6 cm/yr, 4.1 cm/yr, 3.1 cm/yr and 1.5 cm/yr, respectively; upwelling velocities in all of these areas will be minimally affected by the hydraulic containment systems.

In the remediation areas located offshore of proposed hydraulic containment systems, the long-term upwelling velocity after remedy implementation will be equal to the rate of groundwater movement through the regional confining unit. These containment systems are assumed to operate for the life of the remedy. The vertical hydraulic conductivity of the regional confining unit was estimated by the testing of 40 core samples collected from the silt and clay within the remediation areas; these data were combined with estimates of the hydraulic gradient across the regional confining unit and the thickness of the silt and clay unit to calculate the upward groundwater flow through the unit. The uncertainty in this calculation was evaluated based on estimates of the uncertainty in vertical hydraulic conductivity, hydraulic gradients and thickness. The mean estimated long-term upwelling velocities through the regional confining unit were estimated to be less than 2 cm/yr in all areas proposed for capping that are located offshore of proposed hydraulic containment systems.

REPORT

Section 1
Introduction

This technical report describes groundwater discharge to the areas in Onondaga Lake where a sediment cap will be placed as part of the remedial activities undertaken to meet the requirements of the ROD for the Onondaga Lake Bottom Subsite. The areas where a sediment cap will be constructed have been geographically grouped into five subareas termed Remediation Areas A through E. The locations of the remediation areas, which have a total area of about 400 acres, are shown on Figure 1. For purposes of cap design, Remediation Area D has been subdivided into four subareas: SMU2-ILWD, western, center, and eastern; Remediation Area A has been subdivided into Model Area A1 and Model Area A2; and Remediation Areas B and C have been subdivided into Model Area B2, Model Area B1/C1, Model Area C2, and Model Area C3.[1] The locations of the remediation areas and model areas are shown on Figure 1. Also shown on Figure 1 are three wetland areas along the lakeshore that will be created as part of the remedial actions: wetlands to replace the spits at the mouth of Ninemile Creek, a wetland area along the eastern shoreline of Wastebeds 1-8 ("connected wetland"), and a wetland area adjacent to Wastebed B and Harbor Brook ("outboard area wetland"). A sediment cap will be placed beneath these wetlands.

Groundwater discharge to Onondaga Lake has been evaluated in detail because groundwater flux through lake sediments can transport contaminants in the sediments into the upper layers of the cap. As a result, understanding the groundwater discharge that will occur through the sediment cap after placement is essential for predicting the long-term performance of the sediment cap. In the analytical and numerical models developed to simulate the performance of the sediment cap (see Appendix B), the parameter describing the rate of groundwater discharge is referred to as the "Darcy velocity." The Darcy velocity is the rate at which groundwater moves upward through the sediment cap. The Darcy velocity is frequently called the "upwelling velocity." The upwelling velocities that are described in this report have been used as inputs to the chemical isolation model used for cap design (see Appendix B).

In much of Remediation Areas A and E, and in Model Area C2, it is anticipated that groundwater discharge through the cap will be similar to that which is occurring today. As a result, evaluations of groundwater discharge following construction of the cap have focused on understanding and quantifying existing rates of groundwater discharge in these areas.

Hydraulic containment systems constructed or proposed for construction along the shoreline reduce the groundwater discharge to the lake in Remediation Areas B and D, and portions of Remediation Areas A and C, to negligible levels by capturing all groundwater flow towards the lake above the regional confining unit (Figure 1). In these areas, evaluations of

[1] For purposes of chemical isolation layer design, each remediation area was subdivided into distinct model areas as shown on Figure 1. In this report, estimates of upwelling velocities in each of the model areas are developed. The methods used to delineate the model areas are presented in Appendix B. Additional detail on how the influence of groundwater conditions factored into model area delineation are provided in Sections 2, 5 and 8 of this appendix. For purposes of evaluation alternatives in the Feasibility Study, Onondaga Lake was separated into eight areas or sediment management units (SMU) for ease of evaluating alternatives in different portions of the lake. The SMU delineations are shown on Figure 1. For the purpose of this document, portions of the lake remedy are referred to in terms of the remediation areas /model areas rather than the SMU delineations.

groundwater discharge following construction of the cap have focused on understanding the component of groundwater discharge that will not be captured by the hydraulic containment systems and continue to flow through the cap following completion of the remedy. The existing rates of groundwater discharge in these remediation areas provide only an upper bound estimate of the amount of groundwater discharge that will occur following construction of the hydraulic containment system. The dominant component of groundwater discharge following construction of the cap will be upward groundwater flow through the underlying regional confining unit. Thus, the evaluations described in this report focused on quantifying groundwater flow through the regional confining (silt and clay) unit.

A detailed description of groundwater flow to Onondaga Lake is contained in Appendix D: Part A to the Onondaga Lake Feasibility Study (FS) titled "Groundwater Flow to Onondaga Lake" (Parsons 2004). In addition, following publication of the FS, the United States Geological Survey (USGS) published an analysis of groundwater flow in the unconsolidated sediments underlying Onondaga Lake and the contiguous glacial valleys (Yager and others 2007a, 2007b; and Kappel and Yager, 2008). The major findings of these studies are summarized in this report.

The analyses of groundwater discharge described in Appendix D of the FS indicated that in areas offshore of where a hydraulic containment system would be constructed upwelling velocities would be less than 2 cm/yr with the containment system in operation. Upwelling velocities in Remediation Areas A and E, without a hydraulic containment system, were estimated during the FS to be higher in near shore areas. Upwelling velocities in Remediation Area A ranged from 300 cm/yr within 20 ft. of the shoreline to less than 2 cm/yr beyond 700 ft. from the shoreline, and upwelling velocities in Remediation Area E ranged from 70 cm/yr near the shoreline to less than 2 cm/yr beyond 300 ft. from the shoreline.

This report focuses on the studies and investigations that have been conducted since the FS was completed to better quantify groundwater discharge to the five remediation areas. Seepage meters and chloride-depth profiles of the sediments were the field methods employed in the pre-design investigations (PDI) to quantify groundwater discharge rates. These methods and the results of these methods are described in this report as well as other methods that were considered to quantify groundwater discharge rates. In addition, as part of the pre-design investigations, many borings have been advanced into the sediments beneath the remediation areas. The data from these borings have provided a good understanding of the characteristics of the sediments and the thickness and continuity of the major stratigraphic units including the regional confining unit. This information has allowed the development of a better understanding of groundwater flow within the sediments than existed at the time the FS was prepared.

The chloride-depth profile method was judged to be the most reliable and accurate method for quantifying the relatively low groundwater discharge rates through the sediments in the remediation areas. This method relies on the observation that the pore waters in the sediments beneath Onondaga Lake have significantly higher chloride concentrations than the lake water as the result of natural brines beneath the lake and migration of leachate from the wastebeds along the shoreline of Onondaga Lake. As a result, there is a significant chloride concentration gradient from the sediments to the lake. The change in chloride concentration with depth below the lake/sediment interface provides information on the rate of upward groundwater flow through the sediment.

The shape of the chloride-depth profile is a function of chloride migration by advection with groundwater and chemical diffusion. If there is no advective transport with groundwater, the chloride-depth profile will be linear as a result of diffusion. If there is upward groundwater flow, the chloride depth profile will be convex, with the convexity a function of the magnitude of the groundwater flow, as shown on the figure below. Analysis of the convexity of the profile is the method that was used to quantify groundwater upwelling velocities. This method is useful for analyzing upwelling velocities that are less than about 50 cm/yr. At greater upwelling velocities, the chloride concentrations do not change significantly with depth.

The figure to the right shows a plot of chloride concentrations in pore water versus depth at a boring located in Remediation Area E (OL-VC-60154). This figure illustrates the large changes in chloride concentrations that occur with depth below the sediment-water interface. The measured chloride data are plotted as dots and chloride concentrations increase from about 359 mg/L at the sediment-water interface to over 15,000 mg/L at a depth of about 9 ft. below the sediment-water interface. The measured chloride data follow a convex profile indicating a relatively small upwelling velocity. Also shown on the figure are the expected chloride depth profiles for upwelling velocities of 0.1 cm/yr, 1 cm/yr, 10 cm/yr and 100 cm/yr. These expected chloride depth profiles illustrate the significant effect that changes in upwelling velocities have on the shape of the chloride depth profile. For example, the chloride depth profile with an upwelling velocity of 1 cm/yr is significantly different than that with an upwelling velocity of 10 cm/yr. The measured chloride data shown on the figure follow a trend similar to that expected with an upwelling velocity of about 1 cm/yr.

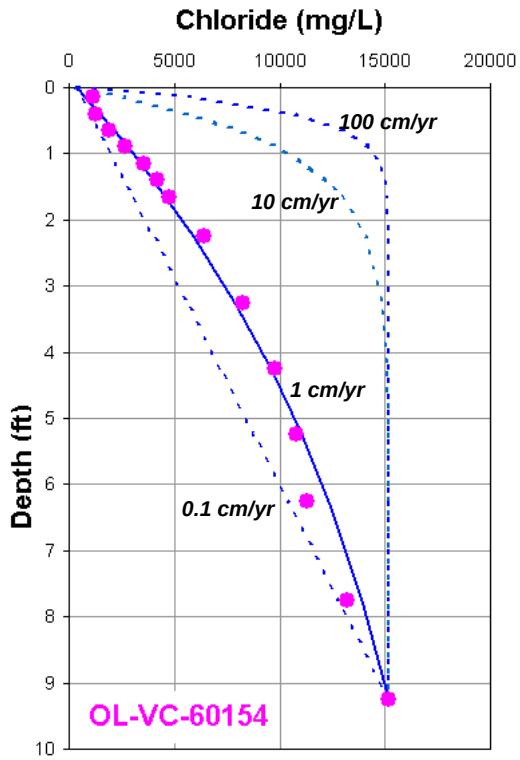

The remainder of this report is organized into eight sections; Section 2 through Section 9. Section 2 of this report describes groundwater conditions in the remediation areas. Section 3 describes the methods used to determine upwelling velocities and compares the methods. Section 4 describes the method used to analyze chloride-depth profiles to calculate upwelling velocities. Section 5 describes upwelling velocities for cap design in remediation areas located in areas without onshore hydraulic containment systems. Section 6 describes an evaluation of uncertainty in calculated upwelling velocities. Section 7 describes analyses of upward groundwater flow through the silt and clay unit, and Section 8 describes upwelling velocities for cap design in areas with onshore hydraulic containment systems. Conclusions are presented in Section 9, and the references cited in the report are listed in Section 10.

Section 2
Groundwater Conditions in Remediation Areas

Geologic Setting

Onondaga Lake overlies a deep, northwest-trending glacial trough in the Vernon Shale, the bedrock formation beneath and in the vicinity of the lake. A schematic block diagram of the southeastern end of the lake, which illustrates the trough, is shown on Figure 2. The trough averages about 300 ft. deep along the axis of the lake and is filled primarily with unconsolidated, fine-grained sediments, although a coarse-grained unit typically occurs overlying till near the base of the unconsolidated sediments. The thickness of the unconsolidated sediments decreases rapidly away from Onondaga Lake, except in the valleys of the main tributaries, which are also underlain by unconsolidated sediments. The stratigraphic sequence observed in most borings advanced beneath the lake and adjacent upland areas are similar:

- Surficial sediments typically described as silt with fine sand and fill material
- Gray clayey marl, gray-brown clayey silty marl (marl unit)
- Brown-gray clay, gray-brown silt and clay (silt and clay unit also termed regional confining unit)
- Gray-brown silt with sand layers (fine sand and silt unit)
- Sand, sometimes with gravel (sand and gravel unit)
- Till, dense clay and silt with sand and gravel (till unit)
- Green, red and gray shale (bedrock)

The silt and clay unit is an important regional confining unit or aquitard that impedes upward groundwater flow to the lake. This unit has been interpreted to be continuous beneath the entire lake, consistent with the interpretation in the USGS report by Yager and others (2007b). A thickness map of this unit based on interpretation of boring logs is shown on Figure 3.

Hydrogeologic cross sections through Remediation Areas A, D and E are shown on Figures 4 to 6 and locations of these sections are shown on Figure 1. These cross sections, at a minimum, depict the silt and clay unit and overlying sediments. Where information is available on the geologic units below the silt and clay unit, this information is also shown. The sections are annotated with notes from the boring logs regarding lithologic observations within each of the geologic units. In general, the marl is described as silt and/or silt and clay though in some logs the marl was noted as consisting of gravel and/or sand sized sediments. In Remediation Area D, relatively thick deposits of Solvay waste generated from the production of sodium carbonate (soda ash) by the Solvay process and other materials contained within the in-lake waste deposits overlie the marl unit (Figure 5). Additional hydrogeologic cross sections are contained in Attachment I.

Onondaga Lake and Groundwater Flow

Onondaga Lake, oriented along a northwest-southeast axis, is approximately 4.5 miles long and one mile wide. The lake has a mean depth of 36 ft. and a maximum depth of 65 ft. which occurs in the southern part of the lake. The average lake level during the past 20 years was

362.9 ft. above mean sea level (AMSL),[2] based on records from the USGS gage on Onondaga Lake (Site 04240495, Onondaga Lake at Liverpool, New York). The surface area of the lake at this elevation is approximately 4.5 square miles, and the volume is approximately 34,600 million gallons. Surface water inflows and outflows from the lake average about 470 cubic ft. per second based on average flows between 1998 and 2002 (Onondaga County, 2003). The groundwater component of the lake water budget is small, estimated to be less than 0.5 percent of surface water inflows (Parsons, 2004). Precipitation on the lake and evaporation from the lake are approximately equal; therefore, the net water budget associated with precipitation and evaporation is small. The average residence time of water in the lake is approximately 100 days.

Regional groundwater flow in both the bedrock and the unconsolidated sediments is towards the valleys of the major tributaries of the lake. Groundwater discharge areas include seven major tributaries: Ninemile Creek, Geddes Brook, Harbor Brook, Bloody Brook, Onondaga Creek, Saw Mill Creek, and Ley Creek. Groundwater flow towards and into the lake originates primarily as precipitation that infiltrates into the unconsolidated sediments bordering the lake. Because the saturated unconsolidated sediments are restricted to a relatively narrow band on either side of the lake, the total recharge area is relatively small, and as a result, recharge to and discharge from the unconsolidated sediments is relatively small. Most of the groundwater in the unconsolidated sediments that flows toward the lake discharges to the tributaries and to ditches and drains along the shoreline with the remainder discharging in near-shore areas of the lake. This occurs, in part, because of the thickening wedge of fine-grained, low-permeability materials beneath the lake and because of dense sodium-chloride brines in the unconsolidated sediments beneath the lake.

Most of the groundwater discharge that occurs to the lake is the result of groundwater flow through the marl and overlying units from the upland areas. These units are typically fine grained, though there are some sand stringers or lenses, as shown on the hydrogeologic cross sections. As a result, groundwater flow rates through these units are not large and most of the groundwater discharge occurs near shore in the littoral zone.

Some groundwater discharge to the lake occurs as the result of upward groundwater flow through the silt and clay unit from the deeper permeable units. The sand and gravel unit and the overlying fine sand and silt unit are the primary deeper permeable units (see Figure 2). These units are primarily recharged where they subcrop around the perimeter of the lake. Groundwater levels in the sand and gravel along the lakeshore are typically well above the lake level indicating the potential for upward groundwater flow. The vertical hydraulic conductivity of the silt and clay unit is estimated to be on the order of 10^{-7} cm/sec and, thus, the total upward groundwater flow through this unit is very small. The potential upward groundwater flow through the silt and clay unit is described in detail in Section 7.

The presence of natural sodium-chloride brines in the unconsolidated sediments beneath the lake complicates the understanding of local groundwater flow conditions. These brines are believed to have originated primarily from the dissolution of soluble minerals in the unconsolidated glacial sediments in the Onondaga Trough that originated from bedrock scour caused by glacial advance and retreat. These brines are comprised primarily of sodium and chloride. In the past, discharge of brines at salt springs was reported to have occurred around

[2] Vertical datum in this report is referenced to the North American Vertical Datum of 1988 (NAVD 88).

much of the shoreline of the southern basin of the lake (Kappel, 2000). These discharges likely occurred in areas where the silt and clay unit thinned or disappeared along the shoreline. The natural discharge of brines has ceased due to extraction of brines from wells along the shoreline. From 1797 to 1917, over 11.5 million tons of finished salt were produced from the springs and wells along the southern shoreline of the lake (USGS, 2000). This represents the salt content from the constant production of 500 gallons per minute (gpm) of brine with a chloride concentration of 60,000 mg/L over this period.

In addition to the natural sodium-chloride brines, there are natural mixed cation brines in the bedrock. These brines formed by the dissolution of evaporate beds within the Vernon Shale and overlying bedrock units. These brines are enriched in calcium, magnesium, and bromide relative to the sodium-chloride brines. In addition to the natural brines, some brines in the subsurface result from seepage of Solvay leachate[3] from the wastebeds. Solvay leachate is comprised primarily of sodium, calcium, and chloride. Solvay leachate typically has sodium to calcium ratios that are less than 1, whereas the natural sodium-chloride brines have sodium to calcium ratios that are greater than 10. The mixed cation brines typically have sodium to calcium ratios in the range of 1.4 to 4. The mixing of relatively fresh groundwater, natural sodium-chloride brines, natural mixed cation brines, and Solvay leachate from the wastebeds have created a wide variety of groundwater quality types in the vicinity of Onondaga Lake. The distribution of groundwater quality provides information on groundwater migration and origin.

Hydraulic Containment Systems

Hydraulic containment systems along the shoreline are an integral part of the lake remedy and remedies for the adjacent upland areas. Two types of hydraulic containment systems have been proposed; containment systems with a barrier wall and containment systems without a barrier wall.

The hydraulic containment systems incorporating a barrier wall will extend along the shoreline from the Willis-Semet area to south of the mouth of Harbor Brook, a total distance of about 6,700 ft. These hydraulic containment systems consists of five primary elements: 1) an impermeable barrier or wall seated in the upper portion of the silt and clay unit; 2) a gravel filled drain, completed to an elevation that is several feet below the elevation of the lowest recorded lake level, with a collection pipe embedded within, 3) wick drains within the lower portion of the fill and within the marl unit, 4) pumps to maintain the water level in the drain below lake level, and 5) a water treatment facility. These hydraulic containment systems are designed to capture the groundwater flowing towards the lake in the materials above the silt and clay unit. In addition, the drains will capture some flow from the underlying units by increasing hydraulic gradients across the confining unit. A schematic of the hydraulic containment system with a barrier wall is shown on Figure 7. A 2,850 ft. section of the hydraulic containment system has already been completed adjacent to the southern section of Remediation Area C and part of Remediation Area D (Willis/Semet IRM Barrier Wall). The impermeable barrier in this area consists of a sealed joint sheet pile wall.

[3] A slurry of Solvay waste and make-up water was discharged to the wastebeds. Solvay leachate refers to the liquid with a high total dissolved solids concentration that was released from the wastebeds during the period when the wastebeds were active. The leachate had a total dissolved solids concentration of about 100,000 mg/L and was a calcium-sodium-chloride type water (Effler, 1996).

Two segments of a hydraulic containment system without a barrier wall are proposed along the shoreline of Wastebeds 1-8; an approximately 1,060 ft. segment east of the mouth of Ninemile Creek and an approximately 6,700 ft. segment along the east side of the wastebeds extending northward from Ditch A (Figure 1). These segments of the hydraulic containment system will consist of four components: 1) a gravel filled drain, completed to an elevation that is several feet below the elevation of the lowest recorded lake level, with a collection pipe embedded within, 2) wells within the lower portion of the fill and within the marl unit that extend to the top of the underlying silt and clay unit, including the area of the former NMC channel sand and gravel deposits, 3) pumps to maintain the water level in the drain below lake level, and 4) a water treatment facility. These hydraulic containment systems will be designed to capture all groundwater flowing towards the lake from Wastebeds 1-8 in the marl and overlying fill units. A schematic of the hydraulic containment system without a barrier wall is also shown on Figure 7.

Groundwater Flow Model

A groundwater flow model has been developed to aid in the evaluation and design of the remedy for Onondaga Lake. The flow model has assisted in the development of the current understanding of groundwater flow conditions in the vicinity of the lake, which guided the detailed studies undertaken to quantify upwelling velocities. The model has been used to quantify the rates and direction of groundwater flow in the unconsolidated materials and in the upper bedrock in the vicinity of Onondaga Lake and to quantify groundwater discharge in the vicinity of Onondaga Lake. The model domain encompasses an area of approximately 30 square miles including all of Onondaga Lake and areas to the west and southwest of the lake. Revisions have been made to the model since the FS; the revised model, referred to as model Version 3.0 (S.S. Papadopulos & Associates, Inc. and O'Brien and Gere, 2009), received conditional approval by the NYSDEC on June 15, 2010. Version 1.0 of the groundwater model is described in Appendix D to the FS (Andrews and Swenson, 2004; and Swenson and Andrews, 2004).

Groundwater Conditions and Model Area Development

Groundwater discharge was an important consideration in developing the cap modeling areas for chemical isolation layer design as shown on Figure 1 and described in Appendix B. Model areas were developed to address variability in conditions across individual remediation areas to allow for robust cap designs, specific to the conditions in a particular portion of the overall remediation area. For example, the groundwater discharge at the mouth of Ninemile Creek is higher than that at other locations within Remediation Area A; therefore, to account for this spatial difference in groundwater upwelling velocities in the chemical isolation layer design, the region of higher upwelling was modeled separately from the remainder of the remediation area (and model inputs were specified separately for the two distinct areas).

In Remediation Area A, following collection of the Phase V and VI chloride-depth profiles it was determined that velocities near the mouth of Ninemile Creek were elevated compared to those in other parts of Remediation Area A. This finding was consistent with the understanding of the underlying sediment/soil structure near the mouth of Ninemile Creek. To explicitly consider the higher upwelling velocity in this area in the cap design, Model Area A2 was differentiated from the remainder of Remediation Area A, which was defined as Model Area A1.

In Remediation Area B, the primary factor in delineating model areas was contaminant concentration. However, the calculated upwelling velocities following onshore hydraulic control suggest higher upwelling velocities in the southeastern half of Remediation Area B. Therefore, separate groundwater upwelling distributions were developed for Model Area B1/C1 and B2 such that the higher upwelling velocities in B1/C1 were specifically considered in the cap design for that area. Groundwater upwelling distributions were also developed for the Wastebeds 1 through 8 connected wetlands.

The influence of the onshore hydraulic containment system was an important consideration in the delineation of model areas within Remediation Area C. The first priority in this area was the concentration and distribution of contaminants; however, the approximate influence of the hydraulic containment system was generally consistent with the delineation based on contaminant distribution. The onshore hydraulic containment system will control upwelling velocities in Model Areas B1/C1 and C3, as shown on Figure 1. In Model Area C2 upwelling velocities will be only minimally affected by the hydraulic containment systems and thus upwelling velocities were based on chloride depth profiles measured in the vicinity of Model Area C2.

Similar to Remediation Area B, Remediation Area D was modeled as four separate areas primarily due to contaminant concentration and distribution. However, groundwater velocities across Remediation Area D generally decrease moving east from the SMU 2 ILWD Area to the Eastern Area. As a result, groundwater distributions were developed for the cap model in each of the four areas of Remediation Area D as well as in three wetland areas along this shoreline (i.e., Wastebed B Outboard Area West, Center, and East).

For purposes of cap modeling Remediation Area E was subdivided into three model areas based on contaminant concentrations and distribution. However, a close review of the groundwater data and underlying geology in Remediation Area E shows a consistent silt/clay unit thickness and does not give any reason to expect spatial variability in upwelling velocities in the offshore areas. This is supported by the scatter in the upwelling data, lack of a clear spatial pattern throughout Remediation Area E, and similarity in upwelling statistics among the data from within each of the three modeling areas. Therefore, the chemical isolation layer design modeling does not use different groundwater upwelling rates in the three model areas, and rather bases each on the full upwelling data set from Remediation Area E.

Section 3
Measurements of Upwelling Velocities

Three types of field methods were implemented in an attempt to quantify groundwater discharge rates to the remediation areas in Onondaga Lake; 1) a piezometer-based method to measure hydraulic heads in the sediment pore waters, 2) seepage meters to directly measure groundwater discharge, and 3) measurement of chloride concentration profiles below the sediment-water interface to estimate groundwater flow rates through the sediments. The piezometer-based method consisted of a network of piezometers with recording devices that were installed within the lake sediments in late 2002 and monitored through July 2003 as part of a study known as the Groundwater Upwelling Investigation (Parsons, 2003). The intent of this method was to measure upward hydraulic gradients within the lake sediments and to covert the hydraulic gradients to upwelling velocities using estimates of the vertical hydraulic conductivity of the sediments. Two studies were conducted to evaluate the use of seepage meters, which directly measure groundwater discharge. An initial study was conducted with six meters in 2005 and a second study was conducted with thirteen seepage meters in 2007. Several field methods were also evaluated to measure and/or estimate sediment chloride concentrations; measurement of sediment conductivity using a direct push conductivity probe, Vibracore sampling with centrifugation of sediment samples to obtain sufficient pore water for analysis of chloride, and in-situ peepers. Each of the field methods implemented in an attempt to quantify groundwater discharge rates is described below. The work plan for the data collection activities and quality assurance plans are described in numerous documents prepared by Parsons (2003, 2005a, 2005b, 2006, 2007a, 2007b, 2007c, 2007e, 2007f, 2007g, 2007h, 2007i, 2008a, 2008b, 2008c, 2008d, 2008e, 2008f, 2008g, 2009a, 2009b, 2009c, 2009d, 2009e, and 2009f).

In addition to the quantitative methods implemented in the field, an additional method was used to qualitatively screen the lake bottom for locations with potentially anomalous groundwater discharge rates such as subaqueous springs and seeps. This method consisted of towing a conductivity and temperature sensor near the lake bottom and analyzing the data for anomalous temperature and conductivity readings that might potentially indicate areas of elevated groundwater discharge. Two surveys were conducted: one in 2005 and a second in 2007. This qualitative investigation of groundwater discharge is described below followed by a discussion of the quantitative methods.

Other techniques for estimating groundwater fluxes were considered but rejected as not feasible for use in Onondaga Lake. An excellent review of field techniques for estimating water fluxes between groundwater and surface water has been published by the USGS (Rosenberry and LaBaugh, 2008). A technique frequently used for quantitatively estimating groundwater fluxes is temperature. The seminal paper regarding this issue is Bredehoeft and Papadopulos (1965) "Rates of vertical groundwater movement estimated from earth's thermal profile." Temperature techniques for estimating groundwater velocities, as noted by Sayles and Jenkins (1982), work best for upwelling velocities of greater than 50 cm/yr. A recently developed technique for using temperature to quantify groundwater discharge is based on collecting time-series data at various depths below the sediment-water interface and evaluating how the temperature signal is attenuated with depth. A description of this method is contained in Keery and others (2006). An evaluation of this method indicated that the resolution of this method was on the order of 200 cm/yr. Recent advances in fiber-optic temperature sensing have indicated the potential of

this technique to accurately define temperatures at the sediment water interface but the technique does not yet lend itself to the quantitative estimation of upwelling velocities (Day-Lewis and others, 2006).

Temperature and Conductivity Survey

Two temperature and conductivity surveys were conducted in the lake to identify areas of groundwater discharge. These surveys were designed to qualitatively identify areas of groundwater discharge, but not to quantify the rate of groundwater discharge. The areas of potential groundwater discharge identified by these methods were then investigated by other methods in an attempt to quantify the discharge rates.

The first survey was conducted on September 7 and 8, 2005 using a Hanna S6T2 temperature and conductivity meter that was towed near the lake bottom from a slowly moving boat. Measurements were conducted in transects along the shoreline east of Ninemile Creek and conducted along the northern portion of the shoreline in Remediation Area E. The measurements along the shoreline east of Ninemile Creek did not identify potential groundwater discharge areas, as neither temperature nor conductivity changed significantly across the survey transects. In Remediation Area E, one potential upwelling location, which was identified by an approximately 1.5°F decrease in temperature and an increase in conductivity, was observed. A seepage meter was located at the observed temperature and conductivity anomaly (meter 60052 as described below).

A second and much more comprehensive temperature and conductivity survey was conducted from April 24 to 26, 2007 in Remediation Areas A and E. For these surveys, a YSI 6600 series multi-parameter sonde was used to measure water temperature, specific conductance, salinity, dissolved oxygen, turbidity, and sensor depth. The sensor was mounted in a custom built steel cage and towed with a 15-ft. jon boat as close to the bottom as possible. As an initial calibration step, the unit was tested on a known brine spring in Onondaga Creek to ensure it would identify a large anomaly in the groundwater discharging through the sediments. This screening step was successful in identifying the location of a large spring in lower Onondaga Creek. The survey was conducted by running transects approximately 25 ft. apart along the shoreline from water depths of about two ft. to six ft. Figures displaying the temperature and conductivity data collected during this survey are contained in Attachment II. For the most part, the temperature and conductivity patterns are consistent and uniform with very few anomalies suggesting potential groundwater seeps. One distinct anomaly of higher conductivity was observed along the shoreline east of the mouth of Ninemile Creek and a seepage meter cluster was located in this area (Seepage Meter Cluster 4-2 as described below). Another conductivity anomaly was observed adjacent to the shoreline east of Harbor Brook and a seepage meter cluster was located in this area (Cluster 7-1 as described below).

Groundwater Upwelling Investigation – 2003

A groundwater upwelling study was conducted in Remediation Area A near the mouth of Ninemile Creek and in Remediation Areas C and D in 2002 and 2003 (Parsons, 2003). The study consisted of vibrating wire piezometers emplaced in pairs at depths of 4.5 and 14.5 ft. below the sediment-water interface at three or four locations along each of six transects oriented approximately perpendicular to the shoreline. The locations of the piezometers are shown on Figure 8. Hydraulic pressures were recorded every twelve hours at these locations from December 27, 2002 through August 1, 2003.

The data from the one transect with three sets of piezometers in Remediation Area A provided relatively consistent estimates of hydraulic heads in the sediments. The piezometer pairs in the transect in Remediation Area A were located 25 ft., 538 ft. and 1,011 ft. from the shoreline. The sediments along this transect are primarily silts with some sands and clays (refer to hydrogeologic cross-section shown on Figure 4; the cross-section trace is shown in Figure 1).

The average upward hydraulic gradient, during the period investigated, calculated as the pressure head difference between the piezometers at a depth of 14.5 ft. and the one at a depth of 4.5 ft., ranged between 0.01 and 0.027 ft. per foot at the three piezometer pairs (Attachment III). The estimated vertical hydraulic conductivity of the sediments based on the lithologic characteristics of the sediments between a depth of 4.5 ft. and 14.5 ft. is approximately 10^{-5} cm/sec. Based on this estimate of the hydraulic conductivity, the upwelling velocity along the transect ranges from about 3 to 8 cm/yr, with the range merely reflecting the variability in the estimate of the hydraulic gradient. There is also uncertainty associated with the hydraulic conductivity estimate.

The piezometer-based method was determined not to be a suitable method for estimating groundwater discharge rates to the lake for purposes of cap design. There were two main reasons why it was judged to not be suitable: 1) it is logistically difficult to collect data from a large number of locations, and 2) it is difficult to obtain reliable estimates of pore water pressures from the vibrating wire piezometers for reasons that could not be fully explained. It is hypothesized that the accumulation of biogenically generated gas in the sand packed interval in which the piezometers were placed led to anomalous pressure measurements.

Seepage Meter Investigations

Two seepage meter investigations were conducted during pre-design investigations for the lake. One was conducted with six seepage meters as part of the Phase I Pre-Design Investigations in 2005 and the second was conducted with 13 seepage meters as part of the Phase III Pre-Design Investigations in 2007. The seepage meters used in this study were an adaptation of the type of seepage meter described by Lee (1977).[4] These two seepage meter investigations are described below.

Seepage Meters – Phase I Investigation

The seepage meters used in the Phase I Investigation were constructed with two-foot diameter PVC housing and an interior acrylic dome. Each meter consisted of two sections: a lower section that was installed into the sediment, and an upper section that housed the dome and a thin-walled Teflon sample bag. The two sections joined at a sealed male-to-female fitting to ensure that there was no leakage. The seepage meters were installed as a two-step process. First, the lower section of the seepage meter was slowly pushed 12 to 18 in. into the lakebed. After a stabilization period of at least 24 hours, the top and bottom sections of the meter were attached with a gasket to create a water-tight seal and bolted together using threaded steel rods. Finally, the four-liter measurement bags were prefilled with 60 ml of water and attached to the seepage meters.

[4] A useful review of seepage meters is contained in Rosenberry (2005) and Roseberry and LaBaugh (2008). The use of seepage meters to investigate groundwater discharge to lakes in central New York is discussed in Schneider and others (2004) and Sebestyen and others (2001).

Three seepage meters were installed in Remediation Area A and three were installed in Remediation Area E at the locations shown on Figures 9 and 12. One of the meters installed in Remediation Area A was located adjacent to a piezometer pair installed as part of the upwelling investigation described above. The meters in Remediation Area A were installed between 325 ft. and 820 ft. from shore, and the meters in Remediation Area E were installed between 200 ft. and 430 ft. from shore based on access and water depth constraints. The meters were monitored approximately weekly from September 16 through November 15, 2005.

There was significant variability in the weekly measurements of upwelling velocities at each of the meters, even though the piezometer data indicated that hydraulic gradients were relatively constant during the period of the study. An analysis of the data that were collected indicates that the volume of water collected in the seepage meter bags was influenced by multiple factors in addition to the ambient flux of groundwater through the sediments. Initially following seepage meter installation, gas production from decaying vegetation appears to have significantly influenced the rate of water accumulation, and as a result, data from the early period are not useful for estimating groundwater fluxes through the sediments. Settlement of the seepage meters was also a major factor influencing the rate of water accumulation resulting from high winds and resulting waves impart forces on the meters. A very small amount of settlement results in a relatively large volume of water accumulation in the collection bags relative to the amount of water accumulation from the ambient seepage flux. As a result, the groundwater flux through the sediments could not accurately be estimated directly from the water that accumulated in the seepage meter collection bags. The measured weekly upwelling velocities at the six seepage meters are shown on figures in Attachment IV.

Lake levels were relatively stable and gas production, at five of the six meters, was relatively constant during the period October 27 to November 15, 2005. Therefore, the amount of water that accumulated in the collection bags during this period can be attributed both to settlement (in part caused by wind and wave action) and ambient groundwater flux. Based on data from this period, the median combined settlement-induced flux and groundwater flux at each of the meters, with the exception of 60053 (SM-6) where gas production varied significantly during this period, are the following:

40013 (SM-1) – 19 cm/yr
40014 (SM-2) – 4 cm/yr
40015 (SM-3) – 44 cm/yr
60051 (SM-4) – 9 cm/yr
60052 (SM-5) – 10 cm/yr

These fluxes represent an upper bound estimate of the groundwater flux as it is likely that the settlement induced flux was significant but insufficient reference data were available to determine the exact amount of settlement.

Seepage Meters – Phase III Investigation

The seepage meters used in the Phase I Investigation were redesigned for the Phase III Investigation based on issues identified with the original meters. The meters were redesigned to reduce impacts of waves (e.g., wave breaks, stabilization poles, etc.) and to reduce settlement. In addition, larger volume bags were used for sample collection and control bags were used at each

meter to assess outside factors influencing water accumulation in the bags. The control bags were based on the design described in Cable and others (2004). In addition, wave height was monitored to account for any influences caused by wave action, centimeter scale measurements of meter elevations were made to assess settlement, and water levels were monitored in the lake and in on-shore monitoring wells to assess changes in horizontal gradients towards the lake during the investigation. A photograph of a redesigned seepage meter is shown in Attachment IV.

Seepage meters were installed at five locations during the Phase III Investigation: three in Remediation Area A, and two in Remediation Area E. Multiple meters were used at each location to assess the reproducibility of results. At three of the locations, three seepage meters were installed in close proximity to each other. At the other two locations, two meters were installed in close proximity to one another. The seepage meters were located as follows:

- Cluster 4-1 was located near the shoreline approximately 900 ft. east of Ninemile Creek to evaluate a temperature and conductivity anomaly at this location. These meters are labeled 40097, 40098, and 40122 on Figure 9.
- Cluster 4-2 was located about 1,300 ft. east of Ninemile Creek to evaluate a temperature and conductivity anomaly at this location. These meters are labeled 40095 and 40096 on Figure 9.
- Cluster 4-3 was located approximately 1,600 ft. east of Ninemile Creek to evaluate potential groundwater discharge from the distal end of a buried former channel of Ninemile Creek. These meters are labeled 40099, 40100, and 40101 on Figure 9.
- Cluster 7-1 was located approximately 350 ft. east of Harbor Brook to evaluate a conductivity anomaly at this location. These meters are labeled 70067, 70068 and 70069 on Figure 12.
- Cluster 7-2 was located approximately 1,000 ft. east of Harbor Brook. These meters are labeled 70065 and 70066 in Figure 12.

The seepage meters were monitored approximately weekly from June through August, 2007. The measured upwelling velocities at each of the seepage meter clusters are shown on figures in Attachment IV.

The results of the Phase III seepage meter study indicated that seepage meters are not a reliable method for measuring small upwelling velocities in Onondaga Lake. The results indicated that seepage meters do not consistently provide a reliable estimate of the “true” upwelling velocity. This conclusion is based on the following observations:

- The seepage meter data from the near-shore portion of Remediation Area A indicate negligible groundwater discharge whereas other lines of evidence (pore water chloride profiles and groundwater modeling) indicate that quantifiable groundwater discharge is occurring.
- The upwelling velocities at seepage meter pairs and triplicates showed little correlation between/among meters.
- The upwelling velocities calculated from the control bags were of the same order of magnitude as the rates calculated from the meters. In addition, upwelling velocities calculated from the control bags do not correlate temporally among locations.

Overall, the lack of reproducibility between/among meters at the five cluster locations indicated that the seepage meters were not a reliable method for estimating upwelling velocities of the magnitude that occur in Onondaga Lake. Therefore the data collected in the seepage meter investigations were not used for the development of the upwelling estimates for the cap design.

Chloride-Depth Profiles

Effler and others (1990) noted that chloride concentrations in the shallow sediments beneath Onondaga Lake increased nearly linearly with depth. They noted that this indicated a diffusive flux of chloride to the lake from a deep source of chloride. The source of chloride is now understood to be primarily halite brines within the glacial deposits that fill the Onondaga Trough and leachate from seepage from the wastebeds. TAMS (2002) noted that the chloride gradients beneath Onondaga Lake were not truly linear and that the deviation from linearity could be used to estimate the upwelling velocity.

The use of chemical concentration gradients in sediments to investigate upwelling velocities was first reported in the literature in 1982 when two studies were published that quantified upwelling velocities in the Pacific Ocean. One study used calcium and magnesium ion gradients to quantify upwelling velocities in the range of 1 cm/yr to 20 cm/yr near the Galapagos Islands, and the other study in the equatorial East Pacific Ocean quantified upwelling velocities of about 20 cm/yr using calcium ion gradients and the ratio of helium-4 to helium-2 (Maris and Bender, 1982; Sayles and Jenkins, 1982). Additional studies that have described the use of chemical concentration gradients in sediments to estimate upwelling velocities include Berg and Risgaard-Petersen (1998), Maris and others (1984), and Anati (1994). All of these studies have indicated that the use of chemical concentration gradients is a useful method for quantifying upwelling velocities that are less than approximately 50 cm/yr. Groundwater flow rates through lake sediments were also evaluated using tritium and chloride concentration depth profiles in sediments by Cornett and others (1989).

The section below describes the theoretical basis for the use of chemical concentration gradients in sediments to estimate upwelling velocities, the field methods that were investigated for measuring and/or estimating chloride concentrations in pore water, and the method of data evaluation.

<u>Description of Method</u>

At steady state conditions, the governing equation for vertical migration of chloride by advection with groundwater and diffusion is:

$$0 = -v\frac{\partial c}{\partial z} + D\frac{\partial^2 c}{\partial z^2} \qquad \text{for} \quad 0 \le z \le L \tag{1}$$

with the following boundary conditions:

$$c(z,0) = c_o; \quad c(0,t) = c_o; \quad \text{and } c(L,t) = c_L$$

where: c = chloride concentration,
c_o = chloride concentration at upper boundary;
c_L = chloride concentration at lower boundary;

L = length of domain;
v = seepage velocity (Darcy velocity divided by porosity);
D = sum of diffusion and dispersion coefficients.

An analytical solution to this equation developed by Al-Niami and Rushton (1977) was used to solve Equation 1 and was implemented in a Microsoft Excel spreadsheet to analyze the chloride depth profiles. The upwelling velocity was calculated by solving Equation 1 in an iterative manner until there was a good correspondence between the calculated and the measured chloride depth profile.

In evaluating chloride-depth profiles using Equation 1, it is important to note that the steepest concentration gradients occur near the sediment-water interface. As a result, calculated upwelling velocities are most sensitive to the chloride data collected near the interface. In applying Equation 1 to the evaluation of upwelling velocities for purposes of this report, a preference was given to using only data from the upper 5 ft. of sediment to estimate the upwelling velocity as deviations from linearity, if there were any, were most pronounced in this depth range. All profiles, though, were analyzed using data from the upper 5 ft. as well as data from the entire depth profile, which typically consisted of data to a nominal depth of about 9 ft. below the interface.

Model Parameters

The use of Equation 1 to analyze steady-state concentration profiles requires the definition of the parameter D, which is the sum of the diffusion and dispersive coefficients. The parameter D is defined as:

$$D = \omega D^* + \alpha_L v \qquad (2)$$

where D^* is the diffusion coefficient, ω is coefficient related to tortuosity and α_L is dispersion length.

The coefficient related to tortuosity is defined based on Boudreau (1996) as:

$$\omega = n/(1 - \ln(n^2)) \qquad (3)$$

where n is the porosity.

These parameters are a function of two characteristics of the sediment media, porosity and dispersion length; and a function of the diffusion coefficient of chloride in pore water. For purposes of the analysis of the chloride depth profiles from sediments of Onondaga Lake, the following values for these characteristics were used:

- A porosity value of 0.65 was used for evaluation of chloride depth profiles from Remediation Area C, a value of 0.75 was used for Remediation Area A, and a value of 0.70 was used for Remediation Area E. Sediment porosity was measured at multiple depths at 64 Vibracore locations; the average porosity at these 64 locations is shown on Figure 13. The available porosity data are listed in Attachment V.

- The dispersion length was calculated using equation (26) in Neuman (1990), which was developed to calculate the scale dependence of the dispersion length. This equation is: $\alpha_L = 0.0169L^{1.53}$, where L is length of the flow field in meters (note that equation requires that L be in units of meters). For a flow field length of 5 ft. the calculated dispersion length is about 0.1 ft. The use of this method to estimate the dispersion length and alternative methods for estimating the dispersion length are discussed in detail in Attachment XI.
- The effective diffusion coefficient for chloride was specified as 1.235 cm^2/day based on Felmy and Weare (1991) for a brine at 11º C.

An assumption implicit in the use of Equation 1 to estimate upwelling velocities is that the chloride concentrations in the sediments are at steady state; that is concentrations are not changing with time. A series of evaluations was conducted to determine the time required to reach steady state in shallow sediments after the sediments were disturbed. The calculations indicate that steady state is typically reached within a few decades. These calculations are described in Attachment VIII. In addition, it is assumed that chloride is neither being produced by dissolution nor lost by precipitation or sorption within the sediments. This is a valid assumption in most of the remediation areas but in some locations, particularly in areas with in-lake waste deposits, it appears that this assumption may not be valid. As a result, this method was not used to evaluate upwelling velocities in areas known to contain in-lake waste deposits.

Measurement of Sediment Chloride Concentrations

The initial method used to measure sediment chloride concentrations in sediment pore water was to collect cores using the Vibracore method, section the cores into 1.0 ft. intervals, centrifuge the cores, and then analyze the pore water for chloride and specific conductance. After evaluation of the data from the Phase I Pre-Design Investigation, it was determined that data at closer intervals were required for accurate analysis of the chloride-depth profiles. As a result, in Phase II the cores were sectioned into 0.5-ft. intervals. In Phase III, the upper 2 ft. of core were sectioned into 0.2 ft. intervals, but the pore water centrifuged from these small sections was only sufficient for analysis of chloride and specific conductance. All other pore water samples from Phase III were analyzed for common anions and cations, including chloride, and specific conductance. The cation-anion balance and the correlation between specific conductance and chloride were used to evaluate data quality.

In Phase II, the use of diffusion samplers (peepers) also was investigated for obtaining estimates of chloride concentrations in pore water. Fourteen extended peepers were installed at the five seepage meter clusters to approximate depths of 8 to 9 ft. The stainless steel peepers consist of a series of cells spaced at 0.5 ft. intervals that are filled with deionized water and covered with a membrane. Ions in the sediment pore water diffuse across the membrane and the peeper is kept in place ideally until equilibrium is reached between the cell and the pore water. The peepers in the Phase II investigation were left in place for approximately one week prior to retrieval. Pore water samples were collected from locations adjacent to each of the peepers and the concentrations measured in the pore water by centrifugation were compared to those determined from the peepers. In almost all cases, the measured chloride concentrations in the pore water were higher than the chloride concentrations in the peepers. This is consistent with the results of the laboratory study conducted by Jackson and Anderson (2007) that indicated that chloride equilibrium requires much longer deployment time than one week. Diffusion samplers

were also installed in each of the five seepage meters cluster in the Phase III investigations. These samplers were left in place for approximately three to five weeks and in general the chloride concentrations determined from these diffusion samplers were also lower than those measured in centrifuged pore water. The chloride depth profiles determined from the diffusion samplers in Phase III are shown along with the chloride depth profile from a nearby vibracore location in Attachment XII.

Because it is labor intensive to collect and centrifuge core samples for pore water analyses and to use extended peepers, alternative techniques were investigated for rapidly estimating sediment pore water chloride concentrations. The most promising technique identified was the measurement of sediment conductivity with a probe advanced into the sediment and subsequent conversion of conductivity to equivalent chloride concentrations. The main technical weakness of this technique is that sediment conductivity is not the same as pore water conductivity as a conductivity probe in contact with sediment measures a response that is both a function of the sediment matrix and the characteristics of the pore water. In these investigations it was determined that there was a relatively good correlation between sediment conductivity and pore water conductivity. The relationship between sediment conductivity and pore water conductivity, though, is a function of sediment characteristics and at locations where sediment characteristics were variable, conductivity depth profiles were also variable as the result of changing sediment characteristics.

A Geoprobe SC4000 soil conductivity probe was used for measuring sediment conductivity. The probe uses a four-pole Wenner-type array; current is passed through the outer contacts of this array and voltage is measured on the inner two contacts. Conductivity and temperature measurements were made at 0.05 ft. intervals as the probe was advanced. Most probes were advanced to a depth of approximately 10 ft.

The conductivity data were converted to equivalent chloride concentrations using a conversion factor. A conversion factor of 0.89 was used to convert from conductivity in uS/cm^2 to mg/L chloride in Remediation Areas A, B and C and a factor of 0.80 was used in Remediation Areas D and E. These factors were developed from comparisons of pore water chloride and sediment conductivity data collected in close proximity to each other. The calculated upwelling velocities are not sensitive to the conversion factor as the conversion factor merely scales the chloride depth profile and does not affect the convexity of the profile. Attachment VI contains plots of chloride concentrations and conductivity versus depth for 31 locations where both pore water and sediment conductivity data were collected. In general, the shapes of the depth profiles are similar for both the pore water data and the sediment conductivity data.

There are inherent strengths and weaknesses with both methods used to construct chloride depth profiles. The chloride-depth profiles constructed from chemical analyses of pore water provide a more accurate estimate of actual changes in chemical concentrations with depth because the parameter of interest, chloride, is measured directly. The main weakness with the chloride-depth profiles developed from pore water is related to the fact that the measured concentrations represent an average concentration over the section of core analyzed. As a result, it is not possible to accurately define the chloride-depth profile very near the sediment-water interface where the chloride concentrations change rapidly with depth. The sediment-conductivity data collected with the Geoprobe conductivity probe, on the other hand, are an approximate analog for chloride concentrations in pore water, but because the probe does not measure pore water properties alone; variations in conductivity measurements with depth are

also related to changes in the physical/chemical properties of the sediment. This method, though, allows variations in conductivity near the sediment water interface to be determined very precisely. Recognizing the strengths and limitations of the two methods leads to the conclusion that both methods can be used to provide reliable estimates of upwelling velocity.

Field Investigations

Chloride-depth profiles were constructed and used to calculate upwelling velocities at 356 locations within and in the vicinity of the Remediation Areas[5]. At 156 locations chloride-depth profiles were developed from analyses of pore water collected from cores during the Phase II, Phase III, Phase V and Phase VI Investigations, and at 245 locations chloride-depth profiles were developed from sediment conductivity data collected in the Phase III and Phase IV Investigation in 2007 and 2008[6]. Pore water data from 72 locations sampled as part of the Lake RI and 10 locations as part of the Phase I Pre-Design Investigation were not used for estimating upwelling velocities because of a limited number of depth-discrete samples collected at each location. In addition, sediment conductivity data collected as part of the DNAPL Investigation (Parsons, 2006) near the Causeway and in Phase II were not used for estimating upwelling velocities because of a lack of standardization in collection of the data. The table on the following page lists all of the investigations in which pore water and sediment conductivity data were collected, the number of locations at which data were collected, and comments regarding data collection.

Only limited sediment conductivity data and pore water data were collected for purposes of estimating upwelling velocities in areas with thick Solvay deposits. During the early phases of this study it was determined that chloride-depth profiles in the Solvay deposits could not be interpreted to reliably estimate upwelling velocities. This has been interpreted to be the result of chemical interactions between the pore water and the Solvay matrix that affect pore water chloride concentrations

Initial Data Evaluations

The following steps were completed initially to evaluate the data that were collected:

1. Anion-cation balances were calculated for the pore water analyses; the balances are listed in Attachment V. In a number of instances, the error in the anion-cation balance was greater than twenty percent. Based on an evaluation of chloride concentrations and specific conductance, it was determined that the error was generally attributable to an under-reporting of cation concentrations. Plots were completed of conductivity versus chloride for data from each Vibracore location with applicable data, to identify chloride data that were outliers.
2. Plots of conductivity versus depth and chloride versus depth were developed for each location with co-located Geoprobe and Vibracore data, and a relationship was developed between the conductivity values from the Geoprobe and the chloride concentrations from pore water collected from the cores. These plots are contained in

[5] Upwelling velocities were estimated from the analysis of 474 chloride-depth profiles collected at 356 locations; 167 profiles developed from pore water data and 307 profiles developed from sediment conductivity data. Data from 25 chloride-depth profiles were not analyzable.

[6] At 31 locations chloride-depth profiles were developed from both pore water data and sediment conductivity data.

Attachment VI for 31 locations with Geoprobe and Vibracore data. A linear factor relating the chloride concentration to conductivity was calculated using the Solver routine in Excel in which the sum of the squared differences between calculated chloride concentrations and observed chloride concentrations were minimized. The calculated factors for each of the thirty-one locations are listed in Attachment VI.

Pore-Water and Sediment Conductivity Data

Type	Study Phase	Date	Locations	Comments
Pore Water	RI	1992	72	Borings were advanced throughout the lake to a nominal depth of 3 ft. and generally three to five subsamples from each boring analyzed for chloride. These data were not used to calculate upwelling velocities because of limited depth-discrete data.
	Phase 1 PDI	2005	10	Sediment samples collected at nominal depths of 1, 3, and 5 ft. and pore water collected by centrifuging the samples. These data were not used to calculate upwelling velocities because of limited depth-discrete data.
	Phase II PDI	2006	13	Sediment samples collected at 1 ft. depth intervals to 10 ft. and pore water collected by centrifuging the samples.
	Phase III PDI	2007	21	Sediment samples collected at 1 ft. depth intervals to 10 ft. and pore water collected by centrifuging the samples. Collocated with seepage meters and Geoprobes.
	Phase III PDI Addendum 5	Dec 2007	30	Pore water collected by centrifuging sediments from approximate intervals of 0.0-0.3 ft., 0.3-0.5 ft., 0.5-0.8 ft., 0.8-1.0 ft., 1.0-1.3 ft., 1.3-1.5 ft., 1.5-1.8 ft., 2-2.5 ft., 3-3.5 ft., 4-4.5 ft., 5-5.5 ft., 6-6.5 ft., 7-7.5 ft., 8-8.5 ft., and 9-9.5 ft.
	Phase V	2009	23	Pore water collected by centrifuging sediments from intervals of 0-0.25 ft., 0.25-0.5 ft., 0.5-0.75 ft., 0.75-1.0 ft., 1.0-1.25 ft., 1.25-1.50 ft., 1.50-1.75 ft., 2.0-2.5 ft., 3.0-3.5 ft., 4.0-4.5 ft., 5.0-5.5 ft., 6.0-6.5 ft., 7.5-8.0 ft. and 9.0-9.50 ft..
	Phase VI	2010	69	Pore water collected by centrifuging sediment from same intervals as in Phase V.
Sediment Conductivity	DNAPL Investigation	2006	20	Advanced along the causeway in SMU 2 to a nominal depth of 45 ft. using a Geoprobe fitted with a MIPs and conductivity detector. These data were not used to estimate upwelling velocities.
	Phase II PDI	2006	68	Advanced using Geoprobe method to nominal depth of 10 ft. These data were not used to estimate upwelling velocities.
	Phase III PDI	2007	39	Advanced using Geoprobe method to nominal depth of 10 ft. in proximity to five seepage meters in SMU 4 and SMU 7.
	Phase III PDI Addendum 5	2007	82	Advanced using Geoprobe method to nominal depth of 10 ft.
	Phase IV PDI	2008	124	Advanced using Geoprobe method to nominal depth of 10 ft.

3. Plots of porosity versus depth were prepared for each of the Vibracore locations. These plots are contained in Attachment V. The porosity was determined in the laboratory according to method ATSM D-2216 from samples collected with Vibracore. An average porosity was calculated for each location and the average porosity values at each of the Vibracore locations are shown on Figure 13.

4. Plots of sodium and sodium-calcium ratio versus depth were prepared for each of the Vibracore locations. These plots are contained in Attachment V.

Section 4
Upwelling Velocities Calculated from Chloride-Depth Profiles

The chloride-depth profiles developed from pore water data and sediment conductivity data collected in the littoral zone in, and in the vicinity of, the remediation areas were analyzed using the procedures described in the previous section. Plots of the chloride-depth profiles are contained in Attachment VII. In total, as a result of duplicate and triplicate data collected at some locations, 474 chloride-depth profiles were developed for 356 locations. The analysis consisted of iteratively solving Equation 1, described in Section 3, using various values of the upwelling velocity until a "best fit" between the calculated and the measured chloride depth profile was obtained. The "best fit" was, in the ideal case, defined as a solution in which the sum of the squared differences between the measured and calculated chloride values was minimized. An example of the iterative process is illustrated below for the analysis of the pore water chloride data from location OL-VC-60154. An initial estimate of the upwelling velocity is 0.0 cm/yr, which produces a sum of the squared differences between the calculated and measured values (squared error) of 5220. A second estimate of the upwelling velocity of 2.0 cm/yr[7] produces a squared error of 2871, a third estimate of the upwelling velocity of 1.0 cm/yr produces a squared error of 184 cm/yr, and finally after many more iterations a final solution of 1.1 cm/yr is calculated with a squared error of 172.

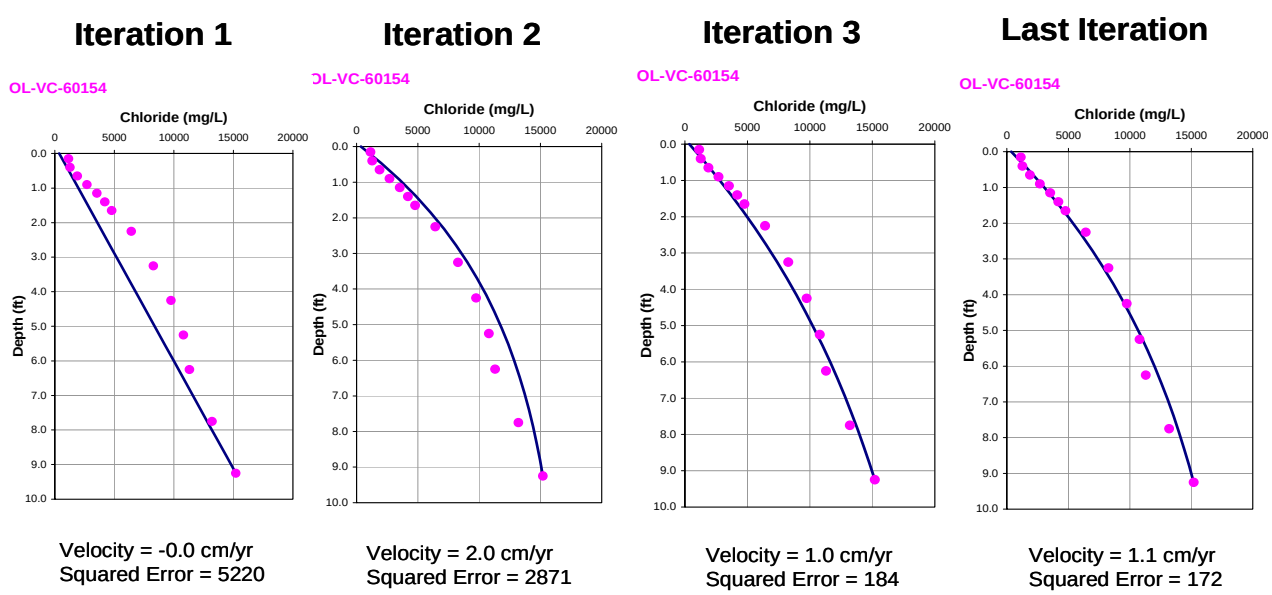

[7] In this text a positive upwelling velocity indicates groundwater flow towards the sediment-water interface. This direction is opposite the standard groundwater convention in which a "positive" velocity indicates downward flow. In Attachment VII, the standard groundwater convention was used; thus for location OL-VC-60154 the "best fit" velocity is listed as "-1.0" rather than "1.0" as described above.

The iterative solutions were calculated with the assistance of the Solver routine in Excel,[8] which is designed to find the solution that minimizes the squared error. In this example, relatively small changes in the upwelling velocity produce large changes in the squared error; for example changing the velocity from 2 cm/yr to 1 cm/yr reduces the squared error from 2871 to 184. This sensitivity of the squared error to the velocity in this example indicates that the upwelling velocity can be accurately quantified from the measured data[9]. The upwelling velocities that were calculated for each of the chloride-depth profiles are shown on Figures 14 through 16 for Remediation Areas A, C, and E, respectively. On these figures, the values from the "best fit" solutions to Equation 1 for each of the chloride-depth profiles that were analyzed are shown on the plots in Attachment VII along with the parameter values used in solving Equation 1.

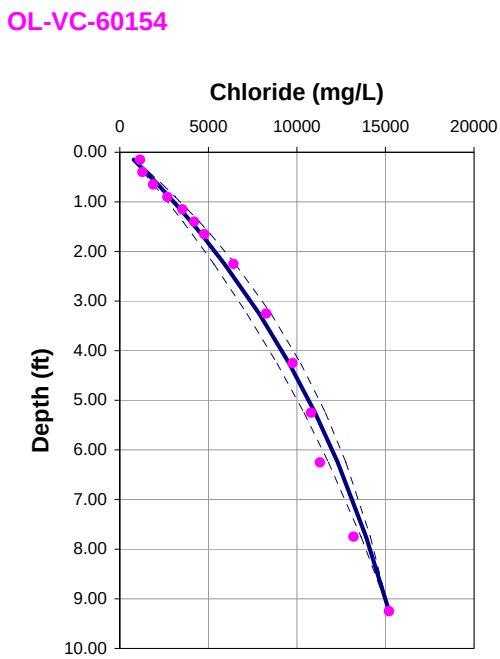

An example plot for pore water data from OL-VC-60154 is shown above. The solid line indicates the "best fit" solution with a velocity of 1.1 cm/yr, and the dashed lines indicate solutions for velocities of 1.1 ± 30% cm/yr. A rigorous quantitative evaluation of the uncertainty associated with the "best fit" solution is described in Section 6.

In analyzing the chloride-depth profiles, a "best fit" solution was calculated based on an analysis of data from the sediments within 5 ft. of the sediment-water interface and a "best fit" solution was calculated based on data from within the upper 10 ft. of the sediment-water interface. "Best fit" solutions were calculated using the two data sets to check the consistency of the calculated upwelling velocity and these results are shown on the plots in Attachment VII. In most cases, similar upwelling velocities were calculated using data from the upper 5 ft. and data from the upper 10 ft. In general for purposes of evaluating the spatial distribution of upwelling velocities, the higher of the two estimates was used and this value is posted on Figures 14 through 16[10].

[8] Microsoft Office Excel 2003 was used for these analyses.

[9] This example oversimplifies the analysis of the data from OL-VC-60154 since in determining the "best fit" solution both the velocity and the concentration at the lower boundary were adjusted in the iteration process.

[10] An exception was when the data from the upper five ft did not correspond to the "best-fit" depth profile as well as data from the upper 10 ft. (or vice versa); in these cases, the "best-fit" solution that better fits the data is the value listed on Table 1 and posted on Figures 14 through 16, and a comment is included in Table 1 and Table VII-1.

At some locations, the measured chloride-depth profile did not exhibit a smooth change in chloride concentrations with depth. As a result, the correspondence between the "best-fit" solution to Equation 1 and the measured data is poor. An example of a chloride-depth profile where the "best-fit" solution poorly matches the observed data is at location OL-GP-40182 where the chloride-depth profile was developed from sediment-conductivity data; the data from this location is shown on the figure to the right. A "best-fit" solution to the entire data set and a "best-fit" solution to the data near the sediment-water interface for this location are also shown on that figure. The upwelling velocity corresponding to the "best-fit" solution to the data near the interface is about 11 cm/yr and the velocity corresponding to the "best-fit" solution to the entire data set is about 2 cm/yr.

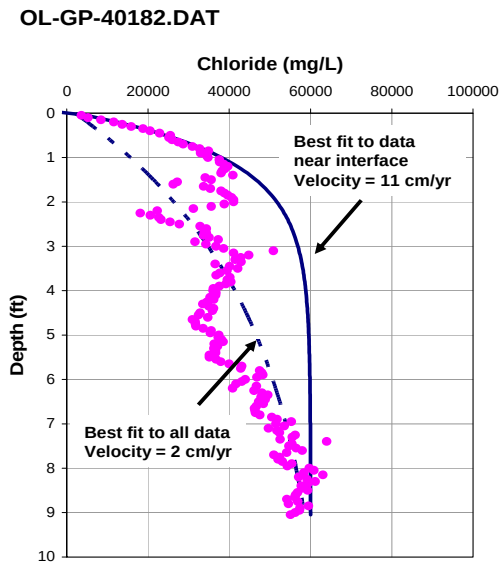

The calculated chloride-depth profiles of the "best-fit" solutions increase monotonically with depth whereas the data from OL-GP-40182 display significant scatter between a depth of about 1 ft. and 5 ft. below the sediment-water interface that is inconsistent with the calculated "best-fit" profiles. The deviation between the form of the measured data and the underlying model could be caused by a number of factors, but insufficient information is available to identify the main factors. It is suspected that a major factor is a poor correspondence between the sediment conductivity reading and the conductivity of the pore water due to variations in lithology with depth and variations in the contact between the probe and the sediment with depth. The sediment-conductivity data from near the sediment-water interface are judged to be more representative of actual conditions because the data provide a smooth chloride-depth profile that is consistent with the analytical model at this sampling location. Therefore, the "best-fit" solution to the data near the sediment-water interface provides a better estimate of actual upwelling velocity than the "best-fit" solution to the entire data set from the upper 9 ft. of sediment.

Table VII-1 includes notes indicating the quality of the upwelling analysis, which is a qualitative assessment of how well the measured data matched the chloride-depth profiles calculated using Equation 1. The quality of the upwelling analysis for about 65 percent of the chloride-depth profiles based on pore water data and for about 54 percent of the chloride-depth profiles based on sediment-conductivity data are judged to be "good." For these chloride-depth profiles the chloride concentrations generally increase monotonically with depth with little scatter and there is a good correspondence between the observed and calculated chloride-depth profiles. For these analyses, there is a high degree of confidence in the calculated upwelling velocities. On the other hand, the quality of the upwelling analysis for about 8 percent of the chloride-depth profiles based on pore water data and about 14 percent of the chloride-depth profiles based on sediment conductivity data are described as "poor." In general, these analyses are judged to be "poor" because the observed chloride concentrations do not increase monotonically with depth as illustrated above for location OL-GP-40182. For these analyses there is significant uncertainty associated with the calculated upwelling velocity. A few of the chloride-depth profiles were not analyzable either because of sparse or sporadic data; a total of

seven of the chloride-depth profiles developed from pore-water data and 18 of the profiles developed from sediment-conductivity data were not analyzable.

At locations where the analysis of the chloride-depth profiles were judged to be poor and that are located within remediation areas that will be unaffected by operation of the hydraulic containment systems, additional borings were advanced in the Phase VI Pre-Design investigation to collect pore-water data with Vibracores to better determine the upwelling velocities. An example of such a location is OL-GP-40182, which is located at the mouth of Ninemile Creek and was discussed above. Plots of the chloride-depth profiles developed from sediment conductivity data from this location and plots of the chloride-depth profiles developed from pore-water data from a Phase VI Vibracore located near (OL-VC-40302) are shown below.

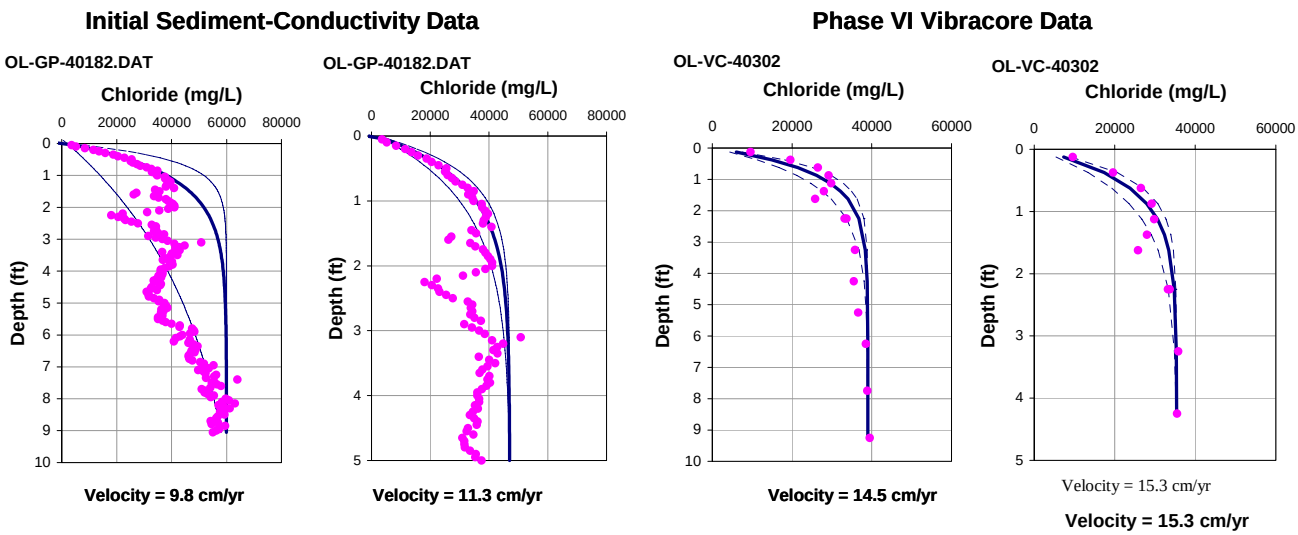

The analysis of the chloride-depth profiles developed from sediment-conductivity data from the upper 10 ft. and the upper 5 ft. from OL-GP-40182 resulted in estimated upwelling velocities of 9.8 cm/yr and 11.3 cm/yr, respectively[11]. These analyses, though, are based solely on fitting the data from the upper 1.25 ft. as the data from greater depths have significant scatter and do not correspond with the calculated chloride-depth profile. The analysis of the chloride-depth profiles developed from pore-water data from the upper 10 ft. and the upper 5 ft. from the Phase VI data collected at OL-VC-40302 resulted in estimated upwelling velocities of 14.5 cm/yr and 15.3 cm/yr, respectively. These data, with the exception of one data point from about 1.5 ft., fit the calculated chloride-depth profiles quite well. As a result, the upwelling velocity calculated from the Phase VI pore-water data is judged to be a better estimate of the actual upwelling velocity at this location.

At some locations, the calculated upwelling velocity based on the "best-fit" solution exceeded a seepage velocity (as defined in Equation 1) of 50 cm/yr, which was judged to be the upper bound velocity that could be estimated by this method. For these locations, Table VII-1 notes that the velocity is greater than the Darcy velocity that corresponds to a seepage velocity of

[11] The NYSDEC has indicated that their analyses of these data produce an upwelling velocity as high as 21 cm/yr (NYSDEC, April 25, 2010).

50 cm/yr[12]. None of the locations where the seepage velocity was estimated to be greater than 50 cm/yr are located within proposed capping areas. The hydraulic containment system proposed to the east of the mouth Ninemile Creek was designed specifically to reduce groundwater upwelling velocities in that portion of Remediation Area A where seepage velocities estimated from the chloride-depth profile method exceeded 50 cm/yr.

[12] The upwelling velocities listed on Table 1 are Darcy velocities. The Darcy velocity by definition is equal to the seepage velocity multiplied by the porosity. Since the porosity is always less than one, the Darcy velocity is always less than the seepage velocity.

Section 5
Upwelling Velocities for Cap Design in Areas without Hydraulic Containment

Groundwater upwelling velocities in Remediation Area E and in Model Areas A1, A2 and C2 are expected to be only minimally affected by operation of the hydraulic containment systems and thus upwelling velocities with the cap are expected to be similar to current upwelling velocities[13]. For each of these areas, a cumulative frequency distribution of upwelling velocities was developed based on the chloride-depth profiles within the areas for use in cap design. In calculating the frequency distributions the following data treatment criteria were used to obtain a data set in which point estimates of upwelling velocities were relatively uniformly distributed within the areas:

1. At locations with upwelling velocity estimates from both pore-water and sediment-conductivity data, the velocity calculated from the pore-water data was selected.
2. At locations with duplicate or triplicate sets of pore-water data or sediment-conductivity data, the highest calculated upwelling velocity from the replicates was selected.
3. When upwelling velocities were calculated from both chloride-depth profiles from the upper 5 ft. and chloride-depth profiles from the upper 10 ft., the higher calculated upwelling velocity was selected unless one of the analyses were judged to be poor.
4. At locations where the 90 percent upper confidence interval on the calculated upwelling velocity was greater than 50 percent of the best-fit value, the value corresponding to the 90 percent upper confidence interval was selected.
5. In Model Area A1, the upwelling velocity in the near shore area that will be affected by the hydraulic containment system was specified as 2.2 cm/yr, which corresponds to the upwelling velocity through the silt and clay unit (refer to Section 8).
6. In Remediation Area E, the upwelling velocity in the near shore area that will be affected by the Harbor Brook containment system was not considered in developing the cumulative frequency distribution of upwelling velocities in Remediation Area E because the area affected by the containment system is only a very small portion of Remediation Area E.
7. In Model Area C2[14] only upwelling estimates from pore-water data were selected as chloride-profiles constructed with sediment-conductivity data were "noisy" and apparently affected by presence of Solvay materials in the sediment.

[13] Exceptions are 1) in that portion of Model Area A1 that is located in proximity to the proposed hydraulic containment system located east of the mouth of Ninemile Creek, and 2) in that portion of Remediation Area E located in proximity to the eastern end of the Harbor Brook hydraulic containment system.

[14] The upwelling velocity frequency distribution for Model Area C2 is based on upwelling velocity estimates from the area offshore of the Department of Transportation turnaround that will be unaffected or only partially affected by hydraulic containment systems as shown on Figure 15.

8. In Remediation Area E there are two small areas with radii of about 25 ft. where many sets of chloride-depth profiles were obtained and for which an upwelling velocity was calculated for each set. A single upwelling velocity was selected to represent the upwelling velocity in each of these areas; this value was specified as the average of the estimates from pore-water data.

These data treatment criteria for developing cumulative frequency distributions of upwelling velocities are biased towards overestimating the actual upwelling velocity, as the higher of the estimates was selected at several decision points.

Results

The upwelling velocities used to calculate the cumulative frequency distributions are listed on Table 1 and the selected data are shown in map view on Figures 14 to 16[15]. On these figures, the values used to develop the cumulative frequency distribution are shown in bold typeface, the values not used are shown in light-grey typeface. Selected statistics of the cumulative frequency distribution for each of the areas, and the number of upwelling velocities used to construct the distribution, are listed below.

	Model Area A1	**Model Area A2**	**Model Area C2**	**Remediation Area E**
count	56	29	10	126
median	1.05	3.22	2.05	1.15
mean	1.64	4.10	3.05	1.51
standard deviation	2.28	2.95	2.75	1.82

The mean calculated upwelling velocity in Model Area A1 is 1.64 cm/yr with a standard deviation of 2.28 cm/yr, the mean upwelling velocity in Model Area A2 is 4.10 cm/yr with a standard deviation of 2.95 cm/yr, the mean upwelling velocity is Model Area C2 is 3.05 cm/yr with a standard deviation of 2.75 cm/yr, and the mean upwelling velocity in Remediation Area E is 1.51 cm/yr with a standard deviation of 1.82 cm/yr. The highest upwelling velocities occur in Model Area A2 and are associated with recent deposits from Ninemile Creek.

Probability plots of the upwelling distributions are shown in graphic form below with the upwelling velocity plotted on a logarithmic scale on the x-axis and the frequency percentile plotted on a probability scale on the y-axis.

[15] The values shown on Figures 14 to 16 represent the values listed on Table 1 in the column labeled "Upwelling Velocity" and the values adjusted for the confidence interval where appropriate.

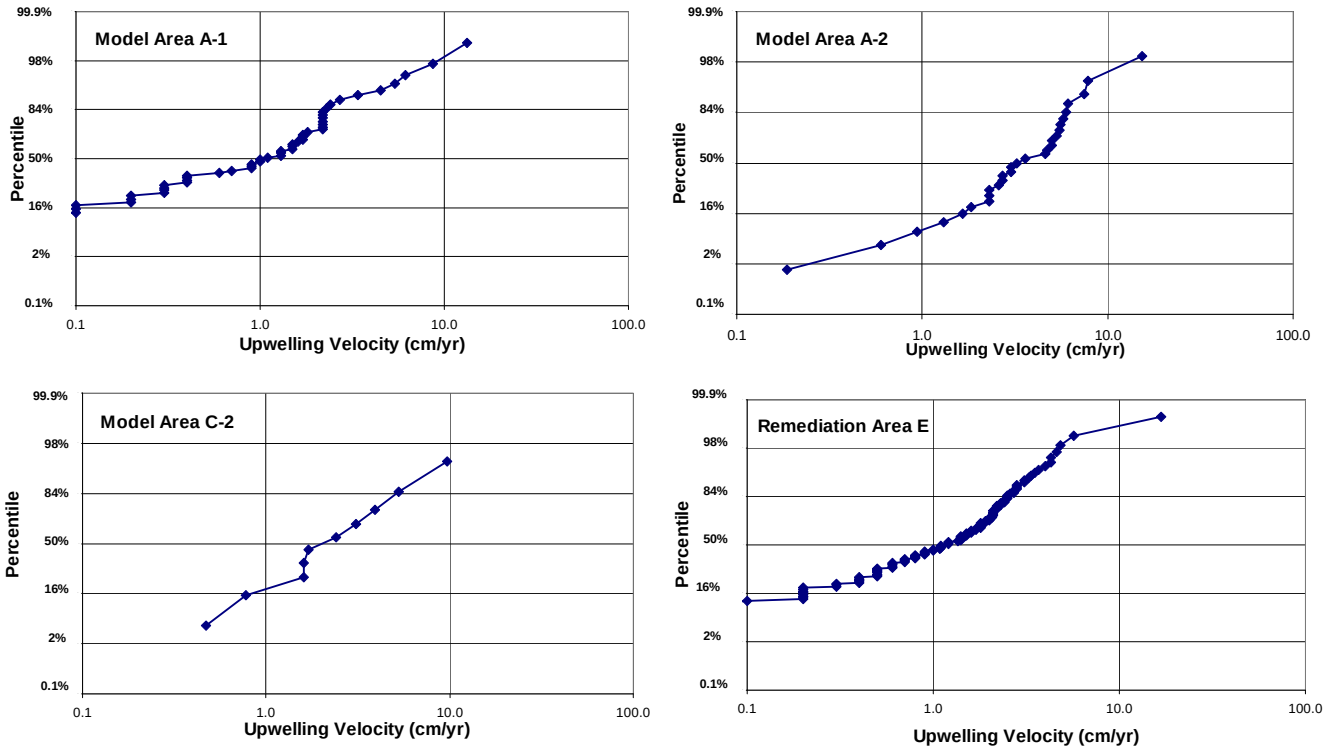

No pore-water or sediment-conductivity data were collected along the spits at the mouth of Ninemile Creek that will be removed and restored as wetlands as part of lake remedy. Under existing conditions, the upwelling velocities on the spits are likely downward because of recharge that occurs on the spits. Following construction of the wetlands, upwelling velocities will be consistent with those observed in adjacent areas in Model Area A2. Therefore, for cap design purposes the upwelling velocities in the proposed wetland area were assumed to be the same as those in Model Area A-2.

Section 6
Evaluation of Uncertainty in Calculated Upwelling Velocities

This section evaluates the uncertainties associated with upwelling velocities calculated with the chloride-depth profile method. In evaluating the chloride-depth profiles, the best estimates of aquifer and chemical parameters have been utilized in the analyses. This section briefly discusses the uncertainty associated with the input parameters, the uncertainty associated with reproducibility of results from co-located borings, and the uncertainty associated with the use of a "best fit" solution to Equation 1 to estimate the upwelling velocity.

Sensitivity to Model Parameters

The sensitivity of calculated upwelling velocities to dispersion length, porosity and chloride factor was evaluated. Sensitivity analyses were conducted using the data from a subset of sample locations (specifically Geoprobe location GP-40168 and Vibracore locations VC-30179, VC-40091, VC-40092, VC-40297, VC-40302, VC-60303, and VC-70058) having estimated upwelling velocities that ranged from 3.3 to 15.3 cm/yr. The sensitivity analyses consisted of the following four evaluations:

1. Increasing the dispersion length from 0.1 ft. to 0.8 ft
2. Decreasing the porosity to the lowest porosity value measured in the vicinity of the location
3. Increasing the factor that converts conductivity to chloride from 0.8 to 1.0 (only for sediment conductivity data)
4. Decreasing the factor that converts conductivity to chloride from 0.8 to 0.64 (only for sediment conductivity data)

The results of these sensitivity evaluations indicate the calculated upwelling velocities are sensitive to porosity and dispersion length, but not very sensitive to the chloride adjustment factor. The porosity and dispersion lengths used in the analyses of upwelling velocities described in Attachment VII and shown on Figures 14 to 16 are the best-estimates of the parameter values. The results of the sensitivity evaluations for porosity and dispersion length that were conducted for the chloride-depth profiles from the selected sample locations are contained in Attachment XI.

Reproducibility of Results

The reproducibility of calculated upwelling velocities was evaluated by comparing the upwelling velocities calculated from sediment conductivity data with those calculated from the Vibracore data at each of the thirty locations with both types of data and by comparing calculated upwelling velocities from multiple sediment-conductivity borings advanced close to one another. Overall the calculated velocities from co-located Vibracore and sediment-conductivity borings compare well. The results of these evaluations are listed on Table 2 and plots of these data are contained in Attachment IX.

At 47 locations, multiple sets of sediment conductivity data were collected. The upwelling velocities at locations with multiple sets of conductivity data are listed on Table 3. At most locations, the upwelling velocities calculated from each set of data are similar.

The reproducibility of calculated upwelling velocity was also assessed by comparing sediment conductivity data taken in different seasons at the same location. Chloride profiles based on sediment conductivity were obtained during spring and fall seasons at several locations (OL-GP-40183, OL-GP-40184, OL-GP-40185, OL-GP-40186, and OL-GP-70107). The upwelling velocities determined in different seasons for these locations are comparable, except in cases where the data are difficult to analyze due to exceeding the maximum measurement capability of the probe (OL-GP-70107). Distinct seasonal trends could not be reliably identified. At four locations, profiles were obtained during the summer months in both 2007 and 2008 (OL-GP-40074, OL-GP-40010, OL-GP-70053, and OL-GP-70054). The upwelling velocity determinations were comparable, except in cases where the data were difficult to analyze due to the measured values exceeding the maximum measurement capability of the probe.

Model Fit

The uncertainty of the upwelling velocities calculated with a "best fit" solution to Equation 1 was evaluated by calculation of a confidence interval (CI) for the calculated velocity. This uncertainty is primarily related to scatter in the chloride or conductivity depth profile data. The confidence interval is calculated as:

$$b \pm f \cdot s_b \tag{4}$$

where b is the calibrated parameter value, f is the confidence interval factor (for a 90% CI, f=1.645), and s_b is the standard deviation of the estimated parameter value. The standard deviation of a parameter value is a function of the perturbation sensitivities and the observation variances (Aster et al. 2005, Doherty, 2008):

$$s_b^2 = \sigma^2 \left(\underline{X}^T \underline{X} \right)^{-1} \tag{5}$$

where $\underline{X}$ is a matrix of the sensitivities of observations to parameters (calculated using forward difference perturbations) and σ^2 is an *m*-vector containing the observation variance calculated according to (Doherty, 2008):

$$\sigma^2 = \frac{\Phi}{m-n} \tag{6}$$

where Φ is the residual sum of squares, *m* is the number of observations, and *n* is the number of parameters.

Because there is only one parameter, the sensitivity matrix $\underline{X}$ has *m* rows and only one column, making it a vector. As such, calculation of $\underline{X}^T\underline{X}$ is simply:

$$\sum_{i=1}^{m} x_i^2 \tag{7}$$

where x_i is the *i*th row in the sensitivity vector.

The calculated confidence intervals for each of the upwelling velocities are listed on Table 1. At most locations, the confidence interval is relatively small compared to the magnitude of the estimated upwelling velocity.

This formal analysis of uncertainty is based on the assumption that the boundary conditions for Equation 1 are fixed. In practice though, there is some uncertainty relative to the lower boundary condition. For the analyses that were judged to be "good" as listed on Table 1, the uncertainty related to the lower boundary condition is small, but for analyses judged as "fair" or "poor," there may be additional uncertainty related to the magnitude of the lower boundary condition.

Another measure of model fit is the correspondence between the upwelling velocities calculated based on "best-fit" solution to the upper 5 ft. of data and the upwelling velocities based on "best-fit" solution to the upper 10 ft. of data. For locations where the upwelling results from the two sets of analyses are similar, this is an indication that the uncertainty associated with the upwelling estimate is low; whereas, when the two estimates differ significantly it indicates uncertainty regarding the estimated upwelling velocity. The upwelling velocities estimated from the upper 5 ft. of data and the upper 10 ft. of data are listed in Attachment VII.

Summary

The evaluations of the uncertainties in the upwelling velocities quantified with the chloride-depth profile method have indicated a high degree of confidence in the calculated upwelling velocities, but as with all evaluations based on field data, there is some uncertainty associated with individual evaluations of upwelling velocities. The spatial consistency of results, as shown on Figures 14, 15 and 16, increased the confidence associated with estimates at individual locations.

Section 7
Analysis of Upward Groundwater Flow through Silt and Clay Unit

Groundwater discharge in remediation areas offshore from the hydraulic containment systems will be less than current rates following construction and operation of the systems. In areas offshore of the hydraulic containment systems, groundwater discharge will potentially come from two sources; recharge in the area between the lake shore and the hydraulic barrier and upward groundwater flow through the silt and clay layer. Some recharge will occur to the wetlands outboard of the barrier wall as the result of fluctuating lake levels, but the engineered design for these wetlands will create a high permeability layer beneath the wetlands through which any recharge will migrate directly to the lake and thus minimize any migration through the underlying contaminated materials. The locations of proposed outboard wetlands are shown on Figure 1. As a result, the only significant potential source of groundwater discharge is upward migration of groundwater through the silt and clay layer.

Groundwater levels, and hydraulic heads, in the permeable units below the silt and clay unit in Remediation Areas A, B, C and D are higher than the average water level in Onondaga Lake. This creates the potential for upward groundwater flow from the deeper units to the lake. Some of the monitoring wells completed in the sand and gravel unit along the shoreline flow at the surface, which illustrates realization of this potential. The water levels in the sand and gravel in onshore wells in the vicinity of the remediation areas are shown on the figure below (elevations are in feet AMSL)[16]. Water levels in the wells in the vicinity of the lakeshore range from 364 to 372 ft. AMSL. The average lake level is about 362.95 ft. AMSL; therefore, the water level differences between the sand and gravel zone and the lake range from about 1 ft. to 9 ft., with the smallest differences occurring at the sample location in the southeast corner of the lake near the mouth of Harbor Brook.

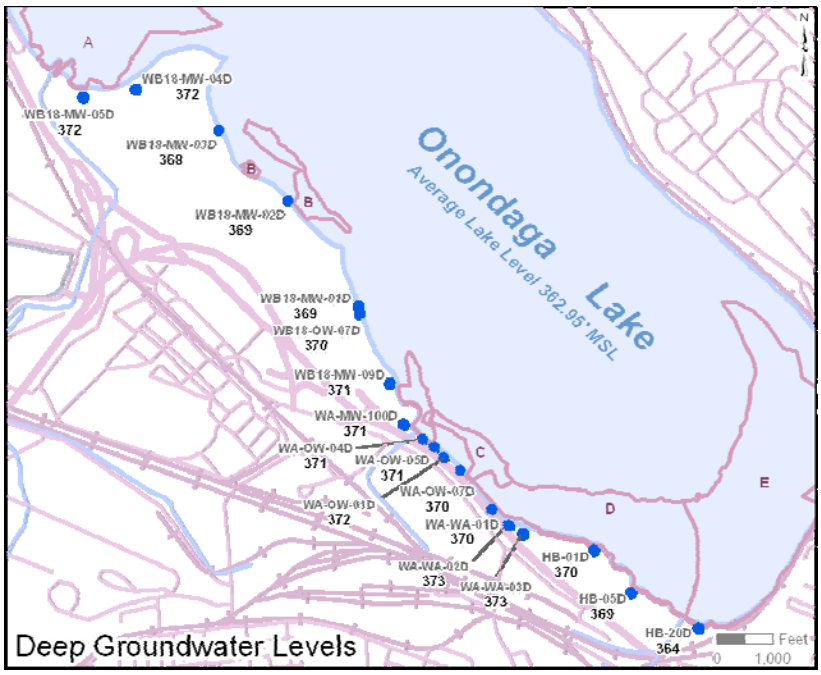

The potential for upward flow from the deep units is proportional to the water level difference. Therefore, the potential for upward flow is smaller in the southeast corner of the lake. The magnitude of the

[16] Water level data represent best estimate of average water levels in the deep zone (O'Brien & Gere, 2009).

upward flow is also related to the thickness and permeability of the silt and clay unit and differences in groundwater density between the sand and gravel zone and the lake.

Several lines of evidence have been used to estimate the upward groundwater flow through the silt and clay unit, and all of these lines of evidence indicate the rate of groundwater flow is very small. From a large-scale perspective, the presence of halite brines in the unconsolidated units beneath the lake provides very strong evidence that the rate of upward groundwater flow through the sediments is very small. The existence of the brine in the sand and gravel aquifer is consistent with only the diffusive flux of chloride across the silt and clay unit as discussed in Appendix D of the Lake FS and in the USGS report by Yager and others (2007b). If upward flow of any appreciable magnitude was occurring across the silt and clay unit, the halite brine in the deep zone, which originated about 16,000 years ago during the end of the last period of glaciation, would have dissipated long ago.

Water-quality data collected from a deep boring (OL-STA-30033) advanced to bedrock in the lake in Remediation Area B also provide qualitative information on the negligible rate of upward groundwater flow through the silt and clay unit. In this boring, pore water samples were collected as the boring was advanced. A plot of water-quality data variations with depth in this

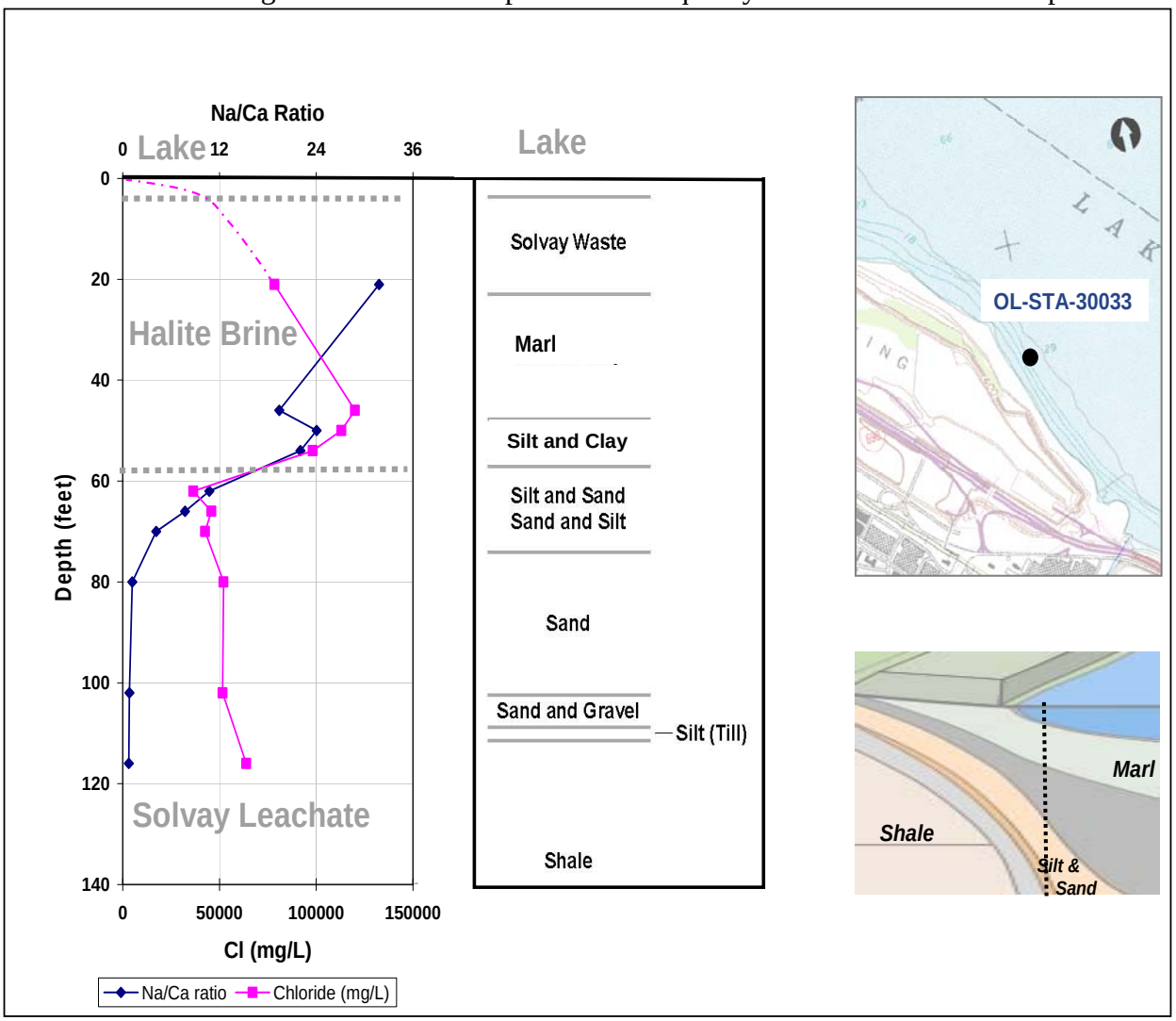

deep boring is shown above along with a geologic log, location map and a schematic cross section with the well location.

An abrupt change in water quality occurs in deep boring OL-STA-3033 at a depth of about 58 feet which corresponds with the contact between the silt and clay unit and the underlying fine sand and silt unit. For example, the chloride concentration in groundwater at a depth of 54 feet was 98,100 mg/L and the chloride concentration at a depth of 62 feet was 36,500 mg/L.. At an upward groundwater velocity of 2 cm/yr, over a period of 60 years, groundwater with chloride concentrations similar to that measured at a depth of 62 feet would have migrated about 10 ft. into the silt and clay unit[17]. The fact that groundwater with lower chloride concentrations has apparently not migrated into the silt and clay unit suggests that the upward groundwater flow rate through the silt and clay unit is significantly less than 2 cm/yr in Remediation Area B.

An estimate of groundwater flow across the silt and clay unit was also made using chloride concentration gradients in an analogous manner to that used to estimate upwelling velocities near the sediment-water interface. Pore water samples were collected in three borings in SMU 2[18] from the upper 8 ft. of the silt and clay unit and analyzed for chloride concentrations in the pore. The pore water chloride data from these borings were interpreted using Equation 1 to quantify groundwater velocity through the silt and clay unit. The calculated velocity through the silt and clay unit at all three borings was less than 0.5 cm/yr. The estimate though has significant uncertainty because the chloride concentration gradient within the silt and clay unit is small due to the fact that this unit is located tens of feet below the sediment-water interface. The results of these evaluations are contained in Attachment X.

A deep boring was advanced in Remediation Area D, approximately 2,000 ft. offshore, into bedrock which was encountered at a depth of 169 ft. below the sediment-water interface. In this boring, unlike the boring in Remediation Area B, all the pore water had the characteristics of a natural sodium-chloride brine. The chloride-depth profile from this boring could not be analyzed to determine upwelling velocities because chloride concentrations in the sand and gravel unit were lower than in the overlying fine sand and silt and the underlying bedrock, likely reflecting changes in water quality induced by historic brine production[19]. A plot of chloride concentrations with depth in this boring (OL-STA-10108), as well as sodium to calcium ratios, are shown on the figure below.

[17] This distance is based on an upwelling velocity of 2 cm/yr, an effective porosity of 0.4, and a 60 year migration time frame.

[18] Borings OL-STA-20042, OL-STA-20053, OL-STA-20058 advanced in May 2006.

[19] The USGS (2000) reported that 11.5 million tons of salt were removed from brines produced from the groundwater system at Onondaga Lake from 1797 to 1917. This represents the salt content from the constant production of 500 gpm of brine with a chloride concentration of 60,000 mg/L over this period. Most of this production occurred from the permeable sand and gravel unit. This production lowered groundwater levels throughout the connected portion of the sand and gravel unit and induced the migration of fresher groundwater from the landward margins of the sand and gravel unit.

The USGS advanced a boring to a depth of 181 ft. near the center of the lake in the profundal zone beyond Remediation Area A. Sediment samples were collected as the boring was advanced and subsequently centrifuged in the laboratory to obtain pore water samples. These samples were analyzed for a number of analytes including calcium, sodium and chloride. The chloride-depth data have been analyzed using the techniques described above to estimate the upwelling velocity. The calculated upwelling velocity is 0.24 cm/yr as shown on the figure below.

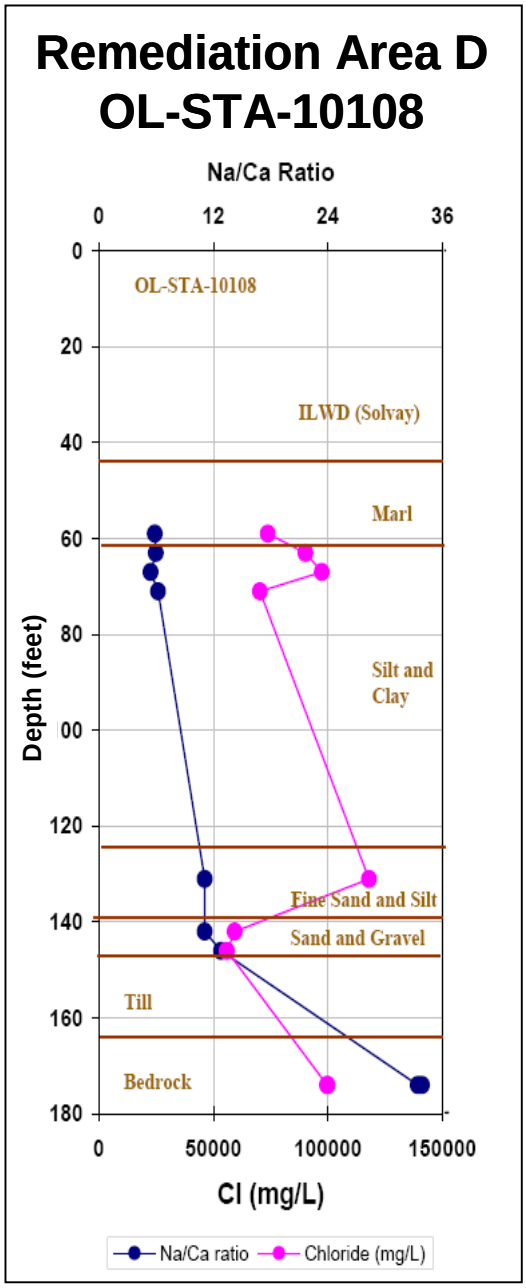

The silt and clay unit typically is described in the field as brown to dark gray clay with some silt with medium to high plasticity. The vertical hydraulic

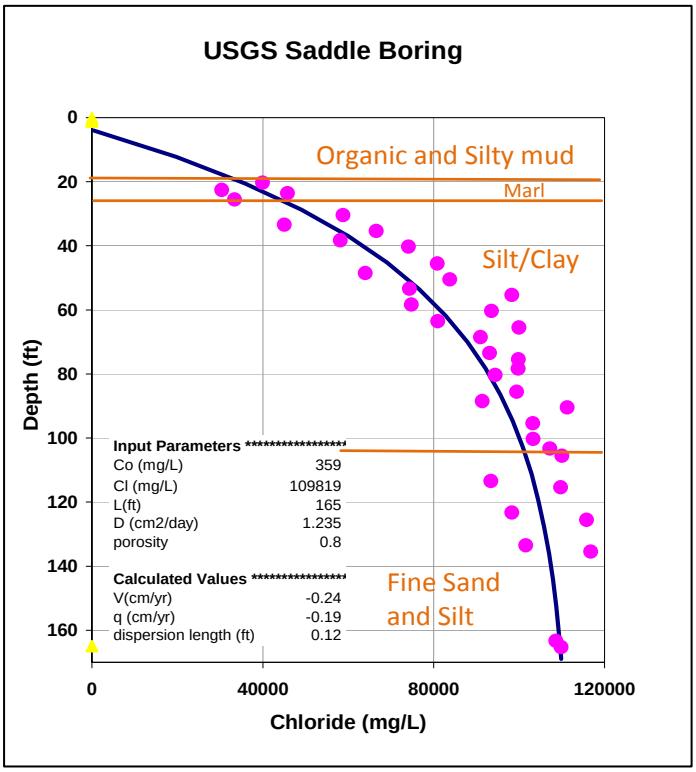

conductivity of the silt and clay unit averages about 1.4×10^{-7} cm/second based on testing of the silt and clay unit within the remediation areas. The vertical hydraulic conductivity of the silt and clay unit was measured[20] in multiple Shelby tube samples collected from eight borings advanced through the silt and clay unit in the Remediation Areas in the Phase VI Pre-Design Investigation. The vertical hydraulic conductivities measured in samples from the eight borings are listed on Table 4 and the locations of the borings are shown on Figure 17. At each boring location, an effective vertical hydraulic

[20] The vertical hydraulic conductivity was measured using a flexible wall permeameter by ASTM D 5084.

conductivity[21] was calculated from the individual measurements of hydraulic conductivity by the following equation:

$$K_{Veff} = \frac{b_T}{\sum_i^n b_i / K_{Vi}} \tag{8}$$

where K_{Veff} is the effective vertical hydraulic conductivity for the silt and clay unit, b_T is the total thickness of the silt and clay unit, n is the number of vertical hydraulic conductivity measurements in the silt and clay unit at the boring, b_i is the thickness corresponding to measurement i, and K_{Vi} is the measured vertical hydraulic conductivity. The effective vertical hydraulic conductivities at the eight borings ranged from 5×10^{-8} cm/sec to 3×10^{-7} cm/sec, a relatively narrow range indicating that the effective vertical hydraulic conductivity of the silt and clay unit is relatively uniform.

In addition, vertical hydraulic conductivity values were calculated from consolidation test results from 11 Shelby tube samples collected from the silt and clay unit beneath Remediation Area D in the Phase I Pre-Design Investigation. The locations of the borings in which these samples were collected are also shown on Figure 17, and the calculated vertical hydraulic conductivies are listed on Table 4. The calculated vertical hydraulic conductivities ranged from 6×10^{-8} cm/sec to 3×10^{-7} cm/sec, a range that is consistent with the data collected in the Phase VI Pre-Design Investigation. The method used to analyze these data and the results of the analyses are described in detail in Attachment XIII.

The thickness of the silt and clay unit beneath the lake is variable, ranging from about 15 ft. to over 70 ft. across the Remediation Areas. A map of the thicknesses of the silt and clay unit beneath much of Onondaga Lake is shown on Figure 3. In much of the eastern part of Remediation Area D and in adjacent Remediation Area E, the silt and clay unit is over 60 ft. thick. The unit is thinnest along the shoreline in the western portion of Remediation Area D, but the unit thickens rapidly away from the shoreline.

The rate of upward groundwater flow through the silt and clay unit can be estimated with Darcy's law: $v = ki$ where v is the upwelling velocity, k is the vertical hydraulic conductivity, and i is the hydraulic gradient. This equation is valid if the density of the groundwater on either side of the silt and clay unit is approximately the same, which is generally the case as brines occur both in the marl overlying the silt and clay unit and in the underlying fine sand and silt unit and the sand and gravel unit. If the density is not the same, the velocity can be estimated with the following equation:

$$v = -k\left(\frac{\partial h_f}{\partial z} + \left(\frac{\rho - \rho_f}{\rho_f}\right)\right) \tag{9}$$

[21] The effective vertical hydraulic conductivity is defined as the value of the vertical hydraulic conductivity that will produce the correct estimate of groundwater flux through the silt and clay unit using the equation $v = K_v$ * *hydraulic gradient* where the hydraulic gradient is the water-level difference across the silt and clay unit divided by the total thickness of the silt and clay unit.

where h_f is equivalent fresh-water head, ρ is average density between two locations where head is measured, and ρ_f is freshwater density (Parsons, 2004; Appendix D: Part A).

The large variations in the thickness of the silt and clay unit result in differences in the upward groundwater flow in Remediation Area D, with the larger upward groundwater flows occurring near the shoreline where the silt and clay unit is the thinnest. Evaluations of potential upwelling velocities were conducted considering the water level differences measured at the various monitoring locations along the shoreline in Remediation Area D and the density variations in groundwater[22]. These evaluations indicate that upwelling velocities will generally be less than 2 cm/yr adjacent to the shoreline where the silt and clay unit is thinnest, to less than 1 cm/yr where the silt and clay unit is greater than about 30 ft. thick[23]. The calculated upwelling velocities at selected monitoring locations, based on water levels in deep and intermediate well pairs, are listed on Table 5.

The silt and clay unit beneath the lake at Remediation Area D appears to be the thinnest adjacent to the East Flume. A boring was advanced and monitoring wells were installed on the spit of land beneath the East Flume and the lake to determine the characteristics of the silt and clay unit and groundwater conditions in this area (boring HB-SB-213 and monitoring wells HB-MW-213D, HB-MW-213I and HB-MW-213S). Monitoring wells HB-MW-213I and HB-MW-213D are screened in the marl above the silt and clay unit and in the sand and silt unit below the silt and clay unit, respectively. Based on the water level difference between these two wells, the thickness of the silt and clay unit and the higher of the two estimates of the vertical hydraulic conductivity described above, the upward groundwater velocity is less than 3 cm/yr[24].

In Remediation Area A offshore of the proposed hydraulic containment system the thickness of the silt and clay unit is slightly greater than 30 ft., and the water level difference between the deep zone and the lake is greater than 9 ft. Based on these parameter values, the estimated upwelling velocity through the silt and clay unit in this area is about 2.2 cm/yr. In Remediation Area B offshore of the proposed hydraulic containment system the thickness of the silt and clay unit ranges from about 20 to 60 ft. and the water level difference between the deep zone and the lake is on the order of 6 ft. Based on these parameters, the upwelling velocity through the silt and clay unit is in the range of 0.4 to 1.3 cm/yr. In Remediation Area C offshore of the proposed hydraulic containment system the thickness of the silt and clay unit ranges from about 15 to 40 ft. and the water level difference between the deep zone and the lake is on the order of 7.5 ft. Based on these parameters, the upwelling velocity through the silt and clay unit is in the range of about 1cm/yr to a little more than 2 cm/yr

---

[22] Groundwater density was estimated based on the total dissolved solids concentrations in groundwater. Standard QA/QC procedures were used to validate the water quality data that were the basis for the measurements of total dissolved solids.

[23] These estimates were calculated using a water-level difference across the silt and clay unit of 7 ft. and vertical hydraulic conductivities for the silt and clay unit in the range of 1.4×10^{-7} cm/yr.

[24] The upward groundwater velocity is calculated based on a vertical hydraulic conductivity of 1.4×10^{-7} cm/sec, a water level difference across the silt and clay unit of 4.92 ft. based on water levels collected on November 3, 2008 (O'Brien & Gere, 2009) and a silt and clay unit thickness of 8 ft. The hydraulic gradient is calculated as the water-level difference divided by the silt and clay thickness. The densities of groundwater at HB-MW-213I and HB-MW-213D are similar as measured total dissolved solids concentrations were 48,900 mg/L and 47,000 mg/L, respectively in November 2008.

Summary

The presence of upward hydraulic gradients from the deep groundwater zones to Onondaga Lake indicates that there is the potential for upward groundwater flow from the deep zones to Onondaga Lake. The hydraulic containment systems that will be operated along the lakeshore at Remediation Area D, portions of Remediation Area A, and portions of Remediation Area B will capture shallow groundwater flowing towards the lake but will have a negligible effect on the potential upward flowing groundwater from the deeper groundwater zones to the lake. The evaluations described above indicate that the upwelling velocities with the hydraulic containment system in operation will generally be less than 2 cm/yr. Upwelling velocities may approach 2 cm/yr along the shoreline in the western portion of Remediation Area D where the silt and clay unit is the thinnest, but upwelling velocities may be much less than 2 cm/yr in the remainder of Remediation Area D where the silt and clay unit is much thicker. Upwelling velocities will be less than or approximately equal to 2 cm/yr in areas offshore of the hydraulic containment systems in Remediation Areas A and B.

Section 8
Upwelling Velocities for Cap Design in Areas with Hydraulic Containment

Based on the multiple lines of evidence described in Section 7, estimates of the upwelling rates in Remediation Areas affected by operation of the hydraulic containment system, and wetland areas located between the containment system and the lake, have been developed. These estimates are based on the assumption that groundwater discharge in the remediation areas and the wetland areas with operation of the hydraulic containment system will be the result only of upward groundwater flow through the silt and clay unit. The rate of groundwater flow through the silt and clay unit is a function of the hydraulic gradient across this unit, the thickness of the unit and the effective vertical hydraulic conductivity of this unit. Contour maps of equal upwelling velocities within Remediation Areas B, C and D have been developed based on best estimates[25] of vertical hydraulic conductivity for the silt and clay unit, thickness of the silt and clay unit, and groundwater level difference across the silt and clay unit. These contour maps are shown on Figures 18, 19, and 20 for Remediation Areas B, C and D, respectively.

For purposes of cap design, upwelling velocities based on best-estimates of groundwater gradient, silt and clay unit thickness and vertical hydraulic conductivity were supplemented by developing cumulative frequency distributions of upwelling velocities based on a consideration of the uncertainty/variability in the estimates of each of these three parameters. The cumulative frequency distributions were calculated using a Monte Carlo approach that is described below, following a discussion of the uncertainty/variability in each of the individual parameters.

Vertical Hydraulic Conductivity

During the Phase VI Pre-Design Investigation the vertical hydraulic conductivity of the silt and clay unit was measured in multiple Shelby tube samples collected from eight borings advanced through the silt and clay unit in the remediation areas and in addition vertical hydraulic conductivity was calculated from consolidation test results from 13 Shelby tube samples collected from the silt and clay unit in Remediation Area D in the Phase I Pre-Design Investigation. For the eight borings in which multiple measurements of vertical hydraulic conductivity were obtained, an effective vertical hydraulic conductivity for the silt and clay unit at that location was calculated. A cumulative frequency distribution of these eight effective vertical hydraulic conductivities is shown on the left-most graph below, in which vertical hydraulic conductivity is plotted along on a logarithmic scale on the x-axis and the percentile frequency is plotted on a probability scale on the y-axis. The data points on the graph plot approximately along a straight line indicating that vertical hydraulic conductivity is log-normally distributed. For purposes of the Monte Carlo simulations used to calculate the uncertainty/variability in estimated upwelling velocities, the uncertainty/variability in the vertical hydraulic conductivity was described by a log normal distribution with a mean of -6.906 log cm/sec (1.24×10^{-7} cm/sec) and a standard deviation of 0.275.

[25] In developing these maps, a vertical hydraulic conductivity of 1.4×10^{-7} was used, the thicknesses shown on Figure 3 were used, and water-level differences based on average levels in sand and gravel unit monitoring wells along the shoreline as shown on page 33 subtracted from average lake levels were used.

For comparison purposes, a probability plot for all 40 individual measurements of vertical hydraulic conductivity was also prepared (the right-most graph above). These data also plot approximately along a straight line, with the exception of one extreme value at each end of the distribution, indicating that these data are also log-normally distributed. The calculated mean and standard deviation of this distribution is -6.80 log cm/sec (1.6×10^{-7} cm/sec) and 0.32, respectively. This distribution is similar to that calculated based on effective vertical hydraulic conductivities.

Thickness of Silt and Clay Unit

The uncertainty in the thickness of the silt and clay unit is related to the accuracy with which the contacts with the overlying marl and underlying silt and fine sand unit were picked

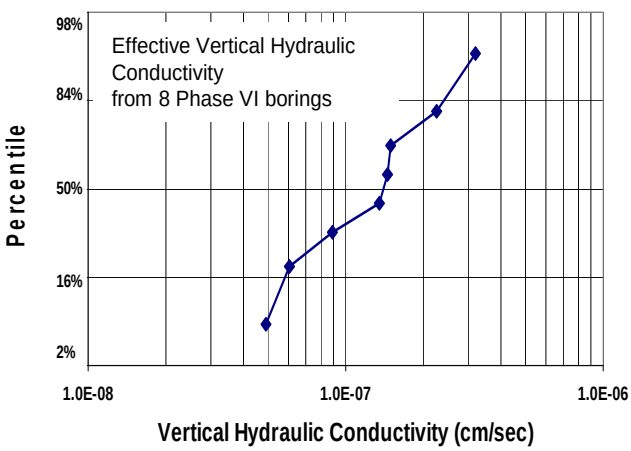

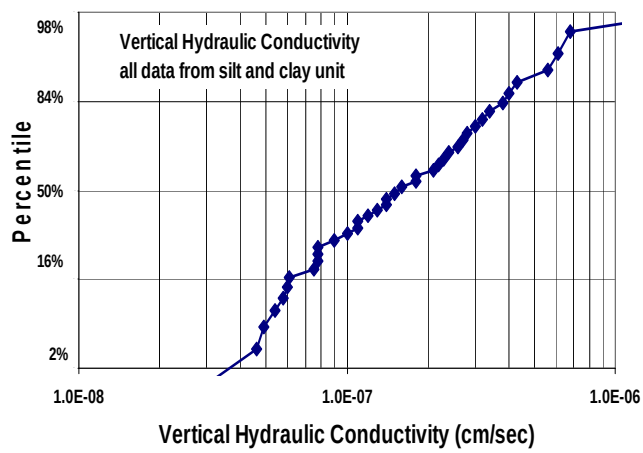

and is related to the density of borings that penetrated the silt and clay unit. The uncertainty in picking the contacts with overlying and underlying units, for purposes of the Monte Carlo simulations, was specified as a normal distribution with ±5 ft. corresponding to a 95 percent degree of confidence. The uncertainty related to density of borings was not explicitly represented in the Monte Carlo simulations as in most areas there is a relatively good density of borings. In addition to the uncertainty described above, the silt and clay thickness varies spatially, according to the contours shown on Figure 3.

Water Level Differences

The groundwater-level difference across the silt and clay unit has not been measured at any location within the remediation areas primarily because of logistical difficulties in obtaining representative water-level measurements beneath the lake. As a conservative assumption, the water-level difference for purposes of the Monte Carlo simulations was specified based on water-levels in monitoring wells completed in the sand and gravel unit along the shoreline and lake water levels. This overestimates the actual water-level difference across the silt and clay unit, as the silt and clay unit is only a portion of the total sediment thickness between the sand and gravel unit and the bottom of the lake. If groundwater-level measurements were available for monitoring wells completed at the base of the marl and at the top of the silt and fine sand unit, the difference in water-levels across the silt and clay unit could be accurately computed and they would likely be smaller than those computed from monitoring wells in the sand and gravel unit and lake level.

For the sand and gravel monitoring wells along the lakeshore, the difference between the groundwater level in the well and lake level[26] was calculated for each date with available groundwater level data. The average and standard deviation of the water-level difference was then calculated for each monitoring location along the shoreline, and these statistics were used in the Monte Carlo simulations (assuming a normal distribution) to represent the uncertainty in water-level difference across the silt and clay unit. The average water-level differences and the standard deviations of the differences are listed in the table below.

	HB HB-01D	HB HB-05D	HB-20D	WA WA-01D	WA MW100D	WA OW-04D	WA OW-05D	WA OW-07D	WB18 MW-02D	MW18 MW-03D	WB18 MW-05D
Remediation Area	D	D	D	D	C	C	C	C	B	B	A
Average (feet)	7.07	5.55	0.71	7.45	8.49	7.74	8.18	7.46	6.26	5.16	9.45
Standard Deviation (feet)	1.16	0.70	0.32	0.45	0.40	0.51	0.56	0.60	0.63	1.05	0.49

Monte Carlo Simulation

The basic model used in the Monte Carlo simulation was the following (i.e., Darcy's Law):

$$V = K_V * \frac{\Delta H}{b} \tag{10}$$

where V is the upwelling velocity, ΔH is the water-level difference across the silt and clay unit, and b is the thickness of the silt and clay unit. This equation assumes that the density of groundwater does not change significantly across the silt and clay unit. The steps in the Monte Carlo analysis were the following:

1. One hundred sets of stochastic random fields were generated for each of the three parameters in the basic model: vertical hydraulic conductivity, water-level difference and silt and clay thickness. For Remediation Area D parameter values were defined on a 50-ft. by 50-ft. grid, and in Remediation Areas B and C parameter values were defined a 25-ft. by 25-ft. grid. In the connected wetland and the outboard area wetland parameters values were defined on a 10-ft by 10-ft grid. The stochastic random vertical hydraulic conductivity fields were generated using the FIELDGEN utility in the computer program PEST (Doherty, 2008). The random fields for thickness of the silt and clay unit were generated by randomly selecting a value from the normal distribution describing the uncertainty in estimated thickness, adding this value to the best-estimate of thickness, and then kriging these values within the domain of interest. The random water-level difference fields were generated by randomly selecting a value from the normal distribution described above at each monitoring well location along the shoreline shown on the figure on page 30 and then kriging the selected values assuming that the water-level difference is constant perpendicular to the shoreline within the domain of interest.

[26] The lake level was specified based on daily data from the U.S. Geological Survey gage 04240495 Onondaga Lake at Liverpool, New York.

2. One hundred sets of parameter combinations were generated by randomly selecting values from 100 sets of random fields generated in the previous step for each parameter.
3. The upwelling velocity was calculated using Equation 10 at each grid cell in Remediation Area D, in Remediation Areas B and C and in the wetland areas for each 100 sets of parameter combinations.
4. The statistics of the calculated upwelling velocities within each subarea in Remediation Area D, in Model Areas B1/C1, B2, and C3, and in the wetland areas were computed. For the outboard wetland area separate statistics were calculated for the eastern, central, and western portions of the area.

Results

Selected statistics on the upwelling frequency distributions generated for each model area and the wetland areas are listed on the table below. These statistics are based on the upwelling velocities calculated at each of the grid cells within the model area in the Monte Carlo simulations. The number of calculated upwelling velocities used to construct the frequency distribution for each model area is listed in the column labeled "count" in the table below. The mean and standard deviation of the log-transformed distributions were used to generate upwelling distributions for the Monte Carlo simulations conducted with the cap model.

Remediation Area	**Area**	**Count**	**Mean (cm/year)**	**Log-Transformed Values**	
				Mean log(cm/yr)	**Std Dev** log(cm/yr)
B and C	**B1/C1**	104700	1.02	-0.09	0.30
	B2	48400	0.51	-0.39	0.29
	C3	76300	1.50	0.07	0.30
	Connected Wetland	131900	1.11	-0.04	0.26
D	**East**	85000	0.37	-0.56	0.34
	Center	51700	0.68	-0.28	0.31
	Western	20000	1.11	-0.06	0.31
	SMU2-ILWD	11900	1.53	0.08	0.31
	Outboard - West	31800	1.73	0.12	0.33
	Outboard - Central	26500	1.22	-0.14	0.44
	Outboard - East	35400	0.06	-1.43	0.39

Probability plots of the distributions generated from the Monte Carlo simulations are shown in graphic form below; the x-axis of each plot is the upwelling velocity plotted on a logarithmic scale and the y-axis is the frequency percentile plotted on a probability scale. Each of the distributions plots approximately as a straight line indicating that the distributions are normally distributed.

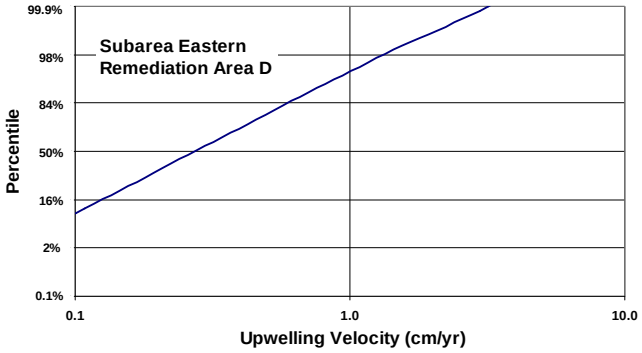
Subarea Eastern
Remediation Area D
Percentile
99.9%
98%
84%
50%
16%
2%
0.1%
0.1
1.0
10.0
Upwelling Velocity (cm/yr)

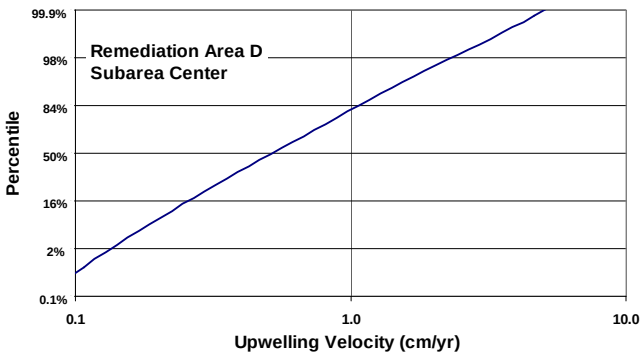
Remediation Area D
Subarea Center
Percentile
99.9%
98%
84%
50%
16%
2%
0.1%
0.1
1.0
10.0
Upwelling Velocity (cm/yr)

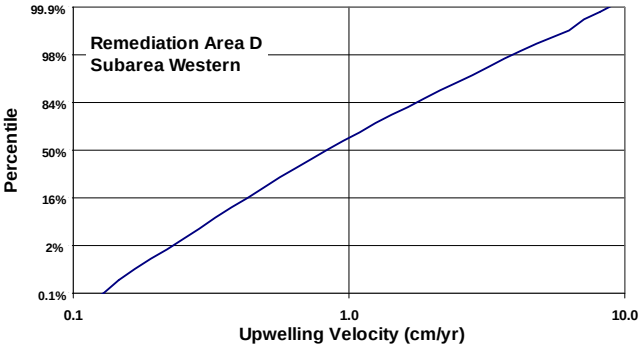
Remediation Area D
Subarea Western
Percentile
99.9%
98%
84%
50%
16%
2%
0.1%
0.1
1.0
10.0
Upwelling Velocity (cm/yr)

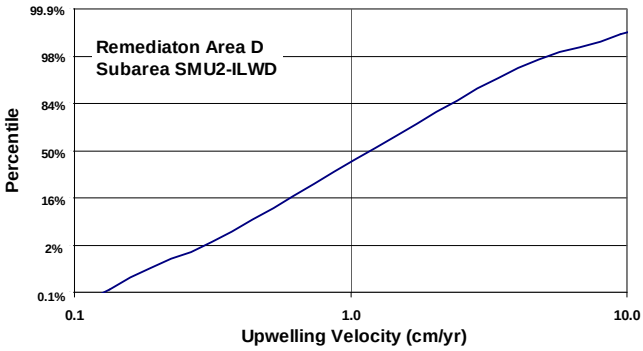
Remediaton Area D
Subarea SMU2-ILWD
Percentile
99.9%
98%
84%
50%
16%
2%
0.1%
0.1
1.0
10.0
Upwelling Velocity (cm/yr)

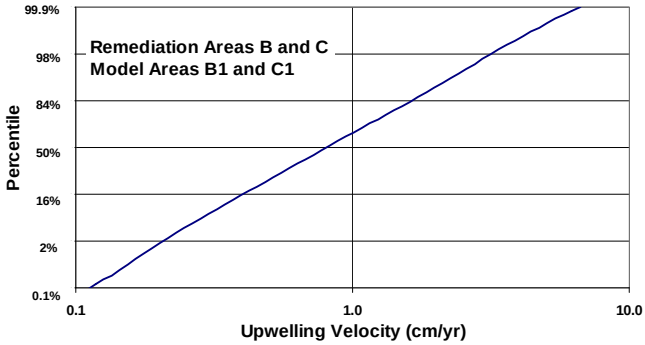
Remediation Areas B and C
Model Areas B1 and C1
Percentile
99.9%
98%
84%
50%
16%
2%
0.1%
0.1
1.0
10.0
Upwelling Velocity (cm/yr)

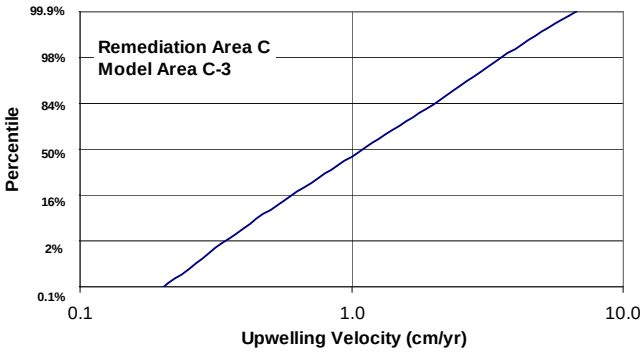
Remediation Area C
Model Area C-3
Percentile
99.9%
98%
84%
50%
16%
2%
0.1%
0.1
1.0
10.0
Upwelling Velocity (cm/yr)

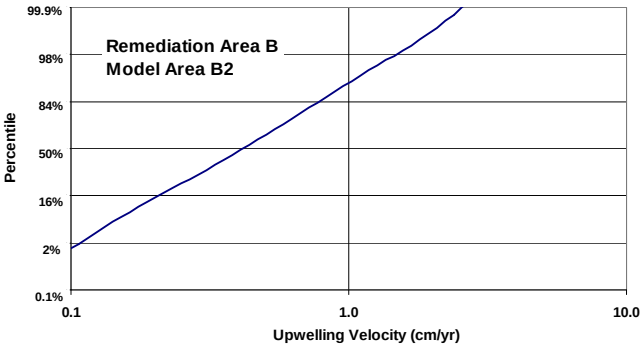
Remediation Area B
Model Area B2
Percentile
99.9%
98%
84%
50%
16%
2%
0.1%
0.1
1.0
10.0
Upwelling Velocity (cm/yr)

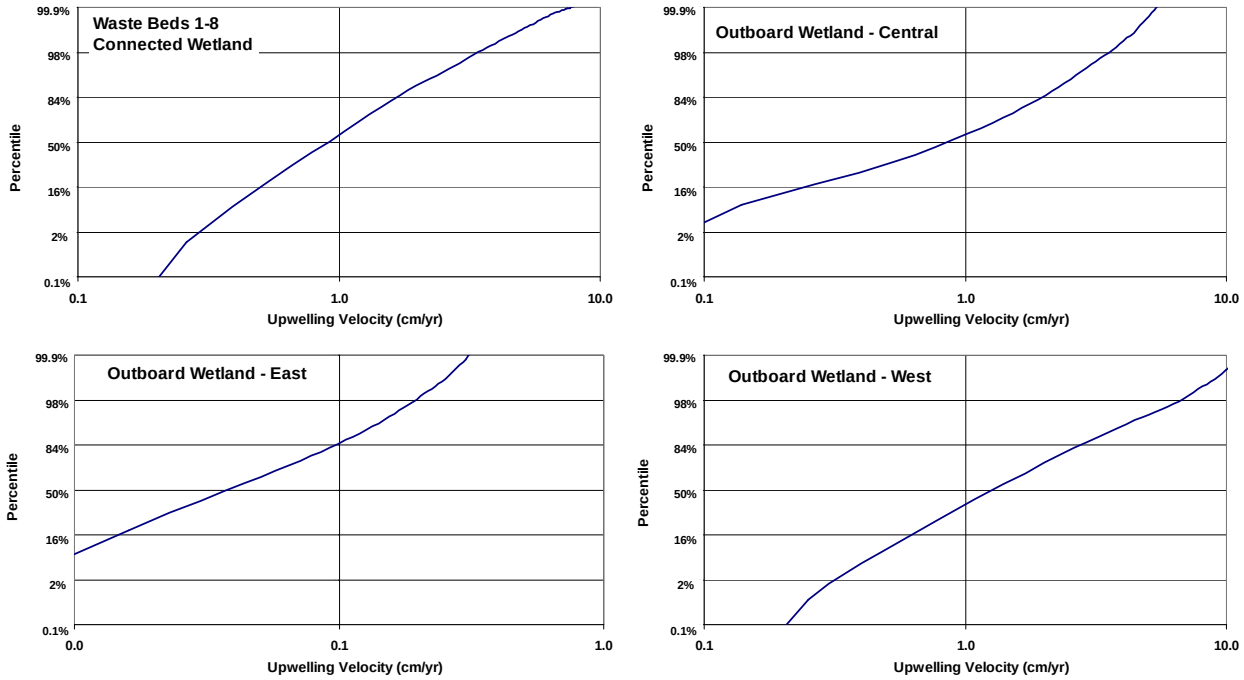

Remediation Area A – Model Area A1

A hydraulic containment system is also proposed along the shoreline of Remediation Area A just east of the mouth of Ninemile Creek because of the high upwelling velocities determined in the area from analysis of chloride-depth profiles constructed from both sediment-conductivity and pore-water data in this area. Conservatively it was calculated that the effect of the containment system on upwelling velocity would extend 500 ft. outward from the shoreline[27]. In the region near the shoreline the average upwelling velocity was calculated to be 2.2 cm/yr with the containment system in operation based on the thickness of silt and clay unit in this area, the average silt and clay vertical hydraulic conductivity in this area, and the water-level difference between the sand and gravel unit and the lake in this area. This value was used in the calculation of the upwelling frequency distribution in Model Area A1 by specifying an upwelling velocity of 2.2 cm/yr at five sample locations present in the influenced area.

[27] The effect of hydraulic containment systems on upwelling velocities was discussed in Appendix D of the FS. A comparison of the tabulated upwelling velocities with distance from shore on pages DA.11-1 and DA.12-1, which show current upwelling velocities and upwelling velocities with hydraulic containment system in place, clearly shows that the effect of the hydraulic containment system extends outward at least 500 ft.

Section 9
Conclusions

This report describes the results of extensive field and analytical studies that have quantified the discharge of groundwater to the areas in Onondaga Lake where a sediment cap will be placed as part of the remedial activities undertaken to meet the requirements of the Record of Decision for the Onondaga Lake Bottom Subsite. The current rates of groundwater discharge in Remediation Areas A and E and Model Area C2, which are similar to discharge rates expected after placement of the cap, have been delineated based on the analysis of chloride depth profiles at more than 200 locations within and in the vicinity of these remediation areas. In Remediation Area D and Model Areas B1/C1, B2 and C3 the rates of groundwater discharge after placement of the cap will be significantly lower than current rates as the result of the construction and operation of a hydraulic containment system along the shoreline. Groundwater discharge rates in Remediation Area D and Model Areas B1/C1, B2 and C3 after placement of the cap were calculated based on groundwater flow rates upward through the underlying regional confining unit (the silt and clay unit).

This report describes a number of methods that were implemented in the field to estimate groundwater discharge rates, which are commonly referred to as upwelling velocities. The evaluation of upward groundwater velocity through the sediment based on the change in chloride concentrations with depth in sediment pore water was determined to be the best method for estimating current upwelling velocities in the remediation areas. This report describes the theoretical bases for the use of this method to estimate upwelling velocities and describes the extensive data collected on chloride concentrations in sediments to accurately delineate the current distribution of upwelling velocities within the remediation areas.

The upwelling velocities within the remediation areas are low. The mean measured upwelling velocity in Remediation Area E is 1.5 cm/yr, and the mean upwelling velocities in Model Areas A1, A2, and C2 are 1.6 cm/yr, 4.1 cm/yr, and 3.1 cm/yr, respectively. In Remediation Area D and Model Areas B1/C1, B2 and C2, calculated upwelling velocities with the hydraulic containment system in place are less than 2 cm/yr.

The data and evaluations described in this report provide an excellent foundation for the design of the remedy for Onondaga Lake. The upwelling velocities that are described in this report will be used in the cap model for purposes of cap design.

Section 10
References

Al-Niami, A., and K. Rushton. 1977. Analysis of Flow Against Dispersion in a Porous Media: Journal of Hydrology 33: 87-97.

Anati, D., 1994. Advection and Diffusion in Marine Sediments: DSDP Site 374 in the Eastern Mediterranean as an Example. Earth and Planetary Science Letters 128:575-589.

Andrews, C. and G. Swenson, 2004. Groundwater Flow to Onondaga Lake. Appendix D: Part A to the Onondaga Lake Feasibility Study. Prepared for Honeywell, Morristown, NJ. By Parsons. November 2004.

Aster, R.C. B. Borchers, and C.H. Thurber (2005), Parameter Estimation and Inverse Problems, International Geophysics Series, vol. 90, Elsevier Academic Press, Amsterdam.

Berg, P. and N. Risgaard-Petersen, 1998. Interpretation of Measured Concentration Profiles in Sediment Pore Water. Chemical Oceanography 43(7): 1500-1510.

Bredehoeft, J.D. and Papadopulos, I.S., 1965. Rates of Vertical Groundwater Movement Estimated from Earth's Thermal Profile. Water Resources Research, 1:325-328.

Boudreau, B. 1996. The Diffusive Tortuosity of Fine-Grained Unlithified Sediments: Geochimica et Cosmochimica Acta 60, no. 16: 3139-3142.

Cable, J., J. Martin, P. Swarzenski, M. Lindenberg and J. Steward, 2004. Advection within Shallow Pore Waters of a Coastal Lagoon, Florida. Ground Water, V42: 1011-102.

Cornett, R. J., B.A. Risto, and D. R. Lee, 1989. Measuring Groundwater Transport Through Lake Sediments by Advection and Dispersion. Water Resources Research, V.25, no. 8.

Day-Lewis, F.D., H. Karam, C. Harvey, J.Lane, 2006. Monitoring Submarine Groundwater Discharge Using a Distributed Temperature Sensor, Waquoit Bay, Massachusetts. EOS Transactions, American Geophysical Union, V.87. no. 52.

Doherty, J. (2008), PEST, Model Independent Parameter Estimation. User's Manual: 5th Edition.

Effler, S. W. editor, 1996. Limnological and Engineering Analysis of a Polluted Urban Lake. Springer-Verlag, New York.

Effler, S., S. Doerr, and C. Brooks, 1990. Chloride in the Pore Water and Water Column of Onondaga Lake, N.Y., U.S.A. Water, Air, and Soil Pollution 51:315-326.

Felmy, A. and J. Weare, 1991. Calculation of Multicomponent Ionic Diffusion from Zero to High Concentration: I. The Sys tem Na-K-Ca-Mg-Cl-SO_4-H_2O at 25º C. Geochimica et Cosmochimica Acta 55:113-131.

Jackson. W. and T. Anderson, 2007. Diffusion Sampler Equilibration Study Using Teflon (PTFE) and Tuffryn Membranes in Onondaga Lake Sediments. Prepared for Parsons, Liverpool, New York, February 24, 2007.

Kappel, W.M. 2000, Salt Production in Syracuse, New York ("The Salt City") and the Hydrogeology of the Onondaga Creek Valley. U.S. Geological Survey Fact Sheet 139-00.

Keery, J., A. Binley, N. Crook, and J. Smith, 2006. Temporal and Spatial Variability of Groundwater-Surface Water Fluxes: Development and Application of an Analytical Method Using Temperature Time Series. Journal of Hydrology, 336:1-16.

Kappel, W.M, and R. Yager, 2008, Ground-water-flow modeling of a freshwater and brine-filled aquifer in the Onondaga Trough, Onondaga County, New York—A summary of findings, U. S. Geological Survey Open-File Report 2007-1409, 12p.

Lee, D.R. 1977. A Device for Measuring Seepage Flux in Lakes and Estuaries. Limnology and Oceanography, 22: 140-147.

Maris, C. and M. Bender, 1982. Upwelling of Hydrothermal Solutions Through Ridge Flank Sediments Shown by Pore Water Profiles. Science, 216: 623-626.

Maris, C., M. Bender, P. Froelich, R. Barnes, and N. Luedtke, 1984. Chemical Evidence for Advection of Hydrothermal Solutions in the Sediments of the Galapagos Mounds Hydrothermal Field. Geochemica et Cosmochimica Acta: 48:2331-2346.

Neuman, S.P. 1990. Universal Scaling of Hydraulic Conductivites and Dispersivities in Geologic Media: Water Resources Research 26, no. 8: 1749-1758.

Neuman, S.P. 2006. Comment on Longitudinal Dispersivity Data and Implications for Scaling Behavior: Ground Water 44, no. 2: 139-141.

Neuzil, C.E., 1986. Groundwater Flow in Low Permeability Environments, Water Resources Research, 22, no. 8: 1163-1195.

New York State Department of Environmental Conservation (NYSDEC) and U.S. Environmental Protection Agency (USEPA), 2005. Record of Decision Onondaga Lake Bottom Subsite of the Onondaga Lake Superfund Site. Town of Geddes and Salina, Villages of Solvay and Liverpool and City of Syracuse, Onondaga County, New York.

Onondaga County, 2003. 2002 Annual Report: Onondaga Lake Ambient Monitoring Program.

Onondaga County, 2004. 2003 Annual Report: Onondaga Lake Ambient Monitoring Program.

O'Brien & Gere, 2008. Wastebeds 1-8 Remedial Investigation Report, Geddes, New York. Prepared for Honeywell, Morristown, New Jersey and Syracuse, New York. April

O'Brien & Gere, 2009. Remedial Investigation Revised Report Wastebed B/Harbor Brook Site.

Parsons, 2003. Groundwater Upwelling Investigation for Onondaga Lake, Syracuse, New York. Prepared for Honeywell, Morristown, New York.

Parsons, 2004. Draft Feasibility Study Report for Onondaga Lake. Prepared for Honeywell, Morristown, New York. November.

Parsons, 2005a. Onondaga Lake Phase I Pre-Design Investigation: Sampling and Analysis Plan. Prepared for Honeywell, Morristown, New Jersey and Syracuse, New York.

Parsons, 2005b. Onondaga Lake Pre-Design Investigation: Quality Assurance Project Plan. Prepared for Honeywell, Morristown, New Jersey. Syracuse, New York.

Parsons, 2006. Onondaga Lake Pre-Design Investigation: Phase II Work Plan. Prepared for Honeywell, Morristown, New Jersey and Syracuse, New York.

Parsons, 2007a. Onondaga Lake Pre-Design Investigation: Phase I Data Summary Report. Prepared for Honeywell, Morristown, New Jersey and Syracuse, New York

Parsons, 2007b, Onondaga Lake Pre-Design Investigation: Phase III Work Plan. Prepared for Honeywell, Morristown, New Jersey and Syracuse, New York.

Parsons 2007c, Onondaga Lake Pre-Design Investigation: Phase III Addendum 1. Prepared for Honeywell, Morristown, New Jersey and Syracuse, New York.

Parsons 2007d, Onondaga Lake Pre-Design Investigation: Phase III Addendum 2 Prepared for Honeywell, Morristown, New Jersey and Syracuse, New York

Parsons 2007e, Onondaga Lake Pre-Design Investigation: Phase III Addendum 3 Prepared for Honeywell, Morristown, New Jersey and Syracuse, New York

Parsons 2007f, Onondaga Lake Pre-Design Investigation: Phase III Addendum 4 Prepared for Honeywell, Morristown, New Jersey and Syracuse, New York

Parsons 2007g, Onondaga Lake Pre-Design Investigation: Phase III Addendum 5. Prepared for Honeywell, Morristown, New Jersey and Syracuse, New York.

Parsons 2007h, Onondaga Lake Pre-Design Investigation: Phase III Addendum 6 Prepared for Honeywell, Morristown, New Jersey and Syracuse, New York

Parsons 2007i, Onondaga Lake Pre-Design Investigation: Phase III Addendum 7 Prepared for Honeywell, Morristown, New Jersey and Syracuse, New York

Parsons 2008a, Onondaga Lake Pre-Design Investigation: Phase IV Work Plan. Prepared for Honeywell, Morristown, New Jersey and Syracuse, New York.

Parsons 2008b, Onondaga Lake Pre-Design Investigation: Phase IV Addendum 1. Prepared for Honeywell, Morristown, New Jersey and Syracuse, New York.

Parsons 2008c, Onondaga Lake Pre-Design Investigation: Phase IV Addendum 2. Prepared for Honeywell, Morristown, New Jersey and Syracuse, New York.

Parsons 2008d, Onondaga Lake Pre-Design Investigation: Phase IV Addendum 3. Prepared for Honeywell, Morristown, New Jersey and Syracuse, New York.

Parsons 2008e, Onondaga Lake Pre-Design Investigation: Phase IV Addendum 4. Prepared for Honeywell, Morristown, New Jersey and Syracuse, New York.

Parsons 2008f, Onondaga Lake Pre-Design Investigation: Phase IV Addendum 7. Prepared for Honeywell, Morristown, New Jersey and Syracuse, New York.

Parsons 2008g, Onondaga Lake Pre-Design Investigation: Phase IV Addendum 8. Prepared for Honeywell, Morristown, New Jersey and Syracuse, New York.

Parsons, 2009a. Onondaga Lake Pre-Design Investigation: DRAFT Phase II Data Summary Report. Prepared for Honeywell, Morristown, New Jersey and Syracuse, New York.

Parsons, 2009b, Onondaga Lake Pre-Design Investigation: DRAFT Phase III Data Summary Report. Prepared for Honeywell, Morristown, New Jersey and Syracuse, New York

Parsons, 2009c, Onondaga Lake Pre-Design Investigation: DRAFT Phase IV Data Summary Report. Prepared for Honeywell, Morristown, New Jersey and Syracuse, New York

Parsons 2009d, Onondaga Lake Pre-Design Investigation: Phase IV Addendum 6. Prepared for Honeywell, Morristown, New Jersey and Syracuse, New York.

Parsons 2009e, Microbead Marker 2008 Pre-Mobilization Field Test Data Summary Report. Prepared for Honeywell, Morristown, New Jersey and Syracuse, New York.

Parsons 2009f, Onondaga Lake Pre-Design Investigation: DRAFT Phase V Work Plan. Prepared for Honeywell, Morristown, New Jersey and Syracuse, New York.

Rosenberry, D. 2005. Integrating Seepage Meter Heterogeneity with the Use of Ganged Seepage Meters. Limnology and Oceanography: Methods, 3: 131-142.

Rosenberry, D. and J. LaBaugh, 2008. Field Techniques for Estimating Water Fluxes Between Surface Water and Ground Water. U.S. Geological Survey, Techniques and Methods 4-D2.

Sayles, F. and W. Jenkins, 1982. Advection of Pore Fluids through Sediments in the Equatorial East Pacific. Science, 217: 245-248.

Schneider, R. T. Negley, and C. Wafer, 2004. Factors Influencing Groundwater Seepage in a Large Mesotrophic Lake in New York. Journal of Hydrology, v310: 1-16.

Sebestyen, S. and R. Schneider, 2001. Dynamic Temporal Patterns of Nearshore Seepage Flux in a Headwater Adirondack Lake. Journal of Hydrology, 247:137-150.

S. S. Papadopulos & Associates, Inc. and O'Brien and Gere, 2009. Honeywell Groundwater Flow Model, Version 3. November 2009.

Swenson, G. and C. Andrews, 2004. Groundwater Model Documentation. Appendix D: Part B to the Onondaga Lake Feasibility Study. Prepared for Honeywell, Morristown, NJ. By Parsons. November 2004.

TAMS Consultants, Inc. 2002. Onondaga Lake Remedial Investigation Report, Syracuse, New York. Prepared for New York Department of Environmental Conservation, Division of Environmental Remediation.

van der Kamp, G., 2001. Methods for Determining the In-situ Hydraulic Conductivity of Shallow Aquitards - An Overview. Hydrogeology Journal, 9: 5-16.

Yager, R.M., W. Kappel, and L. Plummer, 2007a, Origin of halite brine in the Onondaga Trough near Syracuse, New York State, USA: modeling geochemistry and variable-density flow, Hydrogeology Journal, v. 15, no. 7, p. 1321-1339.

Yager, R., W. Kappel, and L. Plummer, 2007b. Halite Brine in the Onondaga Trough Near Syracuse, New York: Characterization and Simulation of Variable-Density Flow. U.S. Geological Survey, Scientific Investigation Report 2007-5058.